# DEVELOPMENT OF NICOTINE LOADED CHITOSAN NANOPARTICLES FOR LUNG DELIVERY


**Hui Wang**

**B. Pharm**

Submitted in fulfilment of the requirements for the degree of

Doctor of Philosophy

School of Clinical Sciences

Faculty of Health

Queensland University of Technology

Australia

2017

# Keywords

Aerosolization;

Biodegradable polymer;

Chitosan;

Controlled drug release;

Dry powder inhaler formulation;

Locomotor activity test;

Microaggregates;

Mouse model for inhalation exposure;

Nanoparticles;

Nicotine addiction;

Nicotine hydrogen tartrate salt;

Nose-only inhalation device;

Powder flowability and dispersity;

Powder long-term stability;

Powder physicochemical properties;

Pulmonary drug delivery;

Smoking;

w/o emulsion crosslinking

# Abstract

Cigarette smoking has become one of the leading causes of preventable deaths all over the world, causing a serious threat to human wellbeing and a tremendous economic burden to governments. The currently available treatment options for smoking cessation are not efficient. The pulmonary delivery of drugs by methods such as dry powder inhaler (DPI) has been recognized as one of the most efficient routes of drug delivery to the targeted area. The lung delivery of nicotine in this way would be expected to mimic the effects of tobacco smoking and could significantly reduce the negative health effects of smoking that result from nicotine addiction.

The aim of this study is to develop nanoparticles with controlled physicochemical properties using biodegradable polymer of chitosan (CS) loaded with nicotine salt for pulmonary delivery as DPI formulations. The outcomes of this project are expected to be a safe and effective CS-based nicotine formulation for pulmonary delivery to treat nicotine dependence. This thesis specially addresses the research questions: (1) how to develop a feasible process to manufacture the nanoparticles suitable for pulmonary drug delivery using biodegradable polymer of CS containing nicotine salt; (2) how to develop an animal model for pulmonary drug delivery from DPI formulation using a nose-only inhalation device.

The current therapeutic options for treatment of smoking addiction have been reviewed, and current advancements of technology in pulmonary drug delivery are summarised. Buccal administration of drugs exhibits a low oral bioavailability, and sublingual tablets and chewing gums can be swallowed before being absorbed. Although nasal spray of nicotine is a fast way to deliver nicotine into the bloodstream,

the rate of absorption is still not as rapid as cigarette smoking. Therefore, it is proposed that delivery of nicotine with sustained drug release profile direct into the deep lung is likely to more effectively mimic the rapid effects of cigarette smoking on a physiological level, which could eliminate patient craving and allow the tapering of nicotine level over time to improve patients' compliance.

Water in oil (w/o) emulsion crosslinking method has been used to fabricate nicotine hydrogen tartrate (NHT)-loaded CS nanoparticles which separate as solid microaggregates. The physicochemical properties of particles are characterized by a series of techniques. Scanning electron microscopy (SEM) and transmission electron microscopy (TEM) shows that the prepared particles are spherical in morphology with rough surface after loading CS particles with NHT. Dynamic Light Scattering (DLS) by Zetasizer determined nanoparticle size ranging from 167.6 nm to 411 nm, while DLS by Mastersizer demonstrated that the microaggregates of these nanoparticles are in the respirable range (<5μm). The surface positive charge as measured by zeta potential tends to decrease with increase of mass ratios of NHT to CS, which is in contrast to the increase of particle size. According to differential scanning calorimetry (DSC), x-ray diffraction (XRD) analysis and attenuated total reflectance-Fourier transform infrared (ATR-FTIR) spectroscopy, the NHT crystallinity is lost when encapsulated in the nanoparticles, indicating it is uniformLy dispersed as a solid solution. On the basis of X-ray photoelectron spectroscopy (XPS) analysis, the amount of NHT loaded on the surface of CS increases proportionally with increasing drug loading in the bulk so there is no surface enhancement.

*In vitro* evaluations of drug release, aerosolization, and stability of formulations have been performed. *In vitro* drug release study through dialysis membrane technique

shows that NHT releases from CS nanoparticles with a prolonged drug release profile up to 4 days. Initial burst release occurred in the first 8 hours due to rapid dissolution of NHT at or close to surface of the nanoparticles, followed by a slow release because of penetration of the release medium into the microaggregates. A mathematical model is designed to correct the discrepancy during drug release measurement due to two barriers to diffusion through the dialysis membrane. It is noted that all the particles show a smooth and rounded morphology after a 6-day release under SEM observations. *In vitro* aerosolization study is determined by twin-stage impinger apparatus. Fine particle fraction (FPF) of NHT-loaded CS nanoparticles is decreased along with increased mass ratios of NHT to CS, which is primarily dominated by the zeta potential of particles. The fine particle dose (FPD) of NHT-loaded CS nanoparticles increases from 1.7 mg to 3.2 mg, respectively from 1:1 to 3:1 based on the same dose of 20 mg in each capsule. In contrast, after mixing inhalable grade lactose with NHT-loaded CS nanoparticles, FPF is improved significantly, which is independent of zeta potential. *In vitro* long term stability test indicates NHT-loaded CS nanoparticles are stable under the storage condition of 25°C and 60% relative humidity and aerosolization of particles does not change significantly in a one-year storage.

*In vivo* locomotor activity test has been used to investigate spontaneous activity in rodents, and evaluate nicotine-mediated behavioural and physiological functions in mice. The locomotor activity test via single subcutaneous injection (s.c.) results in an obvious dose-related effect in mice, with stimulant effects at the intermediate dose (0.5 mg/kg for nicotine; 1.0 mg/kg for NHT-loaded CS nanoparticles) and depressant effects at the higher dose, indicating that NHT keeps bioactive effects after loading into and release from the CS particles. Locomotor activity test administrated by

inhalation exposure using a nose-only inhalation device under the optimum parameters of flow rate (0.9 L/min) and exposure duration (5 minutes) shows a dose-related travelled distance in one hour, suggesting NHT-loaded CS nanoparticles are able to mediate mice locomotion behaviour. Furthermore, no allergic airway inflammation is observed by histological analysis of lung sections post 24 hours inhalation powder exposure to mice.

In summary, this study has established a desirable w/o emulsion crosslinking method to fabricate NHT-loaded CS nanoparticles/microaggregates. Both *in vitro* and *in vivo* evaluations of NHT-loaded CS nanoparticles indicate that prepared particles in this study are suitable to be exploited as DPI formulations for pulmonary delivery. It is proposed that the advancements of knowledge on pulmonary drug delivery from the mouse model will translate to humans and outcomes of this study is promising to provide a more targeted therapy approach for the better management of nicotine dependence in the future.

# Table of Contents

# List of Figures

# List of Tables

# List of Abbreviations

| | |
|---|---|
| $t_{1/2}$ | Half life |
| ATR-FTIR | Attenuated total reflectance Fourier transform infrared |
| CI | Carr's index |
| COPD | Chronic obstructive pulmonary disease |
| CS | Chitosan |
| DLS | Dynamic light scattering |
| DSC | Differential scanning calorimetry |
| ED | Emitted dose |
| EEG | Excipient enhanced growth |
| ENDS | Electronic nicotine delivery systems |
| FDA | U.S. Food and Drug Administration |
| FPD | Fine particle dose |
| FPF | Fine particle fraction |
| FT-IR | Fourier transform infrared spectroscopy |

| | |
|---|---|
| H&E | Hematoxylin and eosin |
| HR | Hausner ratio |
| LC | Liquid chromatography |
| LMW | Low molecular weight |
| MRI | Magnetic resonance image |
| nAChRs | Nicotinic acetylcholine receptors |
| NHT | Nicotine hydrogen tartrate |
| NHT-CS NPs | Nicotine-loaded chitosan nanoparticles |
| NPs | Nanoparticles |
| NRT | Nicotine replacement therapy |
| PBS | Phosphate buffered saline |
| PET | Positron emission tomography |
| PFA | Paraformaldehyde |
| RD | Recovered dose |
| RH | Relative humidity |
| s.c. injection | Subcutaneous injection |

| | |
|---|---|
| SEM | Scanning electric microscope |
| SHS | Second-hand smoke |
| SPECT | Single photon emission computed tomography |
| SS | Sample and separate |
| TEM | Transmission electron microscopy |
| TGA | Therapeutic Goods Administration |
| TSI | Twin stages impinger |
| UV | Ultraviolet–visible spectroscopy |
| XPS | X-ray photoelectron spectroscopy |
| XRD | X-ray diffraction |

# Statement of Original Authorship

The work contained in this thesis has not been previously submitted to meet requirements for an award at this or any other higher education institution. To the best of my knowledge and belief, the thesis contains no material previously published or written by another person except where due reference is made.

QUT Verified Signature

Signature:

Date: 8 June 2017

# Acknowledgements

Three and half years have gone since I started studying my PhD. I owe a great deal of appreciation to numerous individuals who contributed in various ways to assist me in completing this thesis.

First and foremost, I would like to express my sincere appreciation to my dedicated supervisory team: Dr. Nazrul Islam; Prof. Graeme George; Prof. Selena Bartlett; Prof. Changyou Gao.

It was my Principal Supervisor, Dr. Nazrul Islam, who offered me a precious chance to pursue a PhD under his supervision at QUT. I am heartily grateful to him for his strong support throughout this PhD journey. He provided me with chances to apply for excellent postgraduate awards and a supportive reference letter for my job hunting at the final stage of my PhD.

I would like to present my deepest gratitude and admiration to Prof. Graeme George. I am influenced positively by him to stay curious about the unknown and mysteries of science, but also keep optimistic to overcome hardships and look forward to the future. He spent a lot of time and energy supervising me. Although he is my associate supervisor, he read my manuscript a number of times before it was published and gave me a large quantity of helpful and critical comments whether welcome or unwelcome. I regard Prof. George as my respectful supervisor as well as my surrogate grandfather. When I was struggling with my research or life, he was always the first person I would choose to share my problems. He put aside his busy schedule to meet with me. I am

grateful for his patient encouragement and belief in my capability to complete this PhD project throughout these three years.

I would like to appreciate Prof. Selena Bartlett as my associate supervisor for her consistent financial support for undertaking a large amount of animal work.

I am heartily indebted to my external supervisor, Prof. Changyou Gao, from University of Zhejiang for his time and advice. He was exceptionally generous to provide me with guidance and suggestions to his best knowledge and resources.

I am deeply thankful to Ms. Joan Holgate for her friendship and contributions in surgical assistance, providing me with valuable advice in animal experimental design and data analysis.

I am sincerely grateful to all technicians who were involved in this PhD project for their superb technical support during laboratory work.

I would like to acknowledge China Scholarship Council and Queensland University of Technology (QUT) for generous scholarship support financially for completion of this PhD study. In the meanwhile, I would like to acknowledge Institute of Health and Biomedical Innovation (IHBI), Translational Research Institute (TRI), and Faculty of Science and Engineering at QUT for providing me access to specialized equipment and laboratory space for my research.

My special thanks to my peer colleagues, Ms. Afrina Afrose, Mr. Omkar Laxman Patkar, Ms. Elia Barajasalonso for their companionship to share joy and sorrow from research that I am not alone in this often gloomy journey to pursue the PhD degree. Many thanks to my dear friends, Dr. Sern Yih Cheah, Dr. Jinzhang Liu, Dr. Longyan

Wang, Ms. Shuang Wang, Mrs. Pat Davis, Ms. Rosemary Lang, Ms. Catherine L Cath, Ms. Danielle Sentinella, Mr Peter Polak for their steady friendship and substantial tolerance with the warmest memories in these three years.

Intellectual pursuit and academic achievements are nothing to me without love of family. I owe a great deal of gratitude to my parents for their selfless love and support for which I am never able to pay them back. They are my cornerstone psychologically to encourage me to stay firm and keep going.

Finally, much appreciation to all those who helped me directly or indirectly in my research work to make this thesis possible. This journey has at times been hard but it has had many rewards as well as challenges and no doubt has made me a stronger woman.

# Publications and Communications

## Journal publications

- **Wang, H**; George, G; Bartlett, S; Islam, N; Gao, C; Nazrul Islam. Nicotine Hydrogen Tartrate Loaded Chitosan Nanoparticles: Formulation, Characterization and in vitro Delivery from Dry Powder Inhaler Formulation; *European Journal of Pharmaceutics and Biopharmaceutics*. **2017**, 113, 118-131.
- Muhsin MD, George G, Beagley K, Ferro V, **Wang H**, Islam N. Effects of chemical conjugation of L-leucine to chitosan on dispersibility and controlled release of drug from a nanoparticulate dry powder inhaler formulation. *Molecular Pharmaceutics*. **2016**; 13(5):1455-66.
- **Wang, H**; George, G; Bartlett, S; Islam, N: Nicotine loaded chitosan nanoparticles for lung delivery from dry powder inhaler (DPI) formulations---impact of nanoparticle surface charge on dispersion (submitted). *Journal of Pharmaceutical Sciences.*

## Manuscripts ready to submit

- **Wang, H**; George, G; Bartlett, S; Islam, N: Nicotine release behaviour from chitosan nanoparticles: Mathematical model for dialysis membrane technique.
- **Wang, H**; Holgate, J; George, G; Bartlett, S; Islam, N: Viability of nicotine-loaded chitosan nanoparticles to modulate locomotor activity via a nose-only inhalation device in non-tolerant mice.

## Conference Papers

- **Hui Wang; Joan Holgate; Graeme George; Selena Bartlett; Nazrul Islam (2016)**: Nicotine-Loaded Chitosan Nanoparticles as Dry Powder Inhaler Formulation for Management of Nicotine Dependence. 2016 American Association of Pharmaceutical Scientists Annual Meeting and Exposition held Nov 13-17, 2016 at Denver, US.
- **Hui Wang; Joan Holgate; Graeme George; Selena Bartlett; Nazrul Islam (2016):** Nicotine-Loaded Chitosan Nanoparticles： a New Pulmonary Drug Delivery for Management of Nicotine Dependence. International Forum of Biomedical Materials held in Aug 1-3, 2016 at Hangzhou, China.
- **Hui Wang; Graeme George; Selena Bartlett; Nazrul Islam (2015)**: Development of Nicotine Hydrogen Tartrate Loaded Chitosan Nanoparticles as Dry Powder Inhaler (DPI) Formulation for Pulmonary Delivery. 2015 American Association of Pharmaceutical Scientists Annual Meeting and Exposition held in Oct 24-29, 2015 at Orlando, US.
- **Hui Wang; Graeme George; Selena Bartlett; Nazrul Islam (2015)**: Controlled Release of Nicotine Loaded Chitosan Nanoparticles as Dry Powder Inhaler (DPI) Formulation. Drug Delivery Australia 2015 Conference held in Nov 19-20, 2015 at Brisbane, Australia.
- **Hui Wang; Graeme George; Selena Bartlett; Nazrul Islam (2014)**: Development of pulmonary delivery of nicotine hydrogen tartrate loaded chitosan as dry powder inhaler (DPI) formulation. IHBI Inspires Postgraduate Conference 2014 held in November 23-24, 2014 at Gold Coast, Australia
- **Hui Wang; Graeme George; Selena Bartlett, Nazrul Islam (2014)**: Development of nicotine-loaded chitosan nanoparticles for pulmonary delivery

from dry powder inhaler formulation. Australian Pharmaceutical Science Association (APSA) Annual Conference 2014 held in December 5-7, 2014 at Brisbane, Australia.

# Chapter 1:

# Introduction

## 1.1 BACKGROUND

Smoking-related disorders have become the major cause of death and mortality in both developed and developing countries, posing a serious threat to human wellbeing and a tremendous economic burden to governments. This will result in an enormous economic burden including direct financial loss (medications, treatments, welfare services and disability benefits) and indirect financial loss (lost productivity and income due to reduced capability or incapacity), and the estimated economic burden induced by nicotine addiction in Australia will exceed $36 billion (Alcohol Education and Research Foundation, 2010). Cigarette smoking is not going to disappear in the near future. Currently, there are very few effective treatment options for people who are suffering from nicotine-related disorders. Recent studies show that pharmacotherapeutic compounds currently used for smoking cessation (e.g., e-cigarette, vareniciline, bupropion) can reduce tobacco consumption and seeking behaviour significantly, however, they have some therapeutic limitations: side effects such as nausea, depression, even suicidal thoughts and serious neuropsychiatric symptoms Kuehn (2009); substantial dosing is required to overcome the gut and enter the brain. Therefore, continued research for strategies of smoking cessation remains a critical priority.

Pulmonary drug delivery is a modern and popular therapy approach which combines inhalation and respiratory treatments in attempt to help restore or improve breathing function in patients with a variety of diseases, conditions, and injuries. It delivers drugs directly into the deep lungs and combines with novel particle formulations to achieve fast and effective therapeutic effects locally and systemically as the lung provides a high absorption area with vast vascularization. This therapeutic strategy has been utilized to treat a variety of disorders and diseases such as asthma and chronic

obstructive pulmonary disease (COPD). In most cases, the efficacy of drugs is limited by their potential capability of reaching to the targeted therapeutic site. Compared to traditional systemic delivery methods, lung delivery therapy has many advantages, including reduced side effects; quicker onset of action; accurate and consistent dosing using an inhalation device.

The products for dry powder inhalers (DPIs) are desirable powder formulations to be applied in the pulmonary delivery therapy when in combination with an efficient metering system and device. DPIs are inhalation devices that patients are able to operate easily and inhale actively. It can deliver the active drug in the dry powder form to the lungs to achieve local or systemic therapeutic effects through the pulmonary route (Islam & Gladki 2008). DPI formulations consist of three types of compositions: pre-formulated small particles, a carrier-based interactive mixture such as drug particles mixed with lactose, and loose agglomerates of drug and excipient particles. When patients inhale actively using a DPI device, the drug particles are separated from the carrier or deagglomerated, and the active pharmaceutical ingredient is delivered into the patient's deep lungs. A variety of factors, e.g. carrier size, surface roughness, shape and presence of fine excipients in the formulations can influence the efficient dispersion of drug from DPI formulations. The deposition site and the deposition patterns of the inhaled aerosol from DPIs depend on three major performance relevant components (a) the anatomical and physiological characteristics of the patient (b) the interactive powder mixture, including physical properties of the aerosol cloud and (c) the design of delivery devices (Stegemann et al 2013, Timsina et al 1994).

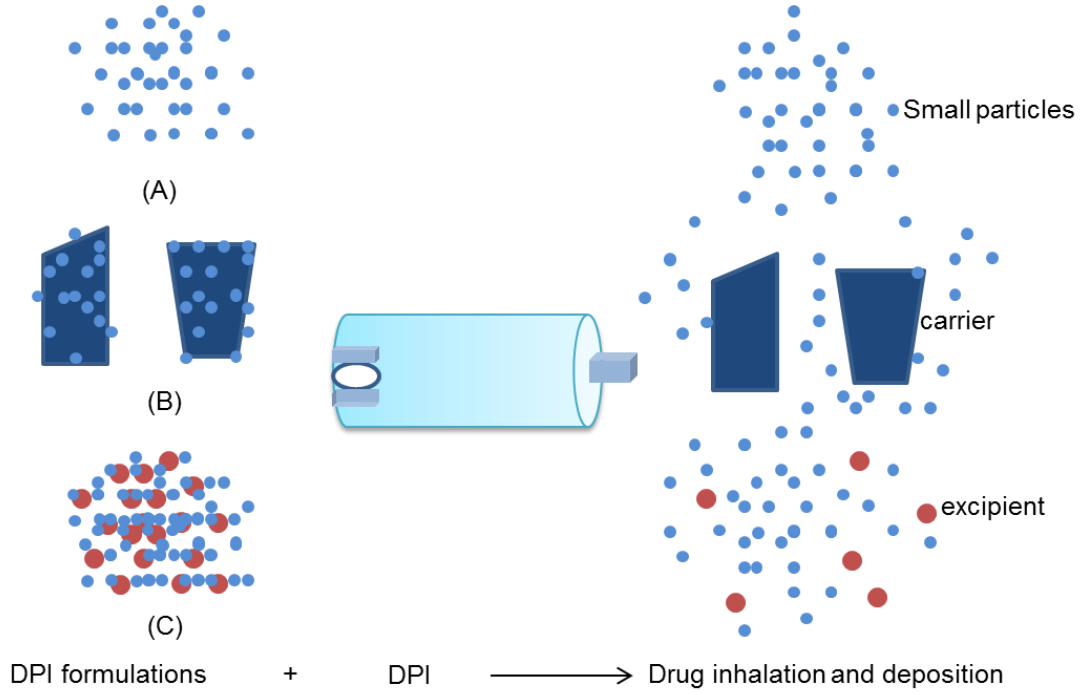


Scheme 1.1 Schematic diagram of DPI formulations and dispersion process: (A) pre-formulated small particles; (B) Carrier-based formulation; (C) loose drug agglomerates or agglomerates of drug and excipient particles;

Particulate drug delivery system via a pulmonary route, including microparticles and nanoparticles, plays a crucial role in the pharmaceutics and clinical medicine. Micro/nanoparticles is generally formed by polymers in the solid and colloidal spheres, and the distinction between microparticles and nanoparticles is related to their specific size cut-offs: diameters of nanoparticles range from 1-500nm; the dimensions of microparticles are in the micron range. Generally, they are composed of biodegradable macromolecular material formed by single or double emulsion methods and can be used as drug carriers (Kohane, 2007). Polymeric micro- and nanoparticles for pulmonary drug administration improve the therapeutic effect of drug by modifying the drug bioavailability. Drug encapsulation in micro- and nanoparticles leads to reducing drug toxicity and prolonging the biological half-life of drug (Mossaad 2014). As a result, the effect of the biopolymer is also an important factor for DPI performance. The currently most prevalent polymers in use for manufacturing

micro/nanoparticles are poly (lactide-co-glycolide) (PLGA), alginate and chitosan. In this study, we select a promising biodegradable polymer of chitosan (CS), which is nontoxic, biocompatible, and biodegradable polysaccharide, to develop a desirable particulate drug delivery system.

Chitosan (CS) is a natural biodegradable polymer derived from crustacean shells (crabs, shrimps and lobsters) and it is also found in some microorganisms, fungi and yeast. CS micro/nanoparticles have been used extensively as drug delivery vehicles due to their excellent bioavailability, better encapsulation, and controlled release with less toxic properties. The properties of CS considerably depend on the molecular weight, degree of deacetylation and viscosity (Li et al 2008), which affect the particle size, particles formation and aggregation. Many studies have showed that several factors are important to affect the characteristics of CS nanoparticles, such as the ratio between crosslinker and polymer (Ajun et al 2009), the molecular weight of the CS (Csaba et al 2009), the CS concentration (Shah et al 2009) and pH (Zhang et al 2004). However, preparations of CS nanoparticles involve organic solvent or high shear force, which pose a harm to drug stability. Besides, the preparation method of emulsion crosslinking is complex and time consuming (Tiyaboonchai 2013). But its minor shortfalls can be ignored when considering its favourable biocompatibility characteristics. In terms of this work, we have achieved the aim of encapsulating appreciable quantities of nicotine within this interesting candidate of CS nanoparticles.

It is important to evaluate the safety and efficacy of formulated inhalation products in animal models prior to use in humans. DPI inhalation devices require active inhalation to operate the devices and deliver the drug to the lungs; however, animals cannot meet this requirement. Hence, the animal models of pulmonary delivery which delivers the

drug via their normal breathing action are necessary. Although a number of apparatus have been designed to evaluate a series of pharmacokinetics parameters, they are only modestly suitable for dry powder inhalation delivery due to limitations in dosing consistency between batches and subjects, excessive wastage of undelivered drug and inability to effectively aerosolize powders of very fine particles (Aoki, Kojo, Yamada, & Onoue, 2012). These apparatus need to be modified to deliver powders of small fine particles that would enable efficient delivery and provide consistency in dose delivery between subjects and between batches.

As discussed above, it is anticipated that the treatment of smoking addiction will be improved with less side effects using the proposed pulmonary drug delivery method. Unlike gums, transdermal patches, sublingual tablets and nasal spray formulations, pulmonary delivery of nicotine can mimic the route of smoking and produce high levels of nicotine to the brain quickly, which offers a more targeted approach that will reduce the amount of drug required and thus reduce side effects and improve patient compliance. As a result, it is hypothesized that the lung delivery of nicotine would mimic the effects of tobacco smoking and would significantly reduce nicotine addiction. The currently available nicotine inhaler formulations (e.g. Nicotrol® and Nicorette® Inhalers) have proven to be undesirable for delivering medicaments into the deep lungs as they deliver nicotine into the mouth for buccal absorption. Currently there is no effective DPI formulation available to deliver nicotine into the deep lung.

The aim of this project is to develop nanoparticles using the biodegradable polymer of CS as the carrier for nicotine for pulmonary delivery for the treatment of nicotine dependence with low dose and controlled release properties. It is anticipated that the

outcome of this study will provide novel therapeutic strategies for better management of patients with nicotine dependence.

## 1.2 AIMS AND RESEARCH PLAN

The goal of this project is to develop a DPI formulation of nicotine for lung delivery as a practicable pharmacotherapeutic strategy that reduce and prevent the development of smoking addiction. This research aims to develop a novel pulmonary nicotine delivery system that mimics the sensory feelings associated with smoking, and at the same time provides a targeted approach that will find the minimal drug dose required for treatment and subsequently eliminate the side effects that have prevented it from being used more effectively as a nicotine cessation therapy. It is anticipated that the treatment of smoking addiction will be improved with least side effects using the proposed inhaled nicotine delivery that could mimic the practices of cigarette smoking. In addition, the potential risks of chronic nicotine inhalation are far lower than the risks of continued smoking. Therefore, the DPI formulation of nicotine developed in this study may be an effective smoking cessation appliance.

**Aim 1:** To develop micro/nanoparticles using a biodegradable polymer with controlled surface properties (size, shape, surface free energy, surface roughness, adhesional properties) that contain nicotine.

*Objectives:*

- To prepare biodegradable polymer (chitosan) nanoparticles that contains nicotine.

- To evaluate the influence of the polymer on the aerosolization performance of nicotine using a controlled water-in-oil emulsion-glutaraldehyde crosslinking method.

- To understand the physicochemical properties of nicotine-loaded CS nanoparticles.

- To identify the specific factors affecting the efficient delivery of prepared nicotine nanoparticles

- To study the dispersibility of blank CS and nicotine-loaded CS nanoparticles

- To study the technology of the controlled release of nicotine from CS nanoparticles.

- To determine whether the process of encapsulating the nicotine nanoparticles has altered the activity of the compound.

**Aim 2:** To construct and optimize a nose-only inhalation device for use in mouse models; to determine the lowest effective dose required to obtain clinically relevant blood levels of nicotine in mice; demonstrate its safety for administering the CS encapsulated nicotine nanoparticles; to test DPI formulations in mice and measure nicotine-mediated locomotor behaviours.

*Objectives:*

- To construct and optimize the nose-only inhalation device with the optimum parameters of flow rate, loading dose to achieve lowest effective dose required.

- To develop the animal models of pulmonary drug delivery from DPI formulations using a nose-only inhalation device.

- To determine whether lung delivery of nicotine alters nicotinic receptor-mediated locomotor behaviour in mice.

- To evaluate the safety and efficacy in mice by administering the CS particles containing nicotine under conditions of inhalation exposure.

- To determine the pharmacokinetics of nicotine-loaded CS from pulmonary delivery of a DPI formulation in mice.

## 1.3 SIGNIFICANCE AND INNOVATION

According to a tobacco report from the World Health Organization (WHO, 2015), smoking-related illness is still the single biggest cause of death worldwide, resulting in the death of more than 7million people a year. Despite the fact that addiction to nicotine, representing more than 40% of brain-related illnesses, generates a serious threat to human wellbeing and further increases susceptibility to other diseases, and poses a huge economic burden to government, there is still a dearth of innovative treatments, and little interest in developing new treatments in the pharmaceutical and biotechnology industry.

Although the currently available drugs, varenicline and bupropion, are used for the treatment of nicotine dependence, both of them cause significant side effects that limits their efficacy. Currently available nicotine formulations include two nicotine inhalation products, Nicotrol® and Nicorette® Inhalers (Pfizer), which are available as nicotine vapour inhalers but less effective in managing nicotine addiction. The nicotine

vapour inhalers deliver nicotine into the buccal areas instead of the deep lungs (Oestergaard et al 2010, Rose et al 2010). In 1997, a DPI formulation of nicotine tartrate was patented using lactose powder for lung delivery; however, this has yet to be developed (Rose et al 1997). In comparison to cigarettes where heat, carcinogens and carbon monoxide produce various adverse effects, a nicotine formulation delivered via the same route would be superior and would offer a safer nicotine delivery system (Andrus PG 1999). We expected that the DPI formulation of nicotine might be an effective technology to reduce the craving for cigarettes and other tobacco products via deep lung delivery of nicotine with very low dose, contributing to an effective treatment for nicotine addiction with a significant reduction in side effects.

This project specifically addresses the significant health priority goals of QUT (Queensland University and Technology), Australia and worldwide generally which comprises ageing welfare and improves Australia's social and economic fabric by improving lifestyle factors that prevent the development of addiction. The outcomes of this research will significantly contribute to current understandings of pulmonary drug delivery that will offer a more targeted therapy approach for the significant number of Australians affected by smoking-related disorders. At the end of this work, it is desirable that we will have synthesized novel intelligent polymer of CS coated nicotine and developed a pulmonary animal model for this drug delivery system. We hope this project will contribute to more effective medications for substance use disorders, reduce direct and indirect costs to society and make improvements to public health and safety and health care delivery.

The innovations of this project are to develop a novel pulmonary drug delivery system and pulmonary animal model and are listed as follows:

- The development of a micro/nanoparticles formulation of biodegradable polymer (CS) containing nicotine.

- An innovative animal model for testing pulmonary delivery of the biodegradable polymers containing nicotine.

- A novel delivery system using a nose-only inhalation device for an animal model that may result in the development of cost effective DPI formulation of nicotine for pulmonary delivery. This delivery system may be applicable to testing a number of drugs in the future.

## 1.4 THESIS OUTLINE

This thesis is presented in a traditional monograph model. Each chapter individually tells a story from development of a particulate drug delivery system through pulmonary route to safety and efficacy tests of formulations on animal models, as such, heading to a primary goal of this research: to develop a practicable pharmacotherapeutic strategy that reduces and prevents the development of nicotine addiction.

**Chapter 2** states the mechanisms of nicotine addiction with a variety of associated side effects, summarises the recent advances in the therapeutic options for smoking addiction and pulmonary delivery technology, and highlights the potential application of nicotine inhalers for smoking cessation based on recent literature. These provide us a general background about this research and highlight the knowledge gaps between literature and practical therapeutic strategies to improve our understanding of significance of treatment of nicotine dependence via pulmonary route.

**Chapter 3** develops an effective way to manufacture micro/nanoparticles of biodegradable polymer, CS, loaded with nicotine hydrogen tartrate (NHT) for pulmonary delivery of nicotine from DPI formulations. The physicochemical properties of particles are determined by a series of experiments such as microscopic study of morphology, particle sizing, surface charge, specific surface area, thermal characteristics and so on. The outcomes of this chapter demonstrate the NHT-loaded CS particles are suitable to be applied for DPI formulation for lung delivery. However, aggregation between nanoparticles (nano-aggregate) is still a common challenge within the nano scale range due to high surface energy.

**Chapter 4** is designed to examine physical characteristics of NHT-loaded CS particles as DPI formulations from a series of *in vitro* studies, including *in vitro* drug release, aerosolization and stability. *In vitro* drug release study showed nicotine released from CS particles surface or diffusion from particles matrix in a sustained and prolonged profile up to 6 days. It is expected to provide the required plasma nicotine concentration for therapeutic effects of nicotine dependence. There is a significant increase in the dispersibility of particles formulations with large lactose carriers compared to formulations without carriers. On the other hand, further comprehensive studies may be needed to better understand the interactions between the charged particles and carriers and the impact of charged particles or agglomerates on the deagglomeration.

**Chapter 5** combines *in vitro* evaluation of efficiency of nose-only inhalation device and *in vivo* examinations of efficacy and safety of nicotine-loaded CS particles as DPI formulations through experiments of locomotor activity test and histological studies on mice. No allergic airway inflammation was observed from histological analysis of

lung sections within 24 hours. It suggests that formulation of nicotine-loaded CS particles may be applicable for exposure studies under this study design.

**Chapter 6** summarises the overall conclusions in this thesis. It concludes the main findings of this study, discusses the significance and limitations of this research and suggests future work.

*Framework of thesis:*

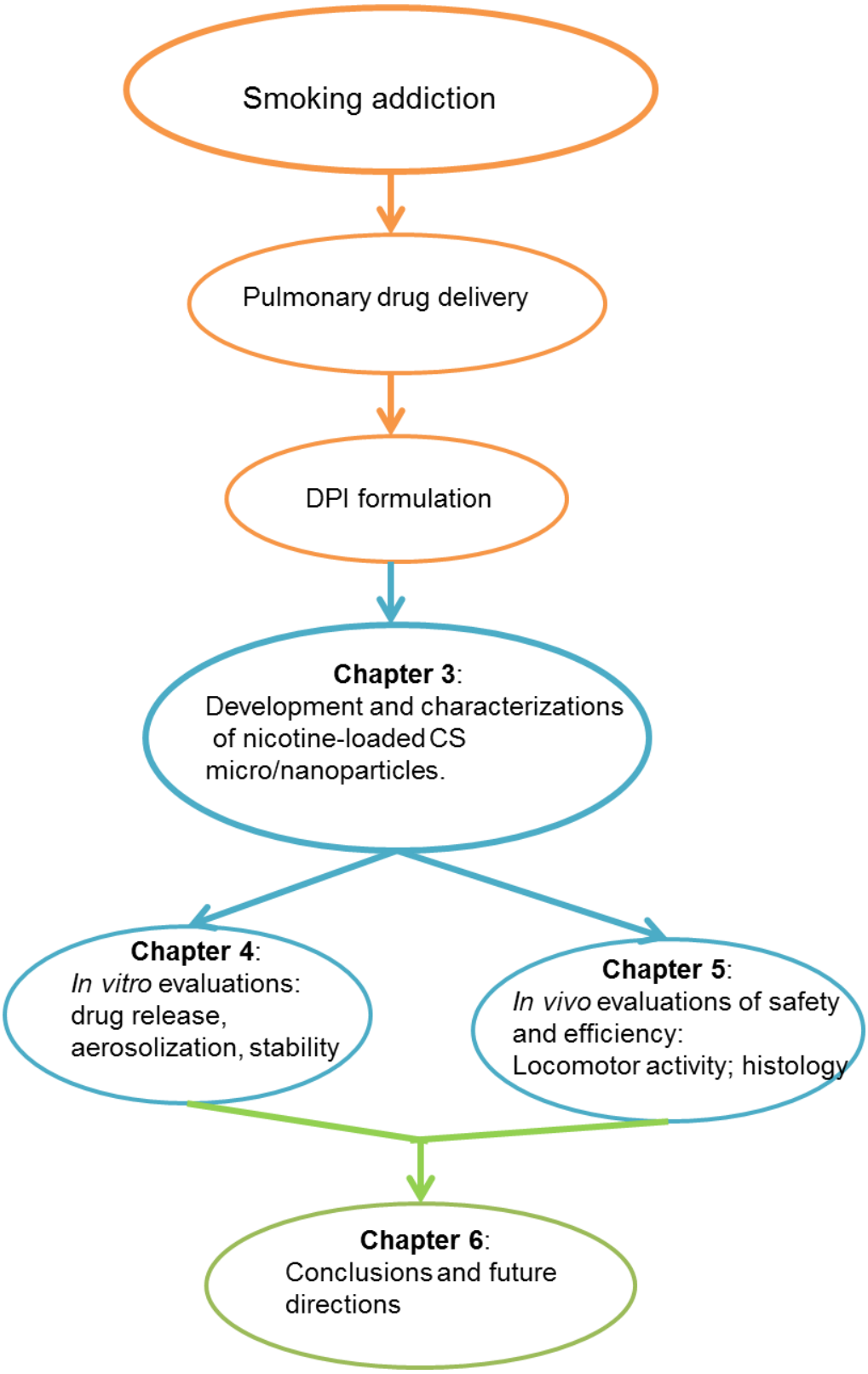

# Chapter 2:

# Literature Review

## 2.1 HISTORICAL BACKGROUND

Tobacco consumption has become one of the leading causes in preventable deaths all over the world, accounting for approximately 20% of all deaths (Jamal et al., 2014) and 90% of lung cancer cases (Stewart & Kleihues, 2003). Cigarette smoking involves inhaling the smoke regularly and habitually owing to the greatly addictive properties of nicotine (N. L. Benowitz, 1988; Aldo Leone, Landini, & Leone, 2010). Nicotine, a potent parasympathomimetic alkaloid and a stimulant drug, is a natural ingredient growing in the roots and accumulating in the leaves of tobacco (N. L. Benowitz, Hukkanen, & Jacob III, 2009). Physician Wilhelm Heinrich Posselt and chemist Karl Ludwig Reimann of Germany isolated nicotine from the tobacco plant in 1828 (Henningfield & Zeller, 2006). Nicotine is a hygroscopic oily liquid, and it is miscible with water in its base form, whereas its salt form is usually solid and water soluble to produce its nitrogenous base (Fu et al., 2010). Nicotine has two enantiomeric forms. Levorotary (S)-isomer is the principal form of nicotine in tobacco; whereas only 0.1–0.6% of total nicotine is in (R)-nicotine (Carmella, McIntee, Chen, & Hecht, 2000). The physiological activity of S-(+)-nicotine is less active than R- (–)-nicotine, while the toxicity of R-(−)-nicotine is more than S-(+)-nicotine. The salts of S-(+)-nicotine are usually dextrorotatory (Obaid, Koyano, Lindstrom, Sakai, & Salzberg, 1999). Nicotine is a weak base at $pK_a$ of 8.0. It is easy to pass through the blood-brain barrier and distribute all over the brain, which its uptake is achieved by active transport and passive diffusion (N. L. Benowitz, 1988). Tritiated S-nicotine tends to be bound in the areas of cerebral cortex, thalamus, hippocampus, hypothalamus, midbrain and brainstem (London, Waller, & Wamsley, 1985). It is reported that the areas of high-affinity nicotine binding showed improved metabolic activity. Short term exposure to nicotine could stimulate central nervous system neurohumoral pathways through

activation of nicotinic receptors, causing release of acetylcholine, dopamine, norepinephrine, serotonin (N. L. Benowitz, 1988). Exposure to nicotine develops a biphasic dose-response relation: low doses of nicotine cause ganglionic stimulation, while high dose of nicotine causes ganglionic depression (Morrison, Goodyear, & Sellers, 1969). The biphasic effects are noted that at low dose of nicotine, cardiovascular effects are mediated by increasing blood pressure and heart rate via the central nervous system; on the other hand, at high dose of nicotine, ganglionic stimulation is mediated from peripheral nervous system. However, extremely high level of nicotine results in hypotension and reduced heart rate intermediated by peripheral ganglionic blockade or central nervous system (N. L. Benowitz, 1988). In addition, the tolerance of nicotine is developed after repeated doses, which may cause adverse effects of nausea, vomiting and pallor and so on (Moura & McMahon, 2016).

Nicotine is only partially responsible for the detrimental effects of smoking as several constituents from cigarette smoke result in the development and progression of cardiovascular damage, particularly atherosclerotic lesions (Aurelio Leone, 2005). Although U.S. Food and Drug Administration (FDA) has approved some therapies which are designed rationally and tested effectively via a combination of numerous animal models for nicotine addiction (Pierce, O'Brien, Kenny, & Vanderschuren, 2012), very few effective drug therapies for nicotine addiction can be effectively applied; even the currently most effective drugs, varenicline and cytisine, can cause significant adverse effects such as nausea and require substantial dosing in order to bypass the gut and enter the brain. Therefore, from these observations, it is clear that a better method of pharmacotherapeutic delivery could help improve efficacy of currently available treatments and lead to the development of novel therapeutics.

## 2.2 ADVERSE EFFECTS OF SMOKING

There are around 5 million smoking-related deaths annually all over the world and there is the expectation of up to 10 million by 2030 (Islam & Rahman, 2012). The positive effects of cigarette smoking include euphoria, ability to concentrate, weight control, and a decrease in daily tension. Nevertheless, the negative effects of smoking associated with high risks of stroke, cardiovascular diseases, respiratory disease and cancer exceed its limited positive effects. It not only shortens the life span among smokers, but also increases overall costs, including direct and indirect costs, and results in the loss of productivity during the life expectancy (Max, 2001). Both the deteriorating health of smokers and aggravating economic impact on society cannot be ignored. A large number of reports have revealed strong associations between tobacco smoke and various neurological, cardiovascular, and pulmonary diseases (Das, 2003). What is worse: cigarette smoke also causes serious health problems of the non-smokers.

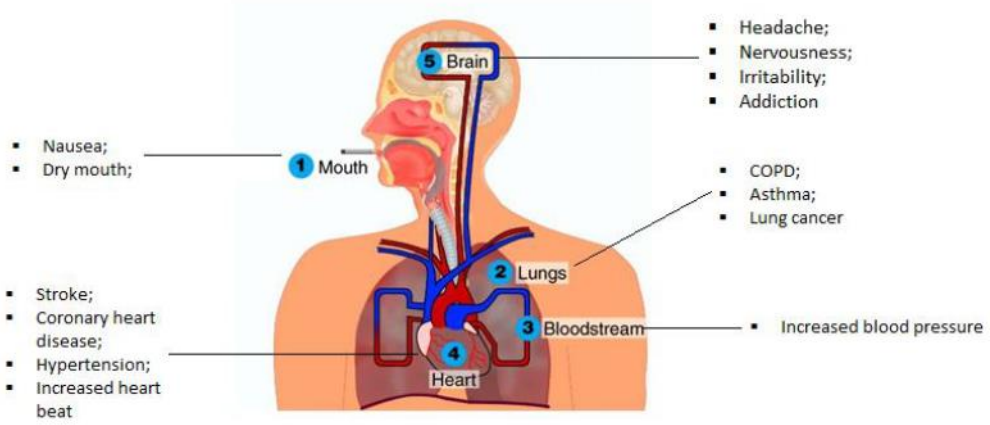


Figure 2.1 Smoking and increased health risk

### 2.2.1 Smoking and Cardiovascular Diseases

The cardiovascular system is the primary target area to be affected by smoking (Aurelio Leone, 1995), The main cardiovascular diseases associated with cigarette

smoking comprise myocardial infarction (Hay & Turbott, 1970), coronary heart disease (Baba et al., 2006), stroke (Burns, 2003), hypertension (Kannel & Higgins, 1990), and abnormal cardiopulmonary function and exercise tolerance (Louie, 2001), all of which emerge a synergistic effect associated with smoking. Various types of cardiovascular damage from smoking have been identified. The first study by Hammond (Hammond & Horn, 1958) demonstrated smoking tended to increase risks of cardiovascular disease. It stated that smokers would suffer a 70% higher rate of death from coronary artery disease than non-smokers (Z. Chen & Boreham, 2002). The smokers age also affects the development of cerebrovascular disease and coronary heart disease (Burns, 2003). The greatest risk for developing coronary heart disease occurs in those under the age of 45. Risks rates increase steeply and considerable death is confined to the seventh and eighth decades of life. Active smoking leads to clinical and anatomical alterations associated with ischaemic pathology, while passive smoking (second-hand smoking) is more likely to trigger functional disorders chronically which are associated with late atherosclerotic changes (Penn, Chen, & Snyder, 1994).

A variety of chemical compounds which are extracted and concentrated from tobacco mixtures are the source of side effects of tobacco smoke associated with the heart and vessels (Byrd, 1992). The tobacco plants and their leaves contain more than 4,000 chemical substances, which results in increasing risks of cardiovascular diseases. But it is known that nicotine addiction contributes to selling more cigarette products. Nicotine is a highly addictive compound found in all tobacco products and plays a major role in contributing to heart and blood vessel lesions and flunk of vascular reconstruction especially after chronic exposure (Benowitz, 2010). Besides, carbon monoxide is also another major component associated with the cardiovascular diseases

induced by smoking. Both of them affects the myocardial oxygen supply/ demand ratio and results in endothelial injury, producing atherosclerotic plaque adversely (Lakier, 1992). Furthermore, the biochemical injury or hypoxic injury of tobacco mechanisms also strongly contributes to these pathogenic behaviours.

### 2.2.2 Smoking and Pulmonary Diseases

Cigarette smoking is responsible for the pathogenesis of many types of pulmonary diseases. Specifically, cigarette smokers have a higher prevalence in respiratory diseases and lung function disorders with a greater mortality rate from chronic obstructive pulmonary disease (COPD) in comparison to non-smokers (Pauwels, Buist, Calverley, Jenkins, & Hurd, 2001). Bronchodilation induced by cigarette smoking decreases the hyperinflated state of lung and favors smaller particles penetrate and depose to deeper and smaller airways via deeper inhalation of smoking. As well, bronchodilation facilitates uptake of carbon monoxide in the lungs. As a result, chronic bronchodilation increases the risk of cardiovascular disease and pulmonary diseases (van Dijk et al., 2010). The way of consuming tobacco is also of importance in the developing disease. For example: pipe and cigar smokers have a higher risk to develop COPD with greater morbidity and mortality rates than cigarette smokers (Pauwels et al., 2001). Tobacco smoke can alter the airway structures and functions, triggering COPD by interfering with the ability of airway epithelial cells to support repair processes (Hangjun Wang et al., 2001). There are many other risk factors for the development of COPD, for example, air pollution, occupational exposures, heredity, and infectious and allergic conditions. Thus, not all smokers will develop clinically significant COPD, but mortality rates are higher among cigarette smokers suffering from COPD (Matthay et al., 2003). It has been reported by some researchers that tobacco smoke inhalation results in a decrease in the level of lung

surfactant phosphatidylcholine (Subramaniam, Bummer, & Gairola, 1995). However, other investigators have demonstrated that no difference in lung lavage phospholipid concentration between smokers and non-smokers was observed (Mancini et al., 1993), which suggests that the effects of cigarette smoke on surfactant and surfactant-producing cells are complicated (Haagsman & van Golde, 1985).

### 2.2.3 Smoking and Asthma

Asthma is abnormalities in airway effects involving both airway inflammation and impaired airflow. It is well documented that smoking or exposure to passive smoking among asthmatics increases the risk rate of asthma-related morbidity and disease severity because of the decline of lung function. It is reported that approximately 25% to 35% of individuals suffering from asthma are tobacco smokers, which is much higher compared with non-smokers (Peters et al., 1999). Also women are more vulnerable to the effects of smoking (M. Stapleton, Howard-Thompson, George, Hoover, & Self, 2011). According to a report by Beckett et al. in 4547 subjects aged from 18 to 30 years old stratified by sex, it is found that cigarette smokers in females are more susceptible to asthma incidence with decreased physical activity and gained weight over time (Beckett, Jacobs Jr, Yu, Iribarren, & Williams, 2001). Asthma is less controlled in asthmatic patients with primary smoking compared with asthmatic non-smokers (Schatz, Zeiger, Vollmer, Mosen, & Cook, 2006).

On the other hand, some of the toxic gases in passive smoking contribute to the development of asthma (M. Stapleton et al., 2011). Environmental smoking exposure among asthmatic patients not only improves severe symptoms, but also lowers quality of life, reduces lung functions, increases health care utilization, and increases hospital

admissions. However, small children are the most vulnerable to tobacco smoke, especially maternal smoking or tobacco smoke at home.

### 2.2.4 Smoking and Lung Cancer

Environmental tobacco smoke, also referred to as second-hand smoke (SHS), has been classified as an important human pulmonary carcinogen (WHO, 2004). A series of epidemiological studies have established and shown a strong association between SHS exposure and lung cancer development; Lung cancer is one of the most prevalent diagnosed cancers and the leading cause of mortality induced by cancer in the world (R. L. Siegel, Miller, & Jemal, 2015). Some researchers report that only a small number of victim who are exposed to an environment of extensive tobacco consumption will suffer from lung cancer (Duan et al., 2013), while epidemiological evidence indicates that cigarette smoking is one of the established risk factors for lung cancer (Alberg, Brock, Ford, Samet, & Spivack, 2013). This controversy has made the mechanisms by which cigarette smoke causes lung cancer unclear. It was estimated that about 90% of male and 75%–80% of female deaths from lung cancer in the United States were due to smoking (Hecht, 2002). More than 60 chemical compounds in the cigarette smoke have been identified to induce cancers potentially, and these carcinogenic components and their metabolites such as N-nitrosamines and polycyclic aromatic hydrocarbons can result in lung cell transformation through activating multiple pathways in different ways (Patrianakos & Hoffmann, 1979). Nicotine tend to trigger tumour promotion and progression associated with properties of antiapoptotic and indirect mitogenic effects (Tonini, D'Onofrio, Dell'Aquila, & Pezzuto, 2013). Lung nodules are often diagnosed among smokers and can be altered to malignant tumours depending on the patients` persistence in smoking (Thun et al., 1997).

These constituents of aromatic amines (e.g.,4-aminobiphenyl, 2-naphthylamine), polycyclic aromatic hydrocarbons, tobacco specific nitrosamines [e.g., 4-(methylnitrosamine)-1-(3-pyridyl)-1-butanone] in tobacco are carcinogens that causes lung cancer or increases the incidence of lung cancer from experimental animals and human beings (Cornfield et al., 2009; Smith et al., 2006). A genotoxic mode of action for some of these carcinogens generates directly electrophilic species capable of forming covalently bound DNA lesions, known as DNA adducts, which are central to the carcinogenic process (Tang et al., 2001). Formation of DNA adducts can initiate carcinogenesis, giving rise to the incidence of mutations (Pfeifer et al., 2002).

### 2.2.5 Nicotine Addiction

Besides a variety of smoking-related diseases, addiction is one of the most notorious smoking-related syndromes and is mainly attributed to nicotine (N. L. Benowitz, 1992). Nicotine withdrawal tends to perform the many adverse effects of smoking cessation such as nervousness, irritability, anxiety, impaired concentration, weight gain and so on which makes the process of quitting smoking extremely undesirable for the smoker despite knowing the negative health impact of continued use (Quist-Paulsen, 2007).

Addiction is a repeated physical behavioural with complicated causes and effects, which depend on the rate and route of nicotine dosing (Polosa & Benowitz, 2011). Essentially, nicotine mimics the actions of the hormone epinephrine and neurotransmitter acetylcholine in the brain (Luty, 2007). The process of nicotine addiction begins with inhalation of nicotine via cigarette smoking. The lungs distil nicotine from the tobacco smoke and allow absorption of nicotine into the arterial bloodstream rapidly (Luty, 2007). This produces a transient exposure of high levels of

nicotine to the brain, where neurotransmitters are released, enhancing the smokers` feelings of pleasure. This exposure acts on nicotinic cholinergic receptors, triggering the increased levels of endorphins, dopamine and other neurotransmitters e.g., glutamate, and γ-aminobutyric acid (GABA) (N. L. Benowitz, 2010). The release of neurotransmitters is particularly essential to the development of nicotine addiction (Vandewater, Park, Carey, & Wilkinson, 2014). Neuroadaptation and tolerance are developed by altering nicotinic receptors and neural plasticity (N. Benowitz, 2008). As discussed above, high nicotine levels travel through body to reach brain within 10 seconds of smoking, followed by a rapid decline only a few minutes after smoking (N. L. Benowitz, 2010). Nicotine from sequential cigarette smoking is capable of overcoming tolerance to produce further pharmacological effects (N. L. Benowitz, 1996). Therefore, smokers have to smoke more and more to maintain the same feelings produced by smoking. Nicotine is metabolized to cotinine primarily by the enzyme CYP2A6.The rate of nicotine metabolism results in variations of tobacco dependence and the response to treatments of nicotine addiction (Shiffman, Ferguson, Dunbar, & Scholl, 2012). An recent popular mediation for treatment of smoking dependence is called varenicline, which acts on specific nicotinic receptor subtypes in the brain based on the mechanisms of nicotine addiction (Figure 2.2) (N. L. Benowitz, 1996).

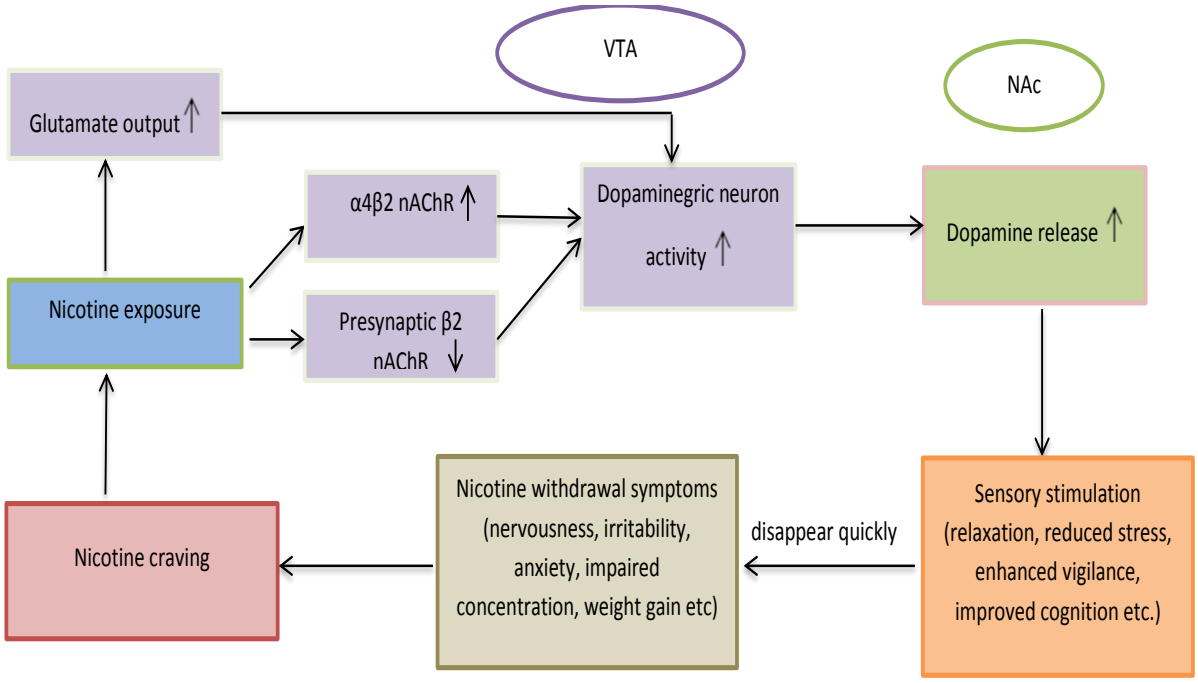


Figure 2.2 The mechanism of nicotine addiction

## 2.3 CURRENT THERAPEUTIC OPTIONS FOR SMOKING ADDICTION

According to the clinical practice guidelines, present pharmacotherapeutics for the treatments of tobacco addiction divide into first-line medications and second-line medications. First-line medications include nicotine replacement therapy (NRT), bupropion (Nides, 2008) and varenicline. Second-line medications are composed of nortriptyline and clonidine (Polosa & Benowitz, 2011). These medications are usually suggested being used in combination prescriptionally.

### 2.3.1 Nicotine Replacement Therapy (NRT)

NRT is the primary medication used for the treatment of tobacco dependence. Available NRT formulations include nicotine chewing gums, transdermal nicotine patches, sublingual tablets, nasal sprays, and inhalers. All of these are now available to be purchased at pharmacies.

The basic mechanism of action is the provision of nicotine without other harmful chemicals via cigarette smoke, replacing partially the nicotine formerly obtained from tobacco smoking through activation of nicotinic receptors in the ventral tegmental area in the brain and trigger release of dopamine subsequently. Thus the severity of withdrawal symptoms and cravings are reduced when smokers try to give up tobacco (J. A. Stapleton et al., 2008). Concerning the safety issue of NRT, attaining nicotine from NRT is significantly reasonable to patients who are not exposed to the many other harmful products of tobacco; nevertheless, smokers absorb nicotine from cigarette. All NRT products appear to be efficacious, leading to a doubling of smokers' quitting chances in comparison with placebo therapy (Shiffman, 2007). However, compared with the route of inhalation, other delivery routes of absorption cause a slow increase in nicotine level in the brain and a slower brain-to-blood ratio (Le Houezec, 2003).

However, NRT could not completely relieve all symptoms of nicotine withdrawal cravings because of its own limitations. The currently available therapeutical systems could not reproduce the high levels of nicotine to reach the brain rapidly achieved through tobacco use. The efficacy of medical nicotine products relies on the pharmacokinetic profiles and dosage of medication. The NRT products take at least a few minutes to achieve lower level of nicotine via systemic venous absorption (Molyneux, 2004). Gum is a slow way to deliver nicotine and dosage is difficult to be adjusted. The plasma concentration obtained from nicotine gum is usually between one-third and two-thirds of that from cigarette smoking (Fagerström, 1987). Slow release and passive administration of nicotine patches are not suitable for urging to relieve smoking craving though transdermal delivery systems ease issues of dosage and patient compliance. The recent nicotine patches are designed for 16h/day and 24h/day (Ma, Kendzor, Poonawalla, Balis, & Businelle, 2016). Nicotine tablets

produce less reinforcement with first pass metabolism, resulting in tolerance with increased nicotine blood levels. Besides, different forms of formulations (nicotine gums, lozenges, patches, nasal sprays, and inhalers) could have different impacts upon withdrawal symptoms and craving. No direct evidence has proved one nicotine delivery system is better than another. In addition, NRT does not fully overcome the issue of weight gain after smoking cessation (Farley, Hajek, Lycett, & Aveyard, 2012). Thus, NRT is less effective for patients who are not motivated to quit or do not expect to experience nicotine withdrawal symptoms. NRT is generally more effective when offered to cigarette smoker regularly who has made a previous quit attempt in conjunction with behavioural support.

It is recommended to use combination treatment such as patch and gum; or patch and inhaler. Combination treatment is more effective on smoking cessation with positive psychological intervention. A report under double blind, placebo controlled and randomised studies demonstrated that combined therapeutical treatments contributed to one year longer abstinence rates than single NRT treatment (Windle et al., 2016).

### 2.3.2 Electronic Nicotine Delivery Device (e-cigarette)

Electronic nicotine delivery systems (ENDS), also called as e-cigarettes were approved by US market in 2007 (Regan, Promoff, Dube, & Arrazola, 2013), followed by some countries worldwide as a drug delivery device for smoking cessation. However, it has not been approved by the Therapeutic Goods Administration (TGA) for use as a nicotine cessation aid in Australia. Therefore, it is illegal to sell or import it without a licence approval within Australia as nicotine is classed as a dangerous poison (Sutherland et al., 2016).

E-cigarettes are battery-powered devices where nicotine is suspended in propylene glycol or glycerine and water. They are breath activated with a micro sensor and produce nicotine mist via heat or ultrasound where. This aerosolizing delivery device is compatible with a disposable cartridge, which contains nicotine in solution of propylene glycol as the humectant. The devices are composed of a battery, a heating element, a power source, and a pressure switch (Trtchounian & Talbot, 2011). All these components are embedded in a tube with a mouthpiece (Figure 2.3), and the construction of device may vary. The newer generation e-cigarettes with high voltage battery power and high temperature may cause thermal breakdown of the solvents to produce toxic chemicals like carbonyls. Currently, three related products are available on the market: delivery devices, cartridges, and refill solutions (Adkison et al., 2013). They still have some common characteristics with pipes, multi-dose inhalers and other drug delivery devices.

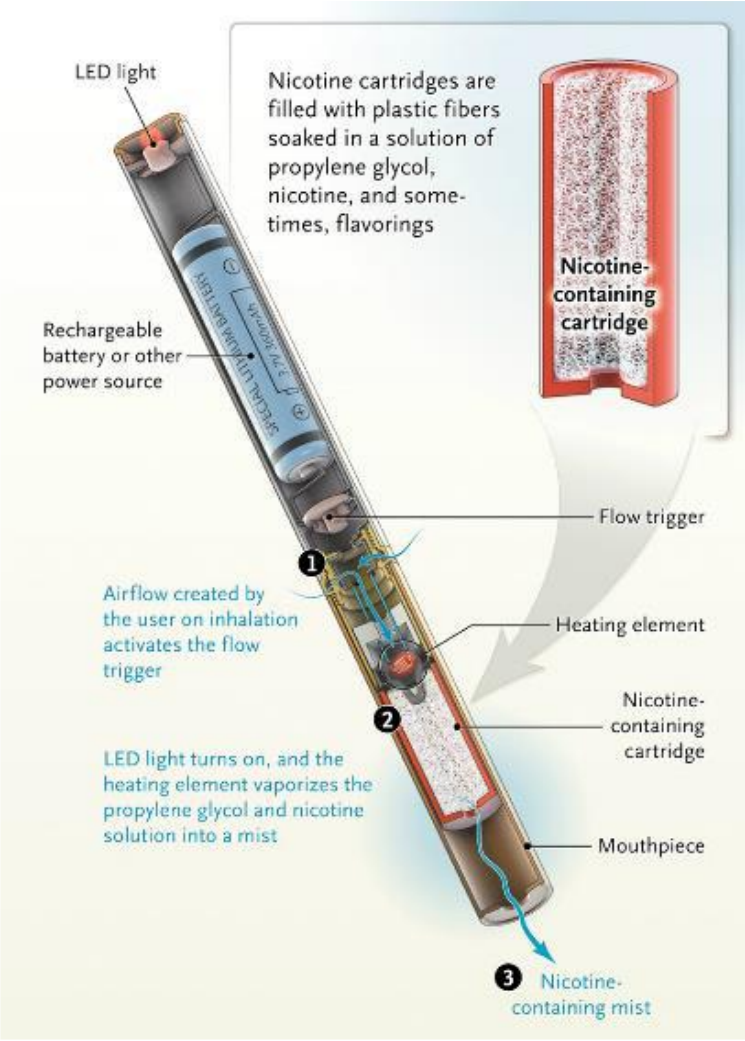


Figure 2.3 The components of e-cigarette (Cobb & Abrams 2011)

In spite of launching on the market in the early stage, the safety of inhaling e-cigarette has not been studied in humans and thus the scientific evidence in terms of safety is limited. The appropriate dose of nicotine which is delivered using e-cigarette also remains unclear and this product has failed to regulate smoking related problems (M. B. Siegel, Tanwar, & Wood, 2011). The effect of long-term use of e-cigarettes is not known and without valid clinical data, the marketing efforts of these products may increase addiction to nicotine, especially in young people. Although some data demonstrate that e-cigarettes may be effective in reducing nicotine cessation, there are no such clinical data demonstrating the efficacy of these products as an efficient tool

to achieve the goal (Drummond & Upson, 2014). In addition the liquid dosage forms of these products are less stable compared to that of solid dosage form. These uncertainties are worrisome to the users. Although no serious adverse effects (e.g. deaths or events requiring hospitalisation) have been reported, most smokers who attempted to use e-cigarette for quitting smoking considered them ineffective (M. B. Siegel et al., 2011). In fact, e-cigarette has become a "bridge product", smokers tend to use it in place where smoking is forbidden. On 25th April, 2011, the FDA had to announce that initial attempt of regulating e-cigarettes as tobacco replacement has failed to regulate them (I. Chen, 2013).

### 2.3.3 Bupropion

Bupropion hydrochloride was regarded to be an effective option for smoking cessation with non-nicotine. It is featured with sustained-release orally preferred over immediate release (Maccaroni, Malpezzi, & Masciocchi, 2009). It is recommended to take Bupropion SR (Zyban®, GlaxoSmithKline) twice daily and bupropion XL (Wellbutrin®, GlaxoSmithKline) once daily. As a selective reuptake inhibitor of dopamine and noradrenalin, bupropion could prevent and reduce craving that accompanies smoking cessation. It is reported that bupropion could improve the chances to quit smoking compared with placebo therapy although the mechanism of bupropion in smoking cessation is not completely understood (Huibers, Chavannes, Wagena, & Van Schayck, 2000). Bupropion in low doses can block brain nicotinic acetylcholine receptor (nAChRs) function, which could decrease the positive reinforcement effects of nicotine (Lerman et al., 2004).

According to some studies comprising over four thousand subjects, it is reported that bupropion arouses a positive effect in smoking cessation consistently (Richmond &

Zwar, 2003). Bupropion is effective to reduce withdrawal symptoms in patients who are motivated to quit smoking. At the same time, it is safe to be applied in patients with cardiovascular disease, but is limited by its occasional increase of blood pressure, which has been reported among smokers with hypertension. In addition, bupropion reduces expired breath CO levels significantly. The major safety issue is associated with seizures and psychosis (Strike & Hatcher, 2015). Insomnia and dry mouth are the other most common adverse effects with bupropion use (Tonstad et al., 2003).

### 2.3.4 Varenicline

Varenicline (Chantix/Champix®) (Figure 2.4) was introduced to market by Pfizer in 2006. Varenicline is able to mediate the reinforcing properties of nicotine in the ventral tegmental area of the brain as a partial selective agonist for the α4β2 nAChR subtypes and improves oral bioavailability and brain penetration significantly as it is produced as cytosine derivative (Tutka & Zatoñski, 2006). Coe suggested that α4β2 nicotinic receptor partial agonists could inhibit activation of dopamine produced by smoking while producing relief from the smoking withdrawal syndrome (Coe et al., 2005). Varenicline has dual effects, that is, on the one hand, it stimulates nAChRs partially without producing the full effect of nicotine agonist action, and on the other hand, it blocks nAChRs to prevent the nicotine from tobacco approaching them (Coe et al., 2005). That is, varenicline displays a higher affinity and less functional effect than nicotine resulting in a smaller release of dopamine. Therefore, varenicline can reduce smoking withdrawal syndrome and reduce the risk of relapse potentially.

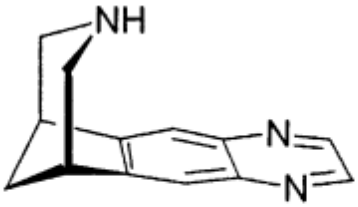


Varenicline

Figure 2.4 Structure of varenicline

Varenicline is an effective option to quit smoking with acceptable safety and tolerability profile. At the same time, it is a tolerated and effective option for treatment of patients with COPD and cardiovascular disease (Tashkin et al., 2011). More participants who were taking varenicline quitted cigarettes successfully than those with bupropion. However, there is few evidence showing that varenicline may prevent relapse (Cahill, Stead, Lancaster, & Polonio, 2012). The major adverse effect of varenicline is nausea, but in most patients nausea tends to subside over time with mild to moderate doses. Varenicline can also produce other side effects such as headache, insomnia and gastrointestinal disorders. In addition, some patients taking varenicline have experienced depression, suicidal thoughts, suicide, and serious neuropsychiatric symptoms (Kuehn, 2009).

## 2.4 PULMONARY DRUG DELIVERY TECHNOLOGY

The route of pulmonary delivery was first reported in 1967 by Herxheimer (Herxheimer, Griffiths, Hamilton, & Wakefield, 1967), and it was recognized as one of the most efficient treatments for delivering drugs to the targeted area because of large surface area of alveoli, small airways, low metabolism and high bioavailability. So far, many advances in pulmonary drug delivery have boosted drug delivery by inhalation locally and systemically, which offers great potential for rapid delivery of small-molecule therapeutics. Rapid absorption of small molecules into the systemic

circulation is due to the large surface area of the alveoli, the highly dispersed property of formulation , and excellent epithelial permeability (Patton & Byron, 2007). Efficiencies of inhaled particles with aerodynamic diameter ranging between 1 and 2 μm is as high as 90% if formulations are inhaled slowly and deeply (Patton & Byron, 2007). Drug delivery through route of lung is a promising technology in which medications are inhaled to the lungs and enter into the bloodstream (Nanjwade, Adichwal, Gaikwad, Parikh, & Manvi, 2011). Aerosol delivery of reformulated drugs is more likely to raise the efficiency of pulmonary drugs exponentially for the treatment of lung disease and systemic diseases. Delivery of small molecules can achieve effects of rapid action, high bioavailability and low metabolism, and macromolecules could be delivered without injections. Pulmonary drugs are currently formulated as solutions, suspensions, emulsions, or micro/nano-nized dry powders, and formulations are aerosolized via a variety of aerosolization devices i.e., nebulizers are for drugs which are formulated in aqueous solution or suspension and then atomized into droplets through some fundamental processes. MDIs are for drugs that are in the forms of suspension or solution under pressure in a liquid propellant. DPIs are for drugs in the form of powder that is fluidized as aerosol particles via subjective inspiratory efforts of patients.

### 2.4.1 Nebulizers

Nebulizers are the oldest method of delivering aerosols to the lungs via pulmonary drug delivery and they still play essential roles in specific diseases such as cystic fibrosis (Daniels, Mills, & Whitaker, 2013), dyspnoea (Boyden et al., 2015) and acute asthma (Cates, Welsh, & Rowe, 2013). Nebulizers are usually applied in the hospitals and ambulatory care settings (Watts, McConville, & Williams III, 2008), and are applicable for drugs which require high dose and little patient compliance and skills.

The new techniques of nebulization have been developed over a few decades, allowing some nebulizers to be portable use outside the home. A new device, Philips' i-neb, incorporating vibrating mesh technology, is designed for a portable device that can be applied outside the home (Denyer & Dyche, 2010). Respimat is a nebulization device, which makes it easy for patients who have difficulties to coordinate the inhalation and pMDI actuation. It produces the slow-moving cloud of aerosol , reducing deposition rate in the mouth-throat and increasing deposition in the lung compared with pMDIs (Hochrainer et al., 2005). However, in many cases, nebulizers are quite bulky. It is suggested to acquire professional guidance to use it. In addition, the usage of it should cooperate with additional tubing and mouth pieces, compressed air and/or oxygen sources, which results in the waste of significant amounts of active medicaments. Besides, only about 10% of dose is actually delivered to the targeted area of the lung from the nebulizers (Zainudin, Biddiscombe, Tolfree, Short, & Spiro, 1990).

### 2.4.2 Metered-Dose Inhalers

Metered dose inhalers (MDI) are portable and convenient for pulmonary drug delivery but their use is largely limited to relatively inexpensive and potent small molecules that can be formulated appropriately in propellants. Ari et al. compared the efficiency between MDIs and nebulizers in a lung model, which is an intubated and mechanically ventilated adult with a tracheostomy tube quantitatively. It showed delivery efficiency of a pMDI is higher than that of nebulizer (Ari, Harwood, Sheard, & Fink, 2015). In this delivery system, drugs are dissolved or suspended in the liquefied propellants. Pressurised metered dose inhalers (pMDIs) are used in respiratory drug delivery extensively; however, pMDIs have been proven inefficient. The deposition rate is only 20%-50% in chlorofluorocarbon (CFC)-propelled and hydrofluoroalkane (HFA)-propelled pMDIs, respectively (Watts et al., 2008). Additionally, these propellants

negatively affect the stratospheric ozone layer making the environmental impact an aversive element (Islam & Rahman, 2012). Over past several decades, the new MDI technologies have developed rapidly in transition to new propellant systems. Isobutane is a commonly used flammable refrigerant, which contributes to lower global warming potentially compared with HFA as propellant (Myrdal, Sheth, & Stein, 2014). Vega group has undertaken exploring isobutane as an alternative to HFA for MDIs (Vega & Toneguzzo, 2012).

### 2.4.3 Dry Powder Inhalers

Dry powder inhalers (DPIs) are easier, more stable and efficient delivery system compared with pMDIs. They have been used extensively to deliver drugs directly to the site of action to achieve local or systemic treatments such as asthma, COPD, tuberculosis (Chan et al., 2013) and infections associated with other pulmonary diseases. They also have been applied for delivery of levodopa to treat Parkinson's disease (Luinstra et al., 2015). Advantages of DPIs are attracting more attentions to boost the development of inhaled medications for pulmonary drug delivery.

The ideal DPI should meet three requirements to achieve most effective aerosol performance (Hoppentocht, Hagedoorn, Frijlink, & de Boer, 2014). The DPI needs to deliver a consistent amount of dose to the airstream. Either the weighting of the dose cavity and container or the dispersion property of compartment during the inhalation plays a vital role in controlling the consistency of delivered dose (Hoppentocht et al., 2014). The second demand of an effective DPI is to provide a consistent delivered fine particle dose (FPD), which requires a consistent amount of active pharmaceutical ingredients from entrained powder to be delivered into respiratory tract under an attainable range of flow rates (Chi Lip Kwok, 2015). The principal adhesive forces

such as van der Waals forces, mechanical interlocking from surface roughness, capillary forces, and electrostatic forces dominate powder performance during inhalation process (Prime, Atkins, Slater, & Sumby, 1997). In addition, the transportation efficiency from generated aerosol to respiratory tract by the inhaled airstream and deposition rate on the target area is highly important to produce an effective DPI product (Frijlink & De Boer, 2004). The aerodynamic particle size distribution and flow rate are particularly dominant in the deposition efficiency (DeHaan & Finlay, 2004). Therefore, it is necessary to consider both the designs of powder formulations and inhalation devices to obtain an optimised inhaler performance.

***DPI Formulations:***

Three types of DPI formulations are currently available, including pre-formulated small particles, a carrier-based interactive mixture, and loose agglomerates of drug and excipient particles (Frijlink & De Boer, 2004). The properties of formulations are affected by morphology, particle size and distribution, surface charge, and surface area and so on, which eventually influence the dispersion property as DPI formulations.

Optimization of flowability and dispersibility of formulations are critically important to develop desirable inhalation powders (Pilcer & Amighi, 2010). Presence of lactose monohydrate types and sieve fractions as carriers is a strategy to improve dispersion properties of inhalation particles (Kaialy, Alhalaweh, Velaga, & Nokhodchi, 2012; Patil, Mahadik, & Paradkar, 2015). Blending drugs with coarse lactose not only enhances the bulk of the formulations; also it improves separation of fine drug particles from formulation to improve dosing consistency of the DPI formulations (Prime et al., 1997). A new method of excipient enhanced growth technology has been introduced

to overcome the limitation of particle size distribution and boost the performance of pulmonary delivery. In the case of this approach, submicron particles composed of drug and hygroscopic excipient are fabricated to minimise loss in the inhaler device and extrathoracic airways (Kleinstreuer, Zhang, & Donohue, 2008). Particle size increases significantly to the ideal size by adjusting the ratio of excipient and drug once hygroscopic excipient interacts with natural warm and humid lung environment, which contributes to depositing particles to lower tracheobronchial and alveolar airways (Behara, Farkas, Hindle, & Longest, 2014; G. Tian, Longest, Li, & Hindle, 2013). However, based on the current literature regarding the implementation of the excipient enhanced growth technology, the relationship between growth of particle size and potential deposition region has not been figured out clearly (Behara et al., 2014).

Several techniques of manufacture have been advanced to obtain the particles in the controlled particle size distribution and surface morphology. Spray-drying is an adequate technique to prepare submicron particles with aerodynamic characteristics favourable for improved dispersion, sustained release and access to deep lungs (Beck-Broichsitter et al., 2012; Sham, Zhang, Finlay, Roa, & Löbenberg, 2004). A new technique of micro-moulded particles is applied to manufacture particles in a narrow particle size distribution with a variety of shapes (Mack, Horvath, Garcia, Tully, & Maynor, 2012). Other techniques for improvement of DPI formulations are based on the adhesive and cohesive nature of the micro-/nanosized particles, which has recently reached the preclinical or clinical productions of anti-asthma and COPD drugs (Begat, Morton, Staniforth, & Price, 2004; Muralidharan, Hayes Jr, & Mansour, 2015; Smyth, 2006).

***DPI designs:***

The design of DPIs on metering system and powder inhaler itself is a key factor to determine the effective dispersion of drug from formulations. A wide range of parameters, for example, material of inhaler device, geometry of the mouthpiece, air flow rate, drug capsule and the way of piercing, influence drug retention in the inhalers as well as aerosol performance of DPI formulations (Stegemann et al., 2013). DPIs are portable to carry, relatively affordable in price, and breath activated. Two main types of DPI system, including single-unit dose and multiple-unit dose, are available to deliver inhaled drugs (Islam & Gladki, 2008). The single-unit devices contain a single dose in gelatin capsule or pre-metered single dose of DPI formulation in disposable blister before use (Islam & Cleary, 2012). This is a common but inconvenient DPI device, because patients have to load an individual dose each time. The Rotahaler® is one of the most familiar single unit dose devices on the market (Srichana, Martin, & Marriott, 1998). The multiple-unit dose devices provide a single dose from pre-metered disposable blister, disks or tubes at each actuation, while the multi-dose devices enable the drugs to be stored in a bulk powder reservoir to meter an individual dose from the bulk (Newman & Busse, 2002). The Turbuhaler® is the first multi-dose example to dispense powders metered from a reservoir of inhaler (Wetterlin, 1988).

Many inhalation devices have been employed in existing DPIs to improve delivery of fine particle fraction (FPF) to site of action therapeutically (Frijlink & De Boer, 2004). Optimisation to break up agglomeration of particles in a turbulent airstream is a feature of DPI devices such as Easyhaler® (Chrystyn & Niederlaender, 2012) and Turbuhaler® (Hirst, Bacon, Pitcairn, Silvasti, & Newman, 2001). *In vivo* trials demonstrate both Easyhaler® and Turbuhaler® have a similar whole lung deposition (18.5±7.8% vs. 21.8±8.2%) from 200µg of budesonide (Hirst et al., 2001), while Easyhaler® tends to

be less sensitive to airflow in the range of 30-60 L/min with lower FPF (Chrystyn, 2006). Genuair® inhaler is another optimised multi-dose inhaler device with medium airflow resistance to improve deagglomeration of inhaled particles (Chrystyn & Niederlaender, 2012). *In vitro* studies reveal consistent emitted dose (ED) and FPF are achieved with reproducible aerodynamic aerosol within 45 - 95 L/min of airflow , and FPF is not dependent on the inhalation volume and storage conditions (Z. Xu, Mansour, & Hickey, 2011). In clinical trials, more patients (110 of 123 patients, mean age 67.6 years) show their preference to Genuair® due to ease of inhalation than Breezhaler® which is a single dose inhaler (Pascual et al., 2015). Besides, design to strengthen the pressure drop is contributing to increase of airflow, which is beneficial to improve FPF deposited in the lungs (Zhou, Tang, Leung, Chan, & Chan, 2014). Some active devices, for example, Exubera® (Hollander et al., 2004), have been combined with other techniques such as gas compression, electronic vibration or motor driven impeller have been introduced to produce inspiration-actuated inhalers to allow effective drug delivery, particularly for child or senior patients suffering from lower lung functions (Islam & Cleary, 2012).

Although DPI and DPI formulations have been advancing significantly in the recent decades due to huge potential to be applied in treatment of respiratory tract diseases, wide variability of deposited FPF in the lung changes from 9% to 78.7% (Islam & Cleary, 2012). This may be from inefficient deagglomeration of particles, insufficient inspiratory force or invalid fluid-particle interaction. As discussed above, the design of an adequate DPI formulation requires the drug to be stored in a solid state with fine dispersion property and high physicochemical stability in the device. Ideally, a DPI device should keep drugs stable physicochemically and be able to produce a reproducible drug dosing (Islam & Gladki, 2008).

### 2.4.4 Soft Mist Inhaler

Respimat® soft mist inhaler (SMI) developed by Boehringer Ingelheim (Dalby, Spallek, & Voshaar, 2004) is an aerosol cloud inhaler with spring generated mechanical power. As the latest generation of inhalers, it is propellant-free and different from the traditional liquid-gas propellants. (Anderson, 2006). A precise engineered nozzle produces two fine jets of liquid with a metered dose of drug solution. A soft mist is generated from the collision of two fine jets of liquid, which results in approximately 65% - 80% fine particle fraction. FPF generated by SMI is much higher than conventional pMDIs and DPIs. As a result, a higher drug deposition in the lungs than oropharynx is achieved as opposed to traditional MDIs and DPIs (Dalby et al., 2004). Respimat® SMI is a water based drug formulation that provides a reliable and consistent dose with each actuation. (Wu, O Adedoyin, & M Mansour, 2011). Several clinical studies have demonstrated that Respimat ® SMI is safe and effective in the application of asthma and COPD treatment in delivering bronchodilators to patients (E. Bateman et al., 2010; Dal Negro & Povero, 2016; Perriello & Sobieraj, 2015). However, Bateman investigated administration of 5 µg tiotropium once daily via Respimat® SMI increases the risk of deaths in COPD patients, particularly in elderly patients (E. D. Bateman, 2013). Thus, tiotropium Respimat® SMI has been withdrawn globally (Beasley, Singh, Loke, Enright, & Furberg, 2012). Regarding the unsure safety, decisions to use Respimat® SMI must be evidence-based carefully (Beasley et al., 2012).

## 2.5 POTENTIAL THERAPEUTIC ROLE OF NICOTINE INHALERS

The products of nicotine dissolution promote the transition across membrane in liquid found in lungs. Nicotine is the primary cause of abuse and dependence of cigarette smoking. It is also the prototypic agonist at acetylcholine receptor-gated ion channels

(Cunningham & McMahon, 2011), although little evidence is shown that nicotine is abused in its pure form. (Balfour, 2004). Currently chewing gums, transdermal patches and sublingual tablets for smoking cessation are available in the market (Lewis, Subramanian, Pandey, & Udupa, 2006), however, a number of practical problems are associated with each nicotine product. A low oral bioavailability is exhibited in the buccal administration of drugs, while sublingual tablets and chewing gums might be swallowed before being absorbed (İkinci, Şenel, Wilson, & Şumnu, 2004). Nasal spray of nicotine is the quickest way of NRT to allow nicotine to reach the brain and enter into the bloodstream. However, the rate of absorption still could not be comparable to cigarette smoking, and lack of acceptability would be caused in the small surface area of nasal cavity resulting from delivered high doses of nicotine (Rigotti, 2002). Therefore, the delivery of nicotine directly into the deep lung is more likely to effectively mimic the rapid effects of cigarette smoking on a physiological level, which could potentially eliminate patient craving and allow nicotine level to be tapered over time alleviating the dependence upon nicotine altogether (Buchhalter, Fant, & Henningfield, 2008).

Nicotine inhaler may be an effective appliance in smoking cessation. The proposed pulmonary drug delivery method is anticipated to improve the treatment of nicotine with less side effects as the potential risks are far lower as opposed to the risks of continued smoking (Henningfield, Fant, Buchhalter, & Stitzer, 2005). Thus, investing in new approaches to develop novel nanoparticles of biodegradable polymer containing nicotine with controlled release profile for pulmonary delivery accompanied by appropriate behavioural counselling, might significantly improve success rates for nicotine addiction. Very recently, an inhalable nicotine formulation (Stenzler, Zamel, Slutsky, & Ellis, 2017) comprising nicotine, lactose, and leucine

applied for a patent as a potential therapeutic formulation for smoking cessation. Currently, no DPI/MDI formulations for pulmonary delivery of nicotine have been approved for the management of nicotine addiction. However, two products, Nicotrol® and Nicorette® Inhalers (Pfizer) are available as nicotine vapour inhaler. These two devices deliver nicotine into the buccal areas, rather than the deep lungs, lowering the maximum plasma concentration and delays the time to reach maximum concentration (Silagy, Lancaster, Stead, Mant, & Fowler, 2004). The current available products are relatively slow compared to the rapid absorption of nicotine via the lungs from smoking, which indicates that the pulmonary delivery method may be advantageous over other routes.

A properly designed nicotine inhaler is critical to improve therapeutical effects through minimising the aerosol loss to the oropharynx and upper airways ensuring consistent dose to reach the deep lung with better dispersibility of formulations. The optimised nicotine inhalers can be achieved by adjusting the principal parameters of inhalation device such as flow rate, particle size distribution, duration of inhalation exposure etc (Silagy et al., 2004). An example would be a pure nicotine delivery inhaler (AERx) comprising a hand-held aerosol mechanical device and a single-unit discardable dosage strip containing nicotine salt (nicotine bitartrate) solution dissolved in water at pH 3.0-3.1 (Cipolla et al., 2008). The mass median aerodynamic diameter (MMAD) is between 2.4 μm and 2.8 μm for 10–30 mg/mL nicotine concentrations. FPF showed a linear relationship with a loaded dose (Moyses, Hearn, & Redfern, 2014). The maximum arterial blood concentration of nicotine was achieved 1 min post administration from inhaled nicotine of AERx Essence (Moyses, et al., 2014). It did not show significant lesions clinically, although mild to moderate acute adverse effects such as coughs and headaches were noted (Cipolla & Gonda, 2015).

Voke® nicotine inhaler is designed based on the MDI technology, containing 20 doses of formulated nicotine with propylene glycol, ethanol, saccharin, menthol, and HFA134a propellant in a MDI reservoir, which mimics 20 cigarettes per pack (Moyses, et al., 2014; Moyses, Hearn, & Redfern, 2015). The delivery of nicotine aerosol is actuated by a plunger within 0.5s after inhalation at a flow rate of at least 2–3 L/min (Beard, et al., 2016), which is different from the typical flow rate of 60 L/min (Pharmacopoeia, 2011). Fine particle dose (FPD) ranging from 0.29 mg to 0.37 mg of nicotine was yielded from 0.43 mg delivered nicotine dose with MMAD less than 5 μm (Moyses, Hearn, & Redfern, 2015). The mean maximum arterial nicotine concentration is achieved at 4.38 ng/mL within 6.5 min post administration from 0.67 mg of nicotine through 6-8 puffs, which is only 5-10 % blood nicotine level after smoking. (Cipolla & Gonda, 2015; Moyses, Hearn, & Redfern, 2014). It indicates nicotine is absorbed slower from Voke® inhaler compared with cigarettes. Mild or moderate side effects such as dizziness, headache, dry throat and cough which are usually associated with cigarette smoking are reported (Moyses, et al., 2015). In the very recent reports, the Staccato® system is at the early stage to develop a nicotine inhaler, where the nicotine in the form of film layer solubilizing in the organic solvents such as ethanol, acetone, hexane or methanol is applied by spray processing (Cipolla & Gonda, 2015). However, the data of product efficacy and human safety are not yet available.

## 2.6 NANOCARRIERS FOR PULMONARY DELIVERY

Biodegradable polymeric nanoparticles as nanocarriers, with optimized physicochemical and biological properties for pulmonary drug delivery has received increasing attention due to their targeted deposition, enhanced drug stability and

absorption, ability for intracellular delivery, sustained release and reduced dosing frequency (Rytting, Nguyen, Wang, & Kissel, 2008).

Various fabrication methods have been applied to produce polymeric nanoparticles. Generally, the drug molecules are either adsorbed or bound to nanopartical surfaces as nanosphere or encapsulated into nanoparticles as nanocapsules (Figure 2.5) (Kumari, Yadav, & Yadav, 2010). Spray drying is the primary particle engineering to manufacture nanoparticles (Chow, Tong, Chattopadhyay, & Shekunov, 2007). This technique applies jets of dissolved or suspended drug in an aqueous or other fluid phases that produces a fine mist through a high pressure nozzle (Bailey & Berkland, 2009). Kuar has reported gum-based porous nanoaggregates containing isoniazid and rifampicin were prepared via spray drying, which is suitable for anti-tubercular pulmonary drug delivery with sustained drug release pattern (R. Kaur et al., 2016). Al-Qadi investigated this process successfully to produce microencapsulated protein-loaded CS nanoparticles as DPI formulation (Al-Qadi, Grenha, Carrión-Recio, Seijo, & Remuñán-López, 2012). However, after spray-drying, the production yield of particles is relatively low (~ 47–50%) (Sosnik & Seremeta, 2015) due to the loss of liquid droplets inside the wall of the drying chamber (Cevher et al., 2006). Besides, the ineffective separation capacity of cyclone and the insufficient forces of liquid atomization affects the formation of appropriate submicron particles, which influences the size and size distribution in the development of the pulmonary drug delivery system (Oliveira, Guimarães, Cerize, Tunussi, & Poço, 2014). Double emulsion/solvent methods have been studied for preparation of polymeric particles, in which droplets of the dispersed phase are emulsified into the continuous phase with surfactants under vigorous homogenization (Iqbal, Zafar, Fessi, & Elaissari, 2015). Multiple emulsions of water-in-oil (w/o) are more widely applied than the oil-in-water

(o/w) (Chu, Utada, Shah, Kim, & Weitz, 2007). The o/w method is usually used to encapsulate insoluble or poorly water soluble drugs such as 5-Fluorouracil (Khang et al., 2001) and Lignocaine (Chung, Huang, & Liu, 2001), while w/o is able to encapsulate most hydrophilic drugs (Iqbal et al., 2015). Although double emulsion systems present a number of advantages, this process of manufacture is complicated and time-consuming (Lambrich & Schubert, 2005). In most cases, organic solvents are involved (Lambrich & Schubert, 2005). The technique of ionotropic gelation crosslinking to prepare nanoparticles is reported extensively in the recent literature (Bailey & Berkland, 2009; Bugnicourt, Alcouffe, & Ladavière, 2014), particularly the use of sodium tripolyphosphate (TPP) as an ionic agent to form the CS nanoparticles (Bugnicourt & Ladavière, 2016). The characters of formed nanoparticles are affected by a series of factors such as size of droplet, stirring speed, viscosity of solution (Rao & Geckeler, 2011).

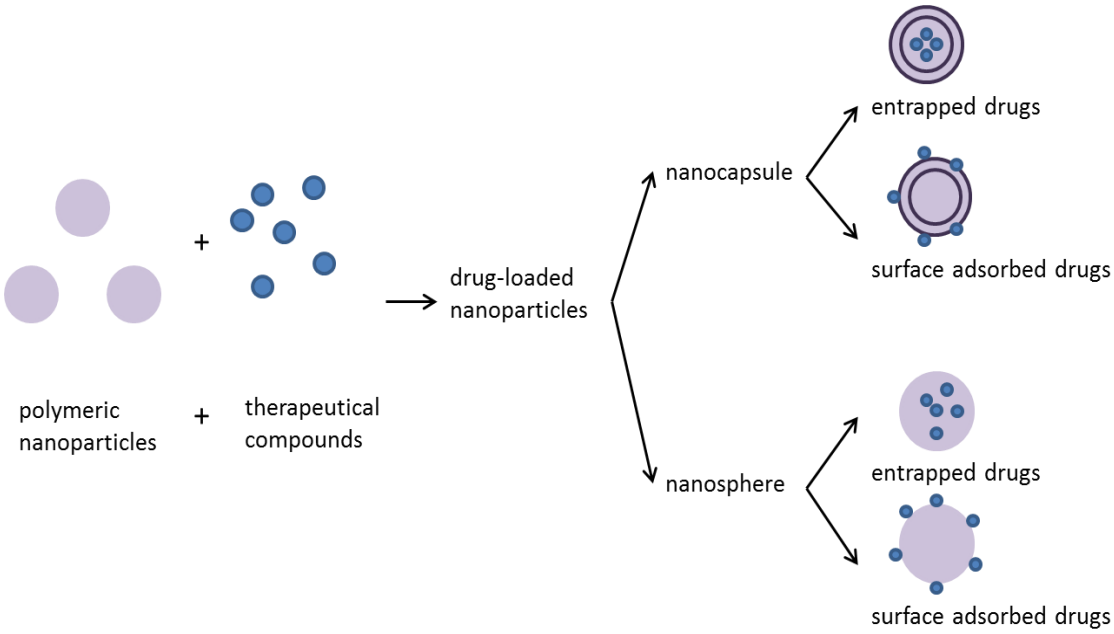


Figure 2.5 Schematic diagram of types of biodegradable nanoparticles: nanocapsule, and nanosphere. The drug molecules are either entrapped inside or adsorbed on the surface.

Poly-D, L-lactide-co-glycolide (PLGA) is one of the most popular biodegradable polymers and has been used extensively for development of nanosystems such as proteins and peptides nanomedicine, nano-vaccines, nanoparticles, as it is metabolised to monomers, lactic acid and glycolic acid in the body with less toxicity. The common methods to prepare PLGA nanoparticles include solvent emulsion-evaporation (Raichur, Nakajima, Nagaoka, Maekawa, & Kumar, 2014), interfacial deposition (Fonseca, Simoes, & Gaspar, 2002) and emulsification-diffusion (Terry, Salaam, Nyairo, Thomas, & Dean, 2014). Gomes et al. demonstrated that entrapped eugenol and trans-cinnamaldehyde with PLGA nanoparticles prepared by emulsion evaporation method could inhibit specific pathogens effectively, which can be used in food systems potentially as antimicrobial delivery (Gomes, Moreira, & Castell‐Perez, 2011). Cardoso et al reported that doxorubicin-loaded galactose-conjugated PLGA nanoparticles could be recognised by human hepatoma cellular carcinoma cells specifically, which has the potential to be used in liver-targeted drug delivery (Margarida Cardoso et al., 2016). However, due to the acidic nature of PLGA monomers, it is recommended to blend with alginate, chitosan, pectin (L. Liu et al., 2004) to overcome this limitation. Arya group investigated and found that topotecan-loaded composite particles of PLGA-chitosan had a synergistic effect on non-small cell lung cancer, which is promising for the treatment of lung cancer (Arya & Katti, 2015).

Nanoparticles of Poly (lactic acid) (PLA) and its copolymers have widely been used as delivery systems for local and systemic applications (Rancan et al., 2009). PLA undergoes scission in the body to monomeric units of lactic acid, which is a natural intermediate in carbohydrate metabolism. The rate of degradation depends on the degree of crystallinity and can be tailored by grafting (Tyler, Gullotti, Mangraviti,

Utsuki, & Brem, 2016). It eases the issue of safe elimination, which has been approved by FDA for use in vaccines, sutures, bone implants and screws (Tyler et al., 2016). In recent decades, formulations incorporated with PLA for targeted and sustained drug delivery has been widely demonstrated. Chen el al. study showed that drug uptake in targeted leukaemia cells could be improved by nanocomposite of nano-$TiO_2$ and PLA nanofibers incorporated with anticancer drug of daunorubicin (C. Chen et al., 2007). Musumeci et al. investigated that docetaxel-loaded PLA/PLGA nanoparticles prepared by a solvent deposition method for intravenous administration could improve drug solubility and achieve sustained release (Musumeci et al., 2006). Montiel-Eulefi et al reported copper-loaded PLA nanoparticles can be applied in the gastric cancer, which showed a cytotoxic effect and increased apoptosis on the gastric cancer cell line MKN-54 (Montiel-Eulefi, Jara, Toro, Garces, & Leal, 2014).

Alginate is an anionic polymer with less toxicity and good biodegradability. It has been employed extensively in the fabrication of particles and bulk gels (Paques, van der Linden, van Rijn, & Sagis, 2014). Nanosystem of alginate, including nanoaggregates, nanospheres and nanocapsules are mostly prepared by complexation (Lertsutthiwong, Noomun, Jongaroonngamsang, Rojsitthisak, & Nimmannit, 2008) and w/o emulsification (T. Chen, Yan, Li, & Tang, 2012). Zahoor et al. prepared alginate nanoparticles, which were 235.5 ± 0 nm in size by cation-induced gelation. Pharmacokinetic and chemotherapeutic performance of encapsulated isoniazid, rifampicin and pyrazinamide with aerosolised alginate nanoparticles were evaluated via the aerosol route in guinea pigs, which showed inhalable alginate nanoparticles are suitable to be applied as a controlled release of antitubercular drug carrier (Zahoor, Sharma, & Khuller, 2005).

## 2.7 CHITOSAN NANOPARTICLES AS A PULMONARY DELIVERY SYSTEM

Chitosan (CS) (Figure 2.6) is a natural biodegradable polymer derived from crustacean shells such as crabs, shrimps and lobsters, microorganisms, fungi and yeast (Kumar, 2000). It is a modified cationic polyaminosaccharide polymer which is the N-deacetylated derivative of chitin (Kumar, 2000). The primary unit of CS is a linear polysaccharide formed by β-(1-4)-linked D-glucosamine (deacetylated unit) and N-acetyl-D-glucosamine (acetylated unit) randomLy, so they are readily available for cross linking (X. Wang, Chi, & Tang, 2008). Due to advantages of CS such as extensive availability, low cost, high biocompatibility, biodegradability, better stability, low toxicity, mild preparation method, ease of chemical modification and versatile routes of administration (Sonia & Sharma, 2011), CS has been used extensively in many fields such as medicine, food and agriculture (Elena Udrea, Hritcu, Popa, & Rotariu, 2011; Sanyakamdhorn, Agudelo, & Tajmir-Riahi, 2013). The properties of CS considerably depend on the viscosity and molecular weight of CS which are dominated by the degree of deacetylation (Li, Liu, Wu, Wu, & Ran, 2008), and its properties affect the particle size, size distribution and particle aggregation. During the past two decades, a substantial amount of work has been published that this polymer is very suitable for preparation of nano- and microparticles for controlled drug release and offers valuable advantages as a drug delivery carrier for both small molecular drugs, like nicotine (Hui Wang, George, Bartlett, Gao, & Islam, 2017), paclitaxel (Majedi et al., 2014), and macromolecules, such as RNA (Ragelle et al., 2014), DNA (Gan, Wang, Cochrane, & McCarron, 2005). A wide range of drug formulations including gels, capsules, tablets, inhalations have been manufactured by CS. (Jonassen, Kjøniksen, & Hiorth, 2012). For example, glycol CS nanoparticles have achieved promising applications in both diagnosis and therapy for cancer (Lee, 2011).

Many studies have showed that several factors are important to achieve the desired characteristics of CS nanoparticles, including the proportion of crosslinking agent and polymer, the molecular weight of the CS, the CS concentration and pH (Agnihotri, Mallikarjuna, & Aminabhavi, 2004). Meanwhile, polymeric micro/nanoparticles for pulmonary drug administration improve the therapeutic effect of drug by modifying the drug bioavailability; in addition, encapsulated drugs in the micro- and nanoparticles contributes to reducing drug toxicity and prolongs the drug release profiles (Mossaad 2014).

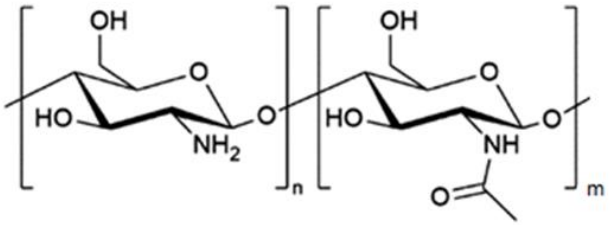


Figure 2.6 Structure of Chitosan (CS)

CS nanoparticles have been used extensively as drug delivery carriers due to their variety of advantages, which were mentioned before. Further studies could involve the use of derivatives of CS to provide better control of properties. Application of CS and its derivatives in lung delivery of various drugs has been extensively reviewed (Islam & Ferro, 2016). Currently most studies focus on the modifications of C2 position which is amino groups , while less attention is paid on the potential application of C6 modification (Islam & Ferro, 2016). In the near future, more modified CS with encapsulated drugs or other conjugated excipients at C6 or both C2 and C6 could be prepared for more practicable pharmacotherapeutic strategies. In addition, toxicities of derivatives of CS in different human organs have not been completely understood although a lot of studies have been reported based on *in vivo* animal models (Archana, Dutta, & Dutta, 2013; Liang et al., 2014). However, there is no doubt that translation

from animal models to humans is still difficult to achieve due to large differences of anatomical structures between animals and humans. Biodegradability is another safety issue to consider in long term human health applications. In particular, the most current techniques involved in organic solvents and use chemical crosslinkers as well as high shear force (Tiyaboonchai, 2003). However, its minor shortfalls can be ignored when considering its favourable biocompatibility characteristics.

## 2.8 ANIMAL MODELS FOR PULMONARY DISPOSITION

With advancements of aerosol and inhalation technology in development of inhalation medications, it is essential to evaluate the efficacy of drug delivery and its bio-activity following encapsulation and release as well as potential toxicity of formulated inhalation products in animal models prior to application in humans. Although several *in vitro* apparatus such as twin-stage impinger (Haghi, Traini, & Young, 2014), multi-stage liquid impinger (Zhou et al., 2013) and cascade impactors (M. Chen, Romay, Li, Naqwi, & Marple, 2016) have been used to evaluate the particle deposition according to the size of particles, these methods could not totally imitate structures of upper and lower respiratory tracts. Rodent models such as rats and guinea pigs are usually employed for pulmonary dosing; however, mice are a greater technical challenge in lung dosimetry and collection of multiple blood samples due to smaller body size and limited volume of body blood.

### 2.8.1 Intratracheal Instillation

Intratracheal instillation is a pioneering work reported by Schanker group (Enna & Schanker, 1972). The rats are placed on a surgical board in a supine position under anesthesia. An insulation blanket is used to maintain 37 °C consistently. The trachea is exposed carefully, following inserting an endotracheal tube between the tracheal

cartilaginous rings. A microsyringe of aqueous tested solutions or suspensions instils into the airways via tube. Then, the lung tissues are removed and homogenized to determine the levels of drug concentration quantitatively using HPLC or LC-MS. Although a substantial number of data for the lung tissue kinetics have been produced from this model (Enna & Schanker, 1972; Lanman, Gillilan, & Schanker, 1973; Schanker & Burton, 1976), a large number of animals are sacrificed to produce a data point due to the destructive tissue sampling. The technique of intratracheal instillation is only applicable to liquid instillation although a variety of more sophisticated and custom-made dosing devices (Hasegawa-Baba, Kubota, Takata, & Miyagawa, 2014; Zhang et al., 2016) have been applied for use in rodent models. Based on the advancement on the tracheostomy, the new techniques such as direct injection to the lung or spray of drug solutions in the lung through orotracheal intubation was applied (Brain, Knudson, Sorokin, & Davis, 1976), but it is still limited for powder administration.

### 2.8.2 Dry Powder Insufflation

As deep lung delivery from dry powder formulations has attracted increasing attentions in the recent years, powder insufflation technique as well as insufflation devices with precise dosing and reproducibility have been employed. In most cases, tracheal access via tracheotomy is essential and it is required 3-5 mL compressed air to insufflate 0.2-5.0 mg powders from devices into the lung (Sakagami, 2006). Penn-Century produced a hand-operated dry powder insufflator™ to aerosolize dry powders and deliver fine particles for small rodent applications (Codrons, Vanderbist, Ucakar, Préat, & Vanbever, 2004). Molina et al. (Molina et al., 2016) compared CeO2 (cerium oxide) nanoparticles distribution from intratracheal instillation and powder insufflation using Penn-Century device. It is found that inhalation insufflation caused

a more significant deposition in the trachea and a more uniform particle distribution within lungs than instillation. In order to achieve deep lung delivery to maximize drug deposition, ventilated administration of aerosol exposure with positive pressure has been employed. However, a substantial amount of test material is required to pursue a desirable biological effect with relatively high dose deposition from powder insufflation due to low ventilation rate of rodents. Furthermore, this technique of powder insufflation relies on the physicochemical characterzations of powder and the way of aerosolization.

### 2.8.3 Inhalation Exposure

Much effort has been made to design devices for inhalation exposure in animal models because neither anaesthesia nor surgery is required. Currently, there are two main options for delivering particles to animals to achieve inhalation exposure, including whole-body exposure and nose-only inhalation exposure (Hu, Adamcakova-Dodd, LehmLer, Gibson-Corley, & Thorne, 2015). Mainelis reported a nose-only exposure chamber with four inhalation ports that was employed to deliver anticancer drug and small interfering RNA to the lungs in mice. The aerosol deposition rate under the size of 130 nm of liposomal nanoparticles was 1.4% at each port after 60 minutes aerosolization (Mainelis et al., 2013). Sinha and his group developed a nose-only inhalation chamber as either nebuliser or DPI depending on the experimental setup for mice (Sinha & Mukherjee, 2012). *In vitro* evaluation test showed drug deposition from DPI was higher than nebulizer (42-57 % vs. 11-26 %) and *in vivo* test demonstrated 80-130 µg/g of voriconazole was found in mice lung tissues from DPI while 40–68 µg/g was detected from nebulizer (Sinha & Mukherjee, 2012). In contrast, a whole-body inhalation exposure apparatus was constructed by Yi group and used for delivery of titanium dioxide nanoparticle aerosol with stable mass concentration, uniform

composition and consistent particle size distribution (J. Yi et al., 2013). This inhalation chamber from whole body exposure requires animal to inhale the drugs from the animal body surface instead of nose administration, which prevents measurement of the oral dose efficiency. Interestingly, a very recent study reported both whole-body inhalation and nose-only inhalation exposure results in the same efficiency in particle deposition under the same administration conditions (Oyabu et al., 2016).

However, it is still a challenge to design the adequate inhalation devices for use in animal models to test the efficacy of inhalation products. The currently available inhalation devices designed for DPI studies require tracheal intubation under ambient pressure or positive pressure, which results in large amount of inhaled particles being deposited by physiological breathing rather than spontaneous respiration. On the other hand, they require whole body exposure to achieve inhalation by spontaneous respiration, while the absorption routes are through percutaneous absorption or orifices other than the nasopharynx. Some test material is toxic if it deposits on the fur of the animals. The nose-only exposure devices seem favourable for animal model studies, however, the duration of exposure is critical to consider carefully with variation of air flow rate, air pressure, aerosol concentration (Lebedová et al., 2016). A large fractions of aerosols deposit nasal cavity as rodents are nose-breathing animals, which results in over-estimation of lung's absorption capacity because plotted blood concentration profiles are the sum of absorptions from nose, gastrointestinal tract and lung (Wolff & Dorato, 1993). Furthermore, a large amount of test material is wasted due to the low efficiency of powder delivery.

### 2.8.4 *In Vivo* Imaging Technique

*In vivo* imaging technique is an approach to assess lung and oropharyngeal depositions in the direct ways to track particle or drug carriers by taking images of lungs, which allows evaluating lung-regional deposition of particles qualitatively and quantitatively. Various options based on the theories of radionuclides, nonionizable radiation and fluorescent dye have been applied to determine particle deposition by capturing pictures of lungs tissues or by autoradiographic technique after sacrificing animals and separation of animal lungs such as gamma scintigraphy (Bennett, Xie, Zeman, Hurd, & Donaldson, 2015), single photon emission computed tomography (SPECT) (Gervais, Poussier, Bardin-Monnier, Karcher, & Thomas, 2014), positron emission tomography (PET) (Barth et al., 2014), magnetic resonance image (MRI) (Abdukayum et al., 2014) and fluorescence imaging (Abdukayum et al., 2014). The images of SPECT and PET are presented in the pattern of 3D, allowing more details on regional lung deposition to be shown, in comparison to the 2D images technique produced by gamma scintigraphy (Nahar et al., 2013). Specifically: (1) Formulations applied to gamma scintigraphy are labelled with gamma ray emitting radioisotopes. It is possible to measure lung deposition regionally via this method. However, due to 2D images from this method, structures of interest maybe overlayed and scanned, which is possible to fail to distinguish among alveoli, small and large airways (Nahar et al., 2013); (2) Formulations applied with SPECT are radiolabelled and subjects are rotated scanned by gamma camera, structures of interest with better anatomical are produced by radionuclide in the 3D construction. Therefore, accuracy is improved significantly by this method (Perring, Summers, Fleming, Nassim, & Holgate, 1994). Nevertheless, the conditions such as redistribution of radiolabelled aerosol, coughing and absorption of radiolabelled signals into blood stream may be associated with this method as it takes as long as 30 minutes to complete scan of regional deposition. (3) The drugs

applied with PET are labelled with positron emitting radioisotopes, which produce high energetic photos by annihilating with electrons and emit spontaneously. The drug of interest is able to be seen as radioactive tracer when merging positron emitting isotopes such as $^{11}C$, $^{13}N$, $^{15}O$ and $^{124}In$, which contributes to progress in pathology, biochemistry, inflammation and cellular response. However, availability of positron emitting radionuclides is primary limitation to applying this technique widely (Saha, MacIntyre, & Go, 1992). In addition, this method is unable to provide lung deposition of inhaled formulations quantitatively. (4) The method of MRI not only offers a way to measure particles deposition in animals quantitatively, but also enables quantification of particles deposited regionally in animals and *in vitro* human airways (Thompson & Finlay, 2012). Richard et al. reported MRI contributed to increase of concentration of particle deposition when drugs are loaded with iron oxide nanoparticles in the application of targeted delivery (Richard et al., 2004). (5) Test drugs tagged with fluorescent particles can be tracked and detected during drug deposition in animals by fluorescence imaging. The limitation associated with this method is that biological tissues could scatter, reflect and absorb emitted fluorescent light, causing interference of light capture by detector and determination of the number of molecules. In addition, most tissues appear to auto-fluoresce, which enhances heterogeneous background signal (D. Yi, Price, Panoskaltsis-Mortari, Naqwi, & Wiedmann, 2010). Currently the common options to overcome this problem are to subtract auto-fluorescence from blank tissue and select emitted light in the region of near infrared of the spectrum (Adams et al., 2007; Diao et al., 2015).

Imaging technique could provide a real picture of drug deposition in the animal lungs locally and regionally. However, the techniques mentioned above are challenging with

expensive cost, high dose required for radiation, safety hazards of radioactivity and specific expertise in handling of radio labelled isotopes.

As discussed above, the author hypothesises that the delivery of pure nicotine to the deep lung using a DPI device with better formulation would be comparable to cigarette smoking and hence would alleviate cravings and nicotine withdrawal with reduced dosage and potential side effects. At the same time, it is anticipated that the polymer encapsulated nicotine delivery will also reduce nicotine craving with controlled formulation. Very recently, Wang et al. demonstrates using the biodegradable polymer of CS as carriers for nicotine hydrogen tartrate (the salt form of nicotine) as DPI formulation, which is able to deliver FPD of nicotine between 1.7 mg and 3.2 mg into lungs with sustained release profiles. It suggests encapsulation of nicotine into CS nnaoparticles may be exploited for sustained release nanoparticulate DPI formulation for treatment of nicotine addiction potentially (Hui Wang et al., 2017).

# Chapter 3:

# Preparation and Characterization of NHT-loaded CS Nanoparticles

Parts of Chapter 3 have been published as below:

**Wang, H;** George, G; Bartlett, S; Islam, N; Gao, C; Nazrul Islam. Nicotine Hydrogen Tartrate Loaded Chitosan Nanoparticles: Formulation, Characterization and in vitro Delivery from Dry Powder Inhaler Formulation; European Journal of *Pharmaceutics and Biopharmaceutics*. 2017, 113: 118-131.

The aim of this chapter is to develop micro/nanoparticles of biodegradable polymer of chitosan (CS) loaded with nicotine hydrogen tartrate (NHT) for pulmonary delivery of nicotine from dry powder inhaler (DPI) formulations. The physicochemical properties such as particle size, flowability, specific surface area etc. of particles are understood by a series of techniques. The NHT-loaded CS (NHT-CS) micro/nanoparticles are prepared using water-in-oil (w/o) emulsion crosslinking method. The morphological studies are characterized using scanning electron microscopy (SEM) and transmission electron microscopy (TEM). Particle size analysis is determined by Zetasizer and Mastersizer. According to differential scanning calorimetry (DSC), x-ray diffraction (XRD) analysis and Attenuated total reflectance-Fourier transform infrared (ATR-FTIR) spectroscopy, the NHT crystallinity is lost when encapsulated in the micro/nanoparticles, indicating it is uniformLy dispersed as a solid solution. On the basis of X-ray photoelectron spectroscopy (XPS) analysis, the amount of NHT loaded on the surface of CS increases proportionally with increasing drug loading in the bulk so there was no surface enhancement.

## 3.1 INTRODUCTION

Novel particle technologies have assisted the advancement of inhalation therapy. The size of particles should be small enough to escape from the mouth, throat and conducting airways and targeted to the deep lung. The performance of the particles deposited is characterized by the aerodynamic diameter, $D_a$. Generally, the particles with large sizes ($D_a$ >5 μm) are deposited in the mouth and upper airways; particles with small size ($D_a$ =1-5μm) are deposited in the lungs; the particles with very small size ($D_a$ <1μm) are able to deliver the drug to the lung epithelium, while mostly they are suspended or exhaled driven by diffusion (Labiris & Dolovich, 2003; Sung, Pulliam, & Edwards, 2007). When the particle-particle aggregation is created, it causes

difficult handling of nanoparticles physically (Grenha, Seijo, & Remunán-López, 2005) as it requires high energy for their deaggregation in dry powder form. To overcome these limitations, nanoparticles incorporating micron carriers such as coarse lactose of different morphologies has been reported (Kho & Hadinoto, 2013; Ungaro, d'Angelo, Miro, La Rotonda, & Quaglia, 2012). Jafarinejad (Jafarinejad et al., 2012) prepared lactose and mannitol micro-scale dry powders containing itraconazole-loaded nanoparticles by spray drying to improve the physical and aerosolization properties. Large biomolecules are not able to cross the alveolar epithelium when they reach it, while nanoparticles are the ideal vehicles for drug transport to the deep lung, avoiding unwanted mucociliary clearance and phagocytic mechanisms (Grenha, et al., 2005). Over the last few decades, nanoparticles have been extensively recognized as valuable drug carriers for pulmonary delivery through dissolving, entrapping or encapsulating to active substance due to its a variety of advantages. Furthermore, nanoparticles are able to deliver drug in the prolonged and sustained period in the lung tissue and systemic circulation, which is beneficial for patients compliance with reduced dose required (Beck-Broichsitter, Merkel, & Kissel, 2012; Colilla, Baeza, & Vallet‐Regí, 2015). The nanoparticles are usually composed of biodegradable polymer, which is degraded in the body and excreted through natural metabolic pathways (Sung, et al., 2007). A variety of molecules have been for systemic and local therapeutic nanoparticles from pulmonary delivery.

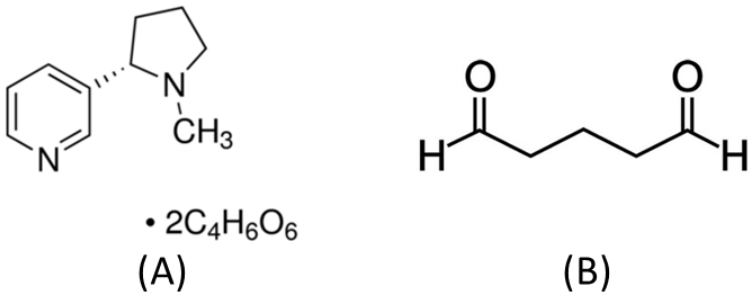


Figure 3.1 Molecular structures NHT (A) and glutaraldehyde (B)

In this study, nicotine hydrogen tartrate (NHT) (Figure 3.1A) was selected as the model drug to prepare the NHT-loaded CS nanoparticles for pulmonary delivery. The targeted size of NHT-loaded CS nanoparticles would be within 500 nm, while the size of micro-aggregate occurred between nanoparticles due to high surface energy are ideal within 5 μm, which is in the respirable range. NHT is more stable than nicotine base, which is a very unstable and hygroscopic oily liquid, causing difficulties in conventional packaging materials (Chauhan, Lin, & Madan, 2012). NHT is a hydrophilic powder, aqueous solubility up to 50 mg/mL and it melts at 89°C (Chauhan et al., 2012).

The aim of this chapter was to demonstrate a strategy to fabricate NHT-loaded CS micro/nanoparticles by using water-in-oil emulsion crosslinking method. Glutaraldehyde (Figure 3.1B) is used as a crosslinking agent for primary amines. The mechanism of this method is to utilize the Schiff base reaction where the 2 units of amine group of CS is crosslinked with one aldehyde molecule, forming a characteristic imine (N=C) bond between aldehyde carbon and primary amine (Agnihotri et al., 2004) (Scheme 3.1).

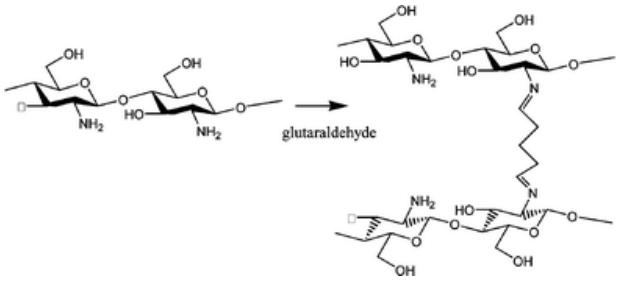


Scheme 3.1 Mechanism of crosslinking of glutaraldehyde with CS (Agnihotri et al., 2004)

## 3.2 MATERIAL AND REAGENTS

Low molecular weight (LMW) CS with the degree of deacetylation of 92% was purchased from Sigma-Aldrich, Australia. 50% aqueous glutaradehyde was purchased from Merck, Australia as the crosslinker for the preparation of nanoparticles. Span 80 was obtained from PCCA, Australia as the emulsifier. Nicotine hydrogen tartrate (NHT) salt powder (≥98%) was purchased from Sigma-Aldrich, Australia. All other chemicals and reagents used were analytical grade.

## 3.3 METHODS

### 3.3.1 W/O Emulsion Crosslinking

***Preparation of blank CS nanoparticles***

Blank CS nanoparticles were prepared by using W/O emulsion-glutaraldehyde crosslinking method (Hui Wang et al., 2017). In order to fabricate blank CS nanoparticles, LMW CS powder was dissolved in 2 w/v% acetic acid to obtain the final concentration 2% CS solution with pH 3.5. About 1mL span 80 was mixed into about 100 mL paraffin oil under vigorously stirring to form a fine dispersion. 3mL of 2% CS solution was added to paraffin oil drop-wise, with the homogenization for 5 minutes using ultraturrax (IKA®) to obtain the W/O emulsion. Then, the mixture was continued stirring at 5000 rpm (IKA® Works (Asia), Inc). After 10 minutes, the stirring

speed reduced to 3000 rpm and the liquid mixture was continued to mix for 3 hours with the addition of 0.2 mL 50% glutaraldehyde every hour for a period of three hours. Finally, the whole mixture was stood for 1 hour, after washing in hexane once and diethyl ether three times. The blank CS nanoparticles were obtained by freeze drying at −80 °C.

***Effect of amount of crosslinking agent on formation of nanoparticles***

Different types of blank CS nanoparticles were prepared with a series of different levels of crosslinking agent (i.e. 0.3mL, 0.6mL, 0.9 mL 50% glutaraldehyde solution in total). All other conditions were same as above. The detailed conditions and results were shown in the Table 3.1. In the following sections and chapters, all the blank CS nanoparticles used for general physicochemical properties tests were prepared by 0.6 mL 50% glutaraldehyde solution, except for emphasizing volume of glutaraldehyde solution used during manufacture process.

***Preparation of NHT-loaded chitosan nanoparticles***

For preparation of NHT-loaded CS nanoparticles, 2 mL of NHT solution in milli-Q water at different concentrations (i.e., 2%, 4%, 6% w/v) was added into 2 mL of 2% CS solution (dissolved in 2% acetic acid) before adding to paraffin oil. This gave loadings which are referred in the following studies as 1:1; 2:1 and 3:1 ratios of NHT: CS. All other conditions were same as above. The detailed conditions and results were shown in the Table 3.1

Table 3.1 Conditions to prepare blank CS and NHT-loaded CS nanoparticles

| Products name | Volume of 2% CS in 2% acetic acid (mL) | volume of 50% glutaraldehyde (mL) | Concentration of NHT solution (%) |
|---|---|---|---|
| Blank CS NPs | 3 | 0.6 | 0 |
| Blank CS NPs-0.3 | 3 | 0.3 | 0 |
| Blank CS NPs-0.9 | 3 | 0.9 | 0 |
| NHT-CS 1:1 | 2 | 0.6 | 2 |
| NHT-CS 2:1 | 2 | 0.6 | 4 |
| NHT-CS 3:1 | 2 | 0.6 | 6 |

### 3.3.2 **Morphological Studies**

The morphological examination of the freeze dried CS nanoparticles and NHT-loaded CS nanoparticles were observed by Scanning Electron Microscopy (Zeiss Sigma VP Field Emission SEM). A tiny amount of freeze dried powder was dropped onto a silicon wafer adhered with an aluminium stub through carbon adhesive tape. The air dried specimen stubs were coated with a conductive layer of sputtered gold (argon gas pressure of 0.5 mbar, current of 30 mA, and coating time of 75 s), followed by observing morphological characterizations of secondary electron images under a high vacuum with an accelerating voltage of 5 kV and a working distance of 6.8 mm. A variety of photomicrographs with different magnifications were captured for blank CS nanoparticles and NHT -loaded CS nanoparticles.

To understand more about individual nanoparticles, the samples were analysed by a TEM. A small amount of powder was suspended in water and TEM analysis were obtained by dropping 6 µl of the prepared suspension onto a copper grid, and dried overnight at room temperature. The examinations were carried out at the accelerating voltage of 200 kV without any further modification or coating.

### 3.3.3 **Particle Size**

The particle size and size distribution of the blank CS and NHT-loaded CS nanoparticles were determined using Zetasizer (Nano ZS 90, Malvern Instruments, UK) by DLS measurements. Lyophilized powder of nanoparticles was dispersed in mineral oil with 1% span 80, and sonicated for 10 minute. Size measurements were performed under a detector angle of 90° at 40°C. All the measurements were performed in triplicate. Reported values were the mean diameter ±SD. Particle sizes and data acquisition were analysed by Malvern Zetasizer Software.

A laser diffraction instrument (Malvern Mastersizer 3000, Malvern Instruments, Malvern, UK) was utilized for measuring the size of micro-aggregates as seen in the SEM images. A 10 mg of NHT-CS and CS powders were suspended in 50 mL of milli Q water with 2 drops of 1% Tween 80 as surfactant. NHT-CS/blank CS suspensions were then added to an automated dispersion unit (Hydro MV, Malvern Instruments, Malvern, UK) to reach an obscuration value of 20 ± 1% and recorded particle sizing in a cycle of 5 measurements over 120 s. Size distribution was determined as relative volume density versus size distribution curves (Malvern Mastersizer 3000® Micro Software v 3.10). Parameters obtained in particle size distribution of mean particle volume D [v, 50] are shown in Table 3.3.

### 3.3.4 **Zeta Potential**

Using this DLS, surface charges (zeta potentials) on nanoparticles were determined at measured pH after freeze drying and a fixed pH (pH=6) to get a clear understanding on the effect of pH on zeta potential. The nanoparticle powders were dispersed in 0.1 mM KCl, following 10 mins sonication and the zeta potential measurements were repeated in triplicate.

### 3.3.5 **Particle Density and Flow Property**

***Bulk density, tap density, Carr's index and Hausner ratio***

The bulk density ($\rho_b$) and tapped density($\rho_t$) of particles were determined by the graduated cylinder measurement (Pilcer, Vanderbist, & Amighi, 2009) as Eq. 3.1 and Eq. 3.2. A certain amount of test samples ($m_0$) were introduced into a dry graduated 10 mL cylinder, after the agglomerates formed during storage were broken up gently to avoid changing the nature of the particles. Apparent volumes ($V_0$) without compacting were noted to calculate the bulk density (g/mL). Then, the formulations were tapped 100 times mechanically by tapped density tester (ERW-SVM101201, ERWEKA, Germany) and the volumes ($V_1$) of cylinder were read to calculate the tapped density (g/mL). Furthermore, Carr's index (CI) and Hausner ratio (HR) were calculated (Varshosaz, Taymouri, & Hamishehkar, 2014) using the Eq. 3.3 and Eq. 3.4 below. All the measurements were performed in triplicate.

$$\rho_b = \frac{m_0}{V_0} \qquad \text{Eq. 3.1}$$

$$\rho_t = \frac{m_0}{V_1} \qquad \text{Eq. 3.2}$$

$$CI = \frac{100(V_0 - V_1)}{V_0} \qquad \text{Eq. 3.3}$$

$$HR = \frac{\rho_t}{\rho_b} \qquad \text{Eq. 3.4}$$

Where $\rho_b$represented the bulk density; $\rho_t$was tapped density; CI was Carr's index and HR was Hausner ratio.

***Angle of repose***

The angle of repose (θ) is an important macroscopic parameter in evaluating the flowability of particles (Varshosaz et al., 2014) as Eq.3.5. It is the angle formed by the horizontal base and the edge of a cone-like pile of granules. A glass funnel of diameter 18 mm and orifice 2 mm was used. The height from the beginning of funnel to end of orifice was 50 mm. The funnel was fixed by in a stand 3 cm above the beaker surface. The cone was built through glass funnel using around 0.50 g of NHT-loaded CS nanoparticles. The height (h) and the diameter (d) of the base of the cone formed by the granules were measured and used to determine θ using the following equation.

$$\theta = \tan^{-1}(\frac{2h}{d}) \qquad \text{Eq. 3.5}$$

### 3.3.6 **Differential Scanning Calorimetry (DSC)**

The thermal characteristics of pure NHT, NHT-CS nanoparticles and blank CS nanoparticles were investigated using differential scanning calorimetry (DSC) in a TA Instruments DSC (model Q100). 1.2 mg samples were accurately weighed in a standard aluminum pan, sealed and taken through a heat-cool-heat cycle between 25°C and 180°C at a constant speed of 10°C/ min under continuous purging of nitrogen atmosphere (10 mL/min). An empty sealed pan was used as a reference. All samples were measured in triplicate.

After DSC test, the aluminium pan of NHT was cut by scissors and observed under microscope. The product inside of aluminium pan subsequently was analysed by attenuated total reflectance Fourier transform infrared (ATR-FTIR).

### 3.3.7 **X-ray Diffraction (XRD)**

Powder X-ray diffraction diagrams of blank CS nanoparticles and NHT-loaded CS nanoparticles were performed with PANalytical X'Pert PRO MPD Powder X-ray Diffractometer. Powder samples were finely ground into XRD sample holders to create

flat surfaces. The X-ray source was CuKα radiation over the range of 4-75° (2θ) at 40 kV and 80 mA. Angular speed was 4°/min.

### 3.3.8 X-ray Photoelectron Spectroscopy (XPS)

The XPS analysis of chitosan and the NHT was performed using a Kratos Axis Ultra Spectrometer (Kratos Analytical, Manchester, UK) equipped with monochromatized aluminium X-ray source (powered at 10 mA and 15 KV), 165 mm radius hemispherical analyser (HSA) and 8-channel electron multiplier (channeltron) detection system. Powder samples were mounted onto stainless steel sample holders using double-sided adhesive tape and the spectra were collected using an analysis area of 700 x 300 µm. Low-resolution wide scans (survey spectrum) in the binding energy scale (0–1200 eV with 1.0 eV steps) were collected at an analyser pass energy of 160 eV. High-resolution narrow scans (multiplex spectra) were collected at 20 eV pass energy with 0.05 eV steps for O1s, N1s and C1s. The data were processed using Casa XPS software Version 2.3.14 and binding energies of the various elements were referenced to the C1s line at 285.0 eV.

### 3.3.9 Attenuated Total Reflectance -Fourier Transform Infrared (ATR-FTIR)

Attenuated total reflectance Fourier transform infrared (ATR-FTIR) spectra was conducted with a Nicolet Nexus 870 FTIR spectrometer equipped with a single reflection diamond crystal attenuated total reflectance (ATR) accessory. External reflection FTIR accessory with an angle of incidence 40° and a mercury cadmium telluride (MCT/A) detector were employed for all ATR spectral acquisitions. NHT, blank chitosan nanoparticles and NHT-loaded chitosan (1:1-3:1) nanoparticles were analysed by ATR. The tiny amount of samples were dropped on the top of a diamond crystal and secured with a high-pressure clamp. The product after DSC measurement of NHT was detected by ATR as well. All spectra were collected at a resolution of 8

$cm^{-1}$ and 64 scans in the range of 4000-600 $cm^{-1}$ and analysed using the spectral analysis software OMNIC (Nicolet Instrument Corp.).

### 3.3.10 BET Specific Surface Area

BET nitrogen adsorption is one of the most common used methods to acquire information about the pore size and specific surface areas of powders consisting of agglomerates of smaller particles. The specific surface area of powders can be evaluated through BET equation, which assumes that the gas volume of monolayer adsorption can be obtained by measuring the adsorbed gas quantity. In this study, the specific surface area of CS nanoparticles and NHT-loaded CS nanoparticle powders were determined by BET surface area measurement. Nitrogen adsorption measurements were carried out at 77 K using an ASAP 2010 volumetric adsorption analyser from Micromeritics (Norcross, GA). Before the measurements, the samples were degassed under vacuum overnight at 473 K.

### 3.3.11 Drug Incorporation

Drug loading was calculated based on the ratio of amount of drug entrapped in the nanoparticles to the total amount of nanoparticles obtained after lyophilisation, which was calculated using Eq.3.6,

$$\text{Drug loading}(\%) = \frac{\text{total drug} - \text{free drug}}{\text{nanoparticle weight}} \times 100 \qquad \text{Eq. 3.6}$$

As the drug loaded nanoparticles were washed with diethyl ether, the amount of washed drug in diethyl ether was calculated to obtain the actual drug loading in nanoparticle. Initially the nanoparticles were separated from the oil phase by centrifugation, free drug was extracted into an excess of PBS (1:5) solutions and quantified by UV spectrophotometry (Beckman Coulter DU 800UV/Vis Spectrophotometer, USA) at the maximum absorbance wavelength of 258 nm. There

was a possibility that a small amount of non-entrapped NHT leached into diethyl ether during washing. To calculate this amount, a 4 mL diethyl ether supernatant after centrifugation was mixed with excess amount of PBS (1:5) under vigorous shaking and kept it an open air at 30°C for 20 minutes for complete removal of diethyl ether. Finally the amount of free drug was measured by UV spectrophotometry. All the free drugs during the diethyl ether three times wash were collected and recorded. The final total free drug was the sum of the free drug in the oil supernatant and ether supernatants. Each sample was repeated three times.

## 3.4 RESULTS AND DISCUSSION

### 3.4.1 Preparation of Nanoparticles

W/O emulsion crosslinking method was applied to prepare blank CS and NHT-loaded CS nanoparticles. Glutaraldehyde was used as a crosslinking agent for primary amines. The mechanism of this method is to utilize the Schiff base reaction where 2 units of amine group of CS is crosslinked with one aldehyde molecule, forming a characteristic imine (N=C) bond between aldehyde carbon and primary amine (Scheme 3.1). The mixture of NHT and CS solution at a series of mass ratios (NHT: CS) from 1:1 to 3:1 at similar fixed conditions was added into the paraffin oil under vigorously homogenization. During this process, it was observed that a clear emulsion changed to opalescent visually upon adding water phase solution into oil phase, which indicated formation of a suspension of nanoparticles. Flocculation was reported to occur on addition of high molecular weight polymer into a dilute dispersion (Abdelwahed, Degobert, Stainmesse, & Fessi, 2006; Gan et al., 2005), so we chose LMW chitosan to improve physical stability and reduce aggregates among nanoparticles. The nanoparticles were dried by freeze-drying through sublimation and desorption under vacuum. Primary physical and chemical characteristics of nanoparticles, were

maintained from freeze-drying, which can also keep the nanoparticles samples under acceptable relative humidity and benefit long-term stability (Abdelwahed et al., 2006).

Both the blank CS nanoparticles and NHT-loaded CS nanoparticles obtained in this experiment showed a light yellow coloration of the powder. In this study, volume ratios of 2% CS solution and glutaraldehyde was 5:1, producing the size of nanoparticles that was below 200 nm and polydispersity <1 (Table 3.2). Weak acid solution is expected to produce the lowest diameter CS nanoparticles (J. Xu et al., 2012). Thus, inter- and intra-molecular cross-linkages of CS and negatively charged glutaraldehyde (Sawyer et al., 1987) were processed in a weak acidic environment of 2% acetic acid. The mean diameter of the blank CS nanoparticles obtained from this work was 167.6±10.2 nm (Table 3.2).

Emulsification behaviour of surfactants mainly relies on their chemical structure especially the hydrophilic-lipophilic balance (HLB). It has been reported that the average diameter of particle increases with increasing HLB value (Kobiasi, Chua, Tonkin, Jackson, & Mainwaring, 2012). Span 80 was selected in this study because of its HLB value of 4.3 (as it is constituted of a small hydrophilic group and one hydrophobic oleate chain), which is favourable for producing desired particle size in paraffin oil. Small hydrophilic group increases steric hindrance and curvature, stabilizing the smaller droplet sizes by reducing surface tension and favoured the formation of stable CS droplet size. We chose the fastest stirring speed (5000 rpm) in this study to obtain the desired size of nanoparticles as there is a relationship between stirring speed and particle size (Ajun, Yan, Li, & Huili, 2009). The relationship between pH and formation of the nanoparticles showed that the mean diameter of the blank CS nanoparticles tend to decrease with increase in pH (J. Xu et al., 2012), and

the CS nanoparticles prepared in weak acid solution were expected to have a minimum diameter. Final nanoparticles were obtained by freeze-drying owing to the advantages of drying samples through sublimation and desorption under vacuum. It not only maintains the primary physical and chemical characteristics of nanoparticles, it also keeps acceptable relative humidity for nanoparticle samples and benefits long-term stability (Abdelwahed et al., 2006).

In order to obtain less aggregated and uniform size of NPs, we anticipated that the application of ultrasonic agitation during homogenization may overcome aggregation and produce narrow particle size distribution. Homogeneity is believed to be a process of equilibrium between aggregation and mixing. Theoretically, homogenization is slower than the process of aggregation, which results in larger nanoparticles; on the other hand, if the time scale of homogenization is faster than aggregation, the nanoparticle size is supposed to be smaller and less aggregated (Karnik et al., 2008). We tended to use ultrasonic agitation to extend the time scale of aggregation during homogenization (Figure 3.1). The application of ultrasonic agitation obtained consistent blank CS particles with diameters around 30 nm, however, the emulsion was too stable to recover the blank CS nanoparticles. We were interested in exploring reasons for this phenomenon. During the ultrasonic emulsification of two immiscible liquids, coalescence occurred, which probably contributed to the collision of small droplets and formation of the continuous phase (Gaikwad & Pandit, 2008). As a result, it was impossible to collect nanoparticles from continuous emulsion phase.

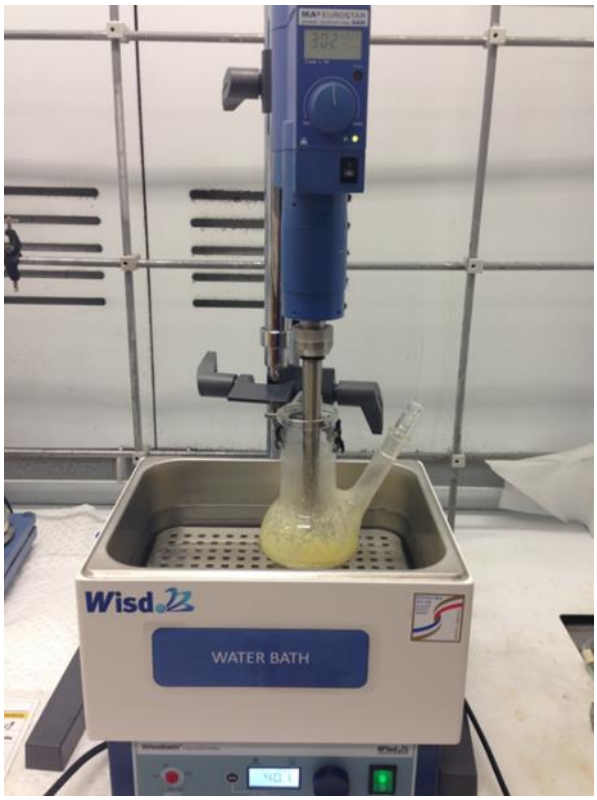


Figure 3.2 Picture of manufacturing of nanoparticles using ultrasonic agitation during homogenization

### 3.4.2 **SEM & TEM**

SEM was applied to observe the shape and surface morphology. Both formulations of blank CS and NHT-loaded CS (1:1) showed nearly spherical shape and smooth surface (Figure 3.3A-B), which suggested that w/o emulsion crosslink technique is successful to obtain a large quantity of nanoparticles. However, the rougher surface was noted on the particles when the weight ratios of NHT and CS were over 2:1 (Figure 3.3 C, D), suggesting that NHT was accumulated on the CS nanoparticle surface with aggregation or adhesion among nanoparticles to some extent. All the size of nanoparticles from SEM images were found to be <1 μm. The similar results were also obtained from TEM that blank CS nanoparticles showed nearly spherical shape and

smooth surface. NHT-loaded CS nanoparticles had a rougher surface (Figure 3.4B) compared with those of blank CS nanoparticles.

A shortcoming of nanoparticles was that serious aggregation occurred among nanoparticles, which is also a common challenge within the nano-scale range due to high surface energy. Additionally, freeze drying made nanoparticles size increase after drying according to the report by Dudhani (Dudhani & Kosaraju, 2010) because of aggregation from the strong inter- and intra-molecular hydrogen bond.

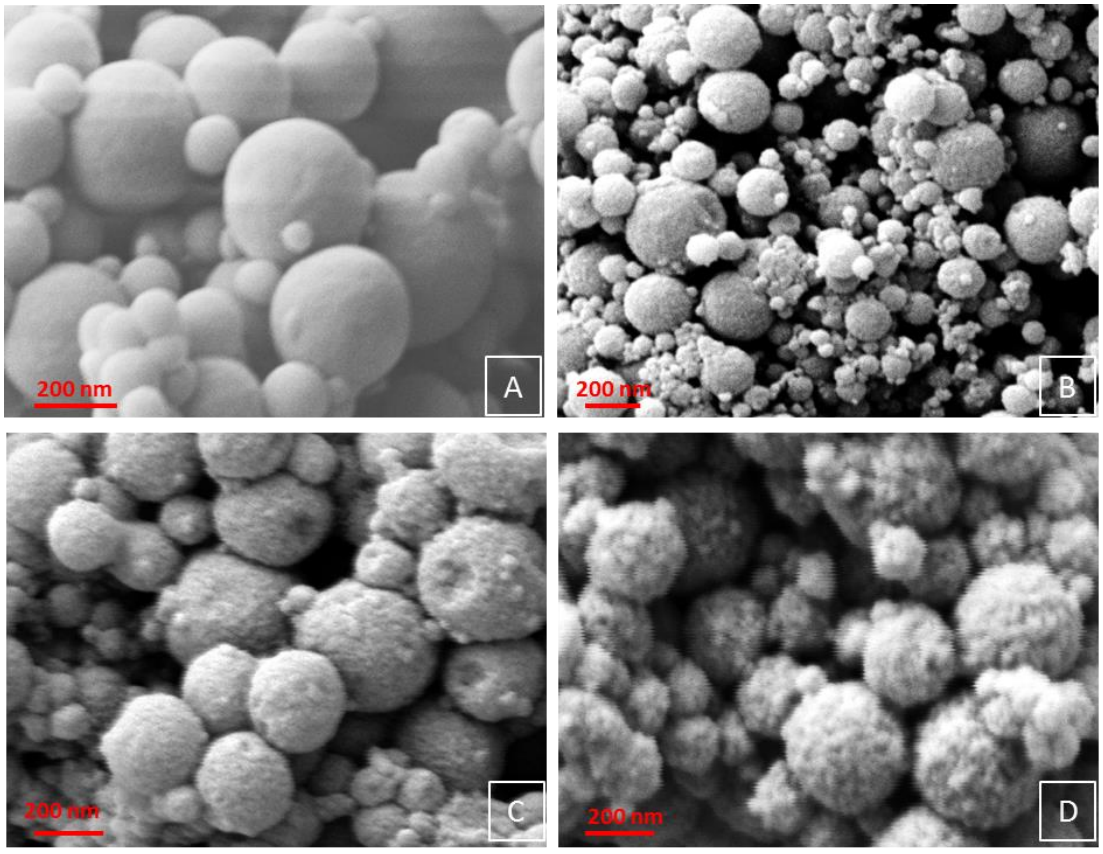


Figure 3.3 SEM images of different ratios of drug and CS (A) Blank CS nanoparticles; (B) Drug-loaded CS nanoparticles (1:1); (C) Drug-loaded CS nanoparticles (2:1); (D) Drug-loaded CS nanoparticles (3:1)

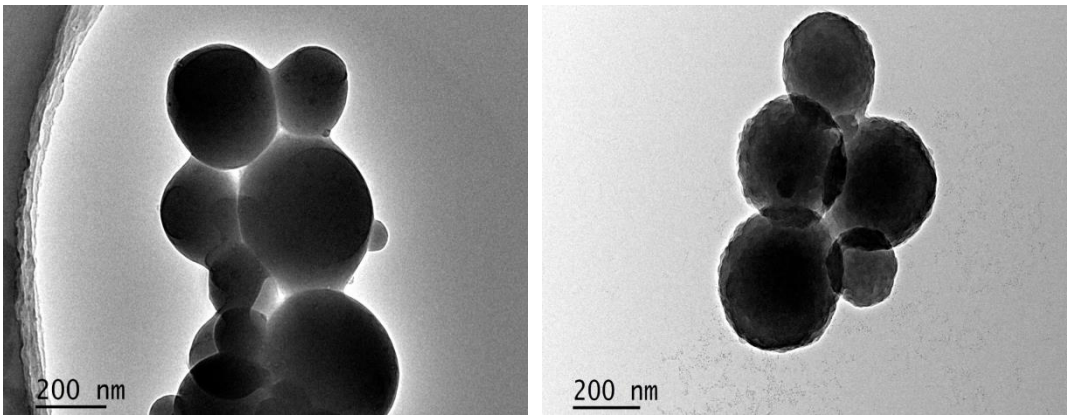


Figure 3.4 TEM images of (A) blank CS nanoparticles; (B) NHT-loaded CS (3:1) nanoparticles

### 3.4.3 Particle Size and Size Distribution

Figure 3.5 and Table 3.2 showed the mean particle size and size distribution of CS nanoparticles and NHT loaded CS nanoparticles from the DLS. DLS analysis of CS nanoparticles from 1:1 to 3:1 showed unimodal size distribution. The average diameter of the blank CS nanoparticles was 167.6±10.2 nm with PDI of 0.084±0.03. Mean particle size of NHT-loaded CS nanoparticles increased with the increased mass ratios of NHT and CS as increased solids within increased concentration of the NHT contribute to a larger droplet during the formation of nanoparticles under other same conditions. Specifically, the average particle size of NHT-CS (1:1) nanoparticles was 198.3±7.5 nm with PDI of 0.161±0.05. The average size of NHT-CS (2:1) nanoparticles increased moderately to 204.4±3.9 nm with PDI of 0.106±0.071, while NHT-CS (3:1) nanoparticles demonstrated a maximum particle size of 411.2±63.4 nm with a PDI of 0.393±0.526. It indicated individual particles were in the nano range (<1 μm) obtained in this work, which were suitable for administration of delivery to deep lungs. It should be noted that the sizes of nanoparticles determined by DLS (Table 3.2) were different from those measured by SEM (Figure 3.3) due to two different methods being applied. DLS is based on laser light scattering to give a particle size measurement, while SEM is based on direct imaging using back-scattered electrons.

The size observed from SEM images was slightly higher than the size measured by DLS. It is possible that aggregation as seen in Figure 3.3 and Figure 3.4 arising from the strong inter- molecular hydrogen bonding was not broken because we used dry powder of nanoparticles during sample preparation for SEM analysis. CS is a hydrogel polymer, so CS nanoparticle clusters tend to be formed by self-adhesion through Brownian motion among nanoparticles themselves. In addition, intra- or intermolecular hydrogen tends to lead intra- or intermolecular aggregation of particles in polar solvent (Berger, Reist, Mayer, Felt, & Gurny, 2004) (X.-G. Chen, Lee, & Park, 2003). The formation of CS self-aggregates was confirmed by SEM and TEM (Figure 3.3, Figure 3.4).

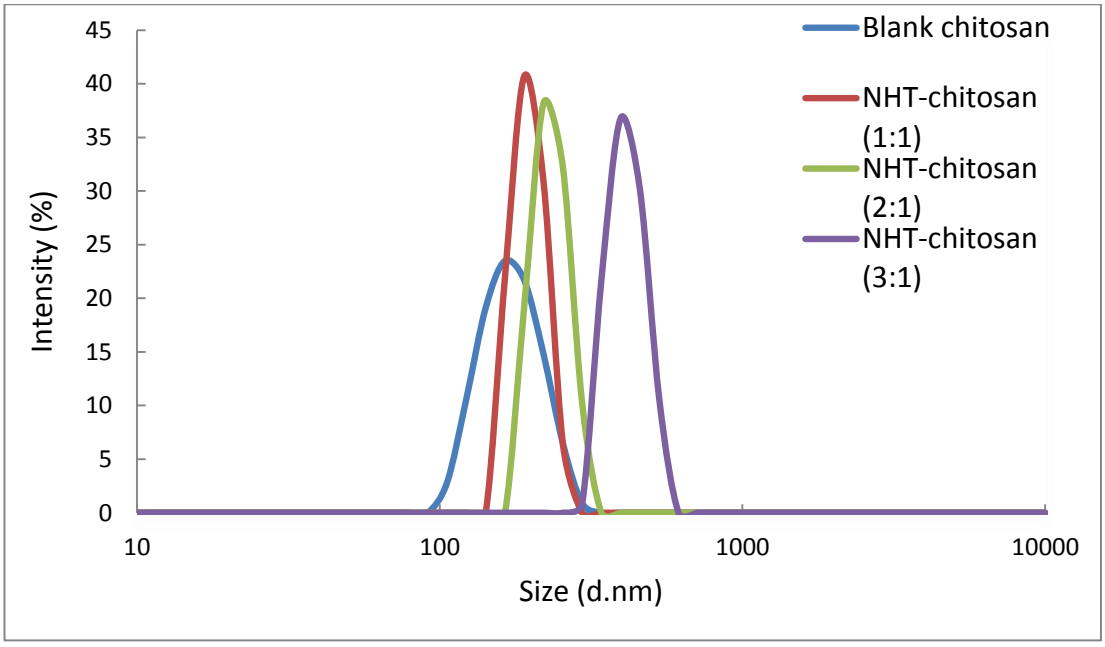


Figure 3.5 Comparable particle size distribution between blank CS nanoparticles and different weight ratios of NHT to CS nanoparticles from 1:1 to 3:1 (n=3)

Table 3.2 Characteristics of nanoparticle prepared by different ratios of NHT and CS (n=3)

| | z-average size (d.nm) | PDI | Zeta potential (+ mV) | pH |
|---|---|---|---|---|
| blank | 167.6±10.2 | 0.084±0.03 | 20.1±1.4 | 5.83 |
| NHT-CS | 198.3±7.5 | 0.161±0.06 | 19.0±1.2 | 4.55 |
| NHT-CS | 204.4±3.9 | 0.106±0.07 | 14.2±0.7 | 3.83 |
| NHT-CS | 411.2±63.4 | 0.393±0.52 | 12.2±0.4 | 3.81 |

As the aggregates of nanoparticles are above one micron (seen by SEM), the actual size of them cannot be measured properly by the DLS and therefore, the size of aggregates was determined using a Mastersizer. The median diameter (D [v,50]) of the aggregates varied between 3.7 and 4.7 µm (Table 3.3), which are within the respirable range (<5µm) and suitable for DPI formulations. Therefore the particles prepared in this study are the mixture of both individual nanoparticles and agglomerates of nanoparticles.

Table 3.3 Aggregate size distribution, represented by volume fractions 50%, D (v, 50)

| | D(v,50) (d.µm) |
|---|---|
| blank CS | 3.73±0.01 |
| NHT-CS (1:1) | 4.23±0.04 |
| NHT-CS (2:1) | 4.20±0.04 |
| NHT-CS (3:1) | 4.73±0.03 |

### 3.4.4 **Zeta Potential**

Zeta potential is associated with the stability of nanoparticles as well as the appropriate dispersion *in vivo*. The surface charge measured by Zetasizer showed all nanoparticles (blank and NHT loaded) were highly positively charged and the amount of charge decreased with increasing NHT concentration in the nanoparticles (Table 3.4). The linearity trend (Figure 3.6, $r^2$= 0.8783) in decreasing surface charge with increased drug loading indicated that the increasing surface coverage of CS nanoparticles with NHT caused the positive charge on nanoparticles to reduce. The reduction of surface charge with drug loading at 1:1 ratio was not significant compared to the blank CS nanoparticle; however, it was highly significant ($P<0.05$) with higher concentration of drug loading (2:1 and 3:1), which implied that the nanoparticle surface positive charges were masked (Muhsin et al., 2016) due to the increased accumulation of NHT on the surface. Although the adhered NHT on the particle surface could not be visible

at 1:1 ratio, higher concentrations of NHT showed a significant amount of drugs are adhered on the particle surface confirmed by SEM images. In addition, as the NHT has a negative charge due to the presence of the tartaric acid salt, the positive charge of the CS amino groups was reduced with increased concentration of NHT in the formulation. Meanwhile, as presented in Table 3.4, surface charges of nanoparticles reduced with increased concentration of NHT and shifted to negative charge at a fixed pH 6. This result suggested that under conditions of reduced protonation of the CS the nanoparticles containing NHT would tend to agglomerate since it is regarded that a low zeta potential (in this case -1.5 to -4.5 mV) would not favour dispersion of the nanoparticles.

Table 3.4 Comparison of zeta potential of nanoparticles prepared at different conditions at pH=6 (n=3)

| **Nanoparticles** | **Zeta potential (mV) at pH 6** |
|---|---|
| blank CS | 18.9±0.3 |
| blank CS-0.3 | 12.8±0.7 |
| blank CS-0.9 | 8.4±0.1 |
| CS NHT (1:1) | -1.50±0.3 |
| CS NHT (1:2) | -3.1±1.1 |
| CS NHT (1:3) | -4.5±1.9 |

NB: blank CS-0.3 means CS particles prepared by 0.3 mL glutaraldehyde; blank CS-0.9 means CS particles prepared by 0.9 mL glutaraldehyde; the rest of particles were prepared by 0.6 mL glutaraldehyde.

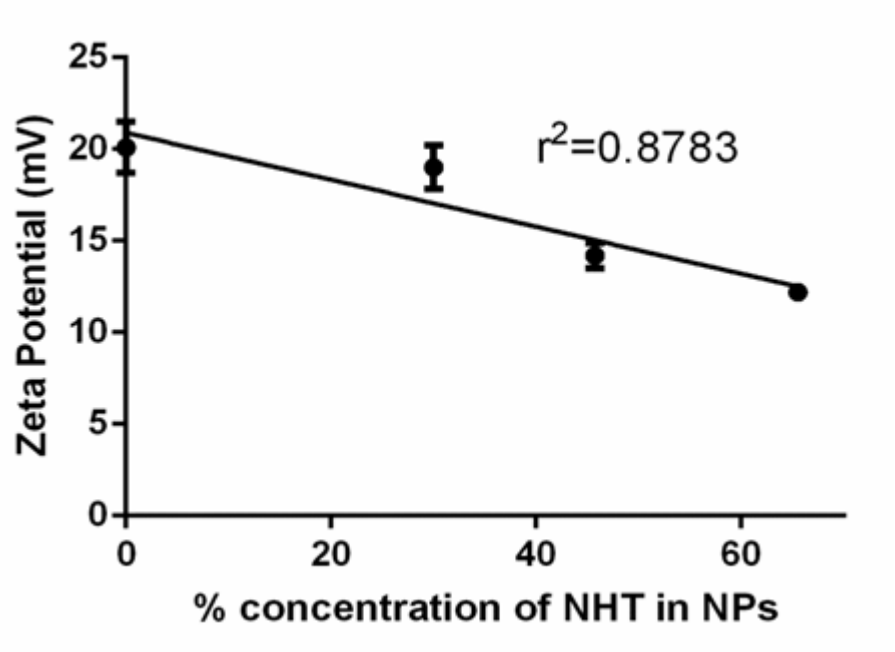


Figure 3.6 The relationship between zeta potential and drug loading

To further study the role of pH on the nanoparticles, we measured the zeta potential of blank CS nanoparticles at different pH levels and the data are presented in Figure 3.7. Blank CS nanoparticles were applied to test the effect of pH on the particle surface charge. The zeta potential was measured in 0.1 mM potassium chloride solution adjusted with 0.1 N NaOH or 0.1 N HCl. A good linearity with a coefficient of determination of 0.9840 was observed where the zeta potential of nanoparticles reduced with increased pH when pH was between 3 and 6 (Figure 3.7). A fixed amount of glutaraldehyde was used for crosslinking, so the number of available amino groups on the CS for protonation was constant. The decrease in zeta potential therefore follows the reduction in the protonation as pH increases. The positive surface charge of CS in acidic medium due to protonation of the amine groups in CS showed repulsive forces (Kiang, Wen, Lim, & Leong, 2004) between nanoparticles, which support these findings. The large amount of drug accumulated on the particle surface resulted in reduced surface positive charge favouring agglomeration. It clearly demonstrated that the pH has a significant effect on the surface zeta potential. In addition, as presented

in Table 3.4**,** when different amount of glutaraldehyde was used for crosslinking, the zeta potential at fixed pH of 6 varied with the degree of crosslinking. The higher intrinsic surface positive charge on the blank CS particles rendered less agglomeration (Gazori et al., 2009) due to the repulsive forces and this resulted in higher FPF of blank CS particles. As a result, the amount of 0.6 mL glutaraldehyde was selected for preparation of CS nanoparticles in this study because of higher postive surface charge on the blank CS nanoparticles. As discussed above, both the effect of pH and degree of crosslinking could affect the zeta potential, which eventually affected the dispersibility of nanoparticles. Therefore, it could be concluded that the surface charge on the CS nanoparticles are highly mediated by an electrostatic interaction in addition to hydrogen bonding or hydrophobic interactions involved in the association process. The positive surface charge of CS in acidic medium due to protonation of the amine groups in chitosan showed repulsive forces (Kiang et al., 2004) between nanoparticles, which support our findings.

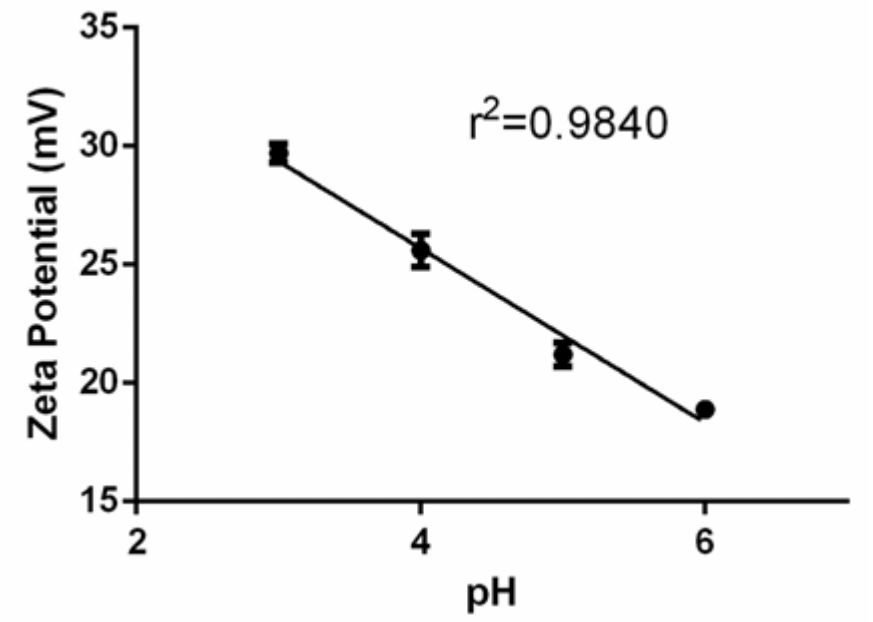


Figure 3.7 The Zeta Potential of blank chitosan nanoparticles under different pH

### 3.4.5 **DSC**

The DSC thermograms of the blank CS, pure NHT and NHT-loaded CS with different drug to polymer weight ratios from 1:1 to 1:3 are shown in Figure 3.8. A broad endothermic peak of CS nanoparticles found to be onset at 82.1°C (peak at 89.04°C), corresponding to loss of bound water from CS nanoparticles (Dudhani & Kosaraju, 2010; Zhang, Yang, Tang, Hu, & Zou, 2008). Pure NHT showed a sharp endothermic peak at 91.0 °C due to a crystalline melting point. However, this peak disappeared during the cool/reheat circle. The deep changes in drug thermal behaviour were found in thermograms of NHT-loaded CS nanoparticles, as the typical peaks of NHT disappeared in terms of NHT to CS mass ratios between 1:1 and 3:1 (Figure 3.8). The endothermic peaks, which were similar to the peaks from CS transition, shifted to a lower temperature with the NHT-loaded CS nanoparticles. It is considered that this is a proof of incorporation of NHT into the matrix of CS nanoparticles, but NHT was also loaded onto the surface of CS nanoparticles as SEM images (Figure 3.3) show. The possible reasons for absence of NHT endothermic peak were: 1) NHT was dissolved into CS nanoparticle matrix as a solid solution and did not crystallize; 2) NHT was converted to its amorphous form within nanoparticles (Chauhan, et al., 2012); 3) the characteristic peaks of NHT and CS were overlapped, so the combined peaks shifted to lower temperature with increasing NHT content. The same phenomenon of disappearance of NHT melting peak from drug loading formulation was also reported by Sneha (Chauhan, et al., 2012).

Inspired by DSC results, the aluminium pan of NHT was cut to be observed under microscope. It was noted that there was a sticky brown gel in the aluminium pan instead of white powder which is the original status of NHT (Figure 3.9). The NHT after heating appears to be liquid rather than crystalline under the microscope. This

explains why there is no crystallization exotherm when cooling from the melt and the endothermic peak of NHT disappeared after first heating cycle. In order to obtain more knowledge of this product, the FTIR was conducted and demonstrated in the following section (3.4.8).

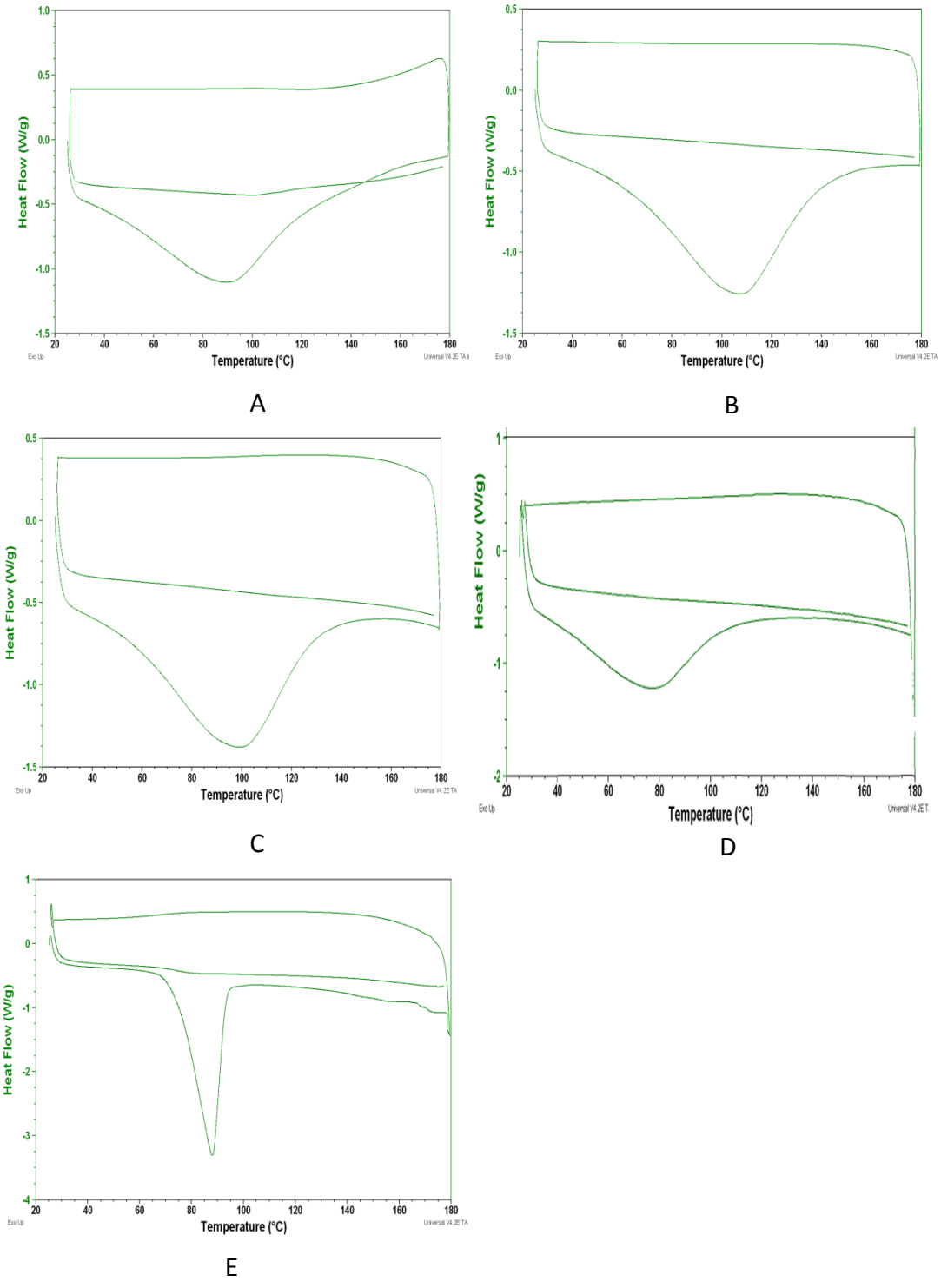


Figure 3.8 DSC (exothermic up) during heat, cool, heat runs of (A) blank CS particles; (B) NHT-loaded CS particles (1:1); (C) NHT-loaded CS particles (2:1); (D) NHT-loaded CS particles (3:1); (E) pure NHT powder

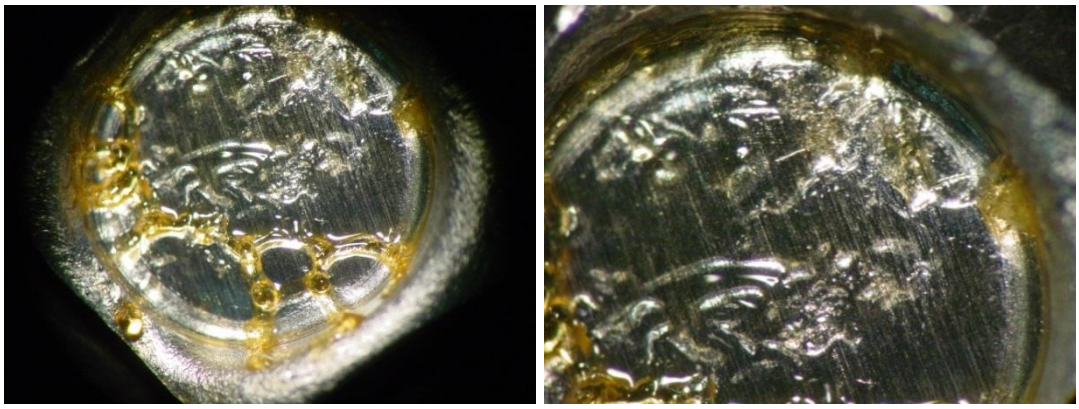

Figure 3.9 The image of NHT under the microscope after DSC heat/cool/heat test

### 3.4.6 **XRD**

Figure 3.10 shows X-ray diffraction patterns of blank CS and NHT-loaded CS nanoparticles. There was only a broad peak in the diffractogram of blank CS at 2θ at 19.04°, which was characteristic of CS as an amorphous polymer. The region under the broad peak was associated with the amorphous phase. In the X-ray diffractogram of pure NHT powder, several sharp identical peaks were observed at the angle of 2θ at 17.50°, 22.96°, 26.06° and 33.24°, indicating that the NHT was existing as the crystalline material. After NHT loading, the diffraction intensities were becoming weaker, which suggested decreased crystallinity within the nanoparticles. Interestingly, the same conclusion was reached from DSC. No characteristic peaks of crystalline NHT were recorded in the XRD spectra of NHT-loaded CS nanoparticles with regards to three different ratios of NHT formulations. Several researchers also reported similar phenomenon ie. the absence of drug XRD peaks after encapsulation of drugs with polymers (Papadimitriou, Bikiaris, Avgoustakis, Karavas, & Georgarakis, 2008). It may be explained that NHT formed an amorphous dispersion within nanoparticles due to interactions that occurred between NHT and drug carriers. This case commonly occurred with amorphous polymers as drug carriers (Karavas, Georgarakis, & Bikiaris, 2006), such as CS. Another potential reason is that NHT

converted to amorphous form attributed to the intermolecular interactions between NHT and CS.

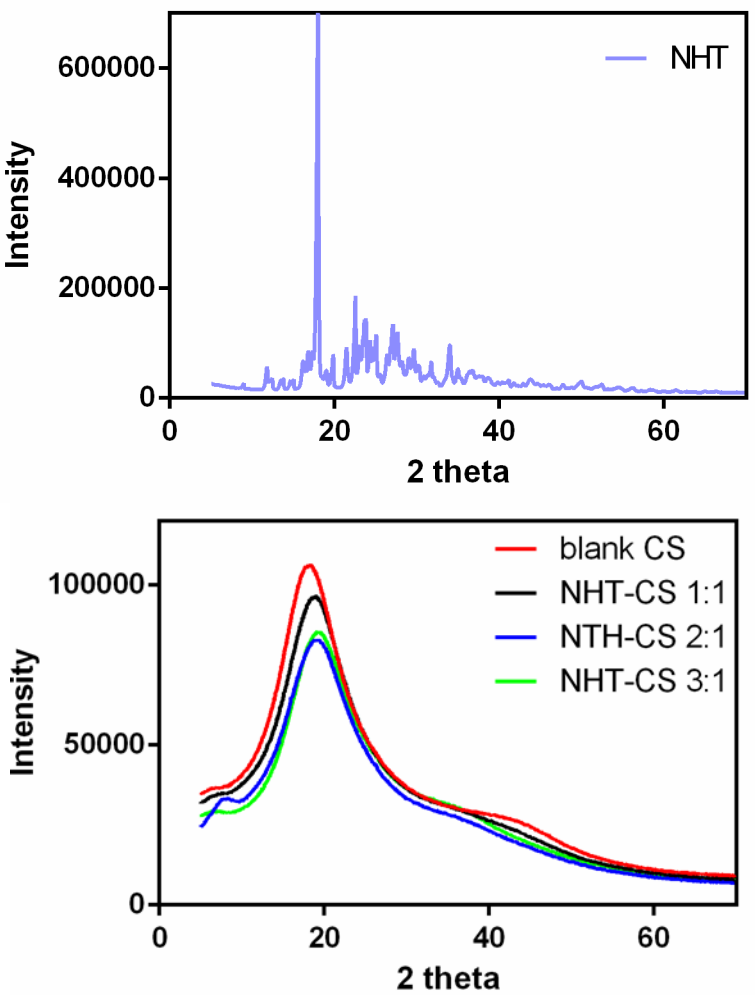


Figure 3.10 The X-ray powder diffractions of (A) NHT; (B) blank CS nanoparticles and NHT-loaded CS nanoparticles

### 3.4.7 **XPS**

As XPS is a surface-specific technique (typically measuring the atomic composition of the first 5 nm) it has been used to determine if there was enrichment or depletion of the NHT at the surface of the CS nanoparticle. Such surface segregation or depletion would affect the release properties of the NHT. The XPS spectra in the C1s, N1s and O1s regions of CS, CS particles, NHT and the particles after loading with NHT at the ratios of 1:1, 2:1 and 3:1 (with respect to the mass of CS) have been analysed and

Table 3.5summarizes the atomic concentrations from these spectra. These can be compared with calculated values from the materials based on composition for all atoms other than hydrogen (which is not detected by XPS). In principle it is difficult to distinguish between CS and NHT based on survey scan data that generate atomic compositions of C, N and O as there are only small differences between the compositions (comparing the calculated values in row 1 and row 4 of Table 3.5). However, when the expanded N1s multiplex spectral data were collected it was found that there was a major difference between CS and NHT due to the ability of XPS to distinguish N+ from N due to a binding energy shift of 2.5eV. It may be seen from Table 3.5 that [N+] is very low in CS from both the starting material and the particle whereas it constitutes, in theory, all of the [N] in NHT and 80% in the actual samples. The concentration of 0.8% [N+] from the original CS and 0.4% [N+] from the particle arise from protonation in the course of extraction from chitin and in subsequent dissolution in acetic acid for particle preparation. It has been noted that solubilisation of CS of MW 295 kDa requires a degree of protonation of 0.5, but this will be lower for the CS studied here which has a MW of 50 to 195kDa.

The composition of NHT has been studied and comprises a single molecule of nicotine which is complexed with two molecules of tartaric acid. One carboxylic acid group from each tartaric acid molecule is hydrogen bonded to the other, leaving one carboxylic acid group to bind to the protonated pyridine and N-methyl pyrrolidine units of nicotine (Perfetti, 1983). The measured value of 0.8 for the ratio $[N^+]/[N1s]$ indicates that not all nicotine groups are associated with two tartaric acid molecules and examination of the N1s multiplex spectrum shows the presence of a weak band at 399.2eV which was consistent with an uncharged pyridine. It must also be recognized

that the NHT may have undergone slight decomposition under the X-ray conditions so the theoretical value is not attained.

In the particle, the surface concentration of NHT compared to the CS may be measured by the ratio of $[N^+]$/[N1s]. If the surface were to be totally covered with NHT then the ratio would be 0.8. When there is no NHT on the surface then it would be given by the value for CS particles i.e., 0.18. The relative amount of charged nitrogen to total nitrogen $[N^+]$/[N1s] may therefore be used as a comparative measure of surface versus bulk composition of NHT in the particle and this was shown in Figure 3.11. In this figure, the value for the blank CS particle has been subtracted, resulting in a linear plot indicating that the surface concentration of NHT is consistent with the bulk concentration i.e., there is no preferential surface segregation of the drug. Thus in the SEM micrograph Figure 3.3D (NHT: CS = 3:1) where there was apparently complete surface coverage of the CS by NHT, the XPS result indicated that there was still 34.4% CS at the surface (i.e. within the first 2nm). Thus the particle is a true solid solution of the two components at all three concentrations studied with neither component acting as an encapsulant. This is consistent with the absence of any crystalline NHT in the particles. This morphology is important when considering the process of *in vitro* nicotine release since NHT is instantly accessible to the PBS solution.

Table 3.5 Calculated and measured atomic concentrations from XPS analysis

| Sample | C1s | N1s | O1s | $[N^+]$ | [O-C=O] | $[N^+]/[N1s]$ |
|---|---|---|---|---|---|---|
| Chitosan calc. | 54.8 | 8.9 | 36.3 | 0.0 | 0.0 | 0.0 |
| Chitosan meas. | 63.0±3.1 | 7.3±0.4 | 28.6±1.4 | 0.8±0.04 | 0.0 | 0.11±0.01 |
| Chitosan NP | 69.4±3.5 | 2.2±0.1 | 28.4±1.4 | 0.4±0.02 | 1.5±0.07 | 0.18±0.01 |
| NHT calc. | 56.2 | 6.3 | 37.5 | 6.3 | 12.5 | 1.0 |
| NHT meas. | 59.1±3.0 | 5.4±0.3 | 35.5±1.8 | 4.3±0.21 | 10.5±0.53 | 0.80±0.04 |
| 1:1 NP | 71.2±3.6 | 2.3±0.1 | 26.4±1.3 | 1.1±0.06 | 2.8±0.14 | 0.48±0.02 |
| 2:1 NP | 66.0±3.3 | 2.5±0.1 | 31.5±1.6 | 1.6±0.08 | 4.7±0.23 | 0.64±0.03 |
| 3:1 NP | 65.0±3.2 | 2.8±0.1 | 32.2±1.6 | 2.0±0.10 | 5.2±0.26 | 0.71±0.04 |

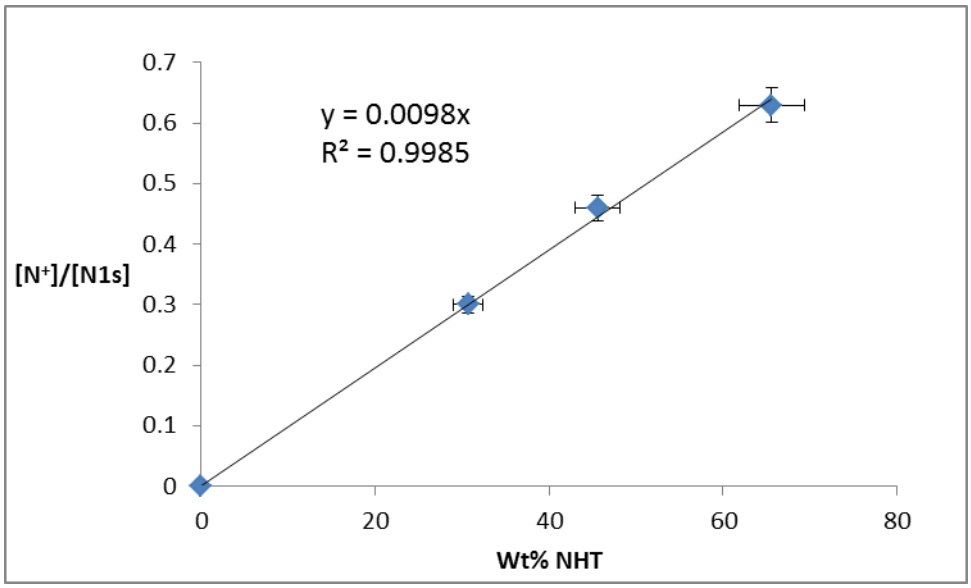


Figure 3.11 Plot of the XPS atom ratio of charged nitrogen [N+] to total nitrogen signal [N1s] from the NHT-loaded particles after subtraction of the signal from a blank CS particle versus the analysed bulk concentration of NHT in weight %.

### 3.4.8 **ATR-FTIR**

Several characteristic bands of CS raw material can be identified from absorbance FTIR spectra (Figure 3.12A) of the original material. The overlapped peaks of the O-H and N-H stretching were recorded at 3400 $cm^{-1}$. At 2870$cm^{-1}$, the peak of $CH_2$ stretching vibration was recorded, which corresponded to pyranose ring. The

characteristic peaks of CS were at 1656 $cm^{-1}$ and 1565 $cm^{-1}$ with high intensity which were attributed to the vibration of amide I (C=O) band and amide II (N-H) band, respectively from the residual N-acetyl groups of chitin. The peak of asymmetric stretching of C-O-C bridge at 1109 $cm^{-1}$ and skeletal vibration involving the O-C-O stretching at 1059 $cm^{-1}$ and 1026 $cm^{-1}$ were assigned to its polysaccharide structure, which is agreement with reports (Peniche et al., 1999). For crosslinked CS nanoparticles, 2 units of amine group of CS is crosslinked with one aldehyde molecule to form a characteristic imine (N=C) bond between aldehyde carbon and primary amine based on the Schiff reaction. However, the characteristic absorbance of C=N stretching, usually ranging between 1600-1700 $cm^{-1}$, was not seen, and this may be associated with overlapping with amide I band. The absorption band at 1715 $cm^{-1}$ was aldehyde group, which results from the polymerization and subsequent crosslinking of glutaraldehyde or possibly from one residual aldehyde of glutaraldehyde that did not react with two amino groups in the CS. These reactions are competitive with the Schiff reaction for crosslinking, indicating that the chemistry of the resulting CS network is complex as recently reported by Liu et al. (C. Liu, Thormann, Claesson, & Tyrode, 2014). The FTIR spectra for NHT (Figure 3.12B) showed an absorption band at 1716 $cm^{-1}$, which was the characteristic band (C=O) of –COOH from NHT. The presence of $-COO^-$ caused a specific band at 1565 $cm^{-1}$. The absorption bands of 1461 $cm^{-1}$, 1268 $cm^{-1}$ 1192 $cm^{-1}$ and 1131 $cm^{-1}$ were associated with O-H bonding and C-O stretching.

The entrapment of NHT into CS nanoparticles was also investigated by FTIR analysis of NHT-loaded nanoparticles with mass ratios between 1:1and 3:1. The obtained spectrum was presented in Figure 3.12B as well. It showed carboxyl peaks of NHT slightly shifted after encapsulation with CS, which was obscured with aldehyde group

at 1719 $cm^{-1}$. In addition, the distinctive absorption bands of amide I, amide II from CS nanoparticles were compromised with NHT, causing a merged absorption band at 1597 $cm^{-1}$ with different intensities affected by the mass ratio of entrapped NHT.

Both DSC and XRD profiles showed that NHT converted to an amorphous form or was present as the nanodispersion in CS nanoparticles. In order to confirm the significant change of NHT in the nanoparticle, FTIR was also employed to detect any possible physicochemical interaction that occurred between the NHT and CS or glutaraldehyde crosslinks from the frequency shifts or splitting in absorption peaks. In this study, we only used one NHT-loaded CS (3:1) nanoparticles formulation as an example. Theoretically, NHT-loaded CS (3:1) nanoparticles were constituted with CS, NHT and glutaraldehyde. The subtraction spectrum (Figure 3.12C) of unloaded CS nanoparticles from the spectrum of NHT-CS (3:1) nanoparticles containing 66% NHT should be comparable to the spectrum of pure crystalline NHT. Surprisingly, it was found that subtracted IR spectrum of blank CS nanoparticles from NHT-CS (3:1) nanoparticles showed a big difference from the IR spectrum of pure NHT. At the same time, the product of NHT after DSC test was also measured by FTIR to distinguish the possible change in chemical structure that occurred to NHT when it experienced heat-cool-heat DSC cycle. Compared with pure NHT powder, FTIR spectrum (Figure 3.12C) of NHT after DSC kept the characteristic peaks of -COOH and -COO- at 1773 $cm^{-1}$ and 1601 $cm^{-1}$, respectively. The bands of O-H and C-O stretching were shifted to lower frequency. However, IR spectrum of unloaded CS subtracted from NHT-CS (3:1) coincided with the spectrum of NHT after DSC test, which strongly confirmed our previous assumption that NHT was encapsulated with CS nanoparticles successfully but some physicochemical changes occurred during this process. Based on the facts discussed above, we concluded that NHT existed as the solid solution in

the CS nanoparticles after encapsulation. This conclusion was consistent with the results from DSC, XRD and ATR-FTIR, as well as supported by the microscope picture of NHT after DSC test (Figure 3.9) which showed the crystalline NHT did not form again on cooling.

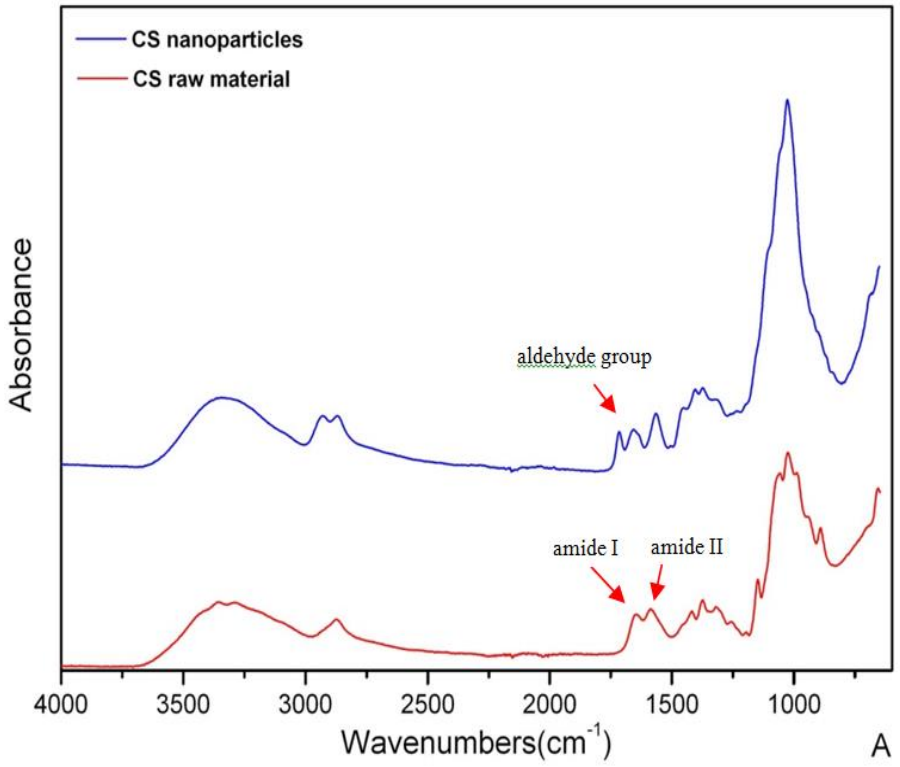

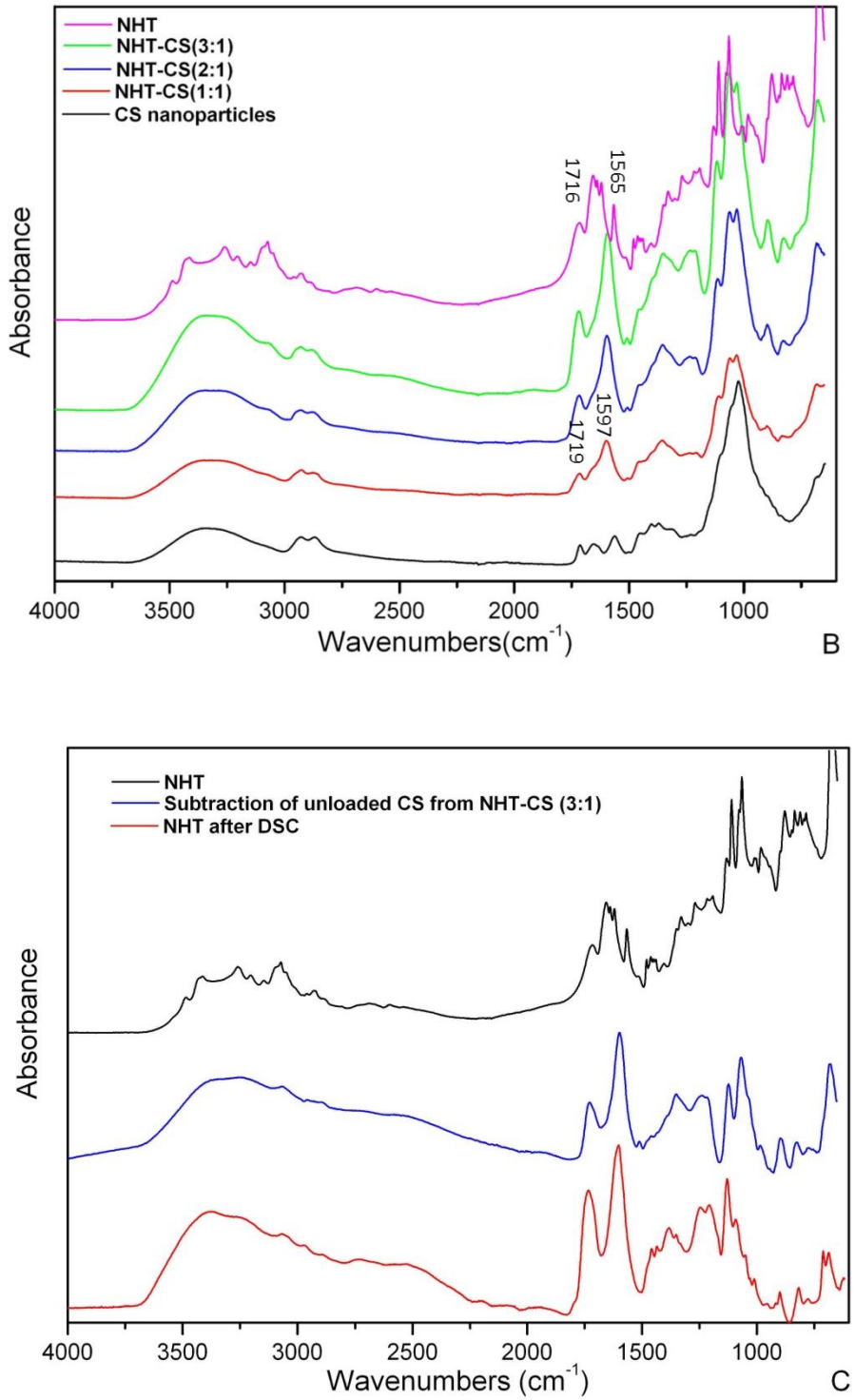


Figure 3.12 Comparisons of FTIR spectrum of (A) CS nanoparticles and CS raw material; (B) NHT-loaded/unloaded CS nanoparticles and NHT; (C) NHT; subtraction of unloaded CS nanoparticles from NHT-CS (3:1) and NHT after DSC test.

### 3.4.9 **BET Surface Area**

Specific surface area of CS and NHT-loaded CS nanoparticles was determined by multipoint BET analysis based on the method developed by Brunauer, Emmett and Teller (Brunauer, Emmett, & Teller, 1938). BET surface area is defined as the ratio A/m of the surface area A to the particles' mass m which is derived from the particles' gas adsorption characteristics shown Eq. 3.7.

$$S_{BET} = \frac{A}{m} = \frac{4\pi r^2}{\rho \cdot \frac{4}{3}\pi r^3} = \frac{3}{\rho \cdot r} \qquad \text{Eq. 3.7}$$

This indicates that specific surface area increases with the inverse of the particle radius and density, assuming all the particles were spherical. In terms of NHT-loaded CS nanoparticles in this study, the density of particles increased with concentration of NHT (Table 3.7), so it is understandable that BET surface area decreased with increased mass ratios of NHT to CS from 1:1 to 3:1 as in Table 3.6. However, blank CS showed smallest BET surface area with 2.5135 ± 0.0202 $m^2/g$ suggesting that serious aggregation occurred between CS nanoparticles compared to those containing NHT. This may have resulted from the smooth surface, which increased cohesion forces among CS nanoparticles.

Table 3.6 BET surface area of blank CS nanoparticles and different weight ratios of NHT to CS nanoparticles from 1:1 to 3:1 (n=3);

| Formulation | BET surface area ($m^2/g$) |
|---|---|
| Blank CS | 3.4222 ± 0.0334 |
| NHT-CS 1:1 | 7.2644 ± 0.0650 |
| NHT-CS 2:1 | 4.6497 ± 0.0493 |
| NHT-CS 3:1 | 2.5135 ± 0.0202 |

### 3.4.10 **Flow Property**

Powder flowability is a critical factor to influence dry power inhalation performance. The flowability of blank CS and different NHT-loaded CS nanoparticles are summarized in Table 3.7. The bulk and tapped density values obtained from the formulations of the blank CS and NHT-CS (1:1) nanoparticles were lower than those obtained from NHT-CS (2:1; 3:1). In terms of NHT loaded nanoparticles, as expected, the more NHT contained into a same amount of formulation, the higher was the density.

CI and HR are two indications to evaluate the powder flowability and respirable fraction. The CI value of < 25% indicates good flowability, while > 25% means poor flowability which is cohesive powder characteristic. In addition, HR value which is less than 1.25 is considered to be good flowability, on the contrast, greater than 1.25 is taken as poor flowabilitly. Either CI or HR is not an absolute number to determine the property of a material; their values would vary depending on the methodology applied to measure them. The CI values of freeze dried nanoparticle powders ranged from 15.4% to 38.9% and HR values were between 1.18 and 1.62. Both formulations of NHT-CS (2:1) (3:1) showed <25% CI and 1.25 HR values, indicating a fluid powder. However, blank CS nanoparticles showed the highest CI and HR values (38.9±0.01%, 1.62±0.01 respectively) with a severe aggregation due to small size, exhibiting poor flowability from cohesive powder. Consequently, the flow properties resulted in this study suggested that higher concentration of NHT to the same amount of CS would reveal better powder flowability, which benefits aerosolization of powders for DPI formulations.

Table 3.7 Physical properties of all CS/NHT-loaded CS nanoparticles tested (mean ± S.D., n = 3)

| | Blank chitosan | NHT-CS (1:1) | NHT-CS (2:1) | NHT-CS (3:1) |
|---|---|---|---|---|
| Bulk density (g/mL) | 0.329±0.01 | 0.364±0.02 | 0.459±0.01 | 0.484±0.01 |
| Tap density (g/mL) | 0.533±0.01 | 0.539±0.01 | 0.572±0.01 | 0.573±0.01 |
| Carr's index | 38.9±0.01 | 31.6±0.01 | 20.0±0.01 | 15.4±0.01 |
| Hausner ratio | 1.62±0.01 | 1.48±0.01 | 1.25±0.01 | 1.18±0.01 |

The results of angle of repose measurements of nanoparticles with and without 10% lactose carriers were shown in Table 3.8. Angle of repose is another general indication for evaluation of the flow properties of powders. The values of angle of repose from nanoparticles without carriers were in the range of 39.9° –50.8°, which was out of the normal acceptable range of 20°–40°. It was observed that the angle of repose reduced with the increased mass contents of NHT to CS nanoparticles. On the other hand, angle of repose decreased significantly after coating 10% lactose carriers, which showed better flow properties compared with corresponding blank CS/NHT-loaded CS nanoparticles without carriers and all the values showed potential good flowability in the range of 26.4°-39.9°.

Table 3.8 Angle of repose of CS/NHT-loaded CS nanoparticles and nanoparticles with 10% lactose carriers (mean ± S.D., n = 3)

| **Drug-loaded chitosan** | **$\theta_1$** | **10% nanoparticles with lactose** | **$\theta_2$** |
|---|---|---|---|
| Blank chitosan nanoparticles | 50.8±0.5 | Blank chitosan | 39.9±0.9 |
| Nicotine-loaded chitosan (1:1) | 49.4±0.3 | Nicotine-loaded chitosan (1:1) | 34.9±3.0 |
| Nicotine-loaded chitosan (2:1) | 44.0±0.9 | Nicotine-loaded chitosan (2:1) | 33.4±0.1 |
| Nicotine-loaded chitosan (3:1) | 39.9±0.9 | Nicotine-loaded chitosan (3:1) | 26.4±0.6 |

### 3.4.11 **Drug Incorporation**

In this study, the drug loading was measured indirectly by measuring the amount of drug remaining in the supernatant (Gomathi et al., 2014). UV spectrophotometry was applied for quantitative analysis of drug loading because direct UV spectrophotometry is applicable to the determination of nicotine quantitatively and its related compounds (Swain et al., 1949; Al-Tamrah, 1999). It is reported that spectrum of nicotine from UV spectrophotometry is characterized by a strong and sharp absorption maximum near 260 nm in water solution, and 259 nm in acidified. The UV spectrum of NHT with different concentrations in PBS showed that the maximum absorbance wavelength (λ max) was 258 nm (Figure 3.13). A zero intercept linear calibration equation for NHT in PBS was obtained to be Y=0.0064X ($r^2$= 0.99745), where X is the drug concentration in μg/mL and Y is the UV absorbance at 258nm (Figure 3.14). The amount of free drug in the supernatant of paraffin oil was determined from the absorbance at the wavelength of 258 nm. Drug loading of NHT-loaded CS nanoparticles were calculated using Eq. 3.6, and the results were calculated in the Table 3.9. The drug loading increased from 30.67±0.84% to 65.59±3.24% as drug-CS mass ratio increased. This suggested the capacity for drug loading decreased as the amount of drug increased.

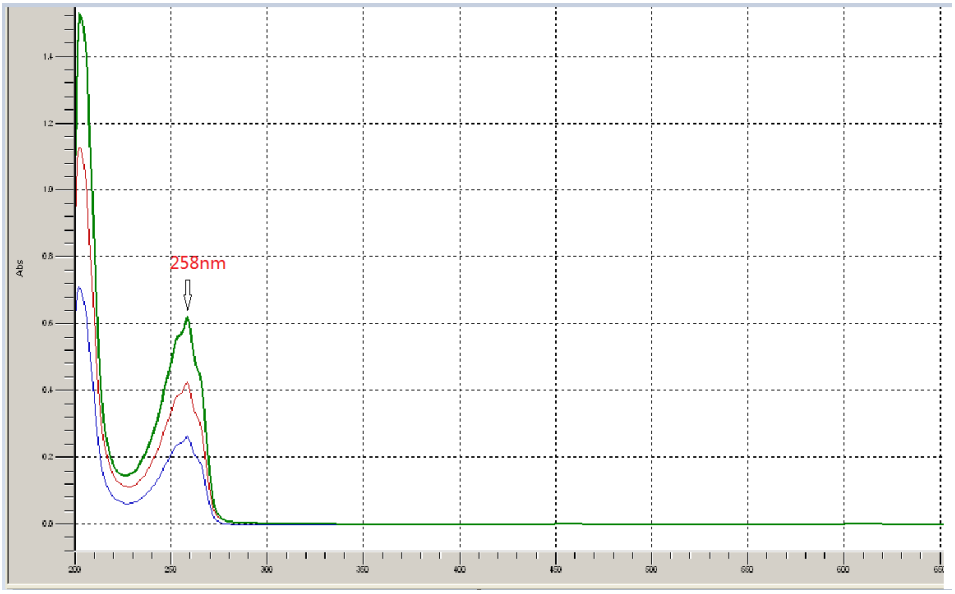


Figure 3.13 UV Scan of maximum absorbance wavelength of NHT in PBS with different concentration ranging from 10-50 µg/mL

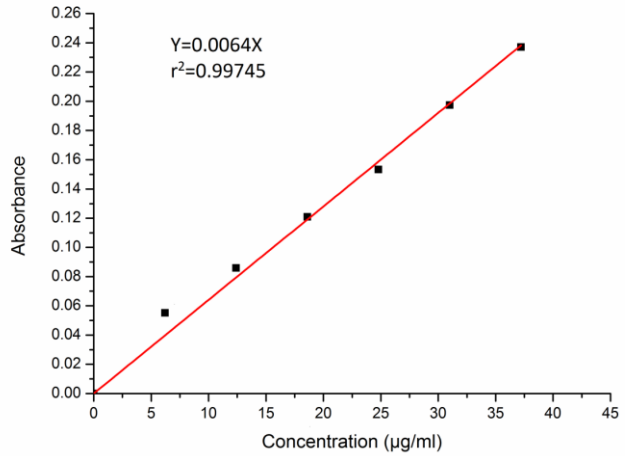


Figure 3.14 Beer-Lamber's calibration curve of nicotine hydrogen tartrate in PBS (n=3)

Table 3.9 Drug loading of different ratios of NHT-loaded CS nanoparticles (n=3)

| | **Drug loading (%)** |
|---|---|
| Blank chitosan NPs | - |
| NHT-CS (1:1) | 30.67±0.84 |
| NHT-CS (2:1) | 45.61±4.41 |
| NHT-CS (3:1) | 65.59±3.24 |

## 3.5 SUMMARY

In this chapter, an effective and feasible way to prepare NHT loaded CS nanoparticles for lung delivery has been established by w/o emulsion crosslinking method. The morphological observations (SEM & TEM) showed that all the particles were spherical and the surface roughness of the particles increased with increased drug loading. The individual particle size and size distribution of blank CS and NHT loaded CS formulations was in the nano range by DLS measurement, showed an increase in diameter with increased NHT content. On the other hand, nano-aggregates were formed among nanoparticles due to high surface energy, while all the aggregates were in the respirable range (<5μm) by laser diffraction determination. The NHT loading depended on the drug/ polymer ratio i.e., the higher the ratio between NHT to CS, the higher the drug loading. Positive surface charge of CS/NHT-loaded CS nanoparticles was reduced with increased concentration of NHT. BET surface area was governed by a variety of combined effects such as particle size, surface charge and cohesion/adhesion forces between particles. In terms of NHT-loaded CS nanoparticles, smaller particle size and higher zeta potential favoured higher BET surface area, which will be beneficial to the powder aerosolization from DPI formulation. In contrast, strong cohesion forces among blank CS nanoparticles are the predominant effect in controlling BET surface area. FT-IR, XRD and DSC indicated that the NHT altered to an amorphous form entrapped in the CS nanoparticles. On the basis of XPS analysis, the amount of NHT loaded on the surface of CS increased proportionally with increasing drug loading in the bulk so there was no surface enhancement. The outcomes of this chapter demonstrated the NHT-loaded CS nanoparticles are suitable to be exploited for DPI formulation for lung delivery, which needs to be confirmed and verified in the following chapters.

# Chapter 4:

# *In Vitro* Evaluation of NHT-loaded CS Formulations

Parts of Chapter 4 have been published as below:

**Wang, H;** George, G; Bartlett, S; Islam, N; Gao, C; Nazrul Islam. Nicotine Hydrogen Tartrate Loaded Chitosan Nanoparticles: Formulation, Characterization and in vitro Delivery from Dry Powder Inhaler Formulation; *European Journal of Pharmaceutics and Biopharmaceutics*. 2017, 113: 118-131.

This chapter will evaluate a series of physical characteristics of NHT-loaded chitosan (CS) and blank CS nanoparticle formulations, which were described in Chapter 3. First of all, the *in vitro* drug release studies are determined indirectly by way of a dialysis membrane technique. A mathematical model is introduced to correct the discrepancy during drug release measurement due to two diffusion barriers of the dialysis membrane. The morphology of particles post-release is investigated by SEM. The second part of work in this chapter is to evaluate *in vitro* aerosolization of the formulations by using a twin-stage-impinger (TSI) apparatus. The aerosolization of nanoparticles is related to the surface charge, and the relationship between surface charge and aerosolization of nanoparticles as DPI formulations is first to be reported in this study. It is also noted that the dispersibility of nanoparticle formulations with large lactose carriers is increased significantly compared to formulations without carriers. Finally, the long term stability of NHT-loaded CS nanoparticles is tested under controlled conditions of 25°C and 60% relative humidity (RH) for one year and formulations were found stable without significant change of FPF during this period.

## 4.1 INTRODUCTION

Aerosolization, controlled release and stability of formulations are three critical efficacy and safety issues to achieve practical drug product in order to develop reliable DPI formulations.

Controlled drug release technology from nanoparticles is one of the most researched areas in the fields of chemical engineering and drug delivery in the recent decades to allow delivery of a variety of drugs to different targeted areas of body with sustained release over a prolonged period of time. Compared with conventional dosage forms, this delivery system is featured with higher efficiency, lower toxicity and better patient

compliance (Uhrich, Cannizzaro, Langer, & Shakesheff, 1999). CS is one of the most widely used polymers for manufacturing nanoparticles. The absorption enhancing effects of CS nanoparticles with small size and marked positive zeta potential were showed to be promising carriers for improving the pulmonary absorption (Chan et al., 2013). CS nanoparticles prepared by cross-linking with glutaraldehyde (Gaspar et al., 2015; Park et al., 2013; Hao Wang, Xu, & Zhou, 2014) have demonstrated sustained drug release from lung delivery.

The release rate of drug from controlled release nano-sized dosage formulations are estimated by several techniques such as direct way of sample and separate (SS) and indirect way of dialysis membrane method to predict the drug release performance in physiological systems. SS provides a simple and direct way to assess the drug release through sampling of the release media, which usually requires high energy separation techniques like centrifugation, ultracentrifugation and ultrafiltration. However, several challenges are involved in the physical separation with high energy separation techniques. Continued drug release occurs during the separation process (Hua, 2014). Additionally, after sampling, a same amount of fresh release media or release buffer is replaced into the release system to maintain the sink condition during drug release study, which results in drug loss during sampling process and increase the discrepancy of concentration between solid phase (nanoparticles) and liquid phase (release medium). The dialysis membrane is used to separate nanoparticles from the released/dissolved drugs, which diffuse through the membrane for quantification, so separating the nanoparticles from the solvent containing the drug to be analysed (Hua, 2014). Drug release from the nanoparticles through the dialysis bag depends on the solubility of the drug from the nanoparticles as well as the diffusion of the dissolved drug through the dialysis membrane, which gives an apparent delay of release of drug

from the nanoparticles. During drug release testing by dialysis bag, the concentration profiles in the acceptor phase are used to assess the release kinetics of drug from nanoparticles. In this process, it is assumed that a steady state concentration gradient of drug is achieved instantaneously in the acceptor phase. The rate limiting properties of the dialysis membrane i.e., small molecular weight cut-off (MWCO), are one of the major obstacles to the steady state diffusion of the dissolved drug as well as the quantification of the diffused/released drug in the acceptor phase (Moreno-Bautista & Tam, 2011). Incomplete release data is likely to be collected with absence of sink condition or high equilibration time (Heng, Cutler, Chan, Yun, & Raper, 2008). Also, dialysis technique is not suitable for drugs which bind to the dialysis membrane (Hua, 2014). The thickness and permeability of membrane is another rate limiting factor that controls the diffusion of the released drug from the nanoparticles. In some references (M.-M. Chen et al., 2015; Khdair et al., 2016; X. Tian et al., 2014), it is assumed that the rate of diffusion across the membrane is faster than the rate of release, so the permeability coefficient of the membrane is ignored and the change in acceptor concentration with time mimics the release rate from the particles. This cannot be generally assumed. One obvious limitation from the general dialysis technique is the accurate quantification of drug release *in vitro*, as the sample is analysed from receiving compartment after it has diffused from nanoparticles through the dialysis membrane. Due to two diffusional barriers, the measured drug release kinetics may be slower than the actual release that would occur *in vivo*. However, in this chapter, the mathematical model modified from a report by Xie et al. (Xie, Beyer, Vogel, Wacker, & Mäntele, 2015) is used to overcome the discrepancy of equilibration times due to diffusion barrier from a dialysis membrane.

For the efficient pulmonary delivery of a drug aerosol particles with an adequate aerodynamic particle size (1 ~5 μm) need to reach the alveolar region of the lungs. However, aggregation among nanoparticles (nano-aggregate) is a common defect within the nano scale range due to high surface energy, which lowers the respirable fractions (Bosquillon, Lombry, Preat, & Vanbever, 2001). Therefore, optimization of aerosolization with an adequate range of particle sizes is still a challenge for development of DPI formulation system. Various strategies have been exploited to reduce aggregations between nanoparticles and improve flowability of dry powders in an attempt to prompt aerosolization performance of inhalation powder particles. In most cases, large coarse lactose carrier are blended with micronized drug particles to improve flowability, reduce aggregation and aid in dispersibility (Bosquillon et al., 2001).

Stability of formulation is another essential characteristic to be considered to produce practical DPI formulations. Storage conditions such as humidity and storage temperature affect the physical and chemical stability of DPI formulation, which results in a significant influence on the aerosolization of formulations. Long term stability test is to provide evidence of how the quality of an active pharmaceutical ingredient varies with time under the variables of a variety of environmental factors such as temperature and humidity. For a formulation to be suitable, physicochemical, pharmaceutical and microbiological characteristics are required to keep stable during its entire shelf-life. During formulation development or feasibility studies, physicochemical and pharmaceutical properties of the formulation are analysed at fixed time intervals of at least 6 months or longer. The other approach to evaluate the stability of formulation is stress testing by exposing the formulation to accelerated humidity and/or temperature without any protective measures.

Overall, a number of factors such as moisture content, particle size, morphology, excipients and storage conditions affect the powder flowability. The aim of this chapter was to evaluate *in vitro* drug release profile, aerosolization performance and long-term stability of DPI formulations of NHT-loaded CS particles. It is expected that the outcome of this chapter will guide the development of *in vivo* evaluations of DPI formulations of NHT-loaded CS particles.

### 4.1.1 Theories and Models of Drug Release

***Zero-order model***

Zero-order release model is an ideal drug delivery model. It is assumed that drugs maintain the constant levels in plasma across the delivery period. The applications of this model can be used to explain the drug dissolution of various classes of modified release pharmaceutical dosage forms, such as oral osmotic tablets, transdermal systems and matrix tablets with low soluble drugs (Freitas & Marchetti, 2005).

Zero order release represents a process of constant amount of drug release from a drug delivery system. The equation can be represented as:

$$Q_t = Q_0 + k_0 t \qquad \text{Eq.4.1}$$

Where $Q_t$ is the amount of drug dissolved or released in time t, $Q_0$ is the initial amount of drug in the system (most often, $Q_0$=0), and $k_0$ is the zero order release constant with the unit of %/h. To study the release kinetics, the release profile is plotted as cumulative % drug release versus time.

***First order model***

First order release model assumes the rate of release process is proportional to the drug concentration based on the different mechanisms of dissolution both alone and in

combination, so the initial rate of process depends on the initial concentration. It is supposed to take place at a constant proportion of the drug concentration available at that time and process never comes to an end. The applications of this model can be used to describe the absorption, distribution and metabolism of dosage forms. The earliest equation of dissolution rate in a linear kinetic process was proposed by Noyes and Whiteney (Noyes & Whitney, 1897) as

$$\frac{dC}{dt} = k_1(C_s - C_t) \qquad \text{Eq. 4.2}$$

Where dC/dt is the rate of concentration change with respect to time, $k_1$ is the first order release constant with the unit of $(time)^{-1}$. The solution to Eq. 4.2 is:

$$\ln[C_s/(C_s - C_t)] = k_1 t \qquad \text{Eq. 4.3}$$

or

$$\log C = \log C_0 - k_1 t/2.303 \qquad \text{Eq. 4.4}$$

Where $C_0$ is the initial concentration of drug and t is the time. To study the release kinetics, the release profile is plotted as log cumulative % of drug remaining versus time.

***Higuchi model***

Higuchi release model was proposed by Higuchi in 1961, aiming to describe a model for the drug's release from a matrix system. This release model was proposed based on the hypotheses: (a) higher drug concentration than drug solubility in the matrix initially; (b) drug diffusion in only one dimension; (c) smaller drug particles compared with system thickness; (d) negligible matrix swelling and dissolution; (e) constant drug

diffusivity; (f) sink conditions in the release environment. Simplified Higuchi model can be represented as:

$$Q = k_H * t^{1/2} \qquad \text{Eq. 4.5}$$

Where $k_H$ is the Higuchi dissolution constant. To study the release kinetics, the release profile is plotted as cumulative % of drug versus square root of time.

***Hixson-Crowell model***

Hixson and Crowell proposed this drug release model in 1931 to describe the proportional relationship between particles' regular area and the cube root of its volume. It is assumed surface area and diameter of particles or tablets is changed during the drug release in the system. The equation is represented as:

$$Q_0^{1/3} - Q_t^{1/3} = k_{1/3}t \qquad \text{Eq. 4.6}$$

$Q_0$ is the initial amount of drug in the dosage form, $Q_t$ is the remaining amount of drug in the dosage form at time t; $k_{1/3}$is a release rate constant. To study the release kinetics, the release profile is plotted as cube root of drug percentage remaining versus time.

***Korsmeyer-Peppas model***

Korsmeyer and Peppas proposed a release model to describe drug release from a polymeric system in 1983. This release model can be represented as:

$$Q = kt^n \qquad \text{Eq. 4.7}$$

Where Q is the fraction of drug release at time t. k is the release rate constant and n is the release exponent. The release mechanism is dependent on the values of n. $n \leq 0.45$ represents a Fickian diffusion mechanism, $0.45<n<0.89$ means non-Fickian

mechanism; n≥0.89 corresponds to case II transport. To study the release kinetics and determine the value of n, the release profile is plotted as log cumulative percentage drug release versus log time.

## 4.2 MATERIAL AND REAGENTS

LMW chitosan (CS) and NHT powder were purchased from Sigma-Aldrich, Australia. Phosphate buffered saline (PBS) tablets were obtained from Sigma-Aldrich, Australia. All other chemicals and reagents used were analytical grade.

## 4.3 METHODS

### 4.3.1 Preparation of NHT-loaded CS Nanoparticles and Mixing Nanoparticles with Large Carriers

***Preparation of NHT-loaded CS nanoparticles***

The details of processes to prepare micro/nanoparticles as DPI formulation were same as section 3.3.1 (See Chapter 3).

***Preparation of mixing nanoparticles with large carriers***

The lyophilized NHT-loaded CS and blank CS nanoparticles were mixed (10%W/W) with inhalation grade lactose monohydrate (Inhalac® 120) microparticles to make binary interactive mixtures using a previously reported hand mixing technique (Liu & Stewart, 1998). The nanoparticles were placed between two layers of lactose particles in a glass test tube together with 3 ceramic beads of approximately 10 mm diameter and shaken vigorously for 5 minutes to ensure adequate mixing. The ceramic beads provide a ball milling effect for breaking up the agglomerates formed during the mixing process.

### 4.3.2 *In Vitro* Drug Release Study by Dialysis Membrane

***Dialysis membrane system set up***

To overcome the limitation of loss of samples during physical separation from the direct way of sample and separate (SS), a system of UV-visible spectrometer and temperature controlled water bath was designed to study the *in vitro* release of NHT from CS nanoparticles from the modified dialysis bag diffusion technique (Pilcer et al., 2009). A dialysis membrane (MW 3500 Da, Yuanye Biotech Ltd, China) was pre-prepared at least 24 hours in advance in deionized water. Dialysis pouch with NHT-loaded CS nanoparticles was mounted into a wide mouth glass reaction flask. Two small stirrer bars were put into donor and acceptor compartments respectively to maintain uniform mixing of media during the process of release. Stirring rate of both acceptor and donor phases was set to gentle stirring at 100 rpm under magnetic stirrer. The dialysis system was kept at the constant temperature thermostatically at 37 °C (set up as Figure 4.1). The volume of acceptor phase ($V_a$) was at least 5 times as much as that of donor phase ($V_d$) to ensure sink conditions. PBS was used as release medium.

UV spectrophotometry analysis was carried out at 258 nm to evaluate the concentration of NHT during drug release. At time t = 0, a certain amount of nanoparticles, obtained as described under Section 3.4.1 was placed into donor compartment. The measured volume, $V_d$ of PBS was then added into the acceptor compartment. Aliquots of 5 mL were taken from receiving compartment for UV spectrophotometry and the released drug concentration was determined at fixed time intervals (0.5, 1, 2, 4, 8, 12, 24h and every 24h until 6 days). After analysis, the liquid was poured back to the acceptor flask immediately. To determine the permeability constant of the dialysis membrane, a plain 1 mg/mL NHT solution dissolved in PBS was placed in the donor compartment and the procedure was repeated using the same

dialysis membrane. All measurements were repeated in triplicate (n=3) and the drug release profile in the acceptor phase was determined directly through linearity ($r^2$=0.9992) of concentration and UV absorbance graph. Cumulative release profiles were determined by a mathematical model in the following section to construct the plots of the cumulative (%) drug release versus time.

The drug release data in this study were obtained under sink conditions, where the back diffusion from receiving to donor phase can be considered negligible, and the thermodynamic activity of permeant in the receiving phase was also negligible compared to that in the donor. The volume enclosed in the dialysis bag was significantly smaller than the receiving phase, so sink conditions were achieved throughout the experiment.

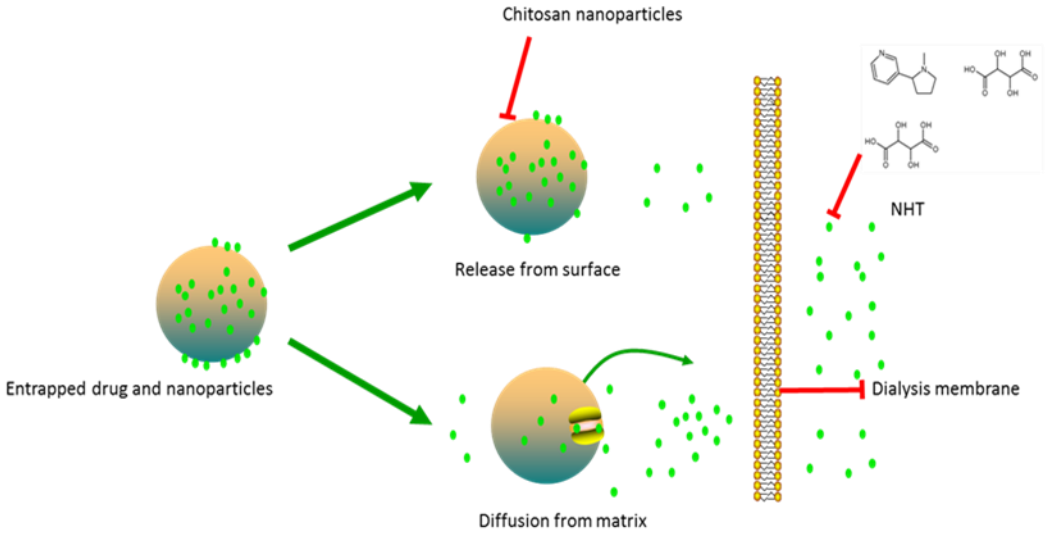


Scheme 4.1 Diagram of NHT released from CS nanoparticles

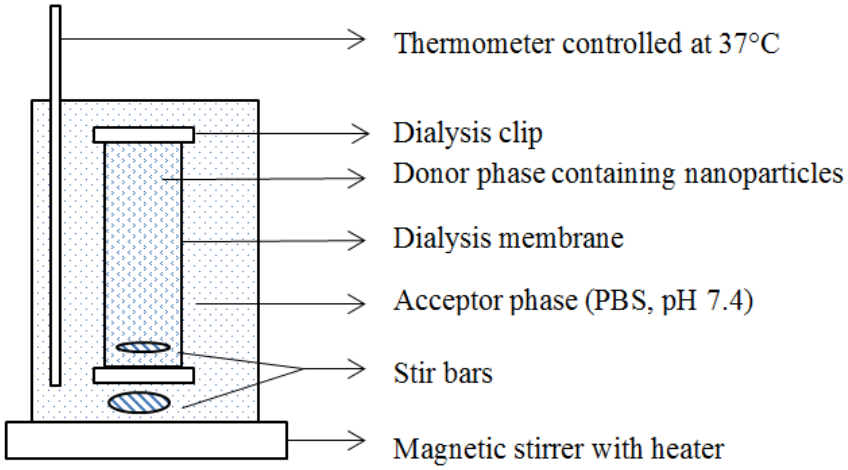


Figure 4.1 Drug release study using dialysis membrane set-up

***Mathematical model for drug release correction***

During dissolution testing by dialysis membrane, the concentration profiles in the acceptor phase are generally employed to estimate the release kinetics of drug from nanoparticles. However, the dialysis membrane diffusion technique has some limitations. The rate limiting properties of the membrane are one of the major obstacles to the quantification of the released drug in the acceptor phase. In order to reduce the

discrepancy of delayed drug release due to diffusion from the dialysis bag to the acceptor compartment and limited membrane permeability, a modified mathematical model (Xie et al., 2015) was used to obtain the corrected release profiles of the model drug used in this study. Although a number of factors such as temperature and pressure affect the diffusion rate, in this study, a simplified mathematical model is based on an optimal condition that only drug permeability constant and concentration gradient between two compartments govern the diffusion rate (Xie et al., 2015). Fick's law (Eq. 4.8) is applicable to describe the rate of change in concentration of acceptor phase (Pedersen, Østergaard, Larsen, & Larsen, 2005) if the system was well stirred.

$$\frac{dC_a}{dt} = \left(\frac{k}{V_a}\right)[C_d(t) - C_a(t)] \qquad \text{Eq. 4.8}$$

Where k refers to a dialysis membrane's permeability coefficient, which is associated with the pore size, thickness and soaked surface area of the dialysis membrane. $C_d$ , $C_a$ are the NHT concentration in the donor and acceptor phases, respectively at time t. $V_a$ is the volume in acceptor compartment.

***Determination of permeability of dialysis membrane***

To determine the permeability coefficient of membrane, the concentration profile of pure NHT passed through dialysis membrane was carried out. The NHT concentration in donor phase can be obtained from Eq.4.9 when a certain amount of pure NHT is put into the donor compartment.

$$C_d(t) = \frac{Q_0 - C_a(t) * V_a}{V_d} \qquad \text{Eq. 4.9}$$

Where $Q_0$ refers to the amount of pure NHT in the donor phase initially; $V_d$ is the volume in donor compartment.

If Eq.4.9 is merged into Eq.4.8, Eq.4.8 can be expressed as:

$$\frac{dC_a}{d_t} = \left(\frac{k}{V_a}\right)\left[\frac{Q_0 - C_a(t) * V_a}{V_d} - C_a(t)\right] \qquad \text{Eq. 4.10}$$

Then, it is solved analytically as:

$$C_a(t) = \left[\frac{Q_0}{V_d + V_a}\right]\left\{(1 - \exp(\frac{kt(V_d + V_a}{V_d V_a})\right\} \qquad \text{Eq. 4.11}$$

Eq.4.11 is simplified as:

$$C_a(t) = C_\infty[1 - \exp(k_m * t)] \qquad \text{Eq. 4.12}$$

Where $C_\infty = \frac{Q_0}{V_d + V_a}$ represents final concentration when the system achieved equilibrium; which was measured by UV directly during the process; $k_m = \frac{k(V_d + V_a)}{V_d V_a}$ is defined as total permeability coefficient. The results of pure NHT release data can be applied to Eq.4.10 to obtain km, after which k was fitted analytically.

***Determination of total permeability coefficient of NHT-loaded CS nanoparticles***

In terms of the NHT-loaded CS nanoparticles, k varied proportionally with the volume of donor phases used during the drug release process.

The parameters of $C_\infty$, $C_a$, t from the drug release of NHT-loaded CS nanoparticles were known, thus, the Eq. 4.10 can be fitted by plotting the experimental data of $C_a(t)$ versus t using software MATLAB®.

To determine the rate of change of concentration in the acceptor phase at each time point, derivative of Eq.4.12 was required as Eq.4.13

$$\frac{dC_a}{dt} = -C_\infty k_m * \exp(k_m * t) \quad \text{Eq. 4.13}$$

$C_d$ can be written as Eq.4.14 according to Eq.4.8:

$$C_d(t) = \frac{V_a}{k} * \frac{dC_a(t)}{dt} + C_a(t) \quad \text{Eq. 4.14}$$

It is noteworthy that k is a constant only if the soaked area does not change. As the different volumes of donor phases have been used, the value of soaked area changes and therefore it is required to correct the k value accordingly. In this way, the concentration of NHT in the donor phase ($C_d$) was obtained.

***Cumulative drug release of NHT-CS nanoparticles***

At any time point t, the total amount of released NHT in the system was accumulated as:

$$Q_r(t) = C_d(t)V_d + C_a(t)V_a \quad \text{Eq. 4.15}$$

Therefore, the cumulative release fraction of NHT from CS nanoparticles was determined by the Eq.4.16

$$F_r(t) = \frac{Q_r(t)}{m(NPs) * \text{drug loading}(\%)} * 100\% \quad \text{Eq. 4.16}$$

Where $m_{(NPs)}$ was the amount of NHT-loaded CS nanoparticles in the dialysis membrane; the value of drug loading regarding different mass ratios of NHT to CS was shown in Table 3.8. The release profiles of NHT from nanoparticles were determined using both the general method (before correction without mathematical model) and modified mathematical models (after correction) to obtain a clear understanding on the drug release from the nanoparticles.

***Release kinetic models***

To understand the mechanism of NHT release from nanoparticles, the release data (up to maximum drug release) were fitted to different kinetic models i.e, zero order, first order, Higuchi model, Hixson-Crowell model and Korsmeyer-Peppas model. The kinetics of drug release from nanoparticles is presented in Table 4.1 and Table 4.2.

***SEM after drug release***

After drug release study, the nanoparticle powders were collected onto the 0.22 µm membrane through repeated filtration and dried overnight in the oven at 60°C. The morphology of fully dried blank and NHT-loaded CS nanoparticles after drug release for 6 days was observed by SEM. All the experimental details of SEM were same as section 3.4.2.

### 4.3.3 *In Vitro* Aerosolization Study

***Formulations without large carrier***

The aerosol performance of DPI formulations of blank CS nanoparticles and NHT-loaded CS nanoparticles were evaluated by applying the twin-stage impinger (TSI, Copley Scientific, Nottingham, UK). Prior to testing, 7 mL and 30 mL of PBS were dispensed to Stage 1 and Stage 2 of the TSI, respectively. The flow rate through the TSI was adjusted to 60±5 L/min by a vacuum pump (D-63150, Erweka, Germany) through a calibrated digital flow meter (Fisher and Porter, Model 10A3567SAX, UK). 20±1 mg of nanoparticle formulations were filled into size 3 hard gelatin capsules (Fawns and McAllan Pty., Australia) which were subsequently inserted into a Rotahaler®. NHT-loaded formulations were aerosolized into the body of DPI device by twisting the capsules at 60±5 L/min for 5 s. After each experiment, Rotahaler, Stage1 (S1) and Stage2 (S2) were washed with PBS separately into suitable volumetric flasks. Washings collected from each stage were filtered through pre-dried and pre-

weighed 0.20 µm pore size filter membrane (Phenomenex, USA). The same filtrations were repeated at least five times until the filtrate was clear without any sign of turbidity. Finally, the particles filtered on the filter membrane were dried overnight at 60 °C until they reached a constant weight and the mass of the nanoparticles were determined gravimetrically. As the NHT is soluble in PBS and the drug-loaded nanoparticles were washed 3 times, the NHT-loaded CS nanoparticles were evaluated both gravimetrically and spectrophotometrically. Initially, the mass of nanoparticles were measured by the method described above. During washing the drug-loaded nanoparticles, the filtrate solutions were collected and the amount of NHT in the solution was determined by UV analysis. Finally, the determined respective amount of NHT was added with the mass of nanoparticles and the actual experimental data was obtained. Therefore, the dispersibility data presented here in this study are the summation of both gravimetric and spectrometric methods. Five capsules were repeated in this procedure.

The aerosolization of DPI formulations was evaluated by four parameters: recovered dose (RD), emitted dose (ED), fine particle fraction (FPF) and fine particle dose (FPD). RD is calculated as the total amount of drug collected from inhaler, S1 and S2. ED is calculated as a percentage of the total amount of particles emitted from the inhaler into S1 and S2 out of RD (Eq. 4.17). FPF is calculated as a percentage of the amount of particles as well as encapsulated/adhered drug deposited in Stage 2 out of RD (Eq. 4.18), which represents a respirable fraction of the delivered dose, and FPD is the mass in milligrams of NHT deposited in the Stage 2 of TSI.

$$\mathrm{ED} = \frac{\mathrm{S1+S2}}{\mathrm{RD}} \times 100 \qquad \text{Eq. 4.17}$$

$$\text{FPF} = \frac{\text{S2}}{\text{RD}} \times 100 \qquad \text{Eq. 4.18}$$

***Formulations with large carrier***

Aerosolization of the drug-loaded CS and mixing nanoparticles (10% W/W) was tested. The freeze-dried nanoparticles were mixed with inhalation grade lactose monohydrate (Inhalac® 120) microparticles as carriers to make binary interactive mixtures using a previously reported hand mixing technique (J. Liu & Stewart, 1998). The dispersibility of this formulation was carried out using the TSI as explained above. To compare the dispersibility behaviour of micronized NHT, the commercially available NHT was ground to inhalable size, mixed with large carriers and the FPF was measured. The NHT in the DPI formulation was analysed using a validated UV spectrophotometric method.

### 4.3.4 Long Term Stability Test

A long term stability study for the NHT-loaded CS nanoparticles was carried out over one year under controlled conditions of 25 °C/60 % relative humidity (RH). The DPI formulations were filled into size 3 hard gelatin capsules, which were stored in stability chambers under the specified conditions of temperature (25 ± 2 °C) and RH (60 ± 5 %). An acceptable RH was maintained by saturated magnesium nitrate slurry. The samples appearance, morphology and FPF were evaluated at different time intervals ($1^{st}$, $2^{nd}$, $12^{th}$ month) for its chemical and physical stability.

### 4.3.5 Statistical Calculations

All statistical analysis (one-way ANOVA with Bonferroni post hoc) was performed using statistical software of SPSS. MATLAB® was applied to analyse and plot drug release experimental data.

## 4.4 RESULTS AND DISCUSSION

### 4.4.1 Controlled Drug Release Study by Dialysis Membrane

***Drug release study by dialysis membrane***

Figure 4.2 presents the normalised data of pure NHT diffused through dialysis membrane from the donor compartment to the receiving compartment. According to the experimental results, NHT achieved equilibrium (0.1 mg/mL) between donor and acceptor phases in seven hours, which confirmed the system setup and dialysis membrane used in this study are reasonable to be applied in this drug release study. The relationship: $C_a(t) = 0.1(1 - e^{-0.6713t})$ ($r^2$=0.9981) was obtained by plotting experimental results to fit Eq. 4.12 analytically. Total diffusion coefficient ($k_m$=0.6713$h^{-1}$) was known through fitted equation. The diffusion constant of dialysis membrane (k=30.2085) was resolved by replacing the values of $V_a$, $V_d$, $k_m$ into $k_m = \frac{k(Va+Vd}{VaVd}$), which was kept constant in the following calculations of NHT-loaded CS nanoparticles since data were collected from the same dialysis membrane.

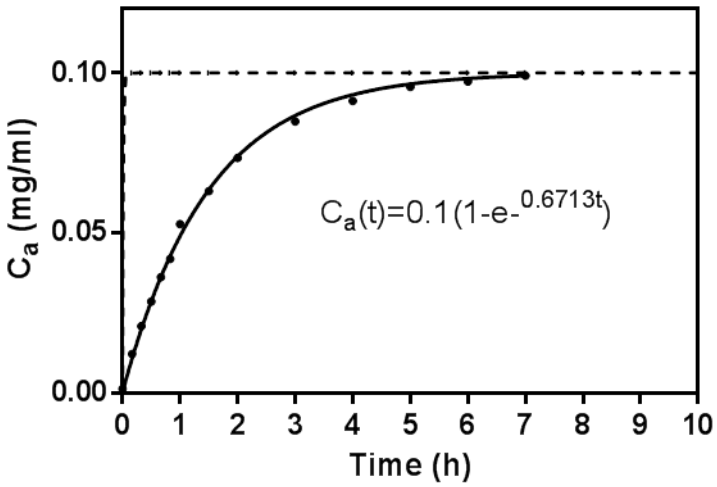


Figure 4.2 Concentrations measured in acceptor phase with time from pure NHT release. ($Q_0$=50 mg, $V_a$=450mL, $V_d$=50mL, $C_\infty$=0.1 mg/h, $k_m$=0.6713$h^{-1}$)

Figure 4.3 showed the normalised concentration profile in the acceptor phase for 6 days. As shown in the figure, pure NHT diffusion reached equilibrium in 7 hours, while the NHT-loaded nanoparticles took longer time to achieve constant concentration. This was because the drug was distributed in the matrix uniformLy and the release took place via diffusion through the matrix. Then, the rate of drug release gradually went down and a longer diffusion time to release was required as drug molecules had to travel a longer distance with the release continuing. In this study, release was terminated at 6 days when the concentrations in the acceptor phases were almost stable. Meanwhile, the concentrations of the donor phases and acceptor phases were measured to be fairly close to each other. Thus, released NHT was considered to be balanced between two phases. $C_\infty$ is the concentration in the acceptor phase by the time of equilibrium. The experimental run of pure NHT was as a control group to obtain dialysis diffusion constant (k), which was constant in the same dialysis system. All the other corresponding values of $k_m$ from NHT-loaded CS nanoparticles were determined by fitting experimental data to the mathematical model (Eq.4.12).

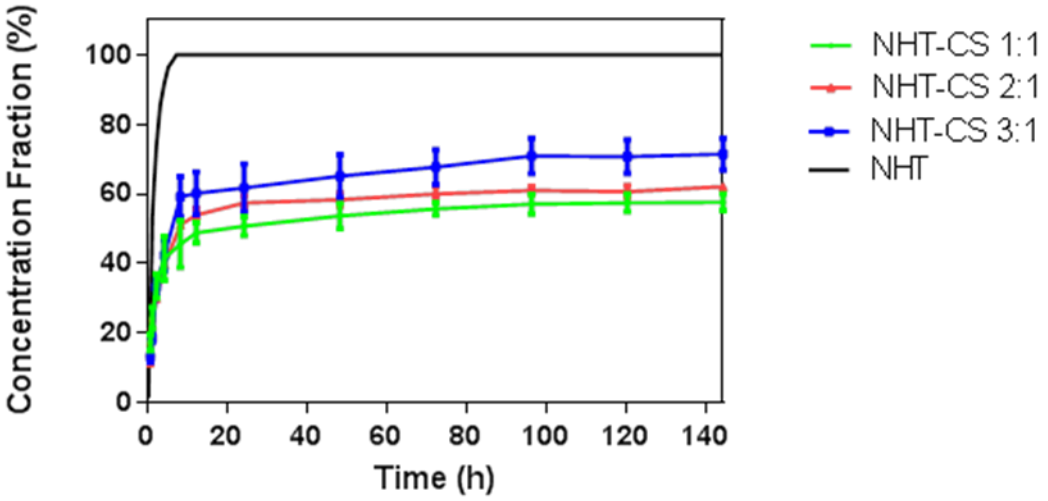


Figure 4.3 Concentration fraction (%) profile in the acceptor phase (data presented as mean ± SD., n = 3)

After determination of $k_m$ and with regards to different weight ratios of NHT-loaded CS nanoparticles respectively, the numerical value for $\frac{dC_a}{d_t}$can be acquired by replacing the derivatives using Eq. 4.13. A series of numerical value of derivatives could describe the rate of change of concentration in the acceptor phase at the point of time t.

Figure 4.4 shows the concentration profiles both in the donor phase ($C_d$) and acceptor phase ($C_a$). The corrected numerical value of $C_d(t)$ was acquired according to Eq. 4.14, with all the known parameters obtained from last two steps. As shown in Figure 4.4 (a, b, c, d), the concentration in the acceptor phase increased continuously, the time to reach equilibrium increased along with increase of mass ratios of NHT to CS. Pure NHT reached equilibrium within 8 hours, while the formulations of NHT-loaded CS (1:1) and (2:1) achieved balance between two compartments in the 12 and 24 hours, respectively. However, the concentration gradient of NHT-loaded CS (3:1) nanoparticles kept increasing until around 12 hours after the start of the drug release test, and two compartments attained the same concentration in 144 hours. It is expected that pure NHT did not share the same release rules with NHT-loaded CS nanoparticles. NHT was dissolved into the PBS the moment it was put into the donor phase, followed by diffusion across the dialysis membrane. On the other hand, NHT on the CS nanoparticles surface was dissolved into PBS at first, and then entrapped drug was released from inside nanoparticles due to drug diffusion following matrix swelling. It was reported the swelling of CS membrane crosslinked by glutaraldehyde reached a stable equilibrium water content in about 15 minute, and the swelling curves remained stable with time under the test condition of 37°C and pH of 7.4 (Gupta & Ravi Kumar, 2000; Silva, Silva, Coutinho, Mano, & Reis, 2004). Thus, the longer equilibrium time

was required with higher drug loading. However, compared with the NHT-CS (1:1; 2:1) groups, NHT-CS (3:1) took longer time to reach equilibrium. The possible explanation for this might be the entrapped drug was gradually released from the CS nanoparticle within the 12 hours. The rate of entrapped drug release slowed down over time, which resulted in a longer drug diffusion time. In this study, the main mechanism of NHT released from chitosan nanoparticles may depend on the drug diffusion within the first release stage considering swelling of CS nanoparticles was a slow process.

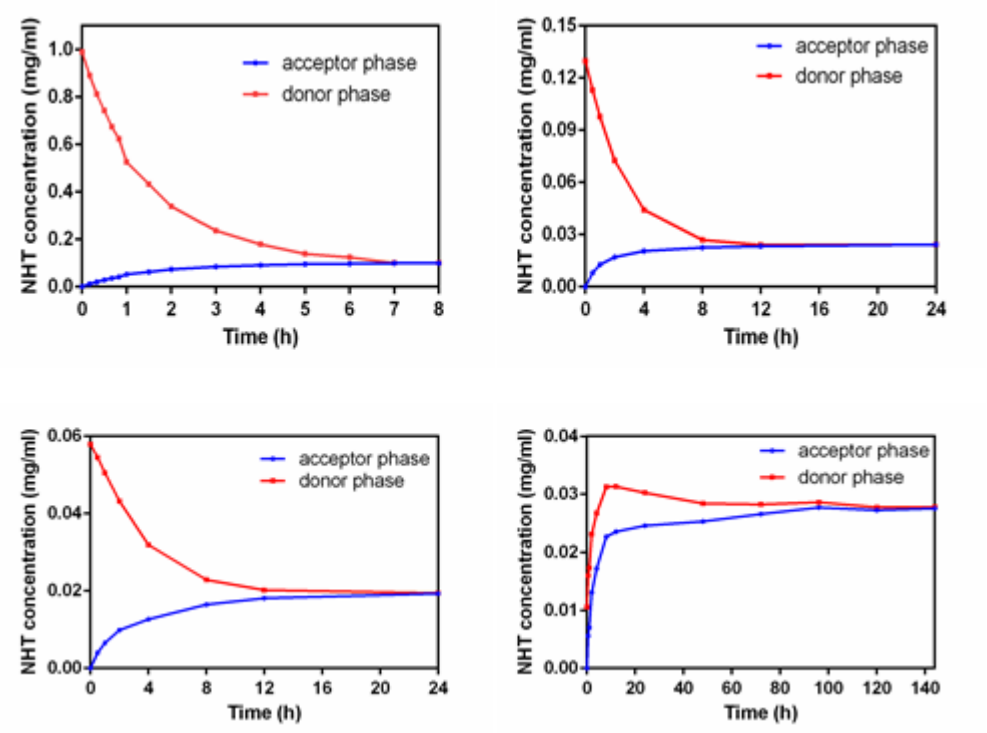


Figure 4.4 The concentration profiles in the donor phase ($C_d(t)$) and acceptor phase ($C_a(t)$) of (A) pure NHT ($V_a$=450mL, $V_d$=50mL); (B) NHT-CS (1:1) ($V_a$=130mL, $V_d$=20mL); (C) NHT-CS (2:1) ($V_a$=250 mL, $V_d$=40 mL); (D) NHT-CS (3:1) ($V_a$=130mL, $V_d$=20mL)

The percentage of cumulative drug release corrected by the mathematical model from the nanoparticle formulation was plotted as shown Figure 4.5. The total cumulative amount of released NHT in the system was determined by Eq. 4.15, and the cumulative drug release (Fr) was calculated according to Eq. 4.16. In terms of the pure NHT

release as a control group, the cumulative release percentage of NHT in the system can be seen constant (100%) during the experiment due to its high solubility and immediate dissolution in the aqueous release medium, which was in accordance with release mechanisms and practical condition as well. According to the drug release profiles (Figure 4.5), the drug was rapidly released from the nanoparticles initially, followed by slight slow release. Initial burst release was attributed to the rapid dissolution of surface or close to surface of adhered/entrapped drug, while the later slow release was because of the penetration of the release medium into the nanoparticles and dissolution of the entrapped drug. Compared with control group, it was obvious that entrapment of NHT in the CS nanoparticles can effectively sustain NHT release. Short-term release profiles (right bottom corner of Figure 4.5) of NHT-loaded CS nanoparticles showed that NHT-loaded CS nanoparticles (3:1) experienced slowest release rate in the initial two hours, achieving a highest cumulative burst release of about 60% in the eight hours when the corresponding values for 2:1 and 1:1 were at 53% and 47%, respectively. At the same time, NHT-loaded CS (3:1) nanoparticles experienced most cumulative release in the duration of 6 days. All the features of release from our study were in accordance with report from Hans (Hans & Lowman, 2002), which indicated that the higher drug loading led to the greater fractional release of drug from the nanoparticles, but the larger particle size resulted in a slower initial burst release and longer sustained release since less area of contact with the release medium contributes to slower dissolution of drug compared with smaller size of nanoparticles. At the end of the period (6 days), all of three drug-loaded CS nanoparticles (weight ratios of 1:1-3:1) achieved the maximum cumulative % release (around 58 ± 3%, 62 ± 1%, and 72 ± 5% respectively). Nicotine-loaded CS nanoparticles as DPI formulations in this study achieved prolonged controlled release from nanoparticles compared with current

nicotine transdermal patch to release accumulative 90% nicotine within periods of 12-24 hours (Lewis et al., 2006; Sha, Zhang, Li, & Shen, 2014). However, not all the drug was released from the nanoparticles within 144 hours. It is estimated that the drug may be associated with vestiges of the positively charged nanoparticles through electrostatic interactions, so lower surface charge favored higher cumulative drug release in PBS, i.e. cumulative drug release of NHT-CS (3:1) was higher than those of NHT-CS (1:1) and NHT-CS (2:1) (Lim et al 2000).

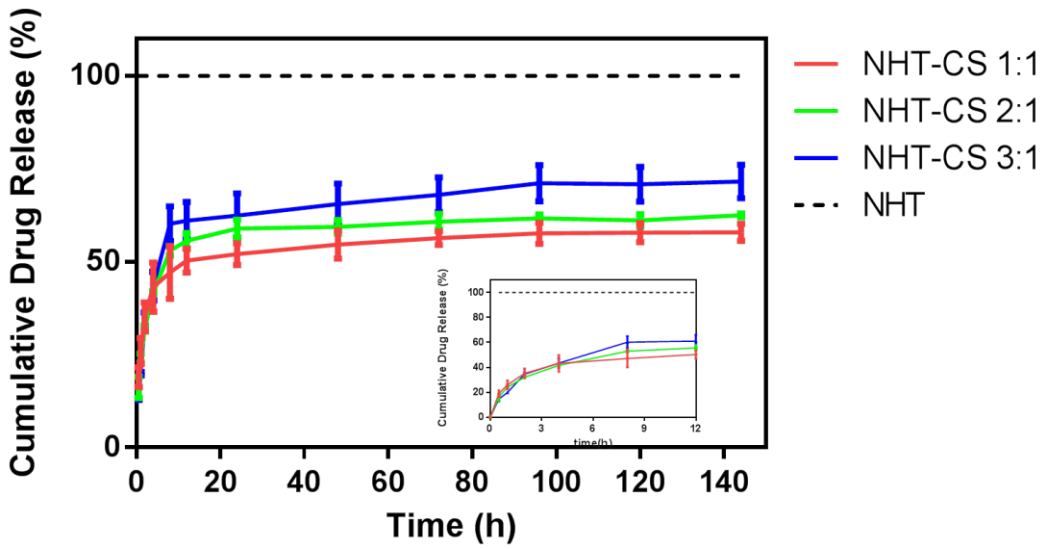


Figure 4.5 Corrected cumulative drug release over a period of 6 days and initial release in the 12 hours (right bottom) (data presented as mean ± SD., n = 3)

Figure 4.6 demonstrated the differences of numerical results of the cumulative drug release between general calculation method and this mathematical model. The general way of dialysis diffusion is based on the assumption that the concentrations of acceptor phase and donor phase are at equilibrium at any point. One obvious limitation from the traditional dialysis technique is the accurate quantification of drug release in vitro, as the sample is analysed from receiving compartment where it has diffused from nanoparticles through dialysis membrane. Due to two diffusional barriers, delayed effect happened during this process, and the measured drug release kinetics may be

slower. However, in this study, a mathematical model based on the approach of Xie (Xie et al., 2015) was set up to overcome the discrepancy of equilibration times due to diffusion barrier from a dialysis membrane. As shown in Figure 4.6, although the corrected cumulative release values did not show significant differences from traditional calculations, especially at ending period (>12 hours) as the systems were under equilibrium conditions, the designed model offered the possibility to measure accurately drug release with time. It can be used to predict real-time release of drug-loaded nanoparticles in order to achieve desired release profiles.

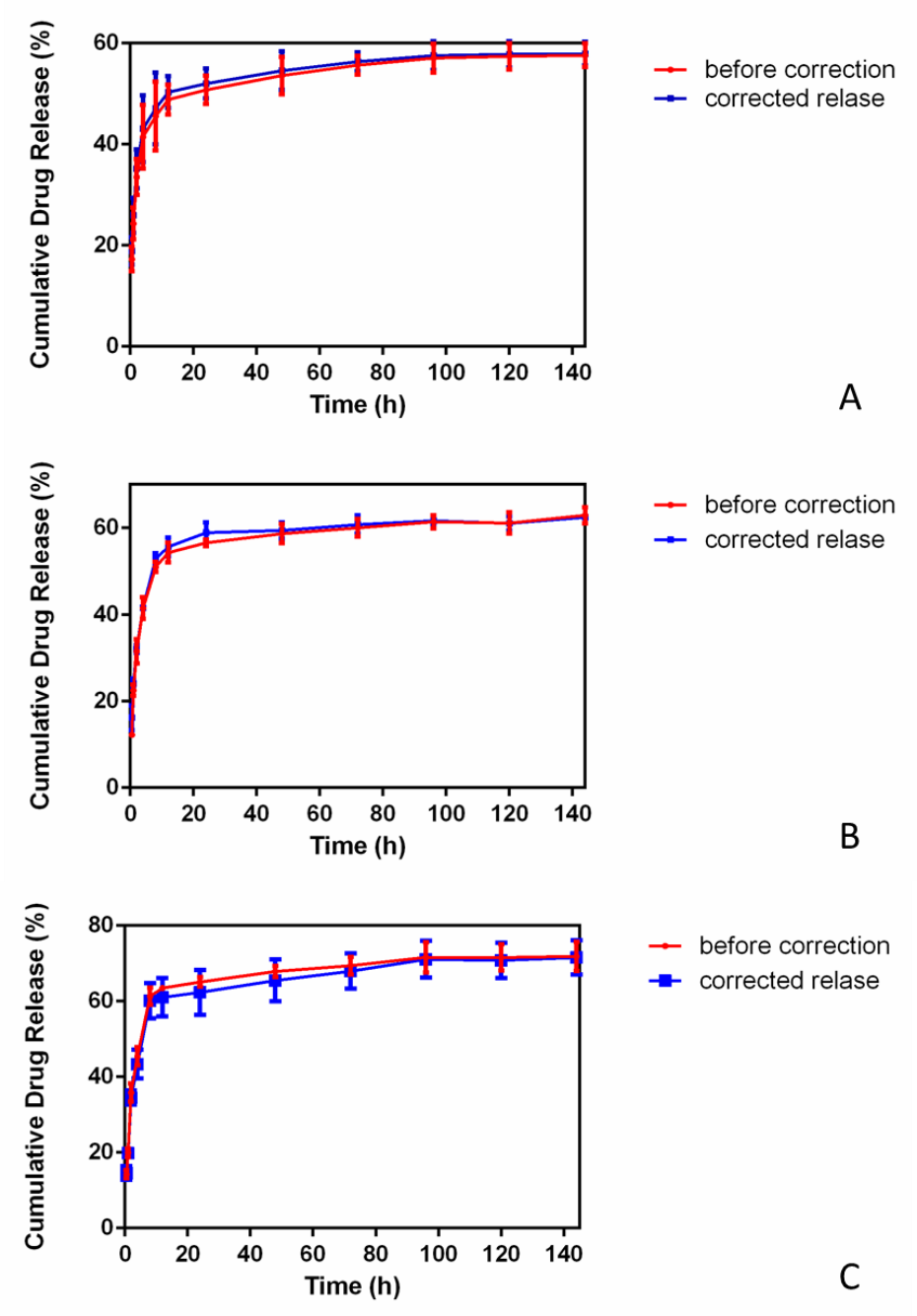


Figure 4.6 Comparisons of before and after corrected drug release (A) NHT-CS (1:1); (B) NHT-CS (2:1); (C) NHT-CS (3:1) (data presented as mean ± SD., n = 3)

### *Kinetics of drug release*

Before the mathematic modelling correction of two-barrier delayed diffusion of dialysis membrane, the original data obtained from acceptor phase of dialysis membrane was fitted to various models, which results referred as before correction. The release data were analysed by linear regression and the highest $r^2$ values were

considered to the best fit model to demonstrate the behaviour of drug release. The rate of release was divided into an initial phase (0-8 hrs) and a terminal phase (8-144hrs) based on a modified report by Lim (S. Lim, Martin, Berry, & Brown, 2000) as it is understandable that the release rate in the burst release stage is faster than that of in the sustained release phase. In an attempt to explore the characteristics of drug release profile, the data were fitted to four different mathematical models, i.e., zero order model, first order model, Higuchi model, and Hixson-Crowell model. The results before mathematic model correction of release rate constants (k) and coefficients of determination ($r^2$) were shown in Table 4.1. The initial phase of release of NHT was faster than that of the terminal phase due to the higher concentration gradient, and this was because of the adherence of the drug on the nanoparticle surface and the defects of pores or cracks within the matrix (S. Lim et al., 2000). As shown in Table 4.1, it indicated that NHT-loaded CS nanoparticles were best characterised by first order model ($r^2$=0.9116-0.9680) and Higuchi model ($r^2$=0.9796-0.9998) with high linearity. The other models were not considered regarding the lower coefficients of determination.

The release data of NHT from all combinations strongly fitted ($r^2$ =0.9567-0.9897, Table 4.1) with Korsmeyer-Peppas model, which demonstrates the release exponent (n) obtained from the slope of a plot of log % cumulative release against log time. For spherical particles if n is 0.45, the release mechanism is considered to follow Fickian diffusion (Siepmann & Peppas, 2001), where drug release occurs through usual molecular diffusion because of a concentration (or chemical potential) gradient. Higher values of n between 0.45 and 0.89 indicate non-Fickian or anomalous transport, where release is controlled by a combination of diffusion and polymer relaxation/erosion. In this study, the drug release exponents (n values) for NHT-CS

(1:1) was less than 0.45, suggesting that the drug release was Fickian diffusion. Whereas, the n values for NHT-CS (2:1) and NHTCS (3:1) were above 0.45 (0.50-0.54), which is an indicative of non-Fickian diffusion due to the higher drug concentration in the nanoparticles.

All data in this report were obtained under sink conditions, where the back diffusion from receiving to donor phase can be considered negligible, and the thermodynamic activity of permeant in the receiving phase was also negligible compared to that in the donor. The volume enclosed in the dialysis bag was significantly smaller than the receiving phase, so sink conditions were achieved throughout the experiment. There is no doubt that dialysis membrane is not suitable for drugs that bind to the membrane. To this purpose the drug concentration in the donor, free from binding, was calculated from dialysis data, as illustrated in Sections 4.3.1, and compared with the concentration in the receiving phase at the corresponding time.

Table 4.1 Release rate constants and correlation coefficients of NHT release from CS nanoparticles before correction

| models | 1:1 | | 2:1 | | 3:1 | |
|---|---|---|---|---|---|---|
| | Initial phase | Terminal phase | Initial phase | Terminal phase | Initial phase | Terminal phase |
| | 0-8 hours | 8-144 hour | 0-8 hours | 8-144 hour | 0-8 hours | 8-144 hour |
| Zero order | $F_r=k_0t$ | | | | | |
| $k_0$ | 6.5888 | 0.0664 | 4.654 | 0.062 | 6.000 | 0.0651 |
| $r^2$ | 0.9279 | 0.8838 | 0.860 | 0.9203 | 0.9167 | 0.8972 |
| | | | | | | |
| First order | $Ln(1- F_r)=-k_1t$ | | | | | |
| $k_1$ | 0.0965 | 0.0017 | 0.072 | 0.00014 | 0.1036 | 0.0021 |
| $r^2$ | 0.9526 | 0.9398 | 0.9196 | 0.9217 | 0.9680 | 0.9116 |
| | | | | | | |
| Higuchi model | $F_r =k_Ht^{1/2}$ | | | | | |
| $k_H$ | 13.289 | 1.3123 | 17.641 | 0.9962 | 22.368 | 1.0542 |
| $r^2$ | 0.9813 | 0.998 | 0.9998 | 0.9845 | 0.9796 | 0.9832 |
| | | | | | | |
| Hixson-Crowell model | $1-(1- F_r)^{1/3}=k_{1/3}t$ | | | | | |
| $k_{1/3}$ | 0.0115 | 0.0002 | 0.0155 | 0.0002 | 0.02 | 0.0003 |
| $r^2$ | 0.9279 | 0.8838 | 0.868 | 0.9203 | 0.9167 | 0.9662 |
| | | | | | | |
| Korsmeyer-Peppas model | $F_r = k_{k-p} t^n$ | | | | | |
| $k_{k-p}$ | 23.7137 | 40.7005 | 20.0309 | 47.1954 | 21.2716 | 55.2205 |
| n | 0.365 | 0.0717 | 0.500 | 0.056 | 0.5408 | 0.054 |
| $r^2$ | 0.9567 | 0.9885 | 0.9542 | 0.9861 | 0.9788 | 0.9815 |

After mathematic modelling correction (described in 4.3.2), the corrected release data were fitted to different kinetic models (Table 4.2) as well to identify the possible drug release mechanism. The highest $r^2$ values were considered to the best fit model to demonstrate the behaviour of drug release. The release rates of drug from nanoparticles depend on either diffusion of dissolved drugs or biodegradation (erosion) of polymer matrix. The release data (after correction, Table 4.2) revealed that NHT-CS

nanoparticles followed Higuchi model (strong linearity, $r^2$ = 0.9127-0.9990) that reflected the drug release from nanoparticles was controlled by diffusion. It has been reported that the prolonged release of water soluble drug from CS-based mico/nanoparticulate systems in PBS is associated with the diffusion of the dissolved drug through hydrated swollen matrix (Learoyd, Burrows, French, & Seville, 2008). Drug release from these formulations also showed good fitting with the first order kinetic in the initial phase ($r^2$ = 0.9328-0.9755), which indicated the amount of initial drug release was a function of drug concentrations as demonstrated in Figure 4.3 and Figure 4.5.

As it knows that diffusion is the main drug release mechanism in this study, the release data of NHT were fitted to Korsmeyer-Peppas model to further understand the mechanism of diffusion from polymeric dosage forms such as Fickian (purely diffiusion) or non-Fickian (combined diffusion/polymer relaxation) behaviour. Specifically, during the initial phase, the drug release exponents (n values) for NHT-CS 1:1 and NHT-CS 2:1 formulations were 0.33 and 0.42 respectively, suggesting that the drug release followed Fickian diffusion governed by purely diffusion as mostly NHT was encapsulated into CS nanoparticles and less NHT on the surface of CS nanoparticles regarding formulations of NHT-CS 1:1 and NHT-CS 2:1 (Hui Wang et al., 2017). As drug loading increased, more NHT were loaded on the surface of CS nanoparticles as well as encapsulated into the CS nanoparticles. As a result, the n values for NHT-CS 3:1 during initial phase was above 0.43, which is an indicative of non-Fickian diffusion governed by diffusion and polymer relaxation due to the rapid dissolution of surface or close to surface of adhered or entrapped NHT. After 8 hours, NHT which were on the surface of CS nanoparticles was washed away, which were

confirmed by SEM images presented in Figure 4.7. Therefore, prolonged drug release in the terminal phase followed Fickian diffusion.

Compared with drug release data between before mathematic model correction (Table 4.1) and after mathematic model correction (Table 4.2), the release constants after correction were lower than before correction except for Korsmeyer-Peppas model, which suggested the mathematic model used in this study was effective to correct delayed diffusion effect occurred by dialysis membrane. However, linearity after correction was not as strong as that of before correction considering lower coefficients of determination after correction. There is no statistically significant difference in the cumulative drug release (Figure 4.6 a, b, c) between before and after mathematical model correction. It was interesting to note drug release of NHT-CS 2:1 during the burst release phase was dominated by diffusion and polymer relaxation before correction which n value for Korsmeyer-Peppas model was above 0.45, while the n value decreased to below 0.45 after correction governed by purely diffusion. Thus it is suggested that drug loading of NHT-CS 2:1 was the critical limit between Fickian and non- Fickian.

Overall, a variety of factors such as drug/CS ratios, concentration and molecular weight of the CS, type and concentration of crosslinking agent, particle size, degree of crosslinking and swelling behaviour of the crosslinked polymer affect the behaviour of drug release polymer nanoparticles. Therefore, it is not straightforward to predict the precise mechanism affecting drug release kinetics where complex processes are involved in releasing drug from nanoparticles. The drug release profiles from the CS nanoparticles with dialysis membrane technique were distinguishable to overcome

discrepancy of delayed drug release, although statistical significance was not detected. These *in vitro* studies demonstrated that the swellable CS nanoparticles developed in this study might have a potential for sustained lung delivery of NHT.

Table 4.2 Release rate constants and correlation coefficients of NHT release from CS nanoparticles after correction

| models | 1:1 | | 2:1 | | 3:1 | |
|---|---|---|---|---|---|---|
| | Initial phase | Terminal phase | Initial phase | Terminal phase | Initial phase | Terminal phase |
| | 0-8 hours | 8-144 hour | 0-8 hours | 8-144 hour | 0-8 hours | 8-144 hour |
| Zero order | $F_r = k_0 t$ | | | | | |
| $k_0$ | 3.4197 | 0.1001 | 4.5393 | 0.0725 | 5.8149 | 0.0998 |
| $r^2$ | 0.7945 | 0.9851 | 0.9206 | 0.7874 | 0.9322 | 0.9774 |
| | | | | | | |
| First order | $Ln(1- F_r) = -k_1 t$ | | | | | |
| $k_1$ | 0.0531 | 0.0022 | 0.0729 | 0.0017 | 0.099 | 0.0033 |
| $r^2$ | 0.9328 | 0.989 | 0.9605 | 0.7997 | 0.9755 | 0.9983 |
| | | | | | | |
| Higuchi model | $F_r = k_H t^{1/2}$ | | | | | |
| $k_H$ | 13.218 | 1.2138 | 16.943 | 0.9073 | 21.558 | 1.4082 |
| $r^2$ | 0.9127 | 0.9998 | 0.9861 | 0.9526 | 0.9852 | 0.999 |
| | | | | | | |
| Hixson-Crowell model | $1-(1- F_r)^{1/3} = k_{1/3} t$ | | | | | |
| $k_{1/3}$ | 0.0114 | 0.0003 | 0.0151 | 0.0002 | 0.0194 | 0.0004 |
| $r^2$ | 0.7945 | 0.9851 | 0.9206 | 0.7874 | 0.9322 | 0.9969 |
| | | | | | | |
| Korsmeyer-Peppas model | $F_r = k_{k-p} t^n$ | | | | | |
| $k_{k-p}$ | 25.5741 | 43.0923 | 22.9456 | 50.8159 | 21.1836 | 50.5126 |
| n | 0.3362 | 0.0635 | 0.4207 | 0.0452 | 0.5221 | 0.0603 |
| $r^2$ | 0.9594 | 0.9896 | 0.9897 | 0.9044 | 0.9835 | 0.9596 |

### 4.4.2 **SEM after Drug Release**

The morphology of the nanoparticles after drug release was determined by SEM in Figure 4.7. An amount of freeze-dried nanoparticles were put into dialysis membrane and PBS as release medium for a period of 6 days before SEM morphological investigation. Comparing drug loaded/unloaded pictures showed that the surface of CS nanoparticles after drug release was still smooth and spherical, though swelling of CS nanoparticles may occur during this process. Obvious differences in morphology of drug-loaded nanoparticles were observed between before and after NHT release. The most distinctive feature of SEM images in comparison between two stages is that a large amount of NHT was loaded onto the surface of CS nanoparticles regardless of mass ratios of NHT and CS before drug release study (Figure 3.3), while the CS particles showed a smoother and more rounded morphology after a 6-day release (Figure 4.7). It is worth noting that SEM images from CS nanoparticles without NHT did not show significant difference between before and after drug release study. The pictures also clearly showed that the porosity of nanoparticles became bigger after drug release visually at the corresponding drug-CS ratio. According to Figure 4.7, the size of nanoparticles was bigger compared with previous pictures (Figure 3.3) because NHT has formed a solid solution with the CS which causing swelling of CS particles to release the NHT and many of the particles looked to be fused together.

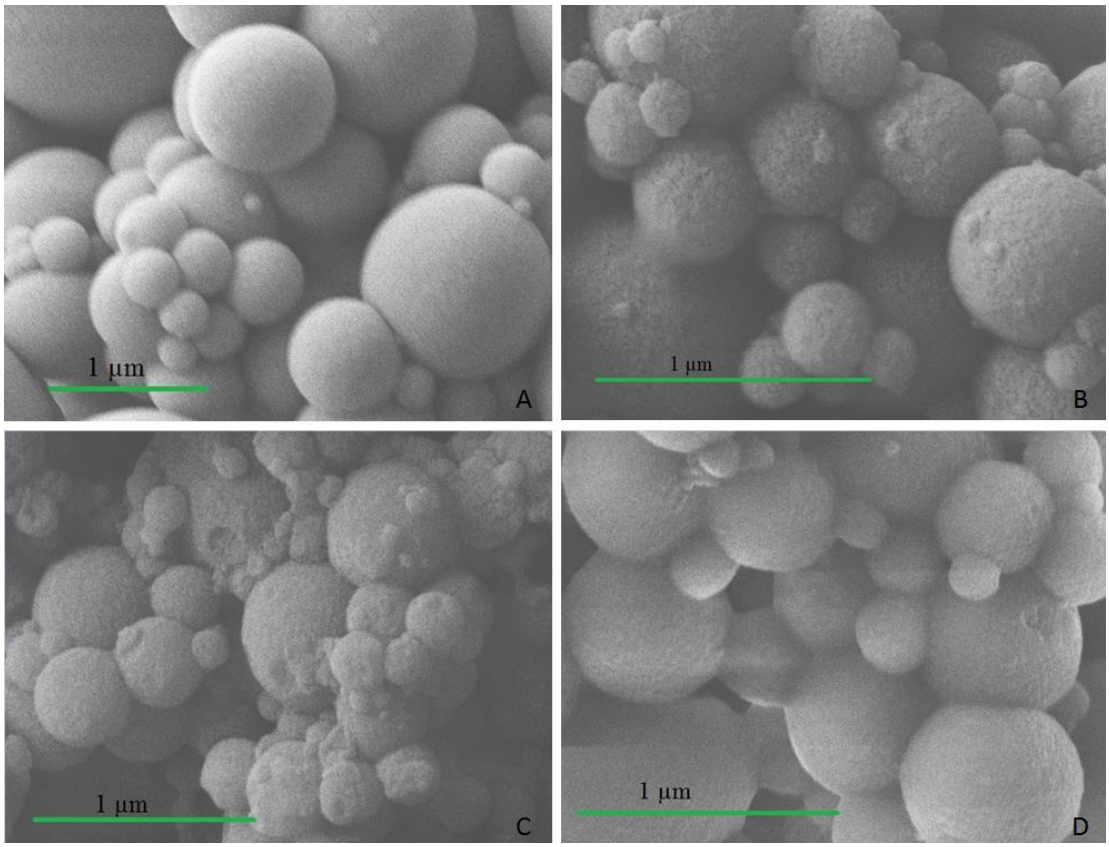


Figure 4.7 SEM images of nanoparticles after immersion in PBS for 6 days from (A) blank chitosan; (B) NHT-loaded CS (1:1); (C) NHT-loaded CS (2:1); (D) NHT-loaded CS (3:1)

### 4.4.3 *In Vitro* Aerosolization Study

***Formulations without large carrier***

Using a twin-stage impinger (TSI), the dispersibility of blank and NHT loaded nanoparticles was investigated and the amount of NHT deposition was determined using both spectrophotometric and gravimetric methods. The relative particle depositions of different formulations were evaluated by parameters: RD, ED, FPF and FPD, which are presented in Table 4.3. Significant differences ($p<0.05$) in all deposition profiles of the aerosolized NHT-loaded CS nanoparticles with CS/NHT mass ratios of 1:1, 1:2 and 1:3 in RD, ED, FPF and FPD were observed. All the formulations exhibited RD ranging from 87.2 % to 92.9 %, which indicated about 7.1% to 12.8% of the particles were lost during the process of evaluation of aerosolization. Some factors that may result in the loss of particles are: 1) adhesion of particles to the capsules and glass walls of the TSI chambers; 2) drug released from the particles in the PBS in case of NHT-loaded particles. The highest FPF of nanoparticles from the blank CS (30.1±0.2 %) which was significantly different ($p = 0.000013$) from NHT-loaded CS of NHT: CS 2:1 (25.9±2.3%) and NHT: CS 3:1 (24.4±1.5%). It was also observed that the FPF from formulation of NHT: CS of 1:1 was higher than those of NHT-loaded CS formulations with mass ratios of NHT and CS of 2:1 and 3:1. The most significant difference (ANOVA, $p= 0.000123$) for FPF in blank CS nanoparticles (30.1±0.2 %) versus NHT: CS of 3:1 (24.4 ± 1.5%), followed by blank CS nanoparticles versus NHT/CS of 2:1 ($p= 0.000884$). No significant differences between the FPF of blank CS nanoparticles and NHT-loaded CS at a ratio of 1:1 were observed. There was no significant difference between mass ratios of drug-loaded CS of 2:1 and 3:1.

Although all drug-loaded CS nanoparticles showed similar ED (75-77%), the blank CS nanoparticles produced a significantly higher FPF than that of the drug-loaded CS nanoparticles (30% vs. 24%, Figure 4.8). It is possible that the CS polysaccharide backbone may contribute to the reduction in interparticle interaction and increase the FPF of the blank CS nanoparticles. The reason behind this could be due to the higher intrinsic surface positive charge on the blank CS nanoparticles rendering less agglomeration due to the repulsive forces and this resulted in higher FPF of blank CS nanoparticles. The decreased FPF of drug-loaded nanoparticles occurred when the mass ratios of NHT and CS increased. A fixed mass of nanoparticles (20 mg of blank and NHT-loaded) was used to aerosolise from the TSI, therefore, the number of nanoparticles reduced in the same mass of formulation (20 mg) with drug loaded nanoparticles. The masking of surface charge of nanoparticles by adsorbed drug on the surface reduced the FPF of NHT- loaded nanoparticles, although all of them have similar ED.

Table 4.3 *In vitro* aerosolization of NHT-loaded /unloaded CS nanoparticles (data presented as mean ± SD., n = 5)

| **Nanoparticle Formulations** | **RD (%)** | **ED (%)** | **FPF (%)** | **FPD (mg)** |
|---|---|---|---|---|
| Blank CS | 87.2±2.4 | 75.5±0.3 | 30.1±0.2 | - |
| NHT- CS (1:1) | 88.3±2.7 | 74.7±0.7 | 29.6±0.9 | 1.71±0.5 |
| NHT- CS (2:1) | 92.5±2.9 | 76.9±2.3 | 25.9±2.3 | 2.5±0.24 |
| NHT- CS (3:1) | 92.9±2.9 | 75.3±2.4 | 24.4±1.5 | 3.18±0.14 |

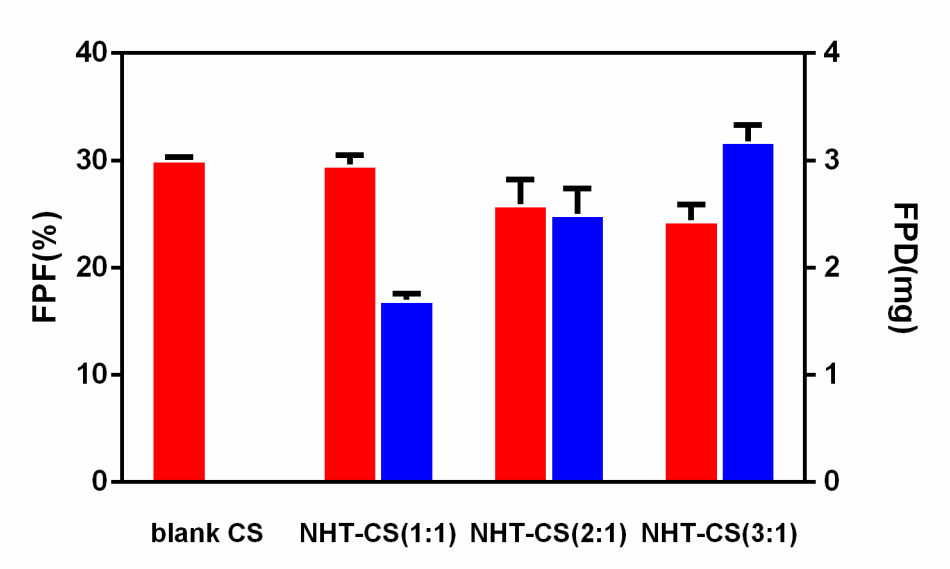


Figure 4.8 Fine Particle Fraction (FPF; red bars) and Fine Particles Dose (FPD; blue bars) of different formulations (data presented as mean ± SD., n = 5)

Capillary forces are generated in the presence of moisture, which has a significant influence on the particle interaction through hydrogen bonding, and it eventually reduces the FPF of nanoparticles. The observed reduction in FPF of drug-loaded nanoparticles was probably attributed to a higher agglomeration tendency caused by the capillary forces due to the presence of highly water soluble drug of NHT, adjoined on the particle surfaces with increased concentration of NHT. Addition of the hydrophilic drug to the CS microspheres that caused an increased agglomeration of particles due to the capillary forces has also been demonstrated (L. Lim & Wan, 1998). The higher amount of drug adjoined on the nanoparticles with high drug loading can be confirmed by SEM images (Figure 3.3, Chapter 3).

Although the FPF of nanoparticles reduced after drug loading, increased FPD of NHT was obtained with increased concentration of NHT in the nanoparticles (Figure 4.8). Forces of particle interactions i.e. mechanical interlocking from surface roughness, capillary forces, electrostatic forces and van der Waals forces (Telko & Hickey, 2005) are the factors that control the effective aerosolization of nanoparticles. In most cases,

the physical interactions due to surface roughness or adhesive/cohesive forces are the dominant forces to obstruct particles aerosolization from the DPI formulations. In addition, surface morphology is an important factor that controls the dispersibility of particles from DPI formulations. The SEM images revealed that the surface smoothness of drug loaded nanoparticles reduced (i.e., roughness increased) with the increase of mass ratios of NHT to CS. Therefore, increased FPD of NHT from nanoparticles occurred due to the increased surface roughness, reduction in contact geometry and cohesion forces among particles. So, the higher FPD of drug loaded nanoparticles was attributed to these surface properties. The enhanced FPD of NHT-loaded nanoparticles were further supported by the Carr's compressibility index presented in Table 3.7 and Table 4.3.The Carr's index of drug loaded CS has been found to be decreased with increasing drug loading, thereby improving the flow property of nanoparticles and increasing the FPD. Furthermore, the particle sizes of drug loaded nanoparticles increased with increased drug loading. The Carr's index also supported the observation that the flow of particles increased with increasing particle size that enhanced the FPD. Increased dispersibility of powders due to increased particle size has been reported (Tuli, George, Dargaville, & Islam, 2012). This can be further explained by the facts that the amount of drug increased in the same mass of nanoparticles dose (20 mg), which indicated a fixed amount of dose contained reduced number of nanoparticles but higher amount of drug in the formulation that increased the FPD. As the total recovery of nanoparticles from the TSI was low, which affected the estimate of the true FPF of nanoparticles, it would be appropriate to take the FPD of nicotine into account rather than FPF of nanoparticles to demonstrate the practical application of the dispersibility data observed in this study. The calculated FPD of NHT increased from 1.71 mg to 3.18 mg (Table 4.3) with increasing concentration of

NHT in the nanoparticles. Since 1.0 g NHT is equivalent to 0.35 g nicotine base, these doses are equivalent to 0.60 mg to 1.12 mg nicotine base delivered into Stage 2 of TSI. Therefore, the FPD (equivalent to 0.60-1.12 mg pure nicotine base) obtained from NHT-loaded CS nanoparticles would be anticipated to deposit in the lower regions of the lung after inhalation, and then undergo initial burst release and subsequent sustained drug release. Thus, it offers the potential to reduce dosing frequency and improve patient compliance.

The relationship between the FPF and zeta potential of nanoparticles was presented in Figure 4.9. The excellent linearity ($r^2 = 0.9849$) of this figure clearly depicted that the FPF of nanoparticles increased with increasing zeta potential at measured pH. CS is a cationic polysaccharide and the glutaraldehyde cross-linked CS nanoparticles without NHT were positively charged (20.1 mV), which reduced (Figure 4.9) with increasing concentration of NHT. The NHT has a negative charge due to the presence of the tartaric acid salt so the positive charge due to protonation of the CS amino groups will be reduced with increased concentration of NHT in the formulation.

Table 4.4 Comparison of zeta potential of nanoparticles at measured pH and fixed pH (data presented as mean ± SD., n = 3)

| **Nanoparticles** | **Measured pH** | **Zeta potential (+ mV)** | **Zeta potential (mV) at pH 6** |
|---|---|---|---|
| Blank CS | 5.83 | 20.1±1.4 | 18.9±0.3 |
| NHT:CS (1:1) | 4.55 | 19.0±1.2 | -1.50±0.3 |
| NHT: CS (2:1) | 3.83 | 14.2±0.7 | -3.1±1.1 |
| NHT: CS (3:1) | 3.81 | 12.2±0.4 | -4.5±1.9 |

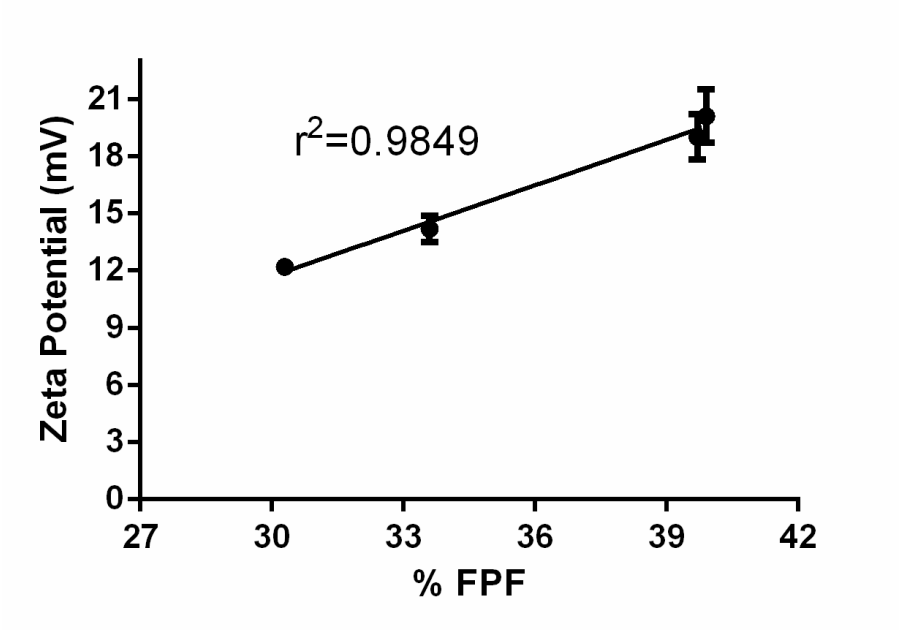


Figure 4.9 Relationship between the zeta potential and FPF of NHT loaded CS nanoparticles (data presented as mean ± SD., n = 3)

The higher FPF from blank CS nanoparticles could be due to the higher surface positive charge contributing to the electrostatic repulsive force among the particles. It is suggested that the intrinsic surface positive charge of CS nanoparticles will enhance the deagglomeration process of nanoparticles resulting in increased FPF with increased charge. As presented in Table 4.4, surface charges of nanoparticles reduced with increased concentration of NHT and shifted to negative charge at a fixed pH 6. This result suggested that under conditions of reduced protonation of the CS the nanoparticles containing NHT tended to agglomerate since it was regarded that a low zeta potential (in this case -1.5 to -4.5 mV) would not favour dispersion of the nanoparticles. To further study the role of zeta potential on the nanoparticle dispersibility, the zeta potential of blank CS nanoparticles (fixed amount of glutaraldehyde) was measured at different pH levels. As Figure 3.7 presented, the zeta potential of nanoparticles was shown to be reduced with increased pH ($r^2$ = 0.984). A fixed amount of glutaraldehyde was used for crosslinking so the number of available

amino groups on the CS for protonation was constant. The decrease in zeta potential therefore followed the reduction in the protonation as pH increased. The positive surface charge of CS in acidic medium due to protonation of the amine groups in CS showed repulsive forces (Kiang et al., 2004) between nanoparticles, which supported these findings. The large amount of drug accumulated on the particle surface resulted in reduced surface positive charge favouring agglomeration. Countering this, deagglomeration of CS-NHT nanoparticle agglomerates might be enhanced due to impaction on the internal wall of the device. Therefore, the significant reduction in FPF from the NHT loaded CS nanoparticles i.e., decreased particle repulsive forces, increased cohesion forces and likewise reduced dispersibility of nanoparticles was observed. This is because the accumulated drug in the nanoparticle reduced the positive zeta potential.

In addition, the increased concentration of drug caused an increase in nanoparticle size (Table 3.2), which reduced the number of nanoparticles. The particle number (N) which gave the number of particles per unit weight of the sample was expressed by the equation:

$$N = \frac{6}{\pi \rho d^3} \qquad \text{Eq. 4.19}$$

where N is the particle number, d is the diameter of the spherical particle and ρ is the density of chitosan (1.54 gm/cm$^3$).

The reduction of particle number with reduced zeta potential in the same mass of formulation caused a reduction in the FPFs. As indicated earlier in the discussion, the loaded drug with higher concentration was likely to reduce the surface charge compared to the blank nanoparticles and thereby FPFs were reduced with increased

drug loading. This rationalizes the lowest FPF of NHT loaded CS nanoparticles at higher drug concentration (NHT: CS of 3:1).

Very insignificant difference was observed between FPF and surface charges produced by the nanoparticles of CS and NHT-CS 1:1. The reason for this may the sum of two effects. The first is that the pH of the solution was higher in the case of the CS compared to the NHT: CS 1:1 nanoparticles so the degree of protonation was less. However, there was a reduced number of amino groups in the nanoparticles due to crosslinking and also the presence of the NHT which will have an overall negative charge. The net reduction in zeta potential is only 1mV. The reason behind this could be that the surface charge was not affected by 1:1 ratio of drug loading as most of drugs the NHT is encapsulated inside the polymer nanoparticles and this concentration was not high enough to cover the nanoparticles surface. The sudden drop of both the FPF and the surface charge produced by the NHT-CS 2:1 and 3:1, compared to the blank CS or NHT-CS 1:1 was probably due to masking more positive charges on nanoparticles by the increased concentration of drug. Additionally, it was possible that the higher agglomeration tendency was caused by the increased capillary forces due to the presence of large amount of highly water-soluble NHT, that were adjoined to the surface of CS nanoparticles. The tendency of increased agglomeration of CS-based microspheres upon the addition of a hydrophilic drug, propranolol hydrochloride has been reported (Lim and Wan, 1998), which supported this possibility. The surface roughness had an impact on the dispersibility (Islam, Stewart, Larson, & Hartley, 2005) of drug and accordingly higher FPF from NHT-loaded nanoparticles was expected as the surface irregularities/roughness increased with increased concentration of NHT. However, it appeared in this study that the surface irregularities or roughness

due to the increased drug loading did not play a dominant role in nanoparticle dispersion.

***Formulations with large carrier***

The nanoparticles of blank CS and NHT-loaded CS were mixed (10% w/w) with inhalation grade lactose microparticles (Inhalac 120, approximately 100 µm size) to see the impact of large carrier on nanoparticle dispersibility. The FPF presented in Figure 4.11 (with carrier), where the large carrier based formulations produced a significant ($p = 0.0001$) elevation in FPF compared with those of carrier-free formulations. The surface charges demonstrated in Figure 4.9 were not seen to contribute to the dispersibility of nanoparticles from the carrier based formulations. The FPFs were slightly higher from samples with lower charge and increased with increasing drug loading in the nanoparticle, suggesting that the large carriers contributed to the reduction of the cohesive forces among the nanoparticles, giving improved de-agglomeration due to the collision effects (Islam, Stewart, Larson, & Hartley, 2004; Kho & Hadinoto, 2013). Because of higher mass of large carriers, the impaction effect was predominant over the charge effect as the charged nanoparticles on a carrier carry the same charge as the free nanoparticles (without carrier). It was explained previously that the intrinsic positive charge on CS nanoparticles led to the increased FPF of nanoparticles with increasing surface charge due to repulsive force among particles that formed loose agglomerates; however, the dispersibility from large carrier based formulation was not in conformity with this argument.

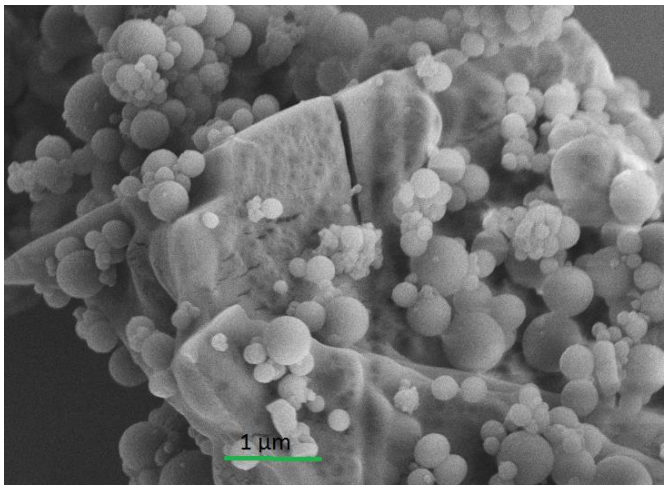


Figure 4.10 SEM images of CS nanoparticles with lactose carrier

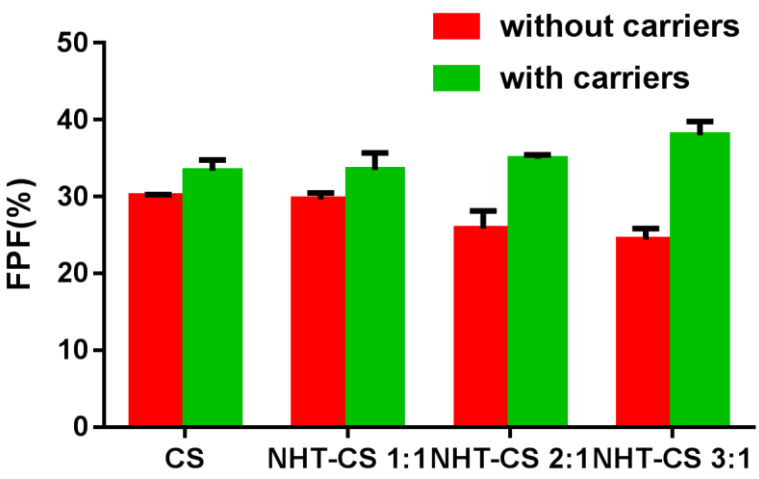


Figure 4.11 FPF of nanoparticles with or without large lactose carriers (data presented as mean ± SD., n = 3)

Once aerosolised the formulation, the agglomerates may be subjected to kinetic forces due to inspiratory flow and inhaler mechanical impaction forces or a combination of both for appropriate deagglomeration and subsequent dispersion (Al-Qadi et al., 2012; Leung et al., 2015; Papadimitriou et al., 2008). The SEM images in Figure 4.10 showed nanoparticles were distributed either as agglomerates or as a single particle on the large lactose carriers. It was suggested these nanoparticles (single or agglomerates) in the

mixture had limited cohesion forces among them and thereby easy detachment occurred due to high impaction. The momentum of any particle is dependent on the mass and the velocity of the carrier and as the larger particles will have greater mass there will be greater momentum transfer or high impaction to detach the surface particles. Therefore, significant mechanical forces were thought to be produced due to the carrier-carrier collisions or collisions between the carrier particles and the internal walls of the inhaler during aerosolization (Coates, Fletcher, Chan, & Raper, 2004). The geometry of the inhaler device, an important factor in drug dispersibility, has been reported to affect the extent of collisions occurring between the inhaler wall and the carrier particles (Coates et al., 2004). The nanoparticulate agglomerates that adhered on the large carriers might be detached as a whole, requiring a much lower velocity than the detachment of a single particle because of the significantly higher inertia for the agglomerates (De Boer, Chan, & Price, 2012). In this study, lactose carriers, mixed with positively charged chitosan nanoparticles were aerosolized via a Rotahaler made of polyvinylchloride. On aerosolization, the lactose particles acquired positive specific surface charge with polyvinylchloride and polypropylene surfaces (Byron, Peart, & Staniforth, 1997; Rowley, 2001). Therefore, the positive electrostatic charge developed on the lactose carrier (depending on the particle size and contact surface) due to the collision between the carriers and device surface during aerosolization probably influenced the overall dispersibility of nanoparticles by repulsive force between the large carriers and the cationic chitosan nanoparticles that resulted in higher FPF. However, this assumption was not supported by the zeta potential of NHT-loaded CS nanoparticles, which showed increased FPF from large carrier based formulations with reduced zeta potential at higher concentration of drug loading (Table 4.5). If the repulsive forces between large carriers with acquired positive surface

specific charge and CS nanoparticles were the contributing factor to increase the FPF, then the blank CS nanoparticles with highest zeta potential would have produced highest FPF and the highest NHT-loaded CS nanoparticles (NHT-CS 3:1) would have showed the lowest FPF. However, the data presented in Table 4.5 showed the highest FPF from large carrier based formulation of nanoparticles with lowest zeta potential. Therefore, it can conclude that the impact of large carriers on FPF was independent of zeta potential.

Table 4.5 Aerosolization studies of blank and nicotine-loaded chitosan nanoparticles with and without large lactose carriers (data presented as mean ± SD., n = 5)

| **Formulations** | **RD (%)** | | **ED (%)** | | **FPF (%)** | |
|---|---|---|---|---|---|---|
| | With carrier | Without carrier | With carrier | Without carrier | With carrier | Without carrier |
| Blank CS | 81.4±3.0 | 90.0±1.4 | 66.6±3.6 | 75.5±0.2 | 33.4±1.4 | 30.8±0.2 |
| CS NHT (1:1) | 81.6±6.1 | 88.3±2.7 | 65.3±1.6 | 74.7±0.7 | 33.5±2.2 | 29.6±0.9 |
| CS NHT (1:2) | 81.3±3.8 | 92.5±2.9 | 71.5±2.6 | 76.9±2.3 | 34.9±0.5 | 25.9±2.3 |
| CS NHT (1:3) | 79.0±3.3 | 92.9±2.9 | 63.0±2.2 | 75.3±2.4 | 38.0±1.8 | 24.4±1.5 |
| NHT | 92.1±4.2 | - | 51.8±6.7 | - | 7.32±2.0 | - |

Another possible factor to increase the FPF could be that the lactose carriers used in this study contained some associated fine particles of lactose (1.5% fine lactose <5µm), which were thought to form loose agglomerates with the nanoparticles that easily detached from the carrier surface, deagglomerated and higher dispersion occurred (Islam et al., 2004). Furthermore, the enhanced FPF of nanoparticles could have happened due to the surface roughness of lactose carriers as well as the nanoparticles. As seen in the SEM images, the nanoparticle surfaces were comparatively rougher with increased concentration of NHT loading and that surface roughness could have played a significant role in the detachment of nanoparticles from carrier surfaces due to limited contact and led to increase FPF. For example, the highest FPF (38.0 %) of NHT-CS 3:1 nanoparticles, which showed very rough surface that

probably experienced less adhesion forces on the lactose rough surface and easy detachment occurred. Although the actual mechanism of nanoparticle dispersion from formulation with or without large carriers was not absolutely clear, this study revealed some key points: i.e., a) the CS nanoparticle dispersion without large carriers was dependent on the deagglomeration process controlled by the surface zeta potential of nanoparticles; b) the presence of large carriers in nanoparticlate DPI formulations accelerated the deagglomeration process by collision and high impaction and was independent of surface zeta potential.

### 4.4.4 **Stability Test**

The stability of inhalation powders is crucial to maintain the aerosolization properties. Temperature and relative humidity during storage are two main factors to affect aerosol performance. Thus, long term stability is required to ensure the efficiency of aerosol performance.

NHT-loaded CS nanoparticles as DPI formulation appeared that the NHT-CS powders remained in the powder form in the one year under conditions of 25°C, 60% RH. The colour of the powders stayed light yellow. SEM showed that the formulations stored for one year showed the same surface structure as those that were freshly prepared (Figure 4.12). In addition, the FPF of nanoparticles stored for up to one year did not show a statistically significant change during storage (Figure 4.13). It indicated that the powder was stable without significant deterioration of aerosolization performance during this period. In terms of drug loading after stability study, it was estimated based on the results of *in vitro* aerosolization study, which NHT-loaded CS nanoparticles were evaluated both gravimetrically and UV spectrophotometrically. During one year storage, the amount of NHT in PBS from each stage of TSI (data presented in

Appendix Table 1, P 219) did not vary significantly compared with freshly prepared particles, which indicated that composition of NHT in the nanoparticles did not change significantly. In other words, that drug loading of NHT-CS nanoparticles did not change significantly in comparison with nanoparticles that were freshly prepared.

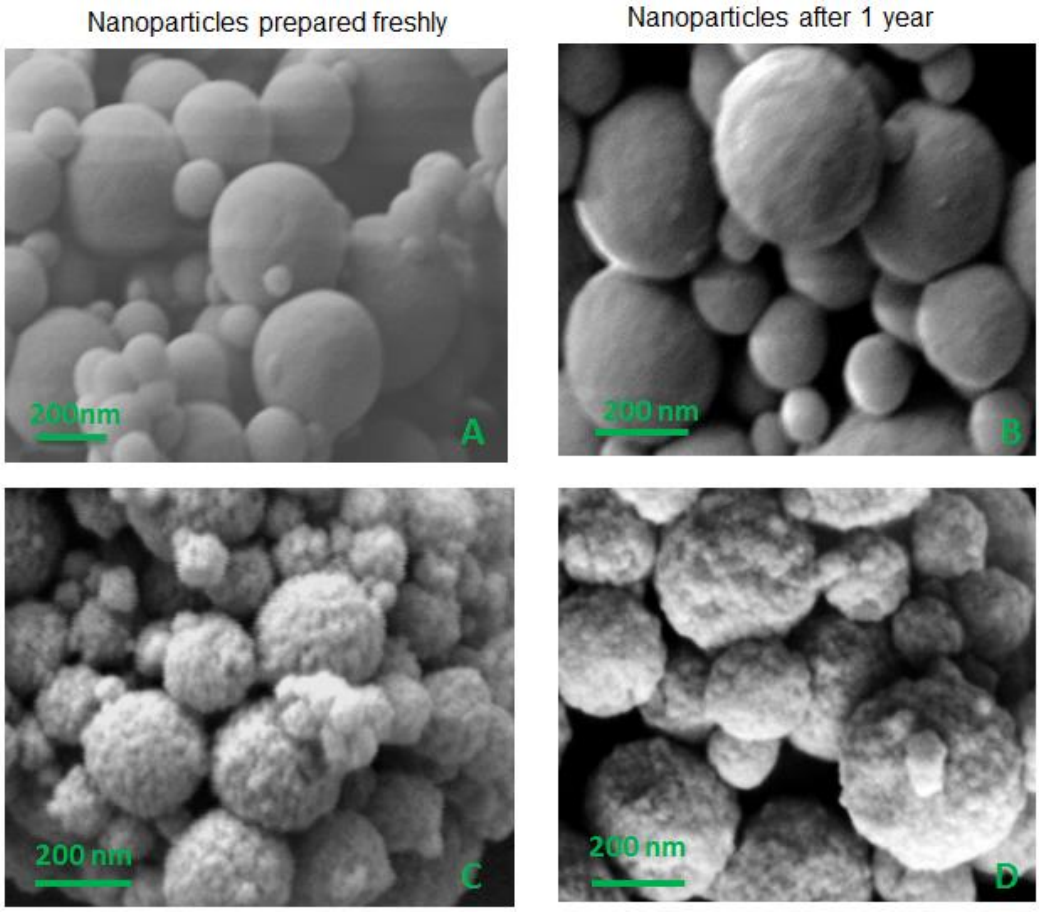


Figure 4.12 SEM of nanoparticles formulations between freshly made (A and C) and after 1 year under room temperature storage and 60% RH (C and D). (A) (B): blank CS nanoparticles; (C) (D): NHT-loaded CS (3:1)

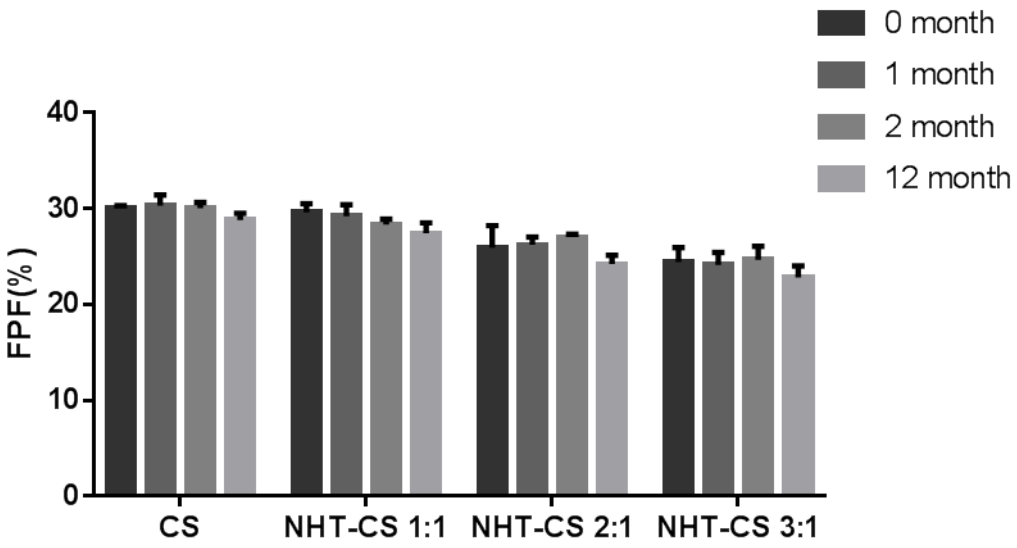


Figure 4.13 *In vitro* aerosolization (FPF) of NHT-loaded CS nanoparticles by TSI in one year under storage condition of 25°C, 60% RH (data presented as mean ± SD., n = 3)

## 4.5 SUMMARY

This chapter showed that both manufacturing process and storage conditions could have a significant effect on effective delivered dose. The powders are a mixture of both individual nanoparticles and their microaggregates. According to *in vitro* drug release profile, NHT loaded CS nanoparticles established in Chapter 3 showed a prolonged drug release up to 4 days at the highest drug loading. Initial burst release is attributed to the rapid dissolution at the surface or close to the surface of adhered/entrapped drug in the nanoparticles, while the later slow release is because of the penetration of the release medium into the microaggregates and dissolution of the entrapped drug. On the basis of the *in vitro* drug release, conversion factor between NHT to nicotine base (1 mg NHT equals 0.35 mg nicotine base), drug loading, and FPD of NHT from the prepared nanoparticles, the predicted plasma concentration will be between 4-7 ng/mL from 1.7 to 3.2 mg of FPDs of the prepared formulations for therapeutic action. These values for NHT-CS 3:1 are similar or above the reported plasma concentrations of

nicotine obtained after inhalation via a device or cigarette smoking (Moyses et al., 2015). FPF of NHT-loaded CS nanoparticles increased with increasing surface charge, which probably enhanced the deagglomeration of nanoparticles by repulsive forces. The use of a lactose carrier removed this effect and FPF of nanoparticles from the large carriers based formulations was significantly higher ($p<0.001$) than those of formulations without carriers and was surface charge independent. The results of this chapter suggest the mechanism of nicotine loaded CS nanoparticle dispersion without large carriers is dependent on the zeta potential, which is linked to the agglomeration or deagglomeration behaviour of nanoparticles. Further comprehensive studies maybe warranted to develop an efficient DPI formulation by understanding the interactions between the charged particles and carriers, the impact of charged particles or agglomerates on the deagglomeration and dispersion. Long term stability study showed the DPI formulations of NHT-loaded CS nanoparticles were stable at the storage condition of 25 °C/60 % RH. The outcomes of *in vitro* evaluations of prepared NHT loaded CS nanoparticles in this chapter are suitable to supply the effective therapeutic concentration after inhalation with sustained release and this provides a direction for *in vivo* animal evaluation tests in the following work.

# Chapter 5:

# *In Vivo* Assessments of NHT-loaded CS Formulations for Pulmonary Delivery

In this chapter NHT-CS nanoparticles are administered to mice lungs via a nose-only inhalation device to assess the drug activity and to determine the potential toxicity issues with pulmonary delivery of the formulations. First, the efficiency of a nose-only inhalation device is evaluated *in vitro* to determine the best parameters of flow rate and delivery period to deposit DPI formulations in the lungs of mice. Investigation of whether the formulation of NHT-CS (3:1) nanoparticle (developed in Chapter 3, designated here as **nano-nicotine**) has altered the activity of NHT by comparing the effect of the unmodified NHT in naïve mice (C57BL/6, 8-10 weeks old) through locomotor activity via a single subcutaneous injection (s.c) was performed. Next, the minimum required inhaled dose of nano-nicotine was determined which caused locomotor activity response similar to the injected (s.c.) dose of unmodified NHT. Finally, histological examination of lung tissues was performed to determine if inhalation of the nano-nicotine caused any lung damage.

## 5.1 INTRODUCTION

Locomotor activity in rodents is commonly used to investigate changes in spontaneous activity in response to pharmacological treatments. It is defined as the movement from one point to another in a specific time period. Nicotine is capable of altering locomotor activity. The locomotor response to nicotine is mediated by various neurotransmitters, producing either a stimulant or depressant motor activity depending on the mouse strain and dose administered (Clarke & Kumar, 1983; Domino, 2001). Stolerman reported locomotor stimulant and depressant effects of nicotine are due to different actions of different type of nicotinic acetylcholine receptors nAChRs (Stolerman, Garcha, & Mirza, 1995). The reinforcing effects of locomotor activity from nicotine is associated with the dopamine release to activate nAChRs subunits in the brain, and then nicotine increases nAChRs intensities through activating α4β2 nicotinic receptors

to modulate the release of several neurotransmitters (Lallemand, Ward, & De Witte, 2007; Marubio et al., 2003). The depressant effect of nicotine is possibly due to blockage of neuronal nAChRs (Mineur & Picciotto, 2010), but the mechanism by which nicotine acts as an inhibitor remains obscure. Both effects of nicotine can be inhibited by the nicotinic antagonists such as mecamylamine (Clarke & Kumar, 1983; Stitzer, Morrison, & Domino, 1970). Therefore, the change in locomotor activity by nicotine exposure in non-tolerant mice is a primary step to predict pharmacological effects of our new nano-nicotine formulation in humans. On the other hand, chronic nicotine exposure in rodents would cause nicotine tolerance, as evidenced by a less depressant phase and a higher dose to induce stimulant locomotor response (Clarke & Kumar, 1983).

Different locomotor activities were observed among various strains due to distinct pharmacogenetic differences (Collins, Miner, & Marks, 1988). In this study, we selected C57BL/6 mice, which are commonly used in bioassays during tobacco ingredient testing. Tsuji reported that mice of the C57 strain could inhale higher volume of smoke in the lungs in comparison to other strains under same exposure conditions in acute cigarette smoke inhalation studies (Tsuji et al., 2011).

The aim of this chapter is to explore a series of optimum parameters *in vitro* to be applied on the nose-only inhalation device and determine the safety and efficacy of nano-nicotine as DPI formulation in mice models *in vivo*. The stimulatory dose of nano-nicotine which is comparable to the effects of free base is selected which is expected to mimic the effects of cigarette smoking.

## 5.2 MATERIAL AND INSTRUMENTS

### 5.2.1 Animals

The protocol was approved by the Queensland University of Technology Animal Ethics Committee and the University of Queensland Animal Ethics Committee, in accordance with the National Institutes of Health (NIH) guidelines for the care and use of laboratory animals.

Male C57BL/6 naïve mice aged 8-10 weeks old (25.0 ±5.0 g) were obtained from the Australian Resource Centre (Perth, Australia). All animals in this study were nicotine naïve prior to the commencement of experimental protocols and were given at least 1 week to habituate to the animal facilities prior to experiment commencement. Mice were single-housed in a clear, ventilated cage (Tecniplast) with unlimited access to food and water. The home cages are temperature controlled with a 12h normal light/dark cycle (lights on 7am: off 7pm). The mice were used only once, and they were sacrificed immediately after testing.

### 5.2.2 Drugs

Nicotine hydrogen tartrate (NHT) powder was purchased from Sigma-Aldrich, Australia. It was ground into inhalable fractions of powders using mortar and pestle. All doses of nicotine in the following work are expressed as the free base of the nicotine (1 mg NHT equals 0.35 mg nicotine base). Based on the results of Chapter 4, to improve aerosolization of nanoparticle powders, both NHT and nano-nicotine were mixed with four times of inhalable grade lactose monohydrate (Inhalac® 120) (see 3.1.1).

### 5.2.3 Nose-only Inhalation Device

***Design of Device***

The nose-only inhalation device for administration of inhalation powder to multiple mice was modified from a previous report by Biswadip (Sinha & Mukherjee, 2012). The scheme of design is shown in Scheme 5.1. The main three parts of this inhalation device are: inhalation chamber, delivery chamber and dosing chamber.

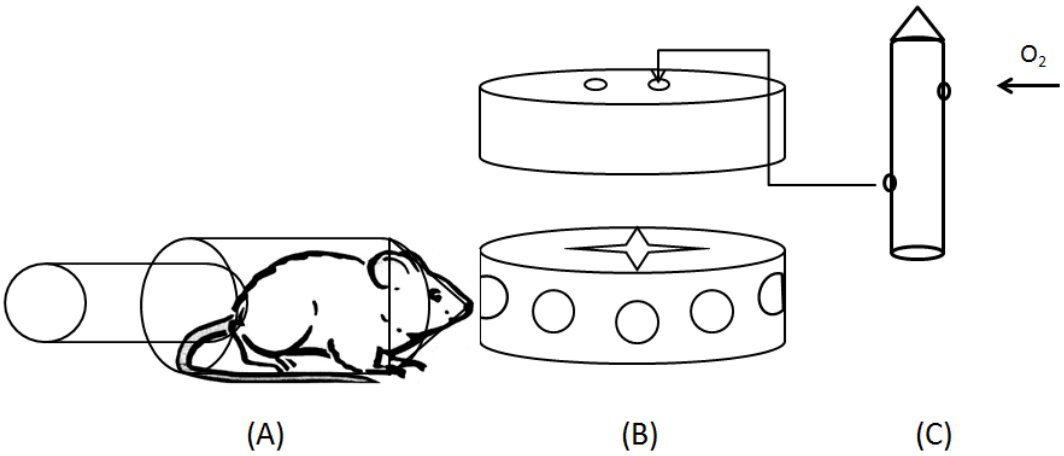


Scheme 5.1 Diagram of (A) inhalation chamber made of 50 mL tapered centrifuge tube; (B) delivery chamber; (C) dosing chamber

***Delivery chamber:*** A round box is in the middle as the delivery chamber with the fan assembled into it to deliver the formulations to the mouse nose and circulate the air. Two holes are made on the screwable cover of the delivery chamber, of which one is to connect the dosing chamber as the entry of the DPI delivery port; the other hole is to connect oxygen/air through pipeline. There are twelve equal holes (exposure ports) across the outer face of delivery chamber to accommodate the mice holding containers, which are termed inhalation chambers.

***Inhalation chamber:*** Each exposure port is connected to an inhalation chamber that transfers aerosolized formulation to the animals. Inhalation chamber are made of the

50mL tapered ends of centrifuge tubes. The tapered bottom of tubes is cut to make a small hole so that only the noses of the mice can tightly fit the holes. The silicone sealant was put between the tubes (inhalation chamber) and delivery chamber to prevent leakage of powder. The other ends of the tapered centrifuge tubes were replaced with the plunger of syringe which is adjusted based on the size of the mouse to prevent the mouse from removing their nose from the inhalation port.

***Dosing chamber:*** Dosing chamber is made of 15 mL tapered end of the centrifuge tube. Two holes are punched on the wall of the tubes. A long plastic pipette was placed into the tube through the hole for pumping air to fluidize the powder. The other hole was connected to the dosing chamber to deliver the drug powder (nano-nicotine powder, NHT powder or blank CS nanoparticles). The dosing chamber from centrifuge tube was turned upside down when the experiment is in process to allow the drug powder to be delivered to delivery chamber. All the holes cut in this system were sealed tightly by adhesive to prevent air leaking from chambers.

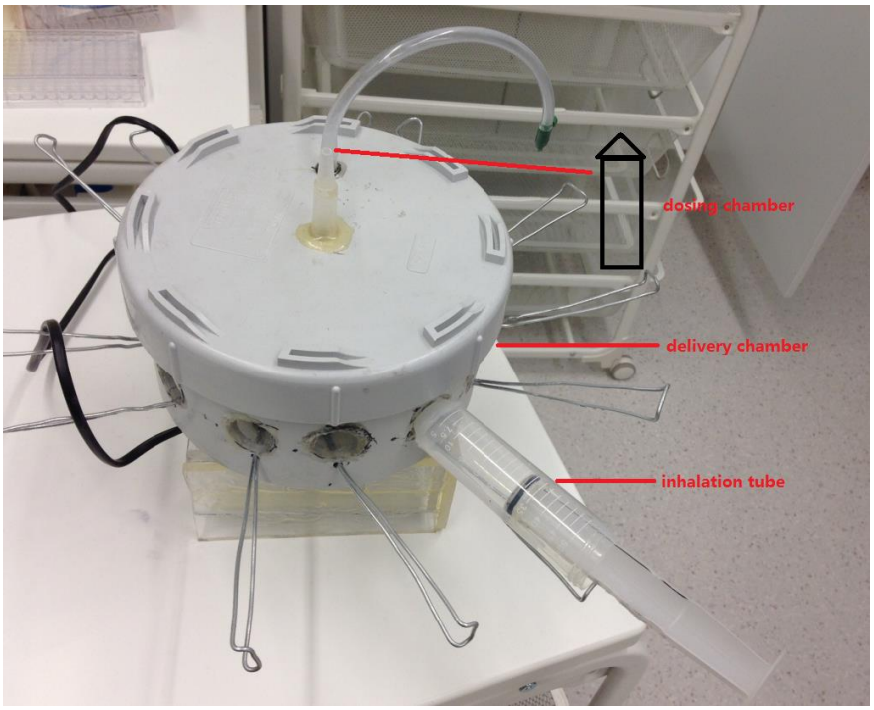


Figure 5.1 Design of nose-only inhalation device

## 5.3 METHODS

### 5.3.1 *In Vitro* Evaluation of Drug Deposition

Efficiency of customised nose-only inhalation device was evaluated by *in vitro* drug deposition test. This procedure was aimed to choose the best aerosolization parameters to collect as much deposited drug on the inhalation ports of inhalation chamber as possible. The selected parameters (e.g. loading dose, delivery time, and flow rate) were applied *in vivo* animal study protocol design. The delivery chamber was connected to the dosing chamber by a rubber pipeline. The other side of dosing chamber was connected to the anaesthesia apparatus to allow control of oxygen flow rate. The loaded powders in the dosing chamber were fluidized after ventilating the oxygen from isoflurane apparatus (V3000PK, Parkland Scientific, Inc. USA). All the junctions of inhalation device were sealed appropriately to prevent the powders leaking and splashing during experiment.

The customised inhalation chamber can accommodate up to twelve mice. Six ports (port No: 2; 4; 6; 8; 10; 12) were blocked using syringe plungers. The other six ports were fixed to animal holder tubes (inhalation chamber) which were made of cut ends of tapered centrifuge tubes to test *in vitro* powder deposition. A weighed piece of cotton, which mimicked the nose of mice, was plugged in each port of animal holder tube. The collected amount of drug on the cotton plugs represented the inhaled amount of drug at the respective ports if the mice were placed into the inhalation tubes. Ground NHT was mixed with inhalation grade lactose monohydrate (Inhalac® 120) microparticles used as carriers to make binary interactive mixtures using hand mixing technique. Amount of powder mixture (1:4 w/w ratio) of NHT (100mg) and lactose (Inhalac® 120) (400 mg) was loaded into dosing chamber. At the selected oxygen flow rate (0.6L/min; 0.9L/min), the powder was delivered to inhalation chamber for 3min or 5min. After powder dosing, the cotton pieces from each port were washed by PBS and collected separately. This process was repeated at least three times by rinsing cottons and squeezing them with a clean tweezers. The volume of the washing from each port was made up to 10 mL with PBS. After filtering through 0.22 μm filter (Millipore), the drug content was analysed by UV spectroscopy with proper dilution with PBS. The powder left in the delivery chamber and dosing chamber was also collected using cotton and PBS, followed by analysing by UV spectroscopy. The total recovered dose was sum of amount of powders in inhalation chamber, dosing chamber and delivery chamber to calculate the mass balance.

### 5.3.2 *In Vivo* Locomotion Behaviour Test

#### *5.3.2.1 General protocol of locomotor activity*

Locomotor activity was monitored with a 16 × 16 photo beam array located above the floor of the enclosure (Figure 5.2). The locomotor activity chambers were 40×40×38

cm divided into 4 enclosures with grid lines marked on the floor. Each enclosure can hold only 1 animal and up to 4 animals can be assessed at any one time. The locomotor activity chambers were monitored with an overhead-mounted video camera connected to a VCR to record mice behaviour which was analysed by Any-maze Software (Stoelting, Wood-dale, IL) which measured the distance the animal travelled every 5 mins.

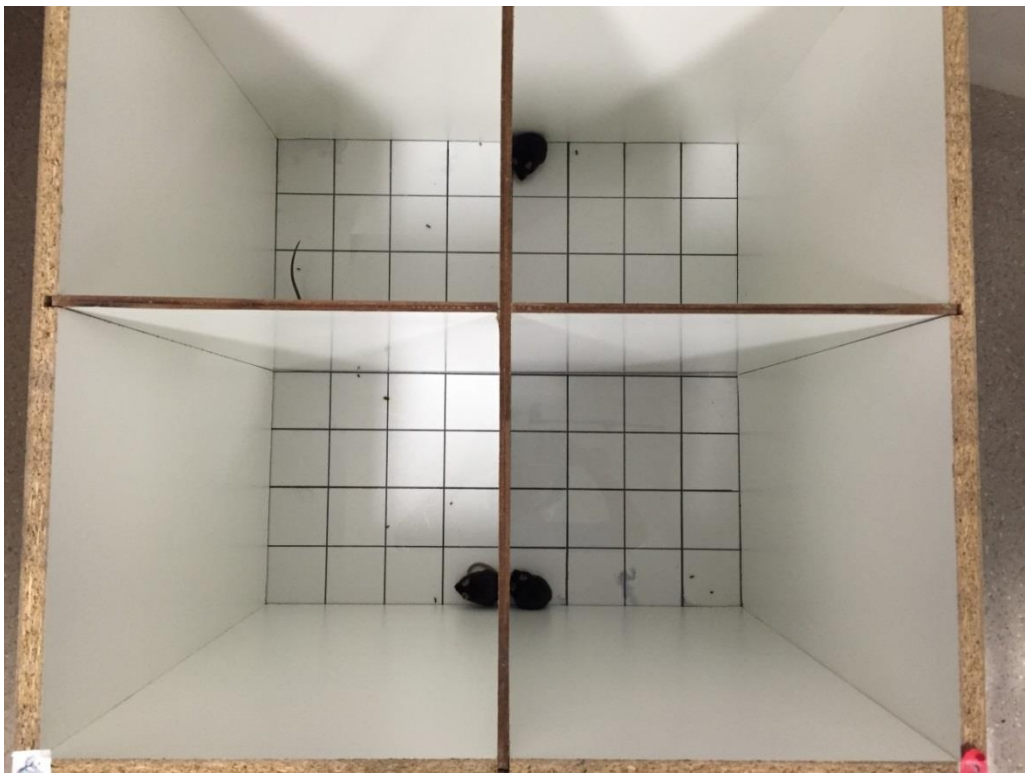

Figure 5.2 The apparatus of locomotor activity chamber

Locomotor studies were run 2 hours per day over four consecutive days. On day 1, mice were placed into the locomotor chamber for 2 hours (8:00am-10:00am, first round) in the morning and returned to home cage afterwards. No data was collected at day 1, allowing mice to acclimatize to the locomotor chamber. On days 2 and 3, mice were placed into the locomotor chamber to be habituated in the first hour, followed by being given a single s.c. injection of physiological (0.9%) saline (10 mL/kg) (Chapter

5.3.2.2) or placed in the nose-only inhalation chambers for 5 mins (Chapter 5.3.2.3). Mice were returned to locomotor chamber for another 1 hour. The purpose of day 2, 3 were to habituate mice to the apparatus and injection or inhalation procedure before the drug test started. On day 4 (drug testing day), mice were placed in the locomotor activity chamber again for 60 min prior to the start of testing, when mice were given a single s.c. injection of drug treatment or placed into the nose-only inhalation chambers with drug treatments. The mice were returned to the activity chamber immediately after the injections or inhalations, and the test sessions lasted for another one hour. After the each session, mice were returned to their home cage. Locomotor activity (distance travelled) was measured from the video recording using AnyMaze software. On the day 4 (drug testing day), travel distances of mice in the first hour were measured as baseline. Once stable baseline were established, changes in distance travelled in the second hour at day 4 with nicotine and nano-nicotine injections or inhalations were compared to the results with the vehicle alone to assess sensitization of nicotine and nano-nicotine in mice. Nicotine naïve mice received s.c. saline injections as a control group on basal activity throughout the experiment. Sensitization was evaluated by a significant increase or decrease in activity with drug administration compared with vehicle group, indicating doses defined in response to drug.

The distance travelled induced by CS only injection was compared with control, determining whether CS only injection cause changes in locomotion behaviour in mice. Afterwards, the travel distance administered by nicotine injection compared to the control to observe the effects of acute injection of nicotine. The comparisons in travel distance by nano-nicotine injection and control to determine whether the bioactivity of nano-nicotine was altered during manufacture process. In the study of in vivo locomotor activity by inhalation, the travel distance administered from CS only

inhalation was seen as control group. The distance travelled exposed to nicotine inhalation to determine the acute effects of nicotine inhalation. The minimum stimulant dose of nano-nicotine was selected from the highest travel distance induced by inhalation of nano-nicotine in comparison with control.

#### *5.3.3.2 Assessment of bioactivity of nano-nicotine via in vivo locomotor test by injection*

To determine whether the nano-nicotine had changed its bio-activity, the locomotor activity procedure was applied. Four different doses of nicotine test groups were set up. They were: 0.25 mg/kg; 0.5 mg/kg; 1.0 mg/kg, 1.5 mg/kg, which were equivalent to NHT powder as 0.71mg/kg; 1.42 mg/kg; 2.84 mg/kg; 4.26 mg/kg respectively. Meanwhile, four different formulated nano-nicotine groups were administered in accordance with nicotine-only groups. They were: 1.10 mg/kg; 2.19 mg/kg; 4.37 mg/kg; 6.56 mg/kg. All drugs were prepared freshly prior to drug test every time in physiological saline (0.9%) and administered as subcutaneous (s.c.) injections in a volume of 10 mL/kg. Doses of nicotine are expressed as mg/kg and were administered using a pseudorandom Latin square design to create test batches and control for potential sources of inter-batch variation.

The dose response curves were used to assess the bio-activity of the nano-nicotine and compared it to nicotine. Mice were randomLy assigned to one of four groups: vehicle (V), CS only (C), nicotine (N) and nano-nicotine (NN) (see Table 5.1). The procedure of locomotor activity test was as general protocol in Chapter 1.3.3.1. On day 4 (drug test day), mice were placed in the locomotor activity chamber for 60 min to collect the baseline prior to the start of testing, then mice were given a single s.c. injection of the assigned treatment: vehicle (n=10) or CS (1.5mg/kg; n=10) or nicotine (n=10) or nano-nicotine (n=10). Changes in distance travelled with CS only, nicotine and nano-

nicotine injections were compared to vehicle as an indicator of whether the nanoparticle manufacture process has altered the activity of the compound.

Table 5.1 Outline of experimental groups (e.g. dose=1 mg/kg)

| Treatment on days | Day 1 | Day 2 | Day 3 | Day 4 |
|---|---|---|---|---|
| First round (8:00 am-10:00 am) | | | | |
| Vehicle (V) | n/a | Sal | Sal | Sal |
| Chitosan (C) | n/a | Sal | Sal | C |
| NHT (N) | n/a | Sal | Sal | N |
| Nana-nicotine (NN) | n/a | Sal | Sal | NN |
| Second round (11:00 am-1:00pm) | | | | |
| | | As above first round | | |
| Third round (3:00 pm-5:00 pm) | | | | |
| | | As above first round | | |

"N"=one of 0.71mg/kg; 1.42 mg/kg; 2.84 mg/kg; 4.26 mg/kg NHT; "NN"=one of 1.10mg/kg; 2.19 mg/kg; 4.37 mg/kg; 6.56 mg/kg formulated nano-nicotine. "C"=blank chitosan; Sal=0.9% saline. n/a means no injection. Three rounds per day.

#### *5.3.3.3 Assessment of viability of nano-nicotine via locomotor test following inhalation*

To determine the minimum stimulant dose required of nano-nicotine to alter mice locomotor activity and compare the inhalation efficiency of inhaled nano-nicotine with nicotine, the locomotor activity of naïve male mice (8-10 weeks old, C57BL/6) was measured following an acute inhalation administration dose of nano-nicotine or nicotine. Blank CS nanoparticle powders were used as the control. As described in the general protocol of locomotor test (1.3.3.1), the animals were habituated to the enclosure for one hour before the drug administration procedure. During the drug inhalation test, the mice were placed in the nose-only inhalation chambers for 5 mins instead of receiving an injection before being returned to the locomotor chamber. We tested blank CS nanoparticles and 3 doses of nicotine and nano-nicotine to determine

the lowest effective dose which was capable of altering locomotor activity using a Latin square design as described above. Four mice were tested per batch and three batches were tested per day. Different doses were loaded in the dosing chamber per batch, i.e 25mg, 50mg, 75mg NHT (labelled as 25N, 50N 75N), and 38.5mg, 76.9mg and 115.4mg nano-nicotine, which were equivalent to corresponding amount of NHT respectively (labelled as 25NN, 50NN 75NN). The test powder (NHT, nano-nicotine or blank CS) with four times of inhalable lactose powders were ground into inhalable grade powder and aerosolized under sufficient fluid pressure with flow rate of oxygen at 0.9L/min for 5 minutes in the 15 mL dosing chamber. In the following contents and figures in this chapter, the dose of nicotine per batch represented as 25N, 50 N, 75N; and equivalent dose of nano-nicotine per batch noted as 25 NN, 50 NN and 75 NN.

### 5.3.3 Histopathological Evaluation and Lung Morphometry

After completion of locomotor activity test, the mice were euthanized with carbon dioxide either immediately or 24 hours post exposure to assess the lungs for potential adverse effects of nicotine and nano-nicotine. The lungs were inflated with 2 mL of 4% (w/v) paraformaldehyde (PFA), and then removed and fixed in a 4% PFA solution containing neutral PBS for at least 72 hours. After fixation, the lungs were stored in the PBS until processing. The specimens of all pulmonary lobes were embedded in paraffin. Sections at a thickness of 5 μm were stained with hematoxylin and eosin (H&E) to examine the histological structure using a brightfield slide scanner (Olympus VS120).

Histological slides were assessed for unpigmented and pigmented macrophages in the alveolar lumen; pigmented macrophage nests in the alveolar lumen; lymphocytic infiltrates in the alveolar interstitium; lymphocytic infiltrates in the peri-vascular area;

neutrophilic granulocytes in the alveolar lumen; pulmonary emphysema; and hyperplasia of the alveolar epithelium. One section per mouse by a cross section between a main stem bronchus and its branching bronchioles was assessed morphometrically. The area of morphometric assessment was selected randomLy using a xyz camera and processed with OlyVIA software (Olympus OlyVIA 2.4).

### 5.3.4 Statistical Analysis

All numerical data presented as mean ± SEM and statistically evaluated using GraphPad Prism 6 (GraphPad Software Co., USA). In the study of in vitro evaluation of nose-only inhalation device, comparison of means between oxygen flow rates of 0.6 L/min and 0.9 L/min as a whole was performed with the unpaired t-test, while the comparison of inhalation port individually between flow rates of 0.6 L/min and 0.9 L/min was processed with two-way ANOVA with Bonferroni's post hoc test. The statistical analysis of the locomotion behaviour and the doses of drug treatment with time were performed as two-way ANOVA, followed by a Bonferroni post hoc analysis. Significant differences were taken into account if p was less than 0.05.

## 5.4 RESULTS AND DISCUSSION

### 5.4.1 *In Vitro* Evaluation of Nose-Only Inhalation Device

The flow rate is one of the most important factors to affect the drug deposition. The drug powder loaded into dosing chamber was forced to flow rapidly towards delivery chamber by sufficient fluid pressure, so the proper flow rate should be selected to aerosolize drug powders as much as possible. In addition, precise ventilation needs to be considered when designing an optimum nose-only inhalation device. The concentration of carbon dioxide in the inhalation chamber is increased with increased duration of animals into the chamber. The suggested ventilation of approaching animal each port is at least 2.5 times as much as that of animal's minute exhaled volume

(Fröhlich & Salar-Behzadi, 2014). The effect of flow rate on drug deposition was evaluated *in vitro* in this study by using 100mg NHT powder with 400 mg lactose as drug carriers. This choice was based on our previous study that the FPF of 10% NHT-loaded CS nanoparticles with lactose carriers was improved significantly compared with the results from nanoparticles without lactose carriers (see section 4.4.4).

After determination of NHT in the PBS by UV, it was found that 0.88±0.04 mg (mean ± SEM) NHT was deposited on average across the six inhalation ports (port No: 1; 3; 5; 7; 9; 11) at 0.6 L/min, while 1.20±0.05mg NHT was collected on average from the six ports at 0.9 L/min. The average deposition rate per port was 21.1% (0.88 mg/port*12 ports/50 mg%100=21.1%) at the oxygen flow rate of 0.6 L/min and 28.8% at the oxygen flow rate of 0.9 L/min. The mean NHT deposition from 0.9L/min was significantly (t-test, $p<0.01$) higher than the mean NHT deposition from 0.6 L/min as presented in Figure 5.3 A. Figure 5.3 B presents the amount of NHT deposited at each individual port of inhalation device. However, when comparison of individual inhalation ports was made between flow rate of 0.6 L/min and 0.9 L/min, the deposition at 0.9L/min was higher than that obtained from 0.6 L/min as a whole, but significance ( two-way ANOVA with Bonferroni's post hoc test, $p<0.05$) was only seen in ports 1, 5 and 11. It is worth noting that six of twelve ports (port No: 2; 4; 6; 8; 10; 12) were blocked during the test process, resulting in lower drug deposition proportion, thus the actual total amount of powder collected from all ports were different from the theoretical amount. The actual mass balance details in the experimental procedure (such as total recovered dose, deposition percentage) have been listed in Appendix A. Consistent with the above findings, the drug deposition was enhanced dramatically with increased flow rate.

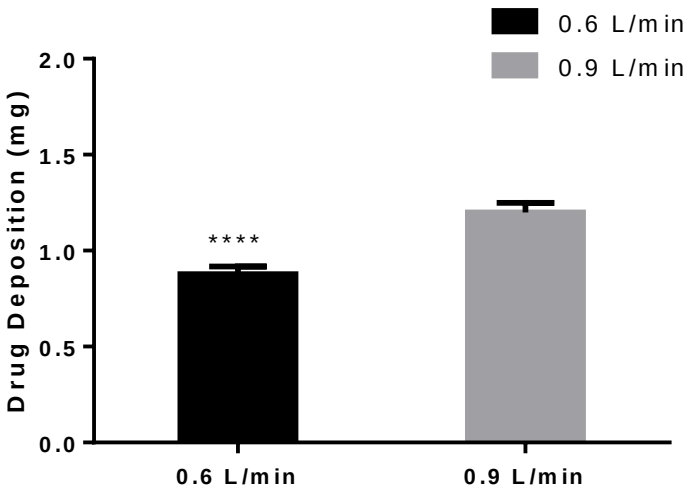


(A)

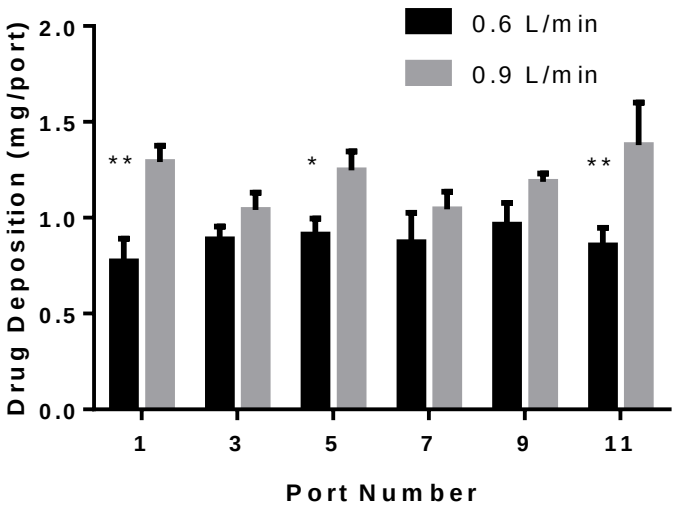


(B)

Figure 5.3 (A) comparison of mean drug deposition at different flow rate. Mean NHT deposition from the flow rate of oxygen of 0.9 L/min (grey) and mean NHT deposition from the flow rate of oxygen of 0.6 L/min (black). (data presented as mean ± SEM., n = 18) (Significant difference from group of 0.9L/min: ****$p<0.0001$). (B) Comparison of effect of flow rate of oxygen on drug deposition at different individual port (data presented as mean ± SEM., n = 3) (Significant difference from group of 0.9L/min: *$p<0.05$, **$p<0.01$)

The nose-only inhalation device in this study was based on a reported design (Sinha & Mukherjee, 2012). A tapered tube was designed as DPI device in this study instead of conventional DPI devices which are available on the market, as generally DPI requires patients to inhale formulation actively, allowing formulation particles to reach the deep lungs properly. However, this definitely cannot be used for animals. In addition, compared to the current 6 mice at a time reported by other group (Sinha & Mukherjee, 2012), the drug deposition rate of our group's device was lower than the reported one (28.8 % vs. 42.67%), which suggested the efficiency of device could be improved potentially.

As discussed above, the drug deposition from flow rate of 0.9 L/min performed much better than those of from 0.6 L/min at all the evaluation sides. The primary reason behind this is that air pressure was insufficient to force powder escaping from dosing chamber and to be delivered to delivery chamber. Besides, more carbon dioxide with water was exhaled from mice when the less oxygen was delivered, causing the overproduction of moisture into the inhalation chambers, which may result in sticky powders to obstruct deaggregation impact events between particles.

### 5.4.2 Assessment of Bioactivity of Nano-nicotine via Locomotor Test by Injection

To explore the effects of nicotine dose on naïve mice locomotor activity, the travel distance against dose of nicotine before and after drug administration was plotted in Figure 5.4. The locomotion distance of mice during habituation period (baseline) Figure 5.4 (A)] was analysed by one-way ANOVA with Bonferroni post hoc analysis, demonstrating no significant difference was observed among groups [$F(5, 43) = 0.2113$, $p>0.05$ ]. It indicated that a stable baseline has been achieved, and any changes of locomotion activity after drug administration resulted from the treatments of drug

instead of some effect of particular locomotor chambers. Under this experimental condition, Figure 5.4 (B) presented the locomotor activity of mice after s.c. injection in the first hour. There was no significant difference between treatments of vehicle (V) and CS only (C) injection, suggesting CS injection did not affect the locomotion activity in mice.

The results of nicotine injections showed the dose of nicotine had the dual effects in locomotion distance with significant difference of treatments statistically [$F(5, 42) = 5.216$, ***$p=0.0008$]. Compared with the vehicle group, s.c. injection of 0.25 N, in the similar level of CS injection, had no effects on locomotor activity, while 0.5 N administration boosted mice locomotor activity significantly (*$p=0.0274$); on the other hand, 1.0 N and 1.5 N decreased locomotor activity considerably visually, though these effects were not statistically significant from vehicle group ($p>0.05$), they were significant different from 0.5 N injection ($p<0.05$).

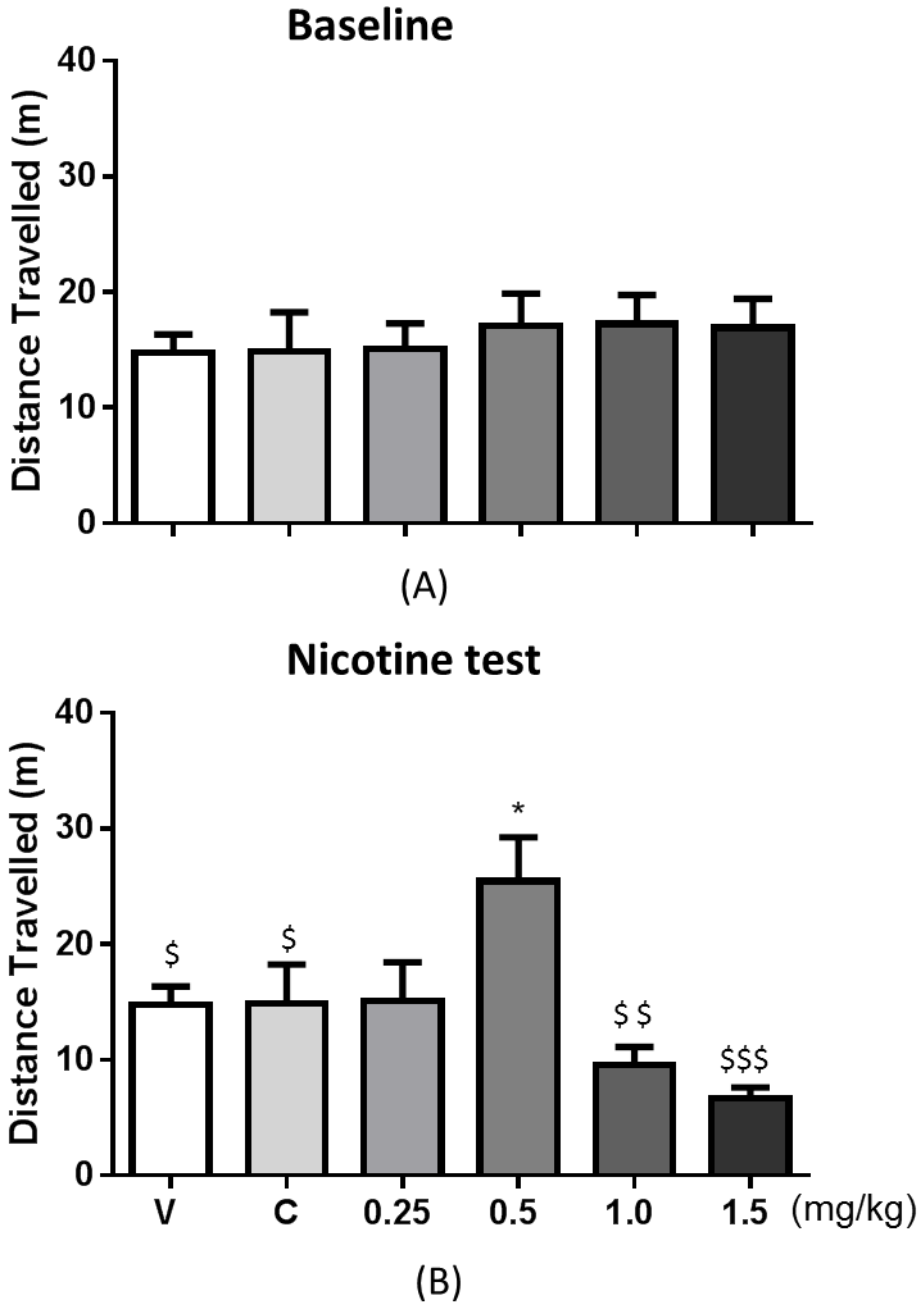


Figure 5.4 Total travel distance of mice in the period of (A) habituation (baseline); (B) nicotine test administered by s.c. injection (n=8-10 per group) (significant difference from group of vehicle: *$p<0.05$, significant difference from group of 0.5N: $^{\$}p<0.05$, $^{\$\$}p<0.01$, $^{\$\$\$}p<0.001$)

The doses of nicotine (0.5 mg/kg, 1.0mg/kg, 1.5 mg/kg) chosen in this study were based on the recommended nicotine dose in mice by Matta et.al (Matta et al., 2007). It was reported that the sensitivity of acute effects of nicotine in mice is less than that in rats. Median effective dose (ED50) dose for seizures in mice is 2-6 mg/kg depending

on strain (Matta et al., 2007). Regarding our study, the markedly depressant effects induced by acute s.c. injection were observed at 1.5 mg/kg, while the stimulant effects were at 0.5 mg/kg. The dose-response relationship between stimulant and depressant effects generally occurs in mice within a narrow dose range and the purpose of this section was to find the minimum nicotine dose in mice which had a stimulant effect. Thus, a lower nicotine dose of 0.25 mg/kg was introduced. The doses of nano-nicotine chosen were based on the drug loading (65%) of nicotine-loaded CS nanoparticles in accordance with corresponding nicotine doses.

The results obtained in this study are agreement with previous reports (Stolerman, Fink, & Jarvik, 1973) (Clarke & Kumar, 1983) that locomotor stimulant effects were developed at low dose of nicotine, followed by a decrease at high dose of nicotine in its locomotor depressant effects, which is governed centrally mediated theoretically (Morrison et al., 1969). The sensitized nicotine group (0.5 N) travelled longest in locomotor activity among all the nicotine test groups, which is supported by Schweitzer that low dose of intravenous nicotine suppresses spinal reflexes (Schweitzer & Wright, 1938), in contrast, the dose of 1.5 N showed sensitized depressant behaviour as high level of nicotine in the brain and blood would cause locomotion disturbances, which has been reported by Stolerman (Stolerman et al., 1973). Overall, the nicotine locomotor stimulant and depressant characters in naïve mice are dose dependent due to the regulations of different types of nAChR on nicotine's stimulant and depressant effects.

A stable baseline with no significant difference [$F(5, 46) = 0.6652$, $p>0.05$] was obtained during habituation period as shown in the Figure 5.5 (A) using one-way ANOVA test. The travel distances from different doses of nano-nicotine were graphed

in Figure 5.5 (B) with significant difference [F (5, 46) = 3.671, **p=0.0071] seen among treatment groups using one-way ANOVA with Bonferroni post hoc analysis. Compared with vehicle group, the injections of CS and 0.25 NN produced similar average travel distance in one hour without statistical difference ($p>0.05$). The treatment of 1.0 NN injection stimulated mice to the maximum average travel distance with significant difference (* p=0.0418) from vehicle group. The dose of 0.5NN increased travel distance, but the effect was not clearly as high as the dose of 1 NN when compared with vehicle group and no significant difference was detected statistically. Marked locomotor depression was observed at 1.5 NN though this effect was not statistically significant from the vehicle group ($p>0.05$).

Furthermore, results were analysed statistically between doses. The travel distance from 1.0 NN injection was as comparator. The significant differences were observed at the treatments of 0.25 NN ($^{\$}p=0.0292$) and 1.5 NN ($^{\$\$}p=0.0014$) from the group of 1.0 NN.

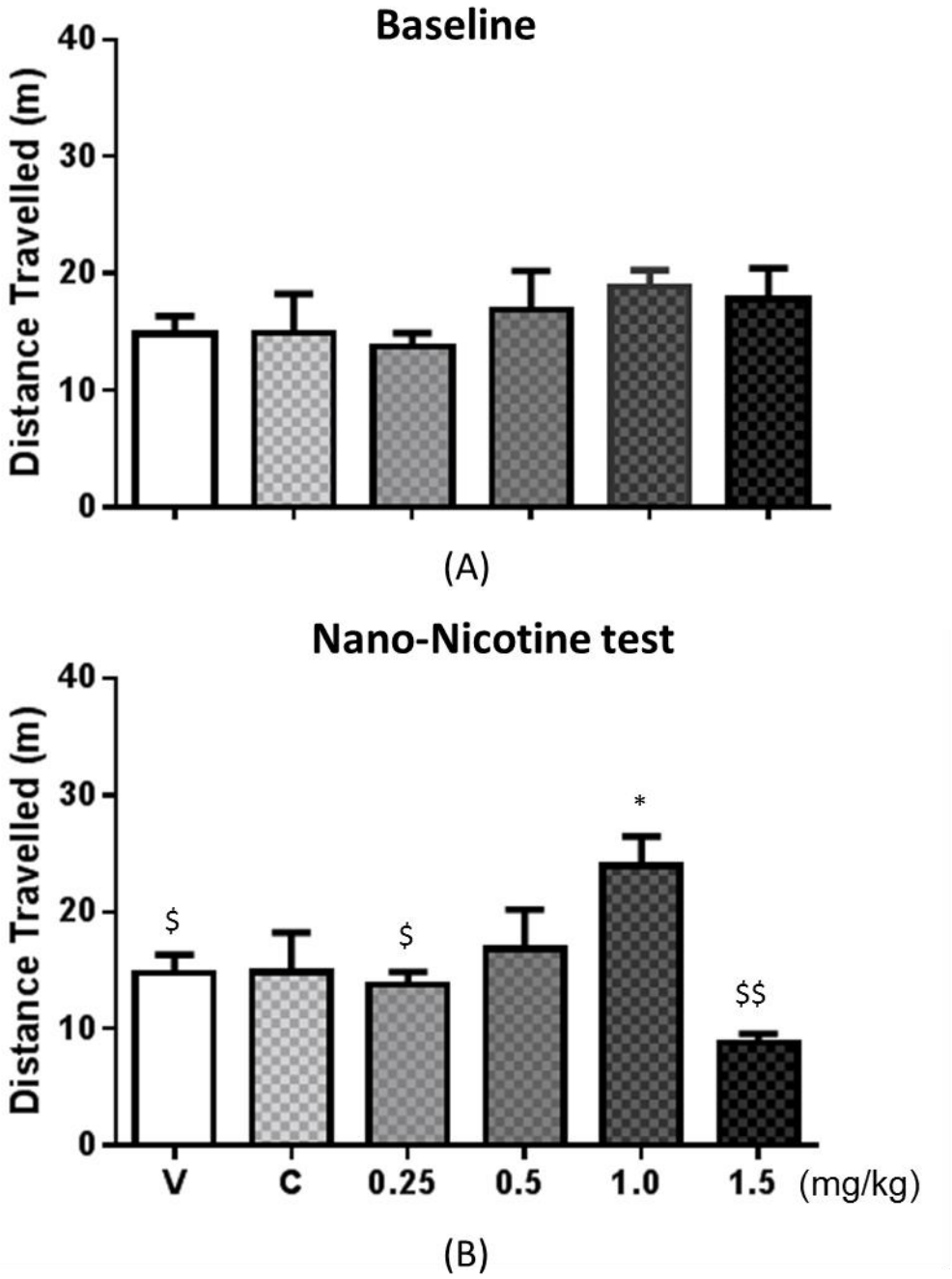


Figure 5.5 Total travel distance of mice in the period of (A) habituation (baseline); (B) nano-nicotine test administered by s.c. injection (n=8-10 per group) (significant difference from group of vehicle: *$p<0.05$; significant difference from group of 1.0 NN: $^{\$}p<0.05$, $^{\$\$}p<0.01$)

The s.c. administration of nicotine induced an obvious dose-related effect in mice locomotor activity and their travel distance was analysed in every 5 minutes in the one

hour post drug injection (Figure 5.6). Statistical analysis from two-way ANOVA with Bonferroni post hoc test showed that there was a main effect [F (55, 473) = 1.819; ***p=0.0006] between factors of time [F (11, 473) = 51.92; p<0.0001] and treatment [F (5, 43) = 3.446; p=0.0105]. The travel distance in the first 5 minutes, the highest peak from all mice during one hour observation, was stimulated greatly by the dose of 0.5 N (**p<0.01) and 1.0 N (*p<0.05) when compared with vehicle group. However, it is uncertain to conclude whether the hyperactivity during this session was as a result of test stress response or nicotine stimulation effects. In the second 5 minute session, the locomotor activity of all mice were reduced substantially, while the doses of 1.0 N (***p<0.001) and 1.5 N (***p<0.001) inhibited mice around zero movement with statistically significant decrease from vehicle group. This maybe an evidence to show acute nicotine administration in high dose could cause mice hypoactive and sleepy. In the following sessions, no significant differences between drug treatment groups were observed compared with vehicle group. This maybe because the nicotine was metabolized into cotinine in the mice bodies which was in agreement with the short half-life ($t_{½}$) around 5.9-6.5 minutes of nicotine in the mice (Petersen, Norris, & Thompson, 1984).

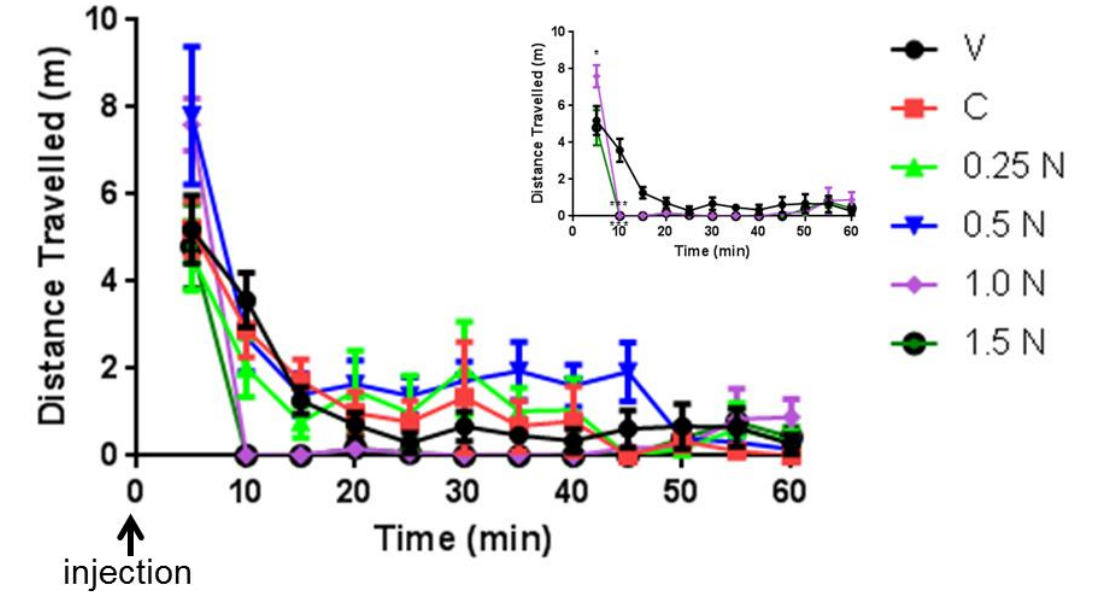


Figure 5.6 The effects of dose administrated by s.c. injection of nicotine on mice locomotor activity with time (n=8-10 per group) (Significant difference from vehicle group: *p<0.05, **p<0.01, ***p<0.001)

Similarly, the locomotor activity of mice with different doses of nano-nicotine injection was analysed in the every 5 minutes by two-way ANOVA with Bonferroni post hoc test as shown in Figure 5.7. No interaction effect [F (55, 506) = 1.222; p=1.222], but significant differences in the effects of time [F (11, 506) = 44.87; ****p<0.0001] and drug treatments [F (5, 46) = 3.671; **p=0.0071] were observed. Substantial increased travel distance was performed in the first five minutes regardless of the doses of nano-nicotine though no significant difference was detected in comparison with vehicle. In the second 5 minutes session, travel distance from all treatment groups reduced considerably, while both treatment groups of 0.5 NN (**p<0.01) and 1.5 NN (**p<0.01) produced decreased travel distance significant statistically compared with vehicle injection. However, it was interesting to note that mice administered with 1.0 NN came back to be hyperactive with statistical significance during test period between 30 (**p<0.01) and 40 (*p<0.05) minutes. It

suggested sufficient concentration of nicotine was available to stimulate releasing nicotinic acetylcholine receptors in the mice brain during this period, which modulated locomotion behaviour of mice. It is supposed to be highly associated with slow and prolonged release system of NHT-CS nanoparticles. Afterwards, no significant differences were observed in the following sessions compared with vehicle group.

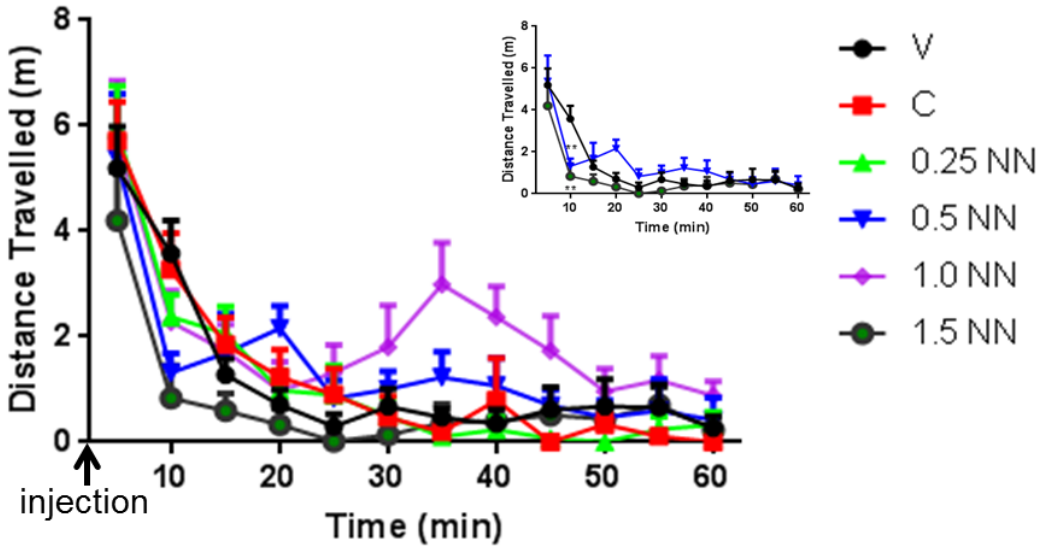


Figure 5.7 The effects of dose administrated by s.c. injection of nano-nicotine on mice locomotor activity with time. (n=8-10 per group) (Significant difference from vehicle group: *p<0.05, **p<0.01, ***p<0.001)

Furthermore, to compare the stimulant effects of nicotine and nano-nicotine in mice locomotor activity clearly, the graphs of 0.5 N and 1.0 NN, which were significantly different from vehicle group statistically, were plotted in Figure 5.8. A marked delayed stimulant response in the treatment of 1.0 NN occurred between 30 and 40 minutes, while no significant effect can be observed in the treatment of 0.5 N in the 5 minutes after s.c. injection was applied. Based on the discussions, it suggested multi doses of nano-nicotine may be required to achieve the same stimulant effect induced by nicotine at the first dose for smokers. However, the delayed stimulant effect of nano-nicotine

will be beneficial to be applied in the clinical practice to reduce side effects of tobacco smoking and maintain a consistent dosing and improve patient compliance.

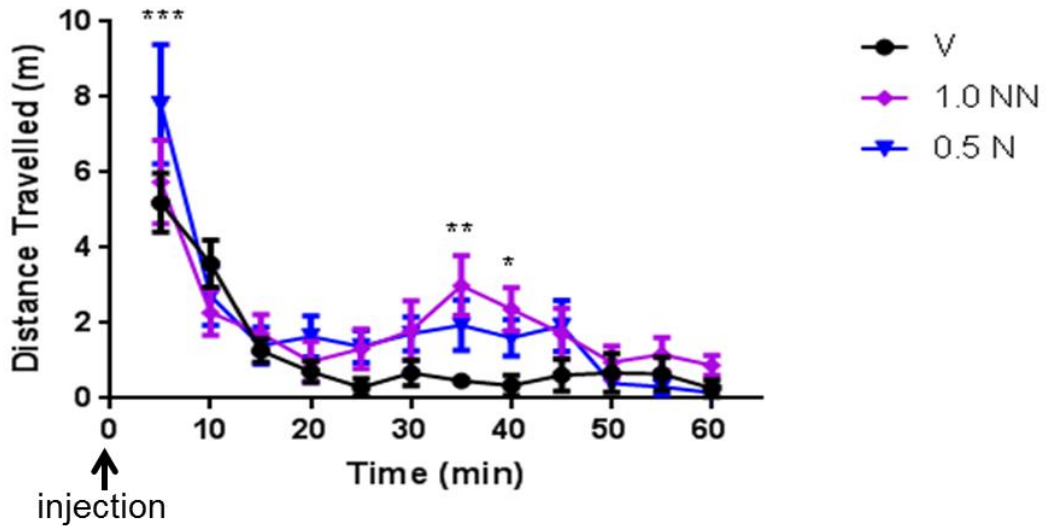


Figure 5.8 Comparison graph between 1.0 NN and 0.5 N administrated by s.c. injection on mice locomotor activity with time. (n=8-10 per group) (Significant difference from vehicle group: *p<0.05, **p<0.01, ***p<0.001)

Based on the results from locomotor activity test by s.c. injection, it is concluded that low dose of nicotine (0.5 N) stimulates hyperactivity in the naïve mice in locomotor sensitivity, while high dose nicotine (1.5 N) depresses locomotor activity. The bioactivity of nano-nicotine was not eliminated during the manufacture process, and the effects of nano-nicotine was like nicotine administration with dual effects, but not as sensitive as nicotine in the naïve animals. This because the nicotine is released from NHT-CS nanoparticles slowly (eg. the cumulative drug release was just around 35% in one hour). Unfortunately, we did not observe the effect of nano-nicotine on naïve mice in a longer period due to the animal ethics concerns and actual operation difficulties.

### 5.4.3 Assessment of Viabilitiy of Inhalation of Nano-nicotine via Locomotor Test

To determine the lowest dose required of the inhaled nano-nicotine to alter locomotor activity, three inhaled doses (25mg, 50mg, 75mg per batch) of nicotine, nano-nicotine and one dose of CS nanoparticles (50mg) as vehicle group were tested on 8-10 weeks old naïve C57BL/6 male mice.

According to the data of *in vitro* evaluation of drug deposition from the novel nose-only inhalation device (section 5.4.1), we knew the flow rate of 0.9 mL/min is superior to 0.6 mL/min for drug deposition. 10.77±1.90mg of 100 mg NHT loaded in the dosing chamber deposited in the 6 delivery ports, so deposited NHT in each port was around 1.8mg. We estimated that loading 100 mg nano-nicotine with 400 mg lactose carriers into the dosing chamber would result in 10.77 mg of NHT delivered to the 6 ports (drug loading=65%, 10.77*65%=7.0 mg) and each mouse will inhale about 1.2 mg (7.0mg/6 mice=1.2 mg) of NHT, which is converted to ~0.4 mg nicotine base (1 mg NHT is equivalent to 0.35 mg nicotine). According to *in vitro* aerosolization study result, FPF of this nano-nicotine formulation was 24.4%, so 97.6 μg of nicotine is expected to be deposited on mouse lung. The average mouse body weight is 25g, so the dose is approximately 4 mg/kg, which is twice as much as the guided dose for mice (Matta et al., 2007). Therefore, 25 mg, 50mg and 75 mg nicotine were chosen to ensure a safe dose was delivered to the mice.

Figure 5.9 (A) showed the mice average total travel distance in the period of habituation (baseline) before nicotine exposure occurred, with no effect of treatment [$F(3, 38) = 0.9177$, $p=0.4415$] when analysed by one-way ANOVA with Bonferroni post hoc analysis test. It suggested that a stable baseline was obtained before drug test. Under this test condition, the acute inhalation of nicotine from different doses caused

a significant treatment effect [F (3, 37) =4.690, **p=0.0071] in mice activity [Figure 5.9 (B)]. As seen in Figure 5.9 (B), the locomotor activity from a dose of 25N was at a similar level to that with vehicle alone ($p>0.05$). At the dose of 50N, the naïve mice were stimulated vigorously to reach the maximum increase in activity compared to the CS only group ($p<0.05$). At a higher dose of 75N the travel activity decreased visually without significant difference from vehicle group.

Furthermore, comparisons were analysed between doses statistically. Though the groups of 25N, 75N were not significant different from vehicle group statistically, the treatments of 25N (*$p<0.5$) and 75N (**$p<0.01$) appeared significantly different from the group of 50N.

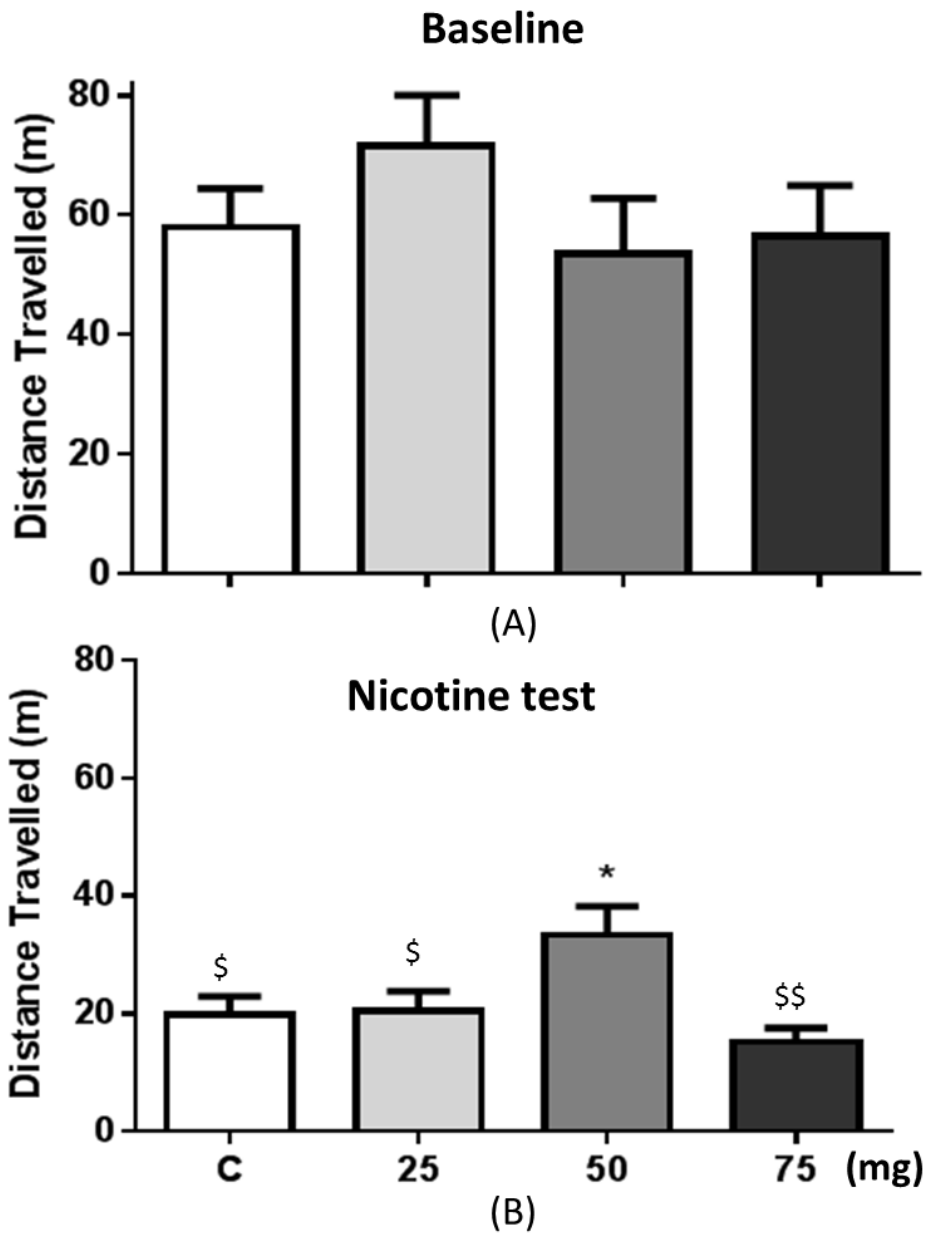


Figure 5.9 Total travel distance of mice with nose-only inhalation exposure in the period of (A) habituation (baseline); (B) nicotine test (n=8-10 per group) (significant difference from group of vehicle: *$p<0.05$; significant difference from group of 50N: $^{\$}p<0.05$, $^{\$\$}p<0.01$).

Figure 5.10 presented the total travel distance of mice between habituation (baseline) and nano-nicotine test. Habituation for 1 hour before drug test produced a stable baseline in mice activity, with no effect of treatment [$F(3, 38) = 0.9692$, $p=0.4173$] observed from one-way ANOVA with post hoc analysis by Bonferroni test. Administration of nano-nicotine caused significant differences in the mice locomotor

activity [F (3, 37) =9.872, ****p<0.0001]. The group of 75NN stimulated locomotor activity significantly (**p<0.01) compared with vehicle group. On the other hand, groups of 25 NN and 50 NN did not alter mice activity behaviour significantly (p>0.5) as compared with vehicle group.

Travel distances from all doses of nano-nicotine were compared between doses. The highest travel distance from dose of 75NN was seen as comparator. Both doses of 25 NN and 50 NN produced the similar level with vehicle group, which were much less than the comparator group with significant differences statistically.

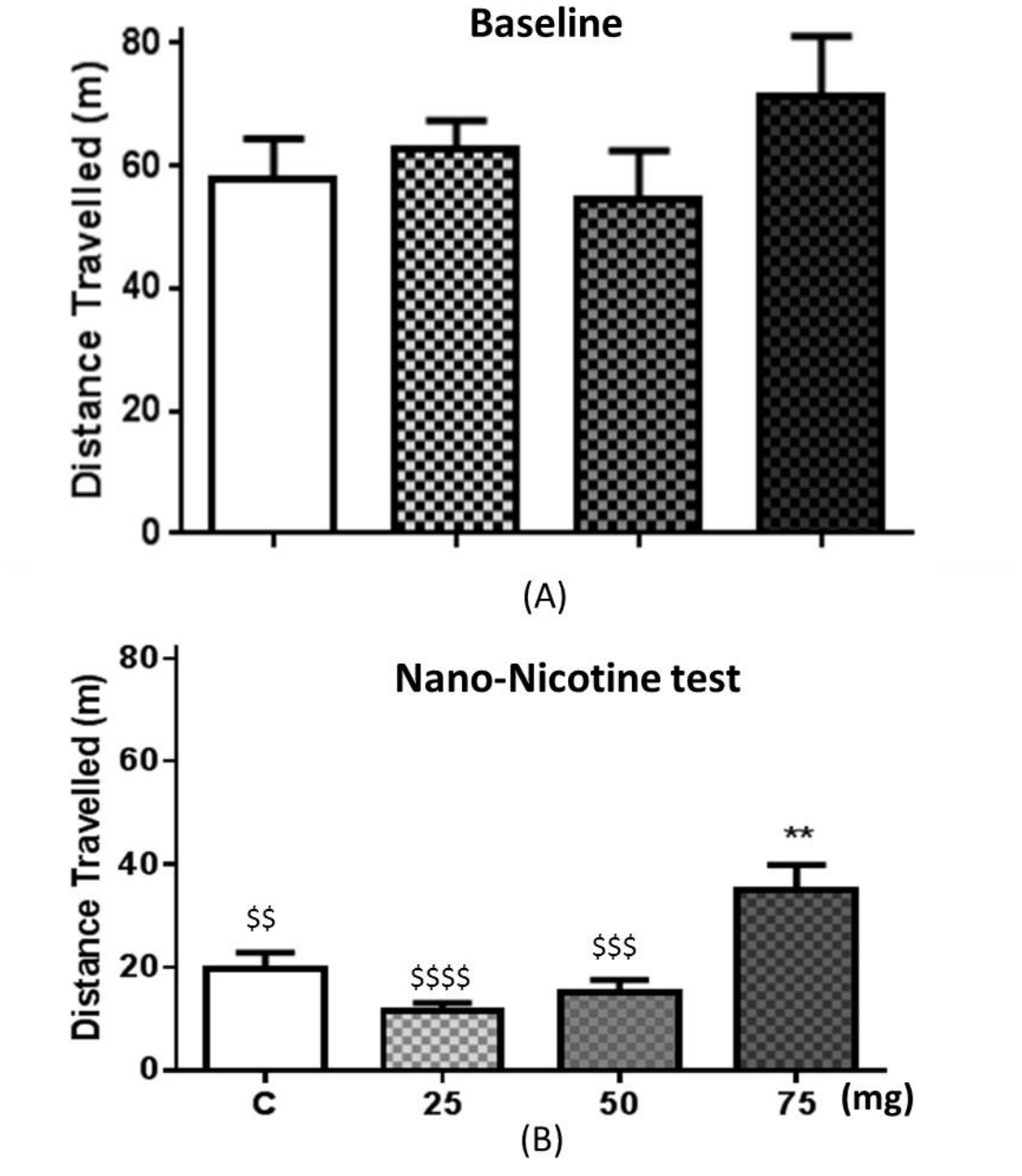


Figure 5.10 Total travel distance of mice with nose-only inhalation exposure in the period of (A) habituation (baseline), producing no differences in baseline activity; (B) nano-nicotine test (n=8-10 per group)(significant difference from group of vehicle: **$p<0.01$; significant difference from group of 75NN: $^{\$}p<0.05$, $^{\$\$}p<0.01$, $^{\$\$\$}p<0.001$, $^{\$\$\$\$}p<0.0001$).

Exposure to inhalable grade of nicotine, nano-nicotine and vehicle of CS nanoparticles powder (after mixing with four times the mass of lactose respectively) produced a dose related response in locomotor activity, which was significant with regards to dose and

treatment factors. To better understand the mechanism of nicotine and nano-nicotine affecting mice locomotion behaviour, the travel distances were plotted in Figure 5.11 in every 5 minutes from all mice and analysed by two-way ANOVA with Bonferroni post hoc analysis test. After inhalation exposure, the first 5 minutes produced highest activity in mice as a result of the fear and stress emotionally from researcher's handling, inhalation device and test process. Hyperactive response induced from stress and fear are consistent with some researchers (Hefner & Holmes, 2007; Strekalova, Spanagel, Dolgov, & Bartsch, 2005). The following activities decreased gradually to the zero at the end of test. There was an interaction effect [F (66, 726) =1.351, *P= 0.0380] on dose treatment [F (6, 66) = 4.562, ***p=0.0006] with time [F (11, 726) = 84.04, ****p<0.0001]. Specifically, the treatments of 25N, 25NN, 50NN, 75N did not resulted in significant travel differences compared with the CS only group. Administration with 50N caused a significant increase (* p<0.05) in the locomotion activity at 15 minutes after inhalation exposure, but no significant differences were observed afterwards. This is mostly possible due to short half-life($t_{1/2}$) of nicotine in mice body. Petersen reported the half-life of nicotine in C57BL mice blood was 5.9-6.9 min when the mice were administrated an i.p injection of nicotine (1.0mg/mL)(Petersen et al., 1984). In other words, smokers have to repeat cigarette smoking frequently to maintain the specific nicotine levels in the body to sustain the effect of the drug because of the rapid elimination rate of nicotine (N. L. Benowitz, 2010). However, the duration of response to 75 NN was longer than 50N, and significant increases in the mice activity were observed at 15 min (**p<0.001), 25 min (**p<0.01) and 30 min (*p<0.05). This is because nicotine has been loaded into CS nanoparticles to achieve sustained and prolonged release, which is in accordance with my previous study in Chapter 4.

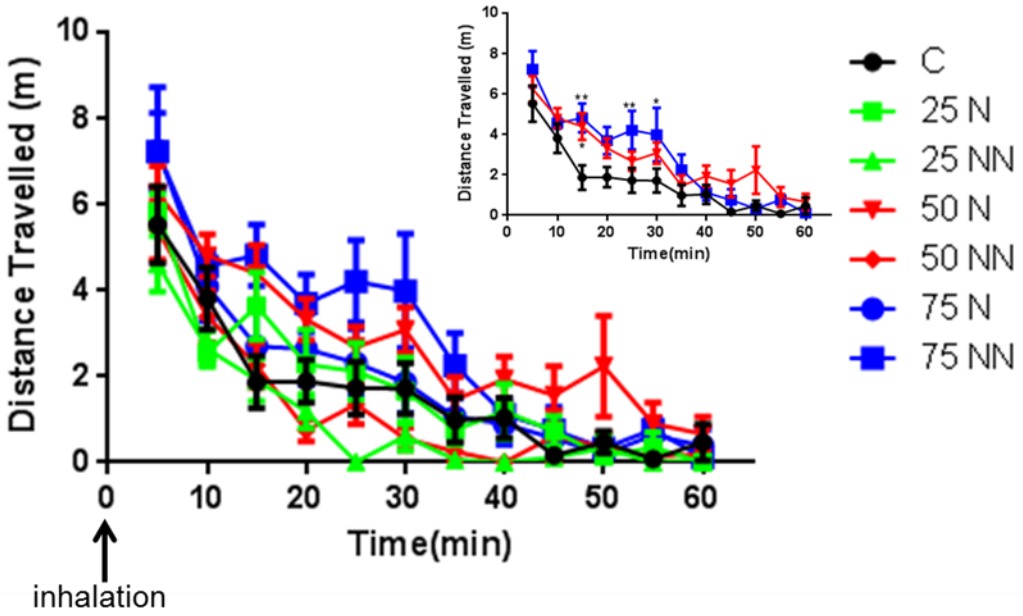


Figure 5.11 The effects of nicotine and nano-nicotine exposure and different levels of drug dose on mice locomotor activity with time. (n=8-10 per group) (Significant difference from CS control: *p<0.05, **p<0.01) (Effects of 50N and 75NN are enlarged on right corner).

The response to nicotine in mice is more sensitive than to nano-nicotine, with a higher dose (75NN) being required to achieve the same level of behavioural activity. Apart from the slow release of nicotine from CS nanoparticles, the greater dose of nano-nicotine that is required may be due to the deposition efficiency of nano-nicotine being lower than NHT powder as nano-nicotine DPI powder is made of floatable LMW chitosan powder. Also, the micro aggregates induced by strong inter-/intra- molecular forces among nanoparticles (see Chapter 3), may prevent nano-nicotine dispersion in high efficiency. The preliminary results in the present study showed inhalation of nicotine presents the dual pharmacological effects on mice locomotion behaviour with increased activity at a dose of 50N and inhibited activity at a dose of 75N, while nano-nicotine exposure evoked dose-dependent increase in travel distance.

The reinforcing effects of locomotor activity from nicotine are associated with the activation of specific nicotine acetylcholine receptor subunits in the brain, resulting in elevated extracellular and synaptic dopamine concentrations (Lallemand et al., 2007). When the nicotine is above a specific concentration in the brain, nicotine stimulates an increase in nicotinic acetylcholine receptors intensities through activating α4β2 nicotinic receptors to modulate the release of several neurotransmitters. Enhanced movement in the locomotor chamber randomLy without stereotypic behaviour was observed in around 10 minutes post exposure, followed by calm to normal spontaneous activity eventually, at which point travel distance was quantitated in one hour of recovery period by Any-maze software.

Overall, all the mice got accustomed to the test chamber and maintained a stable activity prior to inhalation test. Under the conditions of this study, acute administration of 50 N and 75 NN produced the significant increase in the mice locomotor activity. Comparing results of locomotor activity test between 1.0 NN by injection and 75 NN via inhalation, stimulant effects were observed at 30 min and 40 min statistically significantly from 1.00 NN injections, while stimulant effects were noted at 15 min, 25 min and 30 min via 75 NN inhalations. As a result, it is concluded that pulmonary drug delivery is faster and more efficient option to achieve therapeutic effects than injection.

### 5.4.4 **Histopathological Analysis of Lung Tissues**

Representative histological images following acute inhalation exposure (after 1 hour and 24 hours) are presented in Figure 5.12. The section of mice healthy lung tissues (Figure 5.12 A, B) is composed of clear alveolar space, intra-alveolar vessel and thin

wall alveoli, including a single layer of squamous epithelium. Figure 5.12 C, D showed the mice lungs tissues after CS only exposure after 1 and 24 hours respectively. No obvious morphological changes were observed, indicating inhalation of CS nanoparticles with inhalable lactose carrier does not cause airway inflammation. Nicotine exposure in one hour (Figure 5.12 E) did not result in any change, while minimal thickened alveolar wall, hyperplasia of bronchial epithelial cells, mixed inflammatory cell infiltrate (neutrophil, lymphocyte and macrophages) between intra-alveolar vessels occurred post exposure in 24 hours. No lesion was observed after nano-nicotine exposure for one hour (Figure 5.12 G). Nano-nicotine exposure in 24 hours (Figure 5.12 H) induced minimal increased squamous metaplasia, slight thickened alveolar wall and inflammatory infiltrates around the alveolar ducts and adjacent vasculature, which are the commonly observed lesions at the lungs after smoke exposure depending on nicotine concentration and exposure duration (Tsuji et al., 2013).

In this study, we did not observe the severe lesions of lungs in nicotine and nano-nicotine exposure within 24 hours. In the literature, most of the frequent lesions in cigarette smoke exposure using rodents are squamous metaplasia of respiratory epithelium, hyperplasia of metaplastic epithelium and respiratory epithelium, remarkable accumulation of pigmented macrophages in the lungs, and inflammatory cell infiltrates and perivascular lymphocytic infiltrates (Tsuji et al., 2015; Tsuji, Lee, et al., 2011). Tsuji reported emphysematous changes in alveolar ducts and adjacent alveoli occurred in some smoke-exposed mice. A few microscopic lesions were present in sections of other protocol-required tissues from smoke, air or cage control groups, with no clear evidence of a relationship to smoke exposure.

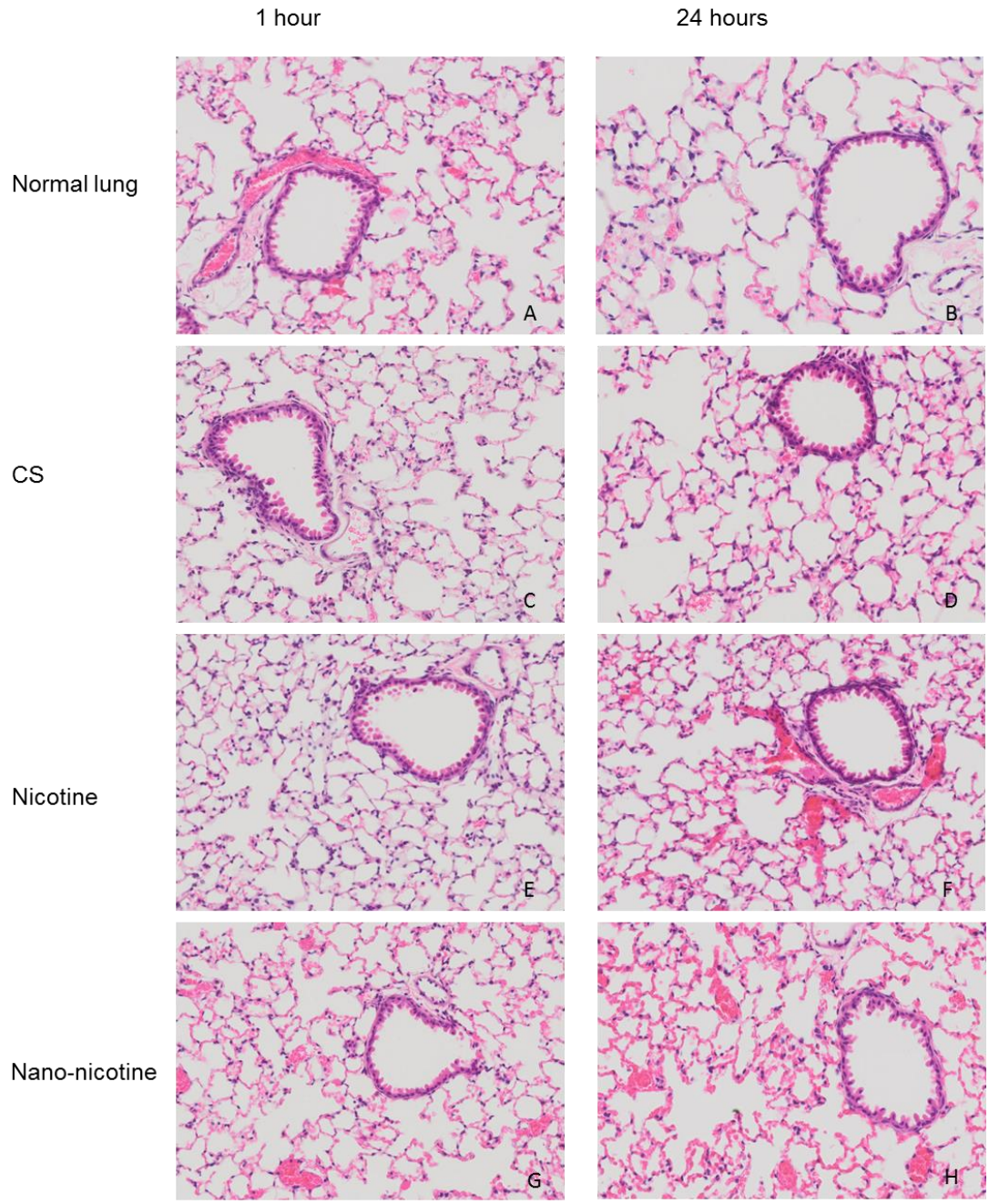


Figure 5.12 Histological changes of lung tissues from different groups (10×40, H&E staining, n=6). (A-B) healthy mice lungs; (C) CS exposure mouse in one hour; (D) CS exposure mouse in 24 hours; (E) nicotine exposure (50mg) mouse in one hour; (F) nicotine exposure (50 mg) mouse in 24 hours; (G) nano-nicotine exposure (75mg) mouse in one hour; (H) nano-nicotine exposure (75mg) mouse in 24 hours

## 5.5 SUMMARY

In this chapter, the locomotor activity of male C57BL/6 naïve mice was examined following acute s.c. injection and inhalation at several concentrations of nicotine and nano-nicotine. During the experimental period, no adverse health effects were observed in any of the animals at any concentrations, nor was there any evidence for residual effects on s.c. injected administration and nose-only inhalation exposure sessions. In terms of experimental results by s.c. injection, nicotine and nano-nicotine produced significant increase in locomotor activity at intermediate concentrations. Minimally effective concentrations for activity increasing effects were 0.5 mg/kg (nicotine) and 1.0 mg/kg (nano-nicotine), respectively. Locomotion activity was decreased with higher concentrations because of blockage of neuronal nAChR. This indicated the formulation of nano-nicotine inhalation powder is bio-active after the process of manufacturing NHT-CS (3:1) particles. Similarly, biphasic effects of dose response on locomotor activity were observed in nicotine and nano-nicotine inhalation. Increased and decreased dose of nicotine and nano-nicotine as a function of exposure concentration play an important role in changing mice locomotion behaviours, which may reflect the CNS-depressant drug-like effects of nicotine. Lowest dose for activity increasing effects were 50 mg per batch/ 4 mice (nicotine) and 75 mg per batch / 4 mice (nano-nicotine), respectively. This suggested the nose-only inhalation device developed by our group is effective to deliver aerosolized powder to mice lungs, which confirmed the result from *in vitro* evaluation of inhalation device. In addition, the formulation of nano-nicotine is promising to develop as DPI formulation for lung delivery, which is a potential therapeutic strategy for better management of nicotine dependence as a kind of nicotine replacement therapies.

In the lung, minimal inflammatory cell infiltration (e.g., macrophages and neutrophils) was increased at the dose of nicotine (50mg) and nano-nicotine (75mg) exposed groups after 24hour exposure compared with healthy mice lungs. Based on the histological images, it is suggested that the exposure of 50mg nicotine per batch and 75 mg nano-nicotine per batch was insufficient to induce the severe pulmonary inflammation associated with tobacco-related lung diseases, indicating that formulation of NHT-CS nanoparticles may be applicable for exposure studies under this study design in C57BL/6 mice, but it is still suggested to observe histopathological changes in a longer period.

# Chapter 6:

# Conclusions

## 6.1 OVERALL CONCLUSIONS

The aim of this study was to develop a pulmonary drug delivery system using nicotine-loaded CS nanoparticles as DPI formulations with the potential for the treatment of nicotine dependence with low dose and controlled release profiles. Thus, this thesis has focussed on discussion of strategies to develop a particulate NHT delivery system from DPI formulations (in Chapter 3), following *in vitro* evaluations of DPI formulations (in Chapter 4); and safety and efficiency tests of formulations on animal models demonstrated in Chapter 5.

Firstly, an effective way to fabricate micro/nanoparticles of biodegradable polymer, CS, loaded with nicotine hydrogen tartrate (NHT) for pulmonary delivery of nicotine from DPI formulations was established. The prepared nanoparticles were characterized using a series of analytical techniques. The particles were spherical under SEM and TEM observations with size ranges between 167.6 and 411 nm by DLS analysis; however, Mastersizer showed aggregation between nanoparticles induced agglomerates between 3.73 and 4.73 μm in diameter due to high surface energy. Drug loading increased along with increase of mass ratios of NHT and CS, achieving highest loading rate at 66% for a ratio of 3:1. There was no surface enhancement of NHT on the nanoparticles since the amount of NHT measured on the surface of CS increased proportionally with increasing drug loading in the bulk according to the XPS analysis. DSC, XRD and FTIR suggested crystallinity of NHT was lost when encapsulated in the CS micro/nanoparticles. Specific surface area and surface charge were two main factors, which eventually affect the drug release and dispersibility of micro/nanoparticles as DPI formulations.

Secondly, *in vitro* drug release, aerosolization and long-term stability were studied to evaluate the DPI formulations of nicotine-loaded CS micro/nanoparticles as DPI formulations. *In vitro* drug release study from dialysis membrane technique (to separate released NHT from the nanoparticles) showed an initial burst release for the first 8 hours followed by the sustained and prolonged release profiles of NHT released from CS particles matrix up to 4 days. The maximum cumulative release (%) achieved was around 65% with respect to highest drug loading formulation. The particles with bigger particle size experienced a slower initial burst release rate but longer sustained release period compared with smaller particles. A mathematical model allowed correction of the discrepancy during drug release measurement due to two diffusion barriers of the dialysis membrane. From TSI studies, the FPF of NHT-loaded CS nanoparticles reduced along with increase of mass ratios of NHT to CS, which is mainly dominated by the surface charge on the nanoparticle aggregates as measured by zeta potential. In contrast, increased FPD of NHT from 1.7 mg to 3.2 mg was obtained with increased concentration of NHT in the nanoparticles. However, dispersibility values of NHT-loaded CS particles with large lactose carriers increased significantly, which were independent of the effect of surface charge. In the long-term stability test, the formulations of NHT-CS inhalation particles were stable at the storage condition of 25°C/60% RH for a one-year observation.

Thirdly, by using a mouse model, effective parameters of nose-only inhalation device were determined at 0.9L/min flow rate and inhalation duration for 5 minute. Safety of inhalation for mice lungs and efficiency to mediate mice locomotion behaviour following administration of NHT-loaded CS particles as DPI formulations were evaluated through locomotor activity test and histological observations. It was found NHT-loaded CS nanoparticles maintained bioactivity and delivered nicotine as

measured through locomotor activity test by injection. This was found to result in hyperactivity in mice at intermediate dose (s.c. single injection: 0.5 mg/kg for nicotine; 1.0 mg/kg for NHT-CS nanoparticles vs. inhalation exposure: the groups of 50N for nicotine; 75 NN for NHT-CS nanoparticles) and, in contrast, hypoactivity at higher challenge doses. After inhalation exposure of NHT-CS particles to mice for 24 hours, there was no allergic airway inflammation observed by histological analysis of lung sections.

In conclusion, this study has successfully established an effective and feasible way to develop NHT-loaded CS nanoparticles as DPI formulations although it involves organic solvent and crosslinking methods that are complex and time consuming. The outcomes of this study suggest that pulmonary delivery, after further work, may provide an alternative treatment approach for nicotine-mediated behaviours. It is anticipated that the advancement of knowledge on pulmonary drug delivery from the mouse model will translate to novel therapeutic strategies for the better management of patients with nicotine dependence in the future, and eventually it may offer a more targeted therapy approach for the significant number of Australians and smokers worldwide affected by smoking-related disorders. At the end of this work, it is expected this project will contribute to more effective medications for substance use disorders, reduce direct and indirect costs to society and make improvements to public health and safety and health care delivery.

## 6.2 LIMITATIONS

A successful nicotine replacement therapy requires delivery of sufficient nicotine in the blood of a smoker to reach the levels achieved from cigarette smoking. Based on this study i.e., *in vitro* drug release (Figure 4.5), conversion factor between NHT to

nicotine base (1 mg NHT equals 0.35 mg nicotine base), drug loading (Table 3.9), and FPD of NHT from the prepared nanoparticles (Table 4.3), the predicted peak plasma concentration will be between 4 and 7 ng/mL from 1.7 to 3.2 mg of FPDs of the prepared formulations in 8 h when the highest drug release was observed. Unlike cigarette smoking where nicotine reaches the brain within a few seconds from inhalation, in the nanoparticle system this will be delayed. As indicated in previous chapters, multiple capsules will likely be required to get the required pharmacological effect and that high dose of chitosan may cause an adverse effect.

## 6.3 FUTURE DIRECTIONS

Developing an effective treatment option from pulmonary delivery with reduced side effects for nicotine addiction is a long term and sustained work. This study is just the tip of an iceberg to explore a better therapeutical option for management of nicotine dependence. There are still many gaps due to complexity of the topic and limited available techniques. Although we have successfully developed a feasible way to prepare particles, it requires a number of studies to improve and optimise current powder formulation techniques and animal models for pulmonary drug delivery. Based on the outcomes to date and a deeper understanding of this project, a few challenges are suggested for future research directions.

Chitosan nanoparticles have been used extensively as drug delivery vehicles due to their excellent bioavailability, better encapsulation, and controlled release with less toxic properties. Further studies could involve the use of derivatives of chitosan to provide better control of properties. However, currently most studies focus on the modifications of amino groups at the C2 position, while less attention is paid on the potential application of C6 modification (Islam & Ferro, 2016). In the near future,

more conjugates of CS with drugs or other excipients at C6 or both C2 and C6 could be prepared for more practicable pharmacotherapeutic strategies. In addition, toxicities of derivatives of CS in human different organs have not been fully understood although a lot of studies have been reported based on in vivo animal models. However, there is no doubt that translation from animal models to humans is still difficult to achieve due to large differences of anatomical structures between animals and humans. Biodegradability is another safety issue to be considered in long term human health applications. In particular, the most current techniques involved in organic solvents and use chemical crosslinkers as well as high shear force. It is suggested that there is a need to develop more mild preparation techniques and search for less or non-toxic crosslinkers.

Further comprehensive studies may be needed to develop an efficient DPI formulation by understanding the interactions between the charged particles and carriers, the impact of charged particles or agglomerates on the deagglomeration and dispersion, which will contribute to improving powders' aerosolization performance and reducing adhesion force among particles.

This study has addressed the safety and efficiency of nicotine-loaded CS particles as DPI formulation from the acute response in an animal model. Future investigations are suggested to consider measuring nicotine-mediated behaviours and clinically relevant blood levels of nicotine and cotinine to examine the efficacy of DPI formulations of NHT-loaded CS particles in reducing nicotine consumption in mice model for the long term.

Further investigations are also suggested to explore more effective inhalation apparatus of dry powders in animal models. The research of DPI is growing fast in the

pharmaceutical studies and has achieved a significant success in the recent decades, but the equipment for studies in animal models is still not yet sufficient. Based on the current reviews (J. Kaur et al., 2008; Kwon et al., 2008), the inhalation devices designed for DPI studies either require tracheal intubation of the test animal under ambient pressure or positive pressure, which results in a large proportion of inhaled particles being deposited by physiological breathing rather than spontaneous respiration; or it requires whole-body exposure to achieve inhalation by spontaneous respiration, while the absorption routes are through percutaneous absorption or orifices other than the nasopharynx. Some material is also toxic when retained on the fur of the animals. The nose-only exposure devices seem favourable for animal model studies, however, the duration of exposure is critical to consider carefully with variation of air flow rate, air pressure and aerosol concentration (Lebedová et al., 2016). Therefore, it is essential to improve inhalation equipment further with joint collaborations from other disciplines such as mechanical engineering, chemistry, biology and neurology and so on.

# Bibliography

Abdelwahed, W., Degobert, G., Stainmesse, S., & Fessi, H. (2006). Freeze-drying of nanoparticles: formulation, process and storage considerations. *Advanced drug delivery reviews, 58*(15), 1688-1713.

Abdukayum, A., Yang, C.-X., Zhao, Q., Chen, J.-T., Dong, L.-X., & Yan, X.-P. (2014). Gadolinium complexes functionalized persistent luminescent nanoparticles as a multimodal probe for near-infrared luminescence and magnetic resonance imaging in vivo. *Analytical chemistry, 86*(9), 4096-4101.

Adams, K. E., Ke, S., Kwon, S., Liang, F., Fan, Z., Lu, Y., . . . Sevick-Muraca, E. M. (2007). Comparison of visible and near-infrared wavelength-excitable fluorescent dyes for molecular imaging of cancer. *Journal of biomedical optics, 12*(2), 024017-024019.

Adkison, S. E., O'Connor, R. J., Bansal-Travers, M., Hyland, A., Borland, R., Yong, H.-H., . . . Hammond, D. (2013). Electronic nicotine delivery systems: international tobacco control four-country survey. *American journal of preventive medicine, 44*(3), 207-215.

Agnihotri, S. A., Mallikarjuna, N. N., & Aminabhavi, T. M. (2004). Recent advances on chitosan-based micro-and nanoparticles in drug delivery. *Journal of Controlled Release, 100*(1), 5-28.

Ajun, W., Yan, S., Li, G., & Huili, L. (2009). Preparation of aspirin and probucol in combination loaded chitosan nanoparticles and in vitro release study. *Carbohydrate Polymers, 75*(4), 566-574.

Al-Qadi, S., Grenha, A., Carrión-Recio, D., Seijo, B., & Remuñán-López, C. (2012). Microencapsulated chitosan nanoparticles for pulmonary protein delivery: In vivo evaluation of insulin-loaded formulations. *Journal of Controlled Release, 157*(3), 383-390.

Alberg, A. J., Brock, M. V., Ford, J. G., Samet, J. M., & Spivack, S. D. (2013). Epidemiology of lung cancer: Diagnosis and management of lung cancer: American College of Chest Physicians evidence-based clinical practice guidelines. *Chest Journal, 143*(5_supplement), e1S-e29S.

Anderson, P. (2006). Use of Respimat® Soft Mist™ inhaler in COPD patients. *International journal of chronic obstructive pulmonary disease, 1*(3), 251-259.

Aoki, Y., Kojo, Y., Yamada, S., & Onoue, S. (2012). Respirable dry powder formulation of bleomycin for developing a pulmonary fibrosis animal model. *Journal of pharmaceutical sciences, 101*(6), 2074-2081.

Archana, D., Dutta, J., & Dutta, P. (2013). Evaluation of chitosan nano dressing for wound healing: Characterization, in vitro and in vivo studies. *International journal of biological macromolecules, 57*, 193-203.

Ari, A., Harwood, R. J., Sheard, M. M., & Fink, J. B. (2015). Pressurized metered-dose inhalers versus nebulizers in the treatment of mechanically ventilated subjects with artificial airways: an in vitro study. *Respiratory care, 60*(11), 1570-1574.

Arya, N., & Katti, D. S. (2015). Poly (d, l-lactide-co-glycolide)–chitosan composite particles for the treatment of lung cancer. *International journal of nanomedicine, 10*, 2997-3011.

Baba, S., Iso, H., Mannami, T., Sasaki, S., Okada, K., Konishi, M., & Tsugane, S. (2006). Cigarette smoking and risk of coronary heart disease incidence among middle-aged Japanese men and women: the JPHC Study Cohort I. *European journal of cardiovascularprevention & rehabilitation, 13*(2), 207-213.

Bailey, M. M., & Berkland, C. J. (2009). Nanoparticle formulations in pulmonary drug delivery. *Medicinal research reviews, 29*(1), 196-212.

Balfour, D. J. (2004). The neurobiology of tobacco dependence: a preclinical perspective on the role of the dopamine projections to the nucleus. *Nicotine & Tobacco Research, 6*(6), 899-912.

Barth, T., Kulenkampff, J., Bras, S., Gründig, M., Lippmann-Pipke, J., & Hampel, U. (2014). Positron emission tomography in pebble beds. Part 2: Graphite particle deposition and resuspension. *Nuclear Engineering and Design, 267*, 227-237.

Bateman, E., Singh, D., Smith, D., Disse, B., Towse, L., Massey, D., . . . Hodder, R. (2010). Efficacy and safety of tiotropium Respimat® SMI in COPD in two 1-year randomized studies. *International journal of chronic obstructive pulmonary disease, 5*, 197-208.

Bateman, E. D. (2013). Tiotropium Respimat increases the risk of mortality: con. *European Respiratory Journal, 42*(3), 590-593.

Beasley, R., Singh, S., Loke, Y. K., Enright, P., & Furberg, C. D. (2012). Call for worldwide withdrawal of tiotropium Respimat mist inhaler. *Bmj, 345*, e7390-e7391.

Beck-Broichsitter, M., Schweiger, C., Schmehl, T., Gessler, T., Seeger, W., & Kissel, T. (2012). Characterization of novel spray-dried polymeric particles for controlled pulmonary drug delivery. *Journal of Controlled Release, 158*(2), 329-335.

Beckett, W. S., Jacobs Jr, D. R., Yu, X., Iribarren, C., & Williams, O. D. (2001). Asthma is associated with weight gain in females but not males, independent of physical activity. *American journal of respiratory and critical care medicine, 164*(11), 2045-2050.

Begat, P., Morton, D. A., Staniforth, J. N., & Price, R. (2004). The cohesive-adhesive balances in dry powder inhaler formulations I: Direct quantification by atomic force microscopy. *Pharmaceutical research, 21*(9), 1591-1597.

Behara, S. R., Farkas, D. R., Hindle, M., & Longest, P. W. (2014). Development of a high efficiency dry powder inhaler: effects of capsule chamber design and inhaler surface modifications. *Pharmaceutical research, 31*(2), 360-372.

Bennett, W. D., Xie, M., Zeman, K., Hurd, H., & Donaldson, S. (2015). Heterogeneity of particle deposition by pixel analysis of 2D gamma scintigraphy images. *Journal of aerosol medicine and pulmonary drug delivery, 28*(3), 211-218.

Benowitz, N. (2008). Clinical pharmacology of nicotine: implications for understanding, preventing, and treating tobacco addiction. *Clinical Pharmacology & Therapeutics, 83*(4), 531-541.

Benowitz, N. L. (1988). Pharmacologic aspects of cigarette smoking and nicotine addiction. *New England Journal of Medicine, 319*(20), 1318-1330.

Benowitz, N. L. (1992). Cigarette smoking and nicotine addiction. *The Medical clinics of North America, 76*(2), 415-437.

Benowitz, N. L. (1996). Pharmacology of nicotine: addiction and therapeutics. *Annual review of pharmacology and toxicology, 36*(1), 597-613.

Benowitz, N. L. (2010). Nicotine addiction. *New England Journal of Medicine, 362*(24), 2295-2303.

Benowitz, N. L., Hukkanen, J., & Jacob III, P. (2009). Nicotine chemistry, metabolism, kinetics and biomarkers. *Nicotine psychopharmacology, 192*, 29-60.

Berger, J., Reist, M., Mayer, J. M., Felt, O., & Gurny, R. (2004). Structure and interactions in chitosan hydrogels formed by complexation or aggregation for biomedical applications. *European Journal of Pharmaceutics and Biopharmaceutics, 57*(1), 35-52.

Bosquillon, C., Lombry, C., Preat, V., & Vanbever, R. (2001). Influence of formulation excipients and physical characteristics of inhalation dry powders on their aerosolization performance. *Journal of Controlled Release, 70*(3), 329-339.

Boyden, J. Y., Connor, S. R., Otolorin, L., Nathan, S. D., Fine, P. G., Davis, M. S., & Muir, J. C. (2015). Nebulized medications for the treatment of dyspnea: a literature review. *Journal of aerosol medicine and pulmonary drug delivery, 28*(1), 1-19.

Brain, J. D., Knudson, D. E., Sorokin, S. P., & Davis, M. A. (1976). Pulmonary distribution of particles given by intratracheal instillation or by aerosol inhalation. *Environmental research, 11*(1), 13-33.

Brunauer, S., Emmett, P. H., & Teller, E. (1938). Adsorption of gases in multimolecular layers. *Journal of the American chemical society, 60*(2), 309-319.

Buchhalter, A. R., Fant, R. V., & Henningfield, J. E. (2008). Novel pharmacological approaches for treating tobacco dependence and withdrawal. *Drugs, 68*(8), 1067-1088.

Bugnicourt, L., Alcouffe, P., & Ladavière, C. (2014). Elaboration of chitosan nanoparticles: Favorable impact of a mild thermal treatment to obtain finely divided, spherical, and colloidally stable objects. *Colloids and Surfaces A: Physicochemical and Engineering Aspects, 457*, 476-486.

Bugnicourt, L., & Ladavière, C. (2016). Interests of chitosan nanoparticles ionically cross-linked with tripolyphosphate for biomedical applications. *Progress in Polymer Science, 60*, 1-17.

Burns, D. M. (2003). Epidemiology of smoking-induced cardiovascular disease. *Progress in cardiovascular diseases, 46*(1), 11-29.

Byrd, J. C. (1992). Environmental tobacco smoke. Medical and legal issues. *The Medical clinics of North America, 76*(2), 377-398.

Byron, P. R., Peart, J., & Staniforth, J. N. (1997). Aerosol electrostatics I: properties of fine powders before and after aerosolization by dry powder inhalers. *Pharmaceutical research, 14*(6), 698-705.

Cahill, K., Stead, L. F., Lancaster, T., & Polonio, I. B. (2012). Nicotine receptor partial agonists for smoking cessation. *Sao Paulo Medical Journal, 130*(5), 346-347.

Carmella, S. G., McIntee, E. J., Chen, M., & Hecht, S. S. (2000). Enantiomeric composition of N′-nitrosonornicotine and N′-nitrosoanatabine in tobacco. *Carcinogenesis, 21*(4), 839-843.

Cates, C. J., Welsh, E. J., & Rowe, B. H. (2013). Holding chambers (spacers) versus nebulisers for beta‐agonist treatment of acute asthma. *Cochrane database of systematic reviews 2013*(9). doi:DOI: 10.1002/14651858.CD000052.pub3

Cevher, E., Orhan, Z., Mülazımoğlu, L., Şensoy, D., Alper, M., Yıldız, A., & Özsoy, Y. (2006). Characterization of biodegradable chitosan microspheres containing vancomycin and treatment of experimental osteomyelitis caused by methicillin-resistant Staphylococcus aureus with prepared microspheres. *International journal of pharmaceutics, 317*(2), 127-135.

Chan, J. G. Y., Chan, H.-K., Prestidge, C. A., Denman, J. A., Young, P. M., & Traini, D. (2013). A novel dry powder inhalable formulation incorporating three first-line anti-tubercular antibiotics. *European Journal of Pharmaceutics and Biopharmaceutics, 83*(2), 285-292.

Chauhan, S. S., Lin, S., & Madan, P. (2012). Preparation and evaluation of nicotine hydrogen tartrate fast dissolving films for smoking cessation. *Asian Journal of Pharmaceutical Sciences, 7*(3), 181-192.

Chen, C., Lv, G., Pan, C., Song, M., Wu, C., Guo, D., . . . Gu, Z. (2007). Poly (lactic acid)(PLA) based nanocomposites—a novel way of drug-releasing. *Biomedical materials, 2*(4), L1-L4.

Chen, I. (2013). FDA summary of adverse events on electronic cigarettes. *Nicotine & Tobacco Research, 15*(2), 615-616.

Chen, M.-M., Huang, Y.-Q., Cao, H., Liu, Y., Guo, H., Chen, L. S., . . . Zhang, Q.-Q. (2015). Collagen/chitosan film containing biotinylated glycol chitosan nanoparticles for localized drug delivery. *Colloids and Surfaces B: Biointerfaces, 128*, 339-346.

Chen, M., Romay, F. J., Li, L., Naqwi, A., & Marple, V. A. (2016). A novel quartz crystal cascade impactor for real-time aerosol mass distribution measurement. *Aerosol Science and Technology, 50*(9), 971-983.

Chen, T., Yan, Q. P., Li, F. R., & Tang, S. Q. (2012). Nanospheres conjugated with Hab18 as targeting carriers for antitumor drug. *Advanced materials research, 535*, 2381-2384.

Chen, X.-G., Lee, C. M., & Park, H.-J. (2003). O/W emulsification for the self-aggregation and nanoparticle formation of linoleic acid modified chitosan in the aqueous system. *Journal of Agricultural and Food Chemistry, 51*(10), 3135-3139.

Chen, Z., & Boreham, J. (2002). Smoking and cardiovascular disease. *Seminars in vascular medicine, 2*(3), 243-252.

Chi Lip Kwok, P. (2015). Electrostatics of pharmaceutical aerosols for pulmonary delivery. *Current pharmaceutical design, 21*(27), 3945-3954.

Chow, A. H., Tong, H. H., Chattopadhyay, P., & Shekunov, B. Y. (2007). Particle engineering for pulmonary drug delivery. *Pharmaceutical research, 24*(3), 411-437.

Chrystyn, H. (2006). Closer to an 'Ideal Inhaler'with the Easyhaler®. *Clinical drug investigation, 26*(4), 175-183.

Chrystyn, H., & Niederlaender, C. (2012). The Genuair® inhaler: a novel, multidose dry powder inhaler. *International journal of clinical practice, 66*(3), 309-317.

Chu, L. Y., Utada, A. S., Shah, R. K., Kim, J. W., & Weitz, D. A. (2007). Controllable monodisperse multiple emulsions. *Angewandte Chemie International Edition, 46*(47), 8970-8974.

Chung, T.-W., Huang, Y.-Y., & Liu, Y.-Z. (2001). Effects of the rate of solvent evaporation on the characteristics of drug loaded PLLA and PDLLA microspheres. *International journal of pharmaceutics, 212*(2), 161-169.

Cipolla, D., & Gonda, I. (2015). Inhaled nicotine replacement therapy. *Asian Journal of Pharmaceutical Sciences, 10*(6), 472-480.

Clarke, P., & Kumar, R. (1983). The effects of nicotine on locomotor activity in non‐tolerant and tolerant rats. *British journal of pharmacology, 78*(2), 329-337.

Coates, M. S., Fletcher, D. F., Chan, H. K., & Raper, J. A. (2004). Effect of design on the performance of a dry powder inhaler using computational fluid dynamics. Part 1: grid structure and mouthpiece length. *Journal of pharmaceutical sciences, 93*(11), 2863-2876.

Codrons, V., Vanderbist, F., Ucakar, B., Préat, V., & Vanbever, R. (2004). Impact of formulation and methods of pulmonary delivery on absorption of parathyroid

hormone (1–34) from rat lungs. *Journal of pharmaceutical sciences, 93*(5), 1241-1252.

Coe, J. W., Brooks, P. R., Vetelino, M. G., Wirtz, M. C., Arnold, E. P., Huang, J., . . . Fox, C. B. (2005). Varenicline: an α4β2 nicotinic receptor partial agonist for smoking cessation. *Journal of medicinal chemistry, 48*(10), 3474-3477.

Collins, A. C., Miner, L. L., & Marks, M. J. (1988). Genetic influences on acute responses to nicotine and nicotine tolerance in the mouse. *Pharmacology Biochemistry and Behavior, 30*(1), 269-278.

Cornfield, J., Haenszel, W., Hammond, E. C., Lilienfeld, A. M., Shimkin, M. B., & Wynder, E. L. (2009). Smoking and lung cancer: recent evidence and a discussion of some questions. *International journal of epidemiology, 38*(5), 1175-1191.

Cunningham, C. S., & McMahon, L. R. (2011). The effects of nicotine, varenicline, and cytisine on schedule-controlled responding in mice: differences in α4β2 nicotinic receptor activation. *European journal of pharmacology, 654*(1), 47-52.

Dal Negro, R. W., & Povero, M. (2016). Acceptability and preference of three inhalation devices assessed by the Handling Questionnaire in asthma and COPD patients. *Multidisciplinary respiratory medicine, 11*(1), 1.

Dalby, R., Spallek, M., & Voshaar, T. (2004). A review of the development of Respimat® Soft Mist™ Inhaler. *International journal of pharmaceutics, 283*(1–2), 1-9.

Daniels, T., Mills, N., & Whitaker, P. (2013). Nebuliser systems for drug delivery in cystic fibrosis. *Cochrane database of systematic reviews 2013*(4), 1-85.

Das, S. K. (2003). Harmful health effects of cigarette smoking. *Molecular and cellular biochemistry, 253*(1-2), 159-165.

De Boer, A., Chan, H., & Price, R. (2012). A critical view on lactose-based drug formulation and device studies for dry powder inhalation: which are relevant and what interactions to expect? *Advanced drug delivery reviews, 64*(3), 257-274.

DeHaan, W., & Finlay, W. (2004). Predicting extrathoracic deposition from dry powder inhalers. *Journal of Aerosol Science, 35*(3), 309-331.

Denyer, J., & Dyche, T. (2010). The Adaptive Aerosol Delivery (AAD) technology: past, present, and future. *Journal of aerosol medicine and pulmonary drug delivery, 23*(S1), S1-S10.

Diao, S., Hong, G., Antaris, A. L., Blackburn, J. L., Cheng, K., Cheng, Z., & Dai, H. (2015). Biological imaging without autofluorescence in the second near-infrared region. *Nano Research, 8*(9), 3027-3034.

Domino, E. F. (2001). Nicotine induced behavioral locomotor sensitization. *Progress in Neuro-Psychopharmacology and Biological Psychiatry, 25*(1), 59-71.

Drummond, M. B., & Upson, D. (2014). Electronic cigarettes. Potential harms and benefits. *Annals of the American Thoracic Society, 11*(2), 236-242.

Duan, Y.-Z., Zhang, L., Liu, C.-C., Zhu, B., Zhuo, W.-L., & Chen, Z.-T. (2013). CCND1 G870A polymorphism interaction with cigarette smoking increases lung cancer risk: meta-analyses based on 5008 cases and 5214 controls. *Molecular biology reports, 40*(7), 4625-4635.

Dudhani, A. R., & Kosaraju, S. L. (2010). Bioadhesive chitosan nanoparticles: Preparation and characterization. *Carbohydrate Polymers, 81*(2), 243-251.

Elena Udrea, L., Hritcu, D., Popa, M. I., & Rotariu, O. (2011). Preparation and characterization of polyvinyl alcohol—chitosan biocompatible magnetic microparticles. *Journal of Magnetism and Magnetic Materials, 323*(1), 7-13.

Enna, S. J., & Schanker, L. S. (1972). Absorption of saccharides and urea from the rat lung. *American Journal of Physiology--Legacy Content, 222*(2), 409-414.

Fagerström, K. (1987). Efficacy of nicotine chewing gum: a review. *Progress in clinical and biological research, 261*, 109-128.

Farley, A. C., Hajek, P., Lycett, D., & Aveyard, P. (2012). Interventions for preventing weight gain after smoking cessation. *Cochrane database of systematic reviews 2012*(1), 1-149.

Fonseca, C., Simoes, S., & Gaspar, R. (2002). Paclitaxel-loaded PLGA nanoparticles: preparation, physicochemical characterization and in vitro anti-tumoral activity. *Journal of Controlled Release, 83*(2), 273-286.

Freitas, M., & Marchetti, J. (2005). Nimesulide PLA microspheres as a potential sustained release system for the treatment of inflammatory diseases. *International journal of pharmaceutics, 295*(1), 201-211.

Frijlink, H., & De Boer, A. (2004). Dry powder inhalers for pulmonary drug delivery. *Expert opinion on drug delivery, 1*(1), 67-86.

Fröhlich, E., & Salar-Behzadi, S. (2014). Toxicological assessment of inhaled nanoparticles: Role of in vivo, ex vivo, in vitro, and in silico studies. *International journal of molecular sciences, 15*(3), 4795-4822.

Fu, H., Machado, P., Hahm, T., Kratochvil, R., Wei, C., & Lo, Y. (2010). Recovery of nicotine-free proteins from tobacco leaves using phosphate buffer system under controlled conditions. *Bioresource technology, 101*(6), 2034-2042.

Gaikwad, S. G., & Pandit, A. B. (2008). Ultrasound emulsification: effect of ultrasonic and physicochemical properties on dispersed phase volume and droplet size. *Ultrasonics sonochemistry, 15*(4), 554-563.

Gan, Q., Wang, T., Cochrane, C., & McCarron, P. (2005). Modulation of surface charge, particle size and morphological properties of chitosan–TPP nanoparticles intended for gene delivery. *Colloids and Surfaces B: Biointerfaces, 44*(2), 65-73.

Gaspar, M. C., Sousa, J. J., Pais, A. A., Cardoso, O., Murtinho, D., Serra, M. E. S., . . . Olivier, J.-C. (2015). Optimization of levofloxacin-loaded crosslinked chitosan microspheres for inhaled aerosol therapy. *European Journal of Pharmaceutics and Biopharmaceutics, 96*, 65-75.

Gazori, T., Khoshayand, M. R., Azizi, E., Yazdizade, P., Nomani, A., & Haririan, I. (2009). Evaluation of Alginate/Chitosan nanoparticles as antisense delivery vector: formulation, optimization and in vitro characterization. *Carbohydrate Polymers, 77*(3), 599-606.

Gervais, P.-C., Poussier, S., Bardin-Monnier, N., Karcher, G., & Thomas, D. (2014). Combination of single-photon emission and x-ray computed tomography to visualize aerosol deposition in pleated filter. *Separation and Purification Technology, 126*, 52-61.

Gomathi, T., Govindarajan, C., Rose H.R, M. H., Sudha, P. N., Imran, P. K. M., Venkatesan, J., & Kim, S.-K. (2014). Studies on drug-polymer interaction, in vitro release and cytotoxicity from chitosan particles excipient. *International Journal of Pharmaceutics, 468*(1–2), 214-222.

Gomes, C., Moreira, R. G., & Castell ‐ Perez, E. (2011). Poly (DL ‐ lactide ‐ co ‐ glycolide)(PLGA) nanoparticles with entrapped trans ‐ cinnamaldehyde and

eugenol for antimicrobial delivery applications. *Journal of food science, 76*(2), N16-N24.
Gupta, K. C., & Ravi Kumar, M. N. V. (2000). Drug release behavior of beads and microgranules of chitosan. *Biomaterials, 21*(11), 1115-1119.
Haagsman, H. P., & van Golde, L. M. (1985). Lung surfactant and pulmonary toxicology. *Lung, 163*(1), 275-303.
Haghi, M., Traini, D., & Young, P. (2014). In vitro cell integrated impactor deposition methodology for the study of aerodynamically relevant size fractions from commercial pressurised metered dose inhalers. *Pharmaceutical research, 31*(7), 1779-1787.
Hammond, E. C., & Horn, D. (1958). Smoking and death rates—report on forty-four months of follow-up of 187,783 men. *Journal of the American Medical Association, 166*(11), 1294-1308.
Hans, M., & Lowman, A. (2002). Biodegradable nanoparticles for drug delivery and targeting. *Current Opinion in Solid State and Materials Science, 6*(4), 319-327.
Hasegawa-Baba, Y., Kubota, H., Takata, A., & Miyagawa, M. (2014). Intratracheal instillation methods and the distribution of administered material in the lung of the rat. *Journal of toxicologic pathology, 27*(3-4), 197.
Hay, D., & Turbott, S. (1970). Changes in smoking habits in men under 65 years after myocardial infarction and coronary insufficiency. *British heart journal, 32*(6), 738-740.
Hecht, S. S. (2002). Cigarette smoking and lung cancer: chemical mechanisms and approaches to prevention. *The lancet oncology, 3*(8), 461-469.
Hefner, K., & Holmes, A. (2007). Ontogeny of fear-, anxiety-and depression-related behavior across adolescence in C57BL/6J mice. *Behavioural brain research, 176*(2), 210-215.
Heng, D., Cutler, D. J., Chan, H.-K., Yun, J., & Raper, J. A. (2008). What is a suitable dissolution method for drug nanoparticles? *Pharmaceutical research, 25*(7), 1696-1701.
Henningfield, J. E., Fant, R. V., Buchhalter, A. R., & Stitzer, M. L. (2005). Pharmacotherapy for nicotine dependence. *CA: a cancer journal for clinicians, 55*(5), 281-299.
Henningfield, J. E., & Zeller, M. (2006). Nicotine psychopharmacology research contributions to United States and global tobacco regulation: a look back and a look forward. *Psychopharmacology, 184*(3-4), 286-291.
Herxheimer, A., Griffiths, R., Hamilton, B., & Wakefield, M. (1967). Circulatory effects of nicotine aerosol inhalations and cigarette smoking in man. *The Lancet, 290*(7519), 754-755.
Hirst, P., Bacon, R., Pitcairn, G., Silvasti, M., & Newman, S. (2001). A comparison of the lung deposition of budesonide from Easyhaler®, Turbuhaler® and pMDI plus spacer in asthmatic patients. *Respiratory Medicine, 95*(9), 720-727.
Hochrainer, D., Hölz, H., Kreher, C., Scaffidi, L., Spallek, M., & Wachtel, H. (2005). Comparison of the aerosol velocity and spray duration of Respimat® Soft Mist™ inhaler and pressurized metered dose inhalers. *Journal of aerosol medicine, 18*(3), 273-282.
Hollander, P. A., Blonde, L., Rowe, R., Mehta, A. E., Milburn, J. L., Hershon, K. S., . . . Levin, S. R. (2004). Efficacy and safety of inhaled insulin (Exubera) compared with subcutaneous insulin therapy in patients with type 2 diabetes results of a 6-month, randomized, comparative trial. *Diabetes care, 27*(10), 2356-2362.

Hoppentocht, M., Hagedoorn, P., Frijlink, H., & de Boer, A. (2014). Technological and practical challenges of dry powder inhalers and formulations. *Advanced drug delivery reviews, 75*, 18-31.

Hu, X., Adamcakova-Dodd, A., LehmLer, H.-J., Gibson-Corley, K., & Thorne, P. S. (2015). Toxicity evaluation of exposure to an atmospheric mixture of polychlorinated biphenyls by nose-only and whole-body inhalation regimens. *Environmental science & technology, 49*(19), 11875-11883.

Hua, S. (2014). Comparison of in vitro dialysis release methods of loperamide-encapsulated liposomal gel for topical drug delivery. *International journal of nanomedicine, 9*, 735.

Huibers, M., Chavannes, N., Wagena, E., & Van Schayck, C. (2000). Antidepressants for smoking cessation: a promising new approach? *European Respiratory Journal, 16*(3), 379.

İkinci, G., Şenel, S., Wilson, C., & Şumnu, M. (2004). Development of a buccal bioadhesive nicotine tablet formulation for smoking cessation. *International journal of pharmaceutics, 277*(1), 173-178.

Iqbal, M., Zafar, N., Fessi, H., & Elaissari, A. (2015). Double emulsion solvent evaporation techniques used for drug encapsulation. *International journal of pharmaceutics, 496*(2), 173-190.

Islam, N., & Cleary, M. J. (2012). Developing an efficient and reliable dry powder inhaler for pulmonary drug delivery–a review for multidisciplinary researchers. *Medical engineering & physics, 34*(4), 409-427.

Islam, N., & Ferro, V. (2016). Recent advances in chitosan-based nanoparticulate pulmonary drug delivery. *Nanoscale, 8*(30), 14341-14358.

Islam, N., & Gladki, E. (2008). Dry powder inhalers (DPIs)—a review of device reliability and innovation. *International journal of pharmaceutics, 360*(1), 1-11.

Islam, N., & Rahman, S. (2012). Improved treatment of nicotine addiction and emerging pulmonary drug delivery. *Drug Discoveries and Therapeutics, 6*(3), 123-132.

Islam, N., Stewart, P., Larson, I., & Hartley, P. (2004). Lactose surface modification by decantation: are drug-fine lactose ratios the key to better dispersion of salmeterol xinafoate from lactose-interactive mixtures? *Pharmaceutical research, 21*(3), 492-499.

Islam, N., Stewart, P., Larson, I., & Hartley, P. (2005). Surface roughness contribution to the adhesion force distribution of salmeterol xinafoate on lactose carriers by atomic force microscopy. *Journal of pharmaceutical sciences, 94*(7), 1500-1511.

Jamal, A., Agaku, I. T., O'Connor, E., King, B. A., Kenemer, J. B., & Neff, L. (2014). Current cigarette smoking among adults—United States, 2005–2013. *Morbidity and mortality weekly report, 63*(47), 1108-1112.

Jonassen, H., Kjøniksen, A.-L., & Hiorth, M. (2012). Effects of ionic strength on the size and compactness of chitosan nanoparticles. *Colloid and Polymer Science, 290*(10), 919-929.

Kaialy, W., Alhalaweh, A., Velaga, S. P., & Nokhodchi, A. (2012). Influence of lactose carrier particle size on the aerosol performance of budesonide from a dry powder inhaler. *Powder Technology, 227*, 74-85.

Kannel, W., & Higgins, M. (1990). Smoking and hypertension as predictors of cardiovascular risk in population studies. *Journal of hypertension., 8*(5), S3-8.

Karavas, E., Georgarakis, E., & Bikiaris, D. (2006). Felodipine nanodispersions as active core for predictable pulsatile chronotherapeutics using PVP/HPMC blends as coating layer. *International journal of pharmaceutics, 313*(1), 189-197.

Karnik, R., Gu, F., Basto, P., Cannizzaro, C., Dean, L., Kyei-Manu, W., . . . Farokhzad, O. C. (2008). Microfluidic platform for controlled synthesis of polymeric nanoparticles. *Nano letters, 8*(9), 2906-2912.

Kaur, J., Muttil, P., Verma, R. K., Kumar, K., Yadav, A. B., Sharma, R., & Misra, A. (2008). A hand-held apparatus for "nose-only" exposure of mice to inhalable microparticles as a dry powder inhalation targeting lung and airway macrophages. *European Journal of Pharmaceutical Sciences, 34*(1), 56-65.

Kaur, R., Garg, T., Malik, B., Gupta, U. D., Gupta, P., Rath, G., & Goyal, A. K. (2016). Development and characterization of spray-dried porous nanoaggregates for pulmonary delivery of anti-tubercular drugs. *Drug delivery, 23*(3), 872-877.

Khang, G., Kim, S. W., Cho, J. C., Rhee, J. M., Yoon, S. C., & Lee, H. B. (2001). Preparation and characterization of poly (3 - hydroxybutyrate - co - 3 - hydroxyvalerate) microspheres for the sustained release of 5 - fluorouracil. *Bio-medical materials and engineering, 11*(2), 89-103.

Khdair, A., Hamad, I., Alkhatib, H., Bustanji, Y., Mohammad, M., Tayem, R., & Aiedeh, K. (2016). Modified-chitosan nanoparticles: Novel drug delivery systems improve oral bioavailability of doxorubicin. *European Journal of Pharmaceutical Sciences, 93*, 38-44.

Kho, K., & Hadinoto, K. (2013). Dry powder inhaler delivery of amorphous drug nanoparticles: Effects of the lactose carrier particle shape and size. *Powder Technology, 233*, 303-311.

Kiang, T., Wen, J., Lim, H. W., & Leong, K. W. (2004). The effect of the degree of chitosan deacetylation on the efficiency of gene transfection. *Biomaterials, 25*(22), 5293-5301.

Kleinstreuer, C., Zhang, Z., & Donohue, J. (2008). Targeted drug-aerosol delivery in the human respiratory system. *Annual review of biomedical engineering, 10*, 195-220.

Kobiasi, M. A., Chua, B. Y., Tonkin, D., Jackson, D. C., & Mainwaring, D. E. (2012). Control of size dispersity of chitosan biopolymer microparticles and nanoparticles to influence vaccine trafficking and cell uptake. *Journal of Biomedical Materials Research Part A, 100*(7), 1859-1867.

Kohane, D. S. (2007). Microparticles and nanoparticles for drug delivery. *Biotechnology and bioengineering, 96*(2), 203-209.

Kuehn, B. M. (2009). Studies linking smoking-cessation drug with suicide risk spark concerns. *Jama, 301*(10), 1007-1008.

Kumar, M. N. R. (2000). A review of chitin and chitosan applications. *Reactive and functional polymers, 46*(1), 1-27.

Kumari, A., Yadav, S. K., & Yadav, S. C. (2010). Biodegradable polymeric nanoparticles based drug delivery systems. *Colloids and Surfaces B: Biointerfaces, 75*(1), 1-18.

Kwon, J.-T., Hwang, S.-K., Jin, H., Kim, D.-S., Minai-Tehrani, A., Yoon, H.-J., . . . Kang, Y.-W. (2008). Body distribution of inhaled fluorescent magnetic nanoparticles in the mice. *Journal of occupational health, 50*(1), 1-6.

Lakier, J. B. (1992). Smoking and cardiovascular disease. *The American journal of medicine, 93*(1), S8-S12.

Lallemand, F., Ward, R. J., & De Witte, P. (2007). Nicotine increases ethanol preference but decreases locomotor activity during the initial stages of chronic ethanol withdrawal. *Alcohol and alcoholism, 42*(3), 207-218.

Lambrich, U., & Schubert, H. (2005). Emulsification using microporous systems. *Journal of Membrane Science, 257*(1), 76-84.

Lanman, R. C., Gillilan, R. M., & Schanker, L. S. (1973). Absorption of cardiac glycosides from the rat respiratory tract. *Journal of Pharmacology and Experimental Therapeutics, 187*(1), 105-111.

Le Houezec, J. (2003). Role of nicotine pharmacokinetics in nicotine addiction and nicotine replacement therapy: a review. *The international journal of tuberculosis and lung disease, 7*(9), 811-819.

Learoyd, T. P., Burrows, J. L., French, E., & Seville, P. C. (2008). Chitosan-based spray-dried respirable powders for sustained delivery of terbutaline sulfate. *European Journal of Pharmaceutics and Biopharmaceutics, 68*(2), 224-234.

Lebedová, J., Bláhová, L., Večeřa, Z., Mikuška, P., Dočekal, B., Buchtová, M., . . . Hilscherová, K. (2016). Impact of acute and chronic inhalation exposure to CdO nanoparticles on mice. *Environmental Science and Pollution Research, 23*(23), 24047–24060.

Lee, P. N. (2011). Systematic review of the epidemiological evidence comparing lung cancer risk in smokers of mentholated and unmentholated cigarettes. *BMC pulmonary medicine, 11*(1), 1.

Leone, A. (1995). Cigarette smoking and health of the heart. *The Journal of the Royal Society for the Promotion of Health, 115*(6), 354-355.

Leone, A. (2005). Biochemical markers of cardiovascular damage from tobacco smoke. *Current pharmaceutical design, 11*(17), 2199-2208.

Leone, A., Landini, L., & Leone, A. (2010). What is tobacco smoke? Sociocultural dimensions of the association with cardiovascular risk. *Current pharmaceutical design, 16*(23), 2510-2517.

Lerman, C., Niaura, R., Collins, B. N., Wileyto, P., Audrain-McGovern, J., Pinto, A., . . . Epstein, L. H. (2004). Effect of bupropion on depression symptoms in a smoking cessation clinical trial. *Psychology of Addictive Behaviors, 18*(4), 362.

Lertsutthiwong, P., Noomun, K., Jongaroonngamsang, N., Rojsitthisak, P., & Nimmannit, U. (2008). Preparation of alginate nanocapsules containing turmeric oil. *Carbohydrate Polymers, 74*(2), 209-214.

Leung, S. S. Y., Tang, P., Zhou, Q. T., Tong, Z., Leung, C., Decharaksa, J., . . . Chan, H.-K. (2015). De-agglomeration effect of the US pharmacopeia and alberta throats on carrier-based powders in commercial inhalation products. *The AAPS journal, 17*(6), 1407-1416.

Lewis, S., Subramanian, G., Pandey, S., & Udupa, N. (2006). Design, evaluation and pharmacokinetic study of mucoadhesive buccal tablets of nicotine for smoking cessation. *Indian journal of pharmaceutical sciences, 68*(6), 829-831.

Li, J., Liu, Z., Wu, Y., Wu, H., & Ran, P. (2008). Chitosan microparticles loaded with mite group 2 allergen Der f 2 alleviate asthma in mice. *Journal of investigational allergology and clinical immunology, 18*(6), 454-460.

Liang, M., Zheng, X., Tu, L., Ma, Z., Wang, Z., Yan, D., & Shen, Z. (2014). The liver-targeting study of the N-galactosylated chitosan in vivo and in vitro. *Artificial cells, nanomedicine, and biotechnology, 42*(6), 423-428.

Lim, L., & Wan, L. (1998). Effect of magnesium stearate on chitosan microspheres prepared by an emulsification-coacervation technique. *Journal of microencapsulation, 15*(3), 319-333.

Lim, S., Martin, G. P., Berry, D., & Brown, M. (2000). Preparation and evaluation of the in vitro drug release properties and mucoadhesion of novel microspheres of hyaluronic acid and chitosan. *Journal of Controlled Release, 66*(2), 281-292.

Liu, C., Thormann, E., Claesson, P. M., & Tyrode, E. (2014). Surface grafted chitosan gels. Part II. Gel formation and characterization. *Langmuir, 30*(29), 8878-8888.

Liu, J., & Stewart, P. J. (1998). Deaggregation during the dissolution of benzodiazepines in interactive mixtures. *Journal of pharmaceutical sciences, 87*(12), 1632-1638.

Liu, L., Won, Y. J., Cooke, P. H., Coffin, D. R., Fishman, M. L., Hicks, K. B., & Ma, P. X. (2004). Pectin/poly (lactide-co-glycolide) composite matrices for biomedical applications. *Biomaterials, 25*(16), 3201-3210.

London, E. D., Waller, S. B., & Wamsley, J. K. (1985). Autoradiographic localization of [3 H] nicotine binding sites in the rat brain. *Neuroscience letters, 53*(2), 179-184.

Louie, D. (2001). The effects of cigarette smoking on cardiopulmonary function and exercise tolerance in teenagers. *Canadian Respiratory Journal, 8*(4), 289-291.

Luinstra, M., Grasmeijer, F., Hagedoorn, P., Moes, J. R., Frijlink, H. W., & de Boer, A. H. (2015). A levodopa dry powder inhaler for the treatment of Parkinson's disease patients in off periods. *European Journal of Pharmaceutics and Biopharmaceutics, 97*, 22-29.

Luty, J. (2007). Nicotine addiction and smoking cessation treatments. *Clinical Topics in Addiction*, 90-100.

Ma, P., Kendzor, D. E., Poonawalla, I. B., Balis, D. S., & Businelle, M. S. (2016). Daily nicotine patch wear time predicts smoking abstinence in socioeconomically disadvantaged adults: An analysis of ecological momentary assessment data. *Drug and alcohol dependence, 169*, 64-67.

Maccaroni, E., Malpezzi, L., & Masciocchi, N. (2009). Structures from powders: Bupropion hydrochloride. *Journal of pharmaceutical and biomedical analysis, 50*(2), 257-261.

Mack, P., Horvath, K., Garcia, A., Tully, J., & Maynor, B. (2012). Particle engineering for inhalation formulation and delivery of biotherapeutics. *Inhalation*, 16-20.

Mainelis, G., Seshadri, S., Garbuzenko, O., Han, T., Wang, Z., & Minko, T. (2013). Characterization and application of a nose-only exposure chamber for inhalation delivery of liposomal drugs and nucleic acids to mice. *Journal of aerosol medicine and pulmonary drug delivery, 26*(6), 345-354.

Majedi, F. S., Hasani‐Sadrabadi, M. M., VanDersarl, J. J., Mokarram, N., Hojjati‐Emami, S., Dashtimoghadam, E., . . . Renaud, P. (2014). On‐chip Fabrication of paclitaxel‐loaded chitosan nanoparticles for cancer therapeutics. *Advanced Functional Materials, 24*(4), 432-441.

Mancini, N., Bene, M., Gerard, H., Chabot, F., Faure, G., Polu, J., & Lesur, O. (1993). Early effects of short-time cigarette smoking on the human lung: a study of bronchoalveolar lavage fluids. *Lung, 171*(5), 277-291.

Margarida Cardoso, M., Peça, I. N., Raposo, C. D., Petrova, K. T., Teresa Barros, M., Gardner, R., & Bicho, A. (2016). Doxorubicin-loaded galactose-conjugated poly (d, l-lactide-co-glycolide) nanoparticles as hepatocyte-targeting drug carrier. *Journal of microencapsulation, 33*(4), 1-11.

Marubio, L., Gardier, A., Durier, S., David, D., Klink, R., Arroyo‐Jimenez, M., . . . Zoli, M. (2003). Effects of nicotine in the dopaminergic system of mice lacking

the alpha4 subunit of neuronal nicotinic acetylcholine receptors. *European Journal of Neuroscience, 17*(7), 1329-1337.

Matta, S. G., Balfour, D. J., Benowitz, N. L., Boyd, R. T., Buccafusco, J. J., Caggiula, A. R., . . . Donny, E. C. (2007). Guidelines on nicotine dose selection for in vivo research. *Psychopharmacology, 190*(3), 269-319.

Matthay, M. A., Zimmerman, G. A., Esmon, C., Bhattacharya, J., Coller, B., Doerschuk, C. M., . . . Hubmayr, R. D. (2003). Future research directions in acute lung injury: summary of a national heart, lung, and blood institute working group. *American journal of respiratory and critical care medicine, 167*(7), 1027-1035.

Max, W. (2001). The financial impact of smoking on health-related costs: a review of the literature. *American Journal of Health Promotion, 15*(5), 321-331.

Mineur, Y. S., & Picciotto, M. R. (2010). Nicotine receptors and depression: revisiting and revising the cholinergic hypothesis. *Trends in pharmacological sciences, 31*(12), 580-586.

Molina, R. M., Konduru, N. V., Hirano, H., Donaghey, T. C., Adamo, B., Laurenzi, B., . . . Brain, J. D. (2016). Pulmonary distribution of nanoceria: comparison of intratracheal, microspray instillation and dry powder insufflation. *Inhalation toxicology, 28*(12), 550-560.

Molyneux, A. (2004). Nicotine replacement therapy. *British medical journal, 328*(7437), 454-456.

Montiel-Eulefi, E., Jara, F., Toro, C., Garces, M., & Leal, P. (2014). Cytotoxic Effect of Double Emulsion (W/O/W) CuSO4 Loaded PLA Nanoparticles on MKN-45 Gastric Adenocarcinoma Cell Line. *International journal of morphology, 32*(1), 61-69.

Moreno-Bautista, G., & Tam, K. C. (2011). Evaluation of dialysis membrane process for quantifying the in vitro drug-release from colloidal drug carriers. *Colloids and Surfaces A: Physicochemical and Engineering Aspects, 389*(1), 299-303.

Morrison, C. F., Goodyear, J., & Sellers, C. (1969). Antagonism by antimuscarinic and ganglion-blocking drugs of some of the behavioural effects of nicotine. *Psychopharmacologia, 15*(5), 341-350.

Moura, F. B. d., & McMahon, L. R. (2016). Differential antagonism and nicotine-induced tolerance/cross-tolerance among nAChR agonists in mice. *The FASEB Journal, 30*(1 Supplement), 1185-1187.

Moyses, C., Hearn, A., & Redfern, A. (2014). Evaluation of a novel nicotine inhaler device. Part 1: arterial and venous pharmacokinetics. *Nicotine & Tobacco Research*, 18-25.

Moyses, C., Hearn, A., & Redfern, A. (2015). Evaluation of a novel nicotine inhaler device: Part 2—Effect on craving and smoking urges. *Nicotine & Tobacco Research, 17*(1), 26-33.

Muhsin, M. D., George, G., Beagley, K., Ferro, V., Hui, W., & Islam, N. (2016). Effects of chemical conjugation of L-leucine to chitosan on dispersibility and controlled release of drug from a nanoparticulate dry powder inhaler formulation. *Molecular Pharmaceutics, 13*(5), 1455-1466.

Muralidharan, P., Hayes Jr, D., & Mansour, H. M. (2015). Dry powder inhalers in COPD, lung inflammation and pulmonary infections. *Expert opinion on drug delivery, 12*(6), 947-962.

Musumeci, T., Ventura, C. A., Giannone, I., Ruozi, B., Montenegro, L., Pignatello, R., & Puglisi, G. (2006). PLA/PLGA nanoparticles for sustained release of docetaxel. *International journal of pharmaceutics, 325*(1–2), 172-179.

Myrdal, P. B., Sheth, P., & Stein, S. W. (2014). Advances in metered dose inhaler technology: formulation development. *AAPS PharmSciTech, 15*(2), 434-455.

Nahar, K., Gupta, N., Gauvin, R., Absar, S., Patel, B., Gupta, V., . . . Ahsan, F. (2013). In vitro, in vivo and ex vivo models for studying particle deposition and drug absorption of inhaled pharmaceuticals. *European Journal of Pharmaceutical Sciences, 49*(5), 805-818.

Nanjwade, B. K., Adichwal, S. A., Gaikwad, K. R., Parikh, K. A., & Manvi, F. (2011). Pulmonary drug delivery: novel pharmaceutical technologies breathe new life into the lungs. *PDA Journal of Pharmaceutical Science and Technology, 65*(5), 513-534.

Newman, S. P., & Busse, W. W. (2002). Evolution of dry powder inhaler design, formulation, and performance. *Respiratory Medicine, 96*(5), 293-304.

Nides, M. (2008). Update on pharmacologic options for smoking cessation treatment. *The American journal of medicine, 121*(4), S20-S31.

Noyes, A. A., & Whitney, W. R. (1897). The rate of solution of solid substances in their own solutions. *Journal of the American chemical society, 19*(12), 930-934.

Obaid, A. L., Koyano, T., Lindstrom, J., Sakai, T., & Salzberg, B. (1999). Spatiotemporal patterns of activity in an intact mammalian network with single-cell resolution: optical studies of nicotinic activity in an enteric plexus. *The Journal of neuroscience, 19*(8), 3073-3093.

Oliveira, A. M., Guimarães, K. L., Cerize, N. N., Tunussi, A. S., & Poço, J. G. (2014). Nano spray drying as an innovative technology for encapsulating hydrophilic active pharmaceutical ingredients (API). *Journal of Nanomedicine & Nanotechnology, 4*, 186.

Oyabu, T., Morimoto, Y., Izumi, H., Yoshiura, Y., Tomonaga, T., Lee, B.-W., . . . Kubo, M. (2016). Comparison between whole-body inhalation and nose-only inhalation on the deposition and health effects of nanoparticles. *Environmental health and preventive medicine, 21*(1), 42-48.

Papadimitriou, S., Bikiaris, D., Avgoustakis, K., Karavas, E., & Georgarakis, M. (2008). Chitosan nanoparticles loaded with dorzolamide and pramipexole. *Carbohydrate Polymers, 73*(1), 44-54.

Paques, J. P., van der Linden, E., van Rijn, C. J., & Sagis, L. M. (2014). Preparation methods of alginate nanoparticles. *Advances in colloid and interface science, 209*, 163-171.

Park, J.-H., Jin, H.-E., Kim, D.-D., Chung, S.-J., Shim, W.-S., & Shim, C.-K. (2013). Chitosan microspheres as an alveolar macrophage delivery system of ofloxacin via pulmonary inhalation. *International journal of pharmaceutics, 441*(1), 562-569.

Pascual, S., Feimer, J., De Soyza, A., Roig, J. S., Haughney, J., Padullés, L., . . . Chrystyn, H. (2015). Preference, satisfaction and critical errors with Genuair and Breezhaler inhalers in patients with COPD: a randomised, cross-over, multicentre study. *NPJ primary care respiratory medicine, 25*, 15018.

Patil, S. S., Mahadik, K. R., & Paradkar, A. R. (2015). Liquid crystalline phase as a probe for crystal engineering of lactose: carrier for pulmonary drug delivery. *European Journal of Pharmaceutical Sciences, 68*, 43-50.

Patrianakos, C., & Hoffmann, D. (1979). Chemical studies on tobacco smoke LXIV. On the analysis of aromatic amines in cigarette smoke. *Journal of Analytical Toxicology, 3*(4), 150-154.

Patton, J. S., & Byron, P. R. (2007). Inhaling medicines: delivering drugs to the body through the lungs. *Nature Reviews Drug Discovery, 6*(1), 67-74.

Pauwels, R. A., Buist, A. S., Calverley, P. M., Jenkins, C. R., & Hurd, S. S. (2001). Global strategy for the diagnosis, management, and prevention of chronic obstructive pulmonary disease. *American journal of respiratory and critical care medicine, 163*, 1256-1276.

Penn, A., Chen, L.-C., & Snyder, C. A. (1994). Inhalation of steady-state sidestream smoke from one cigarette promotes arteriosclerotic plaque development. *Circulation, 90*(3), 1363-1367.

Perfetti, T. (1983). Structural study of nicotine salts. *Beiträge zur Tabakforschung/Contributions to Tobacco Research, 12*(2), 43-54.

Perriello, E., & Sobieraj, D. (2015). The Respimat soft mist inhaler, a aovel inhaled drug delivery device. *Connecticut medicine, 80*(6), 359-364.

Perring, S., Summers, Q., Fleming, J. S., Nassim, M. A., & Holgate, S. T. (1994). A new method of quantification of the pulmonary regional distribution of aerosols using combined CT and SPECT and its application to nedocromil sodium administered by metered dose inhaler. *The British Journal of Radiology, 67*(793), 46-53.

Peters, J. M., Avol, E., Navidi, W., London, S. J., Gauderman, W. J., Lurmann, F., . . . Gong Jr, H. (1999). A study of twelve Southern California communities with differing levels and types of air pollution: I. Prevalence of respiratory morbidity. *American journal of respiratory and critical care medicine, 159*(3), 760-767.

Petersen, D., Norris, K., & Thompson, J. (1984). A comparative study of the disposition of nicotine and its metabolites in three inbred strains of mice. *Drug Metabolism and Disposition, 12*(6), 725-731.

Pfeifer, G. P., Denissenko, M. F., Olivier, M., Tretyakova, N., Hecht, S. S., & Hainaut, P. (2002). Tobacco smoke carcinogens, DNA damage and p 53 mutations in smoking-associated cancers. *Oncogene, 21*(48), 7435-7451.

Pharmacopoeia, B. (2011). Appendix XII C. Consistency of formulated preparations (Vol. BP2011 ). British pharmacopoeia: British pharmacopoeia.

Pierce, R. C., O'Brien, C. P., Kenny, P. J., & Vanderschuren, L. J. (2012). Rational development of addiction pharmacotherapies: successes, failures, and prospects. *Cold Spring Harbor perspectives in medicine, 2*(6), 1-9.

Pilcer, G., & Amighi, K. (2010). Formulation strategy and use of excipients in pulmonary drug delivery. *International journal of pharmaceutics, 392*(1), 1-19.

Pilcer, G., Vanderbist, F., & Amighi, K. (2009). Preparation and characterization of spray-dried tobramycin powders containing nanoparticles for pulmonary delivery. *International journal of pharmaceutics, 365*(1), 162-169.

Polosa, R., & Benowitz, N. L. (2011). Treatment of nicotine addiction: present therapeutic options and pipeline developments. *Trends in pharmacological sciences, 32*(5), 281-289.

Prime, D., Atkins, P. J., Slater, A., & Sumby, B. (1997). Review of dry powder inhalers. *Advanced drug delivery reviews, 26*(1), 51-58.

Quist-Paulsen, P. (2007). The effects of smoking cessation intervention in patients with coronary heart disease: a randomised, controlled trial. *European journal of cardiovascular prevention and rehabilitation, 13*(2), 274-280.

Ragelle, H., Riva, R., Vandermeulen, G., Naeye, B., Pourcelle, V., Le Duff, C., . . . De Smedt, S. (2014). Chitosan nanoparticles for siRNA delivery: optimizing

formulation to increase stability and efficiency. *Journal of Controlled Release, 176*, 54-63.

Raichur, A., Nakajima, Y., Nagaoka, Y., Maekawa, T., & Kumar, D. S. (2014). Hollow polymeric (PLGA) nano capsules synthesized using solvent emulsion evaporation method for enhanced drug encapsulation and release efficiency. *Materials Research Express, 1*(4), 1-15.

Rancan, F., Papakostas, D., Hadam, S., Hackbarth, S., Delair, T., Primard, C., . . . Vogt, A. (2009). Investigation of Polylactic Acid (PLA) Nanoparticles as Drug Delivery Systems for Local Dermatotherapy. *Pharmaceutical Research, 26*(8), 2027-2036. doi:10.1007/s11095-009-9919-x

Rao, J. P., & Geckeler, K. E. (2011). Polymer nanoparticles: preparation techniques and size-control parameters. *Progress in Polymer Science, 36*(7), 887-913.

Regan, A. K., Promoff, G., Dube, S. R., & Arrazola, R. (2013). Electronic nicotine delivery systems: adult use and awareness of the 'e-cigarette'in the USA. *Tobacco control, 22*(1), 19-23.

Richard, J.-C., Zhou, Z., Chen, D. L., Mintun, M. A., Piwnica-Worms, D., Factor, P., . . . Schuster, D. P. (2004). Quantitation of pulmonary transgene expression with PET imaging. *Journal of Nuclear Medicine, 45*(4), 644-654.

Richmond, R., & Zwar, N. (2003). Review of bupropion for smoking cessation. *Drug and alcohol review, 22*(2), 203-220.

Rowley, G. (2001). Quantifying electrostatic interactions in pharmaceutical solid systems. *International journal of pharmaceutics, 227*(1), 47-55.

Rytting, E., Nguyen, J., Wang, X., & Kissel, T. (2008). Biodegradable polymeric nanocarriers for pulmonary drug delivery. *Expert opinion on drug delivery, 5*(6), 629-639.

Saha, G. B., MacIntyre, W. J., & Go, R. T. (1992). Cyclotrons and positron emission tomography radiopharmaceuticals for clinical imaging. *Seminars in nuclear medicine, 22*(3), 150-161.

Sakagami, M. (2006). In vivo, in vitro and ex vivo models to assess pulmonary absorption and disposition of inhaled therapeutics for systemic delivery. *Advanced drug delivery reviews, 58*(9), 1030-1060.

Sanyakamdhorn, S., Agudelo, D., & Tajmir-Riahi, H.-A. (2013). Encapsulation of antitumor drug doxorubicin and its analogue by chitosan nanoparticles. *Biomacromolecules, 14*(2), 557-563.

Sawyer, P. N., Fitzgerald, J., Kaplitt, M. J., Sanders, R. J., Williams, G. M., Leather, R. P., . . . Fries, C. C. (1987). Ten year experience with the negatively charged glutaraldehyde-tanned vascular graft in peripheral vascular surgery: initial multicenter trail. *The American journal of surgery, 154*(5), 533-537.

Schanker, L. S., & Burton, J. A. (1976). Absorption of heparin and cyanocobalamin from the rat lung. *Experimental Biology and Medicine, 152*(3), 377-380.

Schatz, M., Zeiger, R. S., Vollmer, W. M., Mosen, D., & Cook, E. F. (2006). Determinants of future long-term asthma control. *Journal of allergy and clinical immunology, 118*(5), 1048-1053.

Schweitzer, A., & Wright, S. (1938). Action of nicotine on the spinal cord. *The Journal of physiology, 94*(1), 136.

Sha, Y., Zhang, Q., Li, M., & Shen, Y. (2014). Nicotine sustained-release patch. 16.

Sham, J., Zhang, Y., Finlay, W. H., Roa, W. H., & Löbenberg, R. (2004). Formulation and characterization of spray-dried powders containing nanoparticles for aerosol delivery to the lung. *International journal of pharmaceutics, 269*(2), 457-467.

Shiffman, S. (2007). Nicotine replacement therapy for smoking cessation in the "real world". *Thorax, 62*(11), 930-931.
Shiffman, S., Ferguson, S. G., Dunbar, M. S., & Scholl, S. M. (2012). Tobacco dependence among intermittent smokers. *Nicotine & Tobacco Research, 14*(11), 1372-1381.
Siegel, M. B., Tanwar, K. L., & Wood, K. S. (2011). Electronic cigarettes as a smoking-cessation tool: results from an online survey. *American journal of preventive medicine, 40*(4), 472-475.
Siegel, R. L., Miller, K. D., & Jemal, A. (2015). Cancer statistics, 2015. *CA: a cancer journal for clinicians, 65*(1), 5-29.
Siepmann, J., & Peppas, N. (2001). Modeling of drug release from delivery systems based on hydroxypropyl methylcellulose (HPMC). *Advanced drug delivery reviews, 48*(2), 139-157.
Silagy, C., Lancaster, T., Stead, L., Mant, D., & Fowler, G. (2004). Nicotine replacement therapy for smoking cessation. *The cochrane library 2004*(3), 1-106.
Silva, R., Silva, G., Coutinho, O., Mano, J., & Reis, R. (2004). Preparation and characterisation in simulated body conditions of glutaraldehyde crosslinked chitosan membranes. *Journal of Materials Science: Materials in Medicine, 15*(10), 1105-1112.
Sinha, B., & Mukherjee, B. (2012). Development of an inhalation chamber and a dry powder inhaler device for administration of pulmonary medication in animal model. *Drug development and industrial pharmacy, 38*(2), 171-179.
Smith, C. J., Perfetti, T. A., Garg, R., & Hansch, C. (2006). Utility of the mouse dermal promotion assay in comparing the tumorigenic potential of cigarette mainstream smoke. *Food and chemical toxicology, 44*(10), 1699-1706.
Smyth, H. (2006). *Excipients for pulmonary formulations*.
Sonia, T., & Sharma, C. P. (2011). Chitosan and its derivatives for drug delivery perspective. *Advances in polymer science, 243*, 23-54.
Sosnik, A., & Seremeta, K. P. (2015). Advantages and challenges of the spray-drying technology for the production of pure drug particles and drug-loaded polymeric carriers. *Advances in Colloid and Interface Science, 223*, 40-54.
Srichana, T., Martin, G., & Marriott, C. (1998). Dry powder inhalers: the influence of device resistance and powder formulation on drug and lactose deposition in vitro. *European Journal of Pharmaceutical Sciences, 7*(1), 73-80.
Stapleton, J. A., Watson, L., Spirling, L. I., Smith, R., Milbrandt, A., Ratcliffe, M., & Sutherland, G. (2008). Varenicline in the routine treatment of tobacco dependence: a pre–post comparison with nicotine replacement therapy and an evaluation in those with mental illness. *Addiction, 103*(1), 146-154.
Stapleton, M., Howard-Thompson, A., George, C., Hoover, R. M., & Self, T. H. (2011). Smoking and asthma. *The Journal of the American Board of Family Medicine, 24*(3), 313-322.
Stegemann, S., Kopp, S., Borchard, G., Shah, V., Senel, S., Dubey, R., . . . Hippchen, C. (2013). Developing and advancing dry powder inhalation towards enhanced therapeutics. *European Journal of Pharmaceutical Sciences, 48*(1), 181-194.
Stenzler, A., Zamel, N., Slutsky, A., & Ellis, S. (2017). Inhalable nicotine formulations and methods of making and using the same: Google Patents.
Stewart, B. W., & Kleihues, P. (2003). World cancer report. *WHO international agency for research on cancer, 57*, 181-185.

Stitzer, M., Morrison, J., & Domino, E. F. (1970). Effects of nicotine on fixed-interval behavior and their modification by cholinergic antagonists. *Journal of Pharmacology and Experimental Therapeutics, 171*(2), 166-177.

Stolerman, I., Fink, R., & Jarvik, M. (1973). Acute and chronic tolerance to nicotine measured by activity in rats. *Psychopharmacologia, 30*(4), 329-342.

Stolerman, I., Garcha, H., & Mirza, N. (1995). Dissociations between the locomotor stimulant and depressant effects of nicotinic agonists in rats. *Psychopharmacology, 117*(4), 430-437.

Strekalova, T., Spanagel, R., Dolgov, O., & Bartsch, D. (2005). Stress-induced hyperlocomotion as a confounding factor in anxiety and depression models in mice. *Behavioural pharmacology, 16*(3), 171-180.

Strike, M., & Hatcher, S. (2015). Bupropion injection resulting in tissue necrosis and psychosis: previously undocumented complications of intravenous bupropion use disorder. *Journal of addiction medicine, 9*(3), 246-250.

Subramaniam, S., Bummer, P., & Gairola, C. (1995). Biochemical and biophysical characterization of pulmonary surfactant in rats exposed chronically to cigarefte smoke. *Toxicological Sciences, 27*(1), 63-69.

Sutherland, R., Sindicich, N., Entwistle, G., Whittaker, E., Peacock, A., Matthews, A., . . . Burns, L. (2016). Tobacco and e-cigarette use amongst illicit drug users in Australia. *Drug and alcohol dependence, 159*, 35-41.

Tang, D., Phillips, D. H., Stampfer, M., Mooney, L. A., Hsu, Y., Cho, S., . . . Shé, M. N. (2001). Association between carcinogen-DNA adducts in white blood cells and lung cancer risk in the physicians health study. *Cancer research, 61*(18), 6708-6712.

Tashkin, D. P., Rennard, S., Hays, J. T., Ma, W., Lawrence, D., & Lee, T. C. (2011). Effects of varenicline on smoking cessation in patients with mild to moderate COPD: a randomized controlled trial. *Chest Journal, 139*(3), 591-599.

Terry, A. B., Salaam, A. D., Nyairo, E., Thomas, V., & Dean, D. R. (2014). Plga nanoparticles for the sustained release of rifampicin. *Journal of Nanogenomics and Nanomedicine, 2*(1), 1-9.

Thompson, R. B., & Finlay, W. H. (2012). Using MRI to measure aerosol deposition. *Journal of aerosol medicine and pulmonary drug delivery, 25*(2), 55-62.

Thun, M. J., Lally, C. A., Calle, E. E., Heath, C. W., Flannery, J. T., & Flanders, W. D. (1997). Cigarette smoking and changes in the histopathology of lung cancer. *Journal of the National Cancer Institute, 89*(21), 1580-1586.

Tian, G., Longest, P. W., Li, X., & Hindle, M. (2013). Targeting aerosol deposition to and within the lung airways using excipient enhanced growth. *Journal of aerosol medicine and pulmonary drug delivery, 26*(5), 248-265.

Tian, X., Yin, H., Zhang, S., Luo, Y., Xu, K., Ma, P., . . . Fang, J. (2014). Bufalin loaded biotinylated chitosan nanoparticles: An efficient drug delivery system for targeted chemotherapy against breast carcinoma. *European Journal of Pharmaceutics and Biopharmaceutics, 87*(3), 445-453.

Tiyaboonchai, W. (2003). Chitosan nanoparticles: a promising system for drug delivery. *Naresuan University Journal, 11*(3), 51-66.

Tonini, G., D'Onofrio, L., Dell'Aquila, E., & Pezzuto, A. (2013). New molecular insights in tobacco-induced lung cancer. *Future Oncology, 9*(5), 649-655.

Tonstad, S., Farsang, C., Klaene, G., Lewis, K., Manolis, A., Perruchoud, A., . . . Hider, A. (2003). Bupropion SR for smoking cessation in smokers with cardiovascular disease: a multicentre, randomised study. *European heart journal, 24*(10), 946-955.

Trtchounian, A., & Talbot, P. (2011). Electronic nicotine delivery systems: is there a need for regulation? *Tobacco control, 20*(1), 47-52.

Tsuji, H., Fujimoto, H., Matsuura, D., Nishino, T., Lee, K. M., Renne, R., & Yoshimura, H. (2011). Comparison of mouse strains and exposure conditions in acute cigarette smoke inhalation studies. *Inhalation toxicology, 23*(10), 602-615.

Tuli, R. A., George, G. A., Dargaville, T. R., & Islam, N. (2012). Studies on the effect of the size of polycaprolactone microspheres for the dispersion of salbutamol sulfate from dry powder inhaler formulations. *Pharmaceutical research, 29*(9), 2445-2455.

Tutka, P., & Zatoñski, W. (2006). Cytisine for the treatment of nicotine addiction: from a molecule to therapeutic efficacy. *Pharmacological reports, 58*(6), 777-798.

Tyler, B., Gullotti, D., Mangraviti, A., Utsuki, T., & Brem, H. (2016). Polylactic acid (PLA) controlled delivery carriers for biomedical applications. *Advanced drug delivery reviews, 107*, 163-175.

Uhrich, K. E., Cannizzaro, S. M., Langer, R. S., & Shakesheff, K. M. (1999). Polymeric systems for controlled drug release. *Chemical reviews, 99*(11), 3181-3198.

van Dijk, W. D., Heijdra, Y., Scheepers, P. T. J., Lenders, J. W. M., van Weel, C., & Schermer, T. R. J. (2010). Interaction in COPD experiment (ICE): A hazardous combination of cigarette smoking and bronchodilation in chronic obstructive pulmonary disease. *Medical Hypotheses, 74*(2), 277-280.

Vandewater, E. A., Park, S. E., Carey, F. R., & Wilkinson, A. V. (2014). Intergenerational transfer of smoking across three generations and forty-five years. *Nicotine & Tobacco Research, 16*(1), 11-17.

Varshosaz, J., Taymouri, S., & Hamishehkar, H. (2014). Fabrication of polymeric nanoparticles of poly (ethylene‐co‐vinyl acetate) coated with chitosan for pulmonary delivery of carvedilol. *Journal of Applied Polymer Science, 131*(1), 39694-39702.

Vega, J. C., & Toneguzzo, F. (2012). US Patent No.

Wang, H., George, G., Bartlett, S., Gao, C., & Islam, N. (2017). Nicotine hydrogen tartrate loaded chitosan nanoparticles: Formulation, characterization and in vitro delivery from dry powder inhaler formulation. *European Journal of Pharmaceutics and Biopharmaceutics, 113*, 118-131.

Wang, H., Liu, X., Umino, T., Skold, C. M., Zhu, Y., Kohyama, T., . . . Rennard, S. I. (2001). Cigarette smoke inhibits human bronchial epithelial cell repair processes. *American journal of respiratory cell and molecular biology, 25*(6), 772-779.

Wang, H., Xu, Y., & Zhou, X. (2014). Docetaxel-loaded chitosan microspheres as a lung targeted drug delivery system: In vitro and in vivo evaluation. *International journal of molecular sciences, 15*(3), 3519-3532.

Wang, X., Chi, N., & Tang, X. (2008). Preparation of estradiol chitosan nanoparticles for improving nasal absorption and brain targeting. *European Journal of Pharmaceutics and Biopharmaceutics, 70*(3), 735-740.

Watts, A. B., McConville, J. T., & Williams III, R. O. (2008). Current therapies and technological advances in aqueous aerosol drug delivery. *Drug development and industrial pharmacy, 34*(9), 913-922.

Wetterlin, K. (1988). Turbuhaler: a new powder inhaler for administration of drugs to the airways. *Pharmaceutical research, 5*(8), 506-508.

WHO. (2015). *WHO global report on trends in prevalence of tobacco smoking 2015*: World Health Organization.

Windle, S. B., Filion, K. B., Mancini, J. G., Adye-White, L., Joseph, L., Gore, G. C., . . . Eisenberg, M. J. (2016). Combination therapies for smoking cessation: a hierarchical Bayesian meta-analysis. *American journal of preventive medicine, 51*(6), 1060-1071.

Wolff, R. K., & Dorato, M. (1993). Toxicologic testing of inhaled pharmaceutical aerosols. *Critical reviews in toxicology, 23*(4), 343-369.

Wu, X., O Adedoyin, O., & M Mansour, H. (2011). Pulmonary and nasal anti-inflammatory and anti-allergy inhalation aerosol delivery systems. *Anti-inflammatory & anti-allergy agents in medicinal chemistry, 10*(3), 215-229.

Xie, L., Beyer, S., Vogel, V., Wacker, M. G., & Mäntele, W. (2015). Assessing the drug release from nanoparticles: Overcoming the shortcomings of dialysis by using novel optical techniques and a mathematical model. *International Journal of Pharmaceutics, 488*(1), 108-119.

Xu, J., Ma, L., Liu, Y., Xu, F., Nie, J., & Ma, G. (2012). Design and characterization of antitumor drug paclitaxel-loaded chitosan nanoparticles by W/O emulsions. *International journal of biological macromolecules, 50*(2), 438-443.

Xu, Z., Mansour, H. M., & Hickey, A. J. (2011). Particle interactions in dry powder inhaler unit processes: a review. *Journal of Adhesion Science and Technology, 25*(4-5), 451-482.

Yi, D., Price, A., Panoskaltsis-Mortari, A., Naqwi, A., & Wiedmann, T. S. (2010). Measurement of the distribution of aerosols among mouse lobes by fluorescent imaging. *Analytical biochemistry, 403*(1), 88-93.

Yi, J., Chen, B. T., Schwegler-Berry, D., Frazer, D., Castranova, V., McBride, C., . . . Nurkiewicz, T. R. (2013). Whole-body nanoparticle aerosol inhalation exposures. *Journal of visualized experiments*(75), e50263-e50263.

Zahoor, A., Sharma, S., & Khuller, G. K. (2005). Inhalable alginate nanoparticles as antitubercular drug carriers against experimental tuberculosis. *International journal of antimicrobial agents, 26*(4), 298-303.

Zainudin, B., Biddiscombe, M., Tolfree, S., Short, M., & Spiro, S. (1990). Comparison of bronchodilator responses and deposition patterns of salbutamol inhaled from a pressurised metered dose inhaler, as a dry powder, and as a nebulised solution. *Thorax, 45*(6), 469-473.

Zhang, G., Shinohara, N., Oshima, Y., Kobayashi, T., Imatanaka, N., Kawaguchi, K., & Gamo, M. (2016). Comparison of the local pulmonary distribution of nanoparticles administered intratracheally to rats via gavage needle or microsprayer delivery devices. *Journal of Applied Toxicology*. doi:10.1002/jat.3386

Zhou, Q. T., Tang, P., Leung, S. S. Y., Chan, J. G. Y., & Chan, H.-K. (2014). Emerging inhalation aerosol devices and strategies: where are we headed? *Advanced drug delivery reviews, 75*, 3-17.

Zhou, Q. T., Tong, Z., Tang, P., Citterio, M., Yang, R., & Chan, H.-K. (2013). Effect of device design on the aerosolization of a carrier-based dry powder inhaler—a case study on Aerolizer® Foradile®. *The AAPS journal, 15*(2), 511-522.

# Appendix

Table 1. *In vitro* aerosolization study of blank and NHT-loaded CS nanoparticles by TSI in one year under storage condition of 25°C, 60% RH (data presented as mean ± SD., n = 3)

| Formulation | Month | R (mg) | $S_1$(mg) | $S_2$ (mg) | RD (%) | ED (%) | FPF (%) |
|---|---|---|---|---|---|---|---|
| Blank CS | 0 | 5.6±0.1 | 7.4±0.1 | 5.6±0.1 | 90.0±1.4 | 69.9±0.2 | 30.8±0.2 |
| | 1 | 6.2±0.4 | 6.1±0.7 | 5.4±0.1 | 88.8±3.6 | 64.8±2.2 | 30.3±1.1 |
| | 2 | 8.5±0.5 | 7.5±0.3 | 6.9±0.2 | 92.1±0.5 | 62.9±1.8 | 30.1±0.6 |
| ` | 12 | 6.6±0.4 | 6.5±0.2 | 5.7±0.3 | 94.0±2.8 | 64.9±1.6 | 30.3±0.9 |
| NHT-CS 1:1 | 0 | 4.5±0.2 | 8.0±0.2 | 5.3±0.2 | 88.3±2.7 | 74.7±0.7 | 29.6±0.9 |
| | 1 | 5.4±0.3 | 7.5±0.4 | 5.3±0.2 | 91.4±2.1 | 70.4±1.6 | 29.2±1.2 |
| | 2 | 5.2±0.5 | 8.3±0.6 | 5.4±0.2 | 94.6±2.6 | 73.2±2.8 | 28.3±0.6 |
| | 12 | 4.9±0.4 | 7.8±0.5 | 5.2±0.4 | 89.5±2.7 | 72.6±1.3 | 29.1±0.8 |
| NHT-CS 2:1 | 0 | 4.4±0.5 | 9.9±0.4 | 5.3±0.4 | 92.5±2.9 | 76.9±2.3 | 25.9±2.3 |
| | 1 | 4.8±0.3 | 9.5±0.4 | 5.1±0.1 | 96.9±2.6 | 75.2±0.2 | 26.2±0.8 |
| | 2 | 4.8±0.8 | 9.5±0.6 | 5.3±0.2 | 98.2±2.2 | 75.5±3.6 | 27.0±0.3 |
| | 12 | 4.4±0.5 | 9.9±0.1 | 5.0±0.7 | 91.4±3.4 | 77.3±2.8 | 25.8±3.2 |
| NHT-CS 3:1 | 0 | 4.6±0.3 | 9.3±0.8 | 4.6±0.2 | 92.9±2.9 | 75.3±2.4 | 24.4±1.5 |
| | 1 | 4.3±0.2 | 9.4±0.5 | 4.4±0.2 | 90.6±4.2 | 76.1±1.0 | 24.1±1.3 |
| | 2 | 4.7±0.4 | 9.8±0.7 | 4.8±0.2 | 96.4±1.7 | 75.7±2.7 | 24.6±1.4 |
| | 12 | 4.8±0.3 | 9.3±1.1 | 4.4±0.2 | 92.0±3.3 | 74.7±3.3 | 24.1±1.7 |

NB: black CS nanoparticles were measured gravimetrically; NHT-loaded CS nanoparticles were measured gravimetrically and spectrophotometrically.

Table 2. Mass balance between different flow rates (NHT loaded=100mg) (data presented as mean±SEM)

| Flow rate (L/min) | Total recovered dose (mg) | Total all ports collected (mg) | Percentage of Deposition (%) |
|---|---|---|---|
| 0.6 | 27.15±1.14 | 8.72±0.92 | 9.03±1.40 |
| 0.9 | 43.43±4.73 | 10.77±1.90 | 11.21±1.68 |

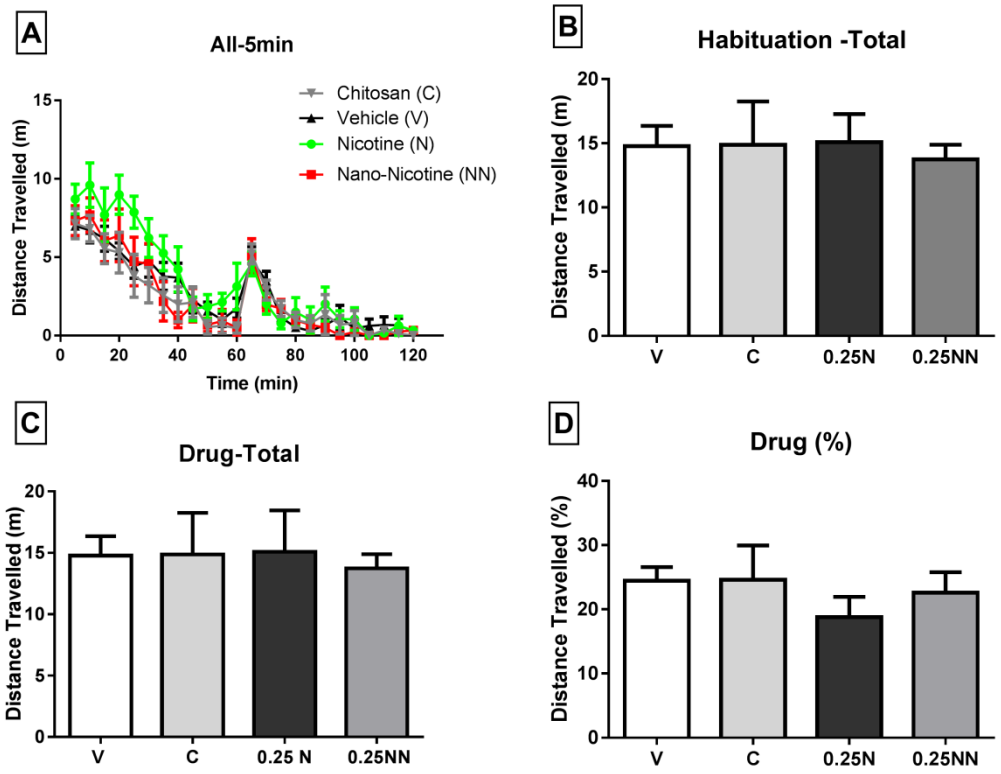


Figure 1. Locomotor activity administrated by 0.25 mg/kg s.c. injection (n=8-10 per group; mean±SEM) (A) travel distance of naïve mice every 5 minutes for 2 hours; (B) travel distance during habituation period; (C) travel distance during one hour of drug test period; (D) the percentage of travel distance in the drug test hour of total travel distance in the two hours;
NB: "N"=nicotine; "NN"=nano-nicotine; "V"=vehicle; "C"=Chitosan

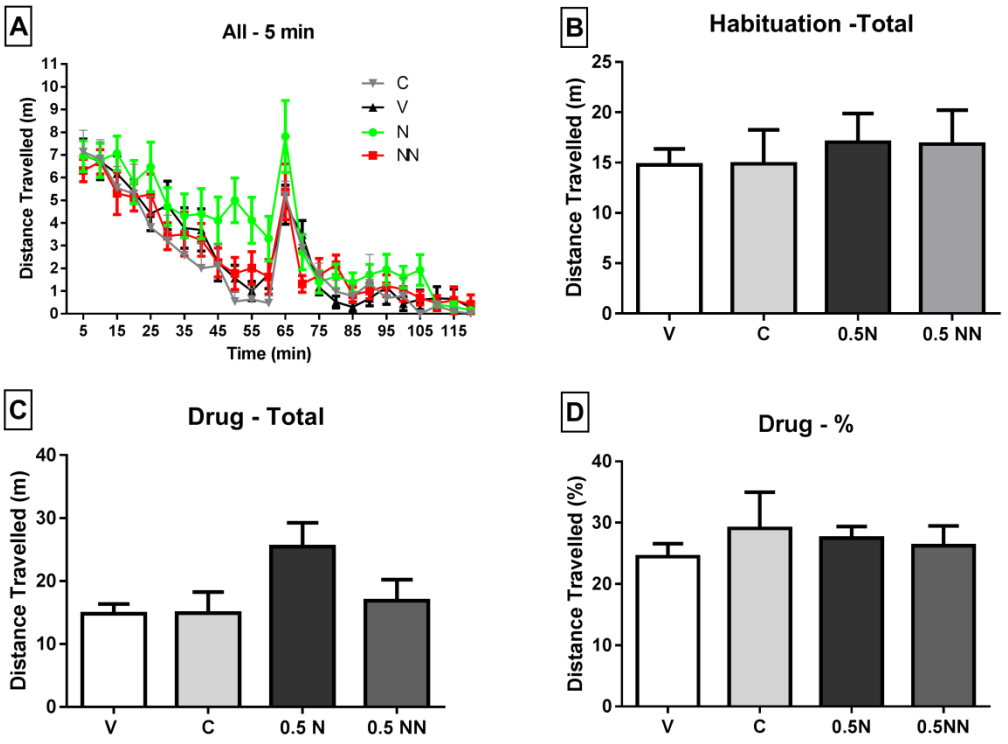


Figure 2. Locomotor activity administrated by 0.5 mg/kg s.c. injection (n=8-10 per group; mean±SEM) (A) travel distance of naïve mice in every 5 minutes for 2 hours; (B) travel distance during habituation period; (C) travel distance during one hour of drug test period; (D) the percentage of travel distance in the drug test hour of total travel distance in the two hours. NB: "N"=nicotine; "NN"=nano-nicotine; "V"=vehicle; "C"=Chitosan

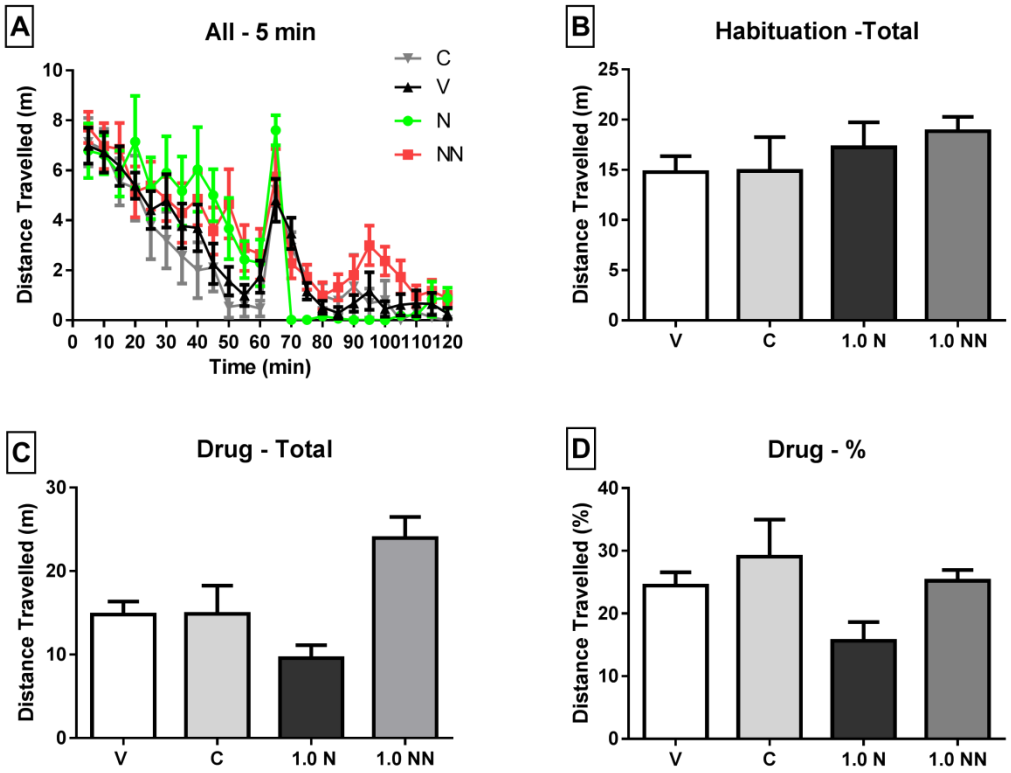


Figure 3. Locomotor activity administrated by 1.0 mg/kg s.c. injection (n=8-10 per group; mean±SEM) (A) travel distance of naïve mice in every 5 minutes for 2 hours; (B) travel distance during habituation period; (C) travel distance during one hour of drug test period; (D) the percentage of travel distance in the drug test hour of total travel distance in the two hours.. NB: "N"=nicotine; "NN"=nano-nicotine; "V"=vehicle; "C"=Chitosan

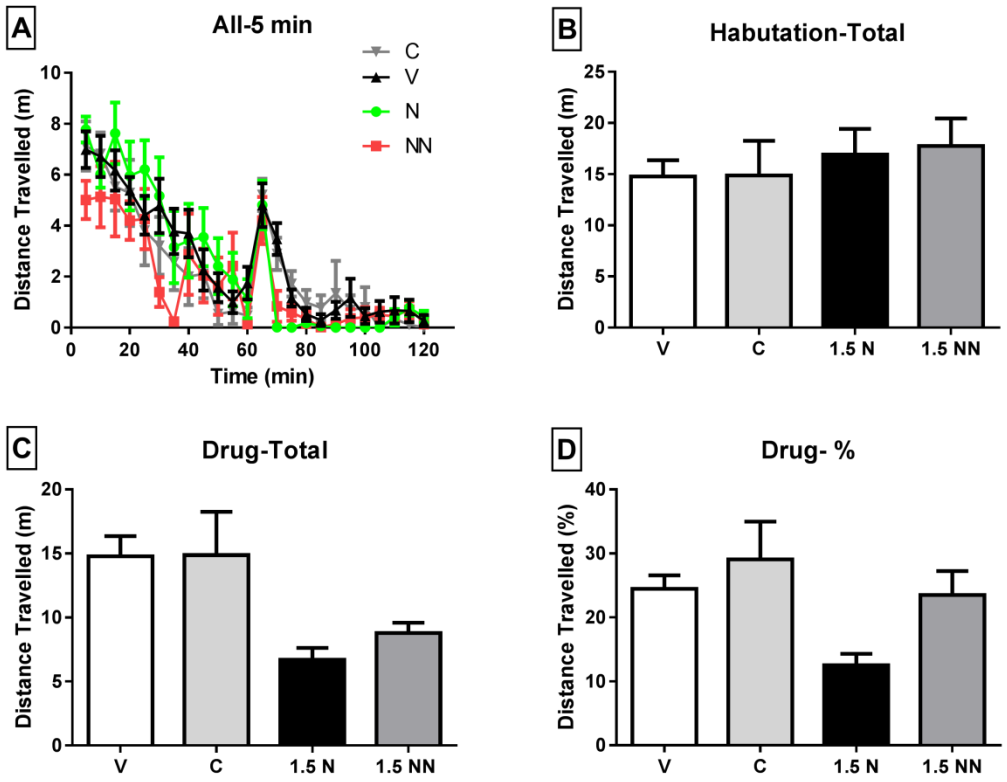


Figure 4. Locomotor activity administrated by 1.5 mg/kg s.c. injection (n=8-10 per group; mean±SEM) (A) travel distance of naïve mice in every 5 minutes for 2 hours; (B) travel distance during habituation period; (C) travel distance during one hour of drug test period; (D) the percentage of travel distance in the drug test hour of total travel distance in the two hours; NB: "N"=nicotine; "NN"=nano-nicotine; "V"=vehicle; "C"=Chitosan

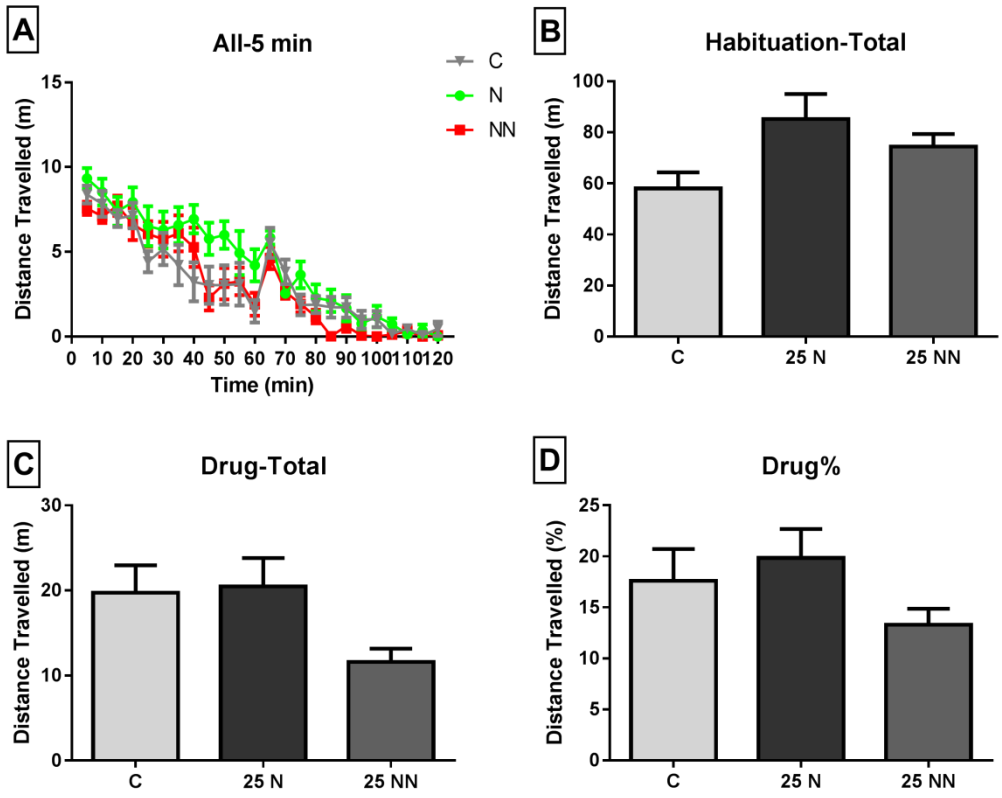


Figure 5. Locomotor activity inhalation exposure for 25mg dose (n=8-10 per group; mean±SEM) (A) travel distance of naïve mice in every 5 minutes for 2 hours; (B) travel distance during habituation period; (C) travel distance during one hour of drug test period; (D) the percentage of travel distance in the drug test hour of total travel distance in the two hours. NB: "N"=nicotine; "NN"=nano-nicotine; "C"=Chitosan/Vehicle

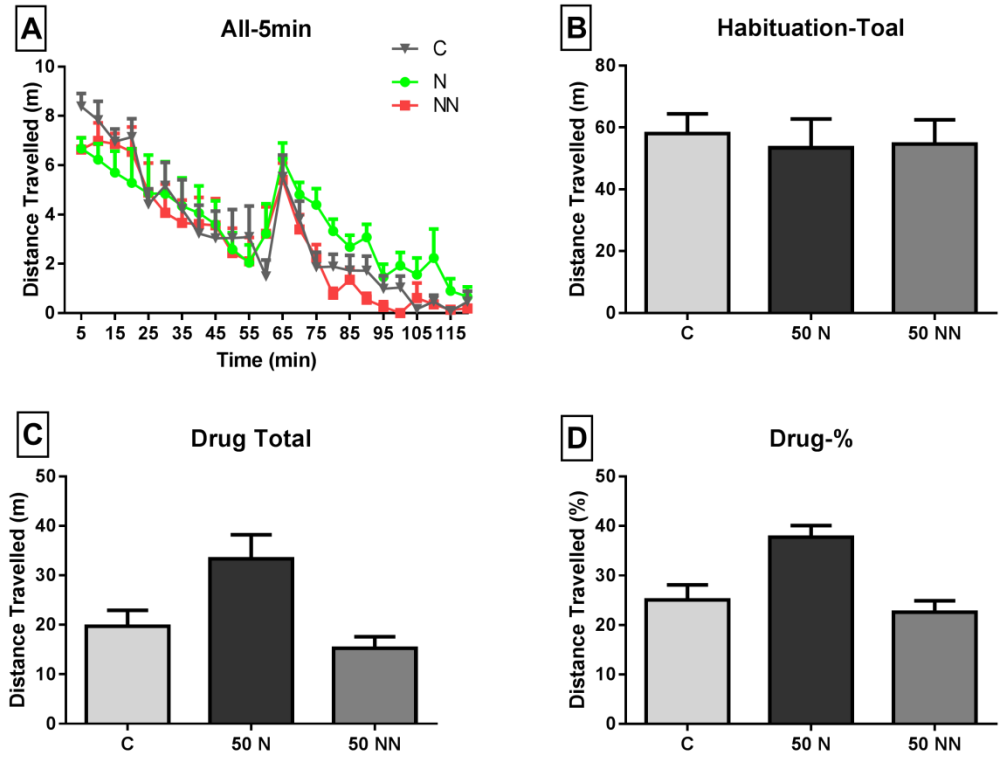


Figure 6. Locomotor activity inhalation exposure for 50 mg dose (n=8-10 per group; mean±SEM) (A) travel distance of naïve mice in every 5 minutes for 2 hours; (B) travel distance during habituation period; (C) travel distance during one hour of drug test period; (D) the percentage of travel distance in the drug test hour of total travel distance in the two hours. NB: "N"=nicotine; "NN"=nano-nicotine; "C"=Chitosan/Vehicle

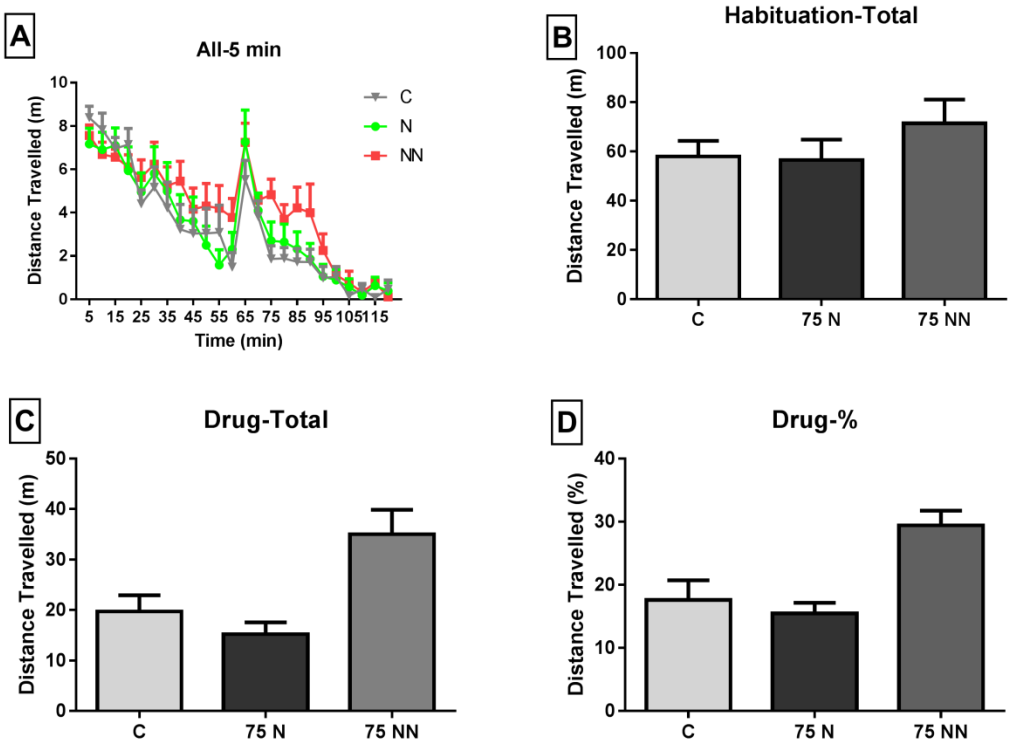


Figure 7. Locomotor activity inhalation exposure for 75 mg dose (n=8-10 per group; mean±SEM) (A) travel distance of naïve mice in every 5 minutes for 2 hours; (B) travel distance during habituation period; (C) travel distance during one hour of drug test period; (D) the percentage of travel distance in the drug test hour of total travel distance in the two hours; NB: "N"=nicotine; "NN"=nano-nicotine; "C"=Chitosan/Vehicle